delayed by T seconds to allow the slicer to make a decision. In practice, this method provides a smaller error variance compared with either the Costas or times-N carrier recovery loops if the receiver is operating at error rates below 0.01. A decision-directed carrier recovery loop can be implemented with or without an adaptive equalizer. Without an adaptive equalizer, the receiver makes a decision based on the most likely transmitted constellation point given the received symbol. This is usually the minimum Euclidean distance between the transmitted and received constellation points. These decisions are then used to generate a phase-error control signal to adjust the erroneous phase of the received constellation points.

The use of an adaptive equalizer in conjunction with a decision-directed loop creates several practical difficulties that need to be overcome. Placing an adaptive equalizer inside the decision-directed loop would cause long symbol delays, and would impair the loop's ability to track phase jitter. This problem is typically solved by placing the adaptive FFE before the carrier recovery loop.

7.10.2 Timing Recovery in QAM Receivers

The primary task of the timing recovery loop is to generate a clock signal at the symbol rate R_S or a multiple of R_S from the received signal. For state-of-the-art QAM receivers, it is not practical to transmit a separate clock signal with the data; the clock signal must be extracted from the received modulated signal using a additional circuitry in the receiver.

In general, the timing recovery methods can be categorized into two classes, which are called the forward-acting [33] and the feedback methods [38–40]. The forward-acting timing-recovery method extracts a timing tone directly from the received signal. The timing tone, which has an average frequency exactly equal to the symbol rate, is used to synchronize the receiver to the detected digital signal. Since the timing tone has some amount of a

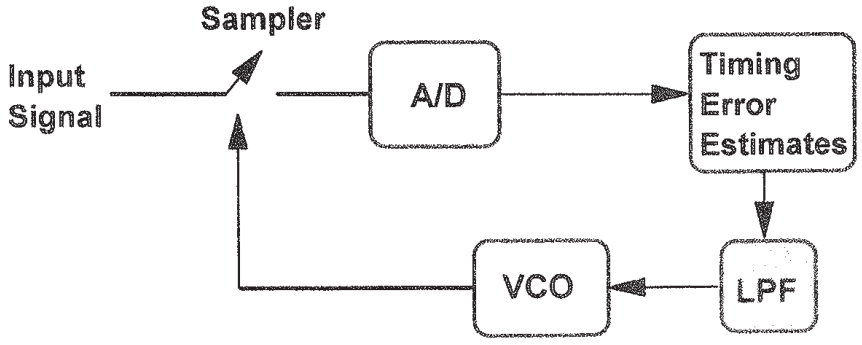


Figure 7.22 A generic block diagram of an MMSE feedback-timing-recovery loop.

phase jitter or a timing jitter, a PLL is typically used to reduce the timing jitter to an acceptable level. In the feedback-timing-recovery methods, a feedback loop is used in conjunction with the PLL to adjust the sampled phase in an iterative way and drive the VCO in order to minimize the timing error.

The most popular-timing-recovery method in the forward-acting category is the spectral-line method. In this method, the timing error τ_k is determined by the zero crossing of the timing tone and PLL. The modulated signal is passed through a timing tone detector such as an envelope detector, LPF, and a PLL, where the resultant signal is used to drive a VCO. The feedback-timing-recovery category can be divided into two different techniques, namely, the MMSE and the baud-rate timing recovery. The operating principles and the advantages and disadvantages of each method are explained as follows: Figure 7.22 shows a basic block diagram of an MMSE timing-recovery loop. The MMSE timing recovery adjusts the timing error to minimize the expected square error between the slicer output (estimated symbols) and the corrected data symbols. Notice that we assumed that the received signal is in baseband and it is sampled every symbol period (T). The MMSE timing-

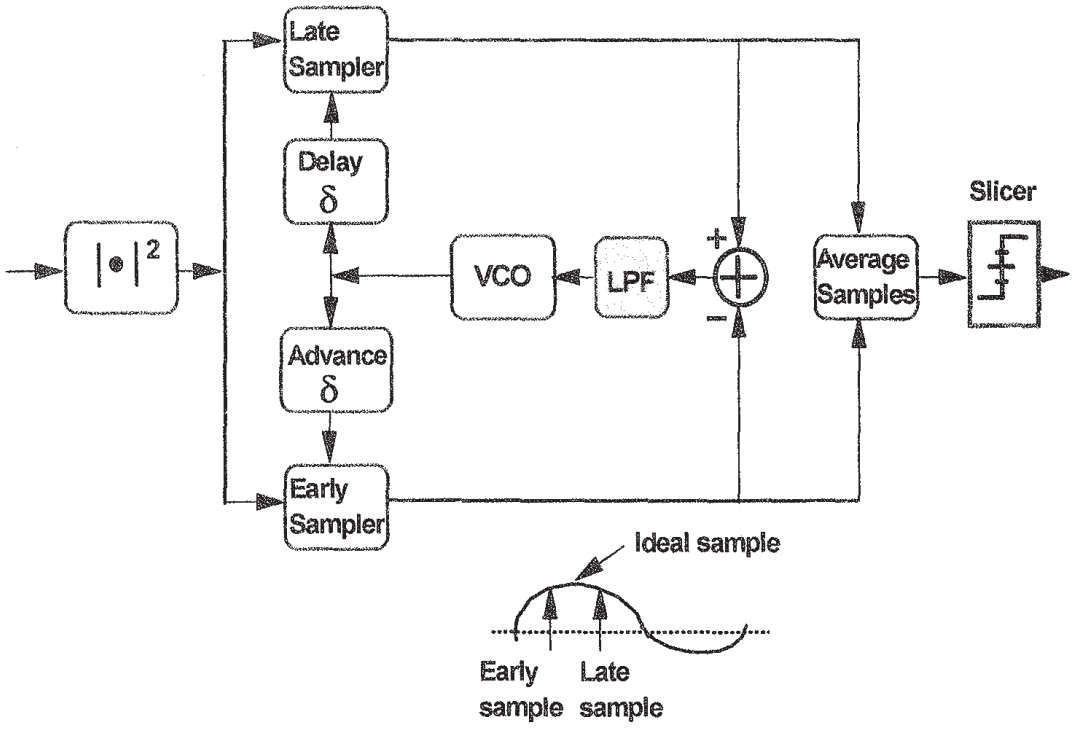


Figure 7.23 A block diagram of an early-late timing recovery loop. After Ref. [40].

recovery method, which is sometimes called the LMS timing recovery, can be implemented using various techniques. The MMSE can be implemented using the stochastic gradient algorithm to minimize the timing error in the same way that it was used for the adaptive equalizer (Section 7.8). The main problem with this approach is that it operates on the input to the slicer, which has been equalized and demodulated. However, both the carrier recovery and the equalizer assumed that the timing recovery has been achieved.

Other timing recovery techniques, which are closely related to the MMSE method, have been reported in the literature. One of the well-known techniques is the *early-late timing recovery* as shown in Figure 7.23 [35]. In this technique, the received baseband waveform is first squared to make all the peaks positive, and then it is sampled at two different times, once before and once after the sampling instant at the same amount of δ. The sampling instant is adjusted by the VCO until the early and late samples are equal. This technique assumes that the received waveform peaks are at the correct sampling points and the waveform around the peak is symmetric. The averaged-timing-error signal is used to drive the VCO, whose output is the desired clock signal. The drawback of this technique is that the waveform peaks of the received signal (in the time domain) do not occur every sampling period for QAM sequences.

7.11 MER and EVM

Now that we understand the operation of the various building blocks of a QAM transmitter and receiver, we are ready to introduce two important parameters, which are related to one another, and which provide one with a very practical tool to test the fidelity of a QAM transmitter and to calibrate the CNR measurement of a QAM receiver under test.

7.11.1 MER and EVM Definition

The first parameter is the SNR due to any impairment. It is equivalent to the SNR for Gaussian noise generated by inter-symbol interference (ISI) that would degrade the transmitter or receiver by the same amount as the impairment. This parameter is also called the modulation-error ratio (MER), which is typically measured on a standard QAM test receiver such as the Agilent 89441A Vector Signal Analyzer, and is defined as follows:

$$MER(dB) = -10 \cdot \log\left\{\frac{\sum_{j=1}^{N}(\delta I_j^2 + \delta Q_j^2)}{\sum_{j=1}^{N}(I_j^2 + Q_j^2)}\right\} \tag{7.30}$$

where I and Q are the ideal QAM constellation data points, δI and δQ are the errors in the received data points relative to the ideal QAM constellation points due to the impairment, and N is the number of points that were captured in the data sample. N in Equation (7.30) is the data sample size, and typically should be much greater than the number of points in the constellation in order to capture a representative sample. In other words, it is a measurement of the constellation-cluster variance due to any impairment and transmitter imperfections measured relative to the ideal constellation point locations.

The related parameter to the MER is the error-vector magnitude (EVM), which is defined as

$$EVM = 100\% \cdot \sqrt{\frac{\frac{1}{N}\sum_{j=1}^{N}(\delta I_j^2 + \delta Q_j^2)}{S_{\max}^2}} \tag{7.31}$$

where S_{max} is the magnitude of the vector to the outermost state of the M-ary QAM constellation. Since the numerator is the same in each case, the EVM and MER are related as follows

$$\frac{EVM^2}{MER} = \frac{\frac{1}{N}\sum_{j=1}^{N}(I_j^2 + Q_j^2)}{S_{\max}^2} = \frac{P_{rms}}{P_{\max}} = 1/R \tag{7.32}$$

where R is the ratio of the peak power to the average power of the M-ary QAM constellation. Thus, Equation (7.32) defines the relationship between the MER and the EVM.

7.11.2 MER and EVM Test Procedure

To accurately measure the MER or EVM of a QAM transmitter, a calibrated reference QAM receiver is needed. Such an instrument is, for example, the Agilent 89441A Vector Signal Analyzer [41]. This instrument can analyze a broad range of performance parameters, including both the MER and the EVM from QPSK to 256-QAM signals. The Agilent 89441A can operate either in continuous or burst data mode. However, for simplicity, we will explain the MER test procedure for a QAM transmitter operating in a continuous mode. The measurement of MER by the Agilent 89441A is done by capturing a number of symbols, analyzing them, and calculating the result. Because of the randomizer, each QAM constellation point should be equally likely. In a typical measurement, the HP89441A calculates the MER of each point, but weights them all equally since they are all equally likely to occur. The Agilent 89441A should be set, for example, to sample (result length) N = 512 symbols per measurement and then average over at least 10 measurements. It is recommended that a

larger number of sample points, particularly for 256-QAM constellations, should be specified.

The Agilent 89441A dynamically tracks the carrier-phase loop, baud loop, and AGC-gain loop. The Agilent 89441A does not perform real-time signal processing so there really is no tracking loop bandwidth. The instrument will determine the best overall carrier phase, baud timing, and AGC gain for the overall sample and will hold those parameters fixed for the entire sample size. The effective carrier, baud, and AGC loop bandwidth will be determined by the size of the data sample. For example, when demodulating 64-QAM signals at 5-Mbaud and using a sample size (result length) of 512 points with 1 point per symbol (512 symbols), the duration of the sample data is 0.2-Mbaud·512 = 0.2-μs·512 ≅ 102-μs. This corresponds to a bandwidth of 10-kHz. In other words, if the carrier phase changes are slow compared to 10-kHz, the change during the sample time will be small and will have small

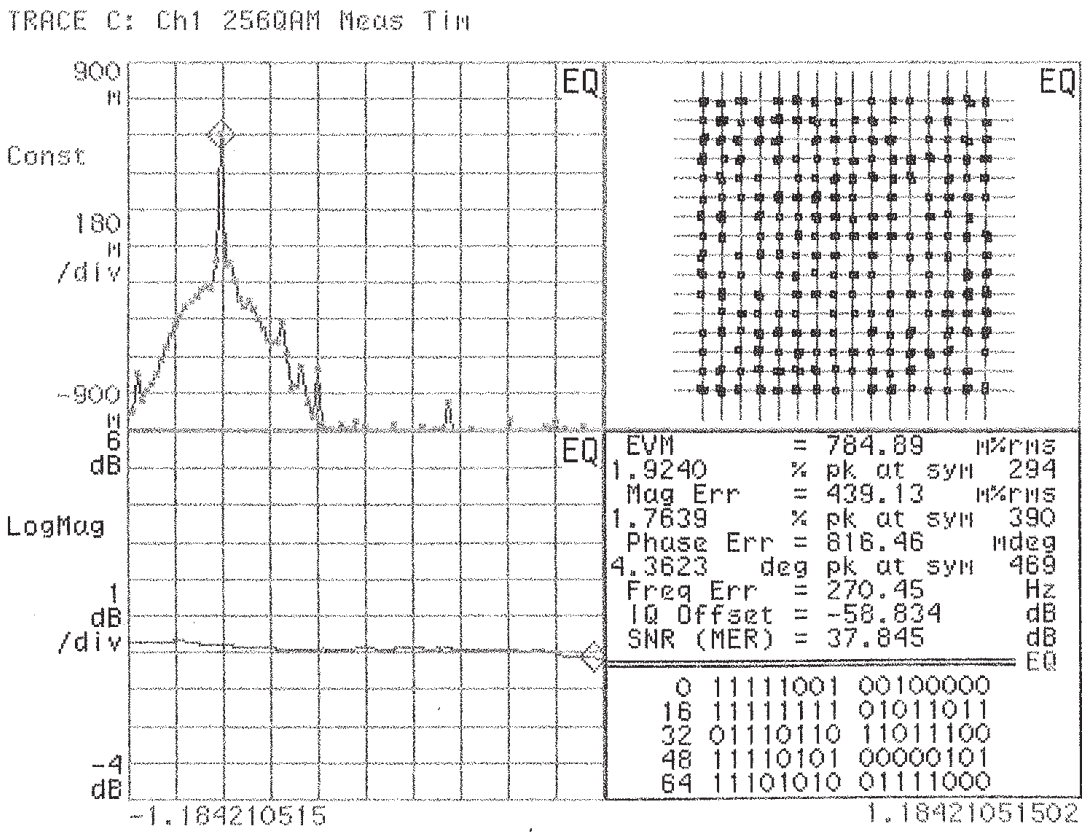


Figure 7.24 Measured MER (37.845 dB) for 256-QAM equalized constellation (99 taps) using Agilent 89441A instrument with a result length = 512 symbols.

small effect on the MER. If the change is fast compared to 10-kHz, the change during the sample time will be significant. A new set of parameters is calculated for each set of samples so the "tracking bandwidth" is in effect determined by the time duration of the result length. When set up to receive ITU-T J.83B type M-ary QAM signals, the Agilent 89441A instrument appears to behave as a well-damped second-order loop with a carrier bandwidth of about 10-kHz. Below 10-kHz, the phase perturbations are reduced at 12-dB per octave. It seems to track these parameters but with loops that are narrower than typically would be used in a QAM receiver. Thus, the Agilent instrument displays the degradations that would affect a real QAM receiver.

Figure 7.24 shows an example of a four-window display of a 256-QAM signal demodulated by the Agilent 89441A. A 256-QAM constellation with the measured EVM and MER parameters is shown in the top and bottom right side window of Figure 7.24. Notice that some of the 256-QAM constellation points are missing from the data sample due to the limited data sample size (N = 512). The impulse response and its Fourier transform are also shown in the top and bottom left side of Figure 7.24. The Agilent 89441A receiver contains an adaptive FIR filter, where the number of symbol-space taps ranges from 3 to 99 (odd values). The adaptation process minimizes the EVM and therefore maximizes the MER. Consequently, the equalized MER will be larger than the unequalized MER. Thus, it is recommended to specify the performance of a QAM transmitter with and without the adaptive equalizer using the Agilent 89441A instrument. The number of equalizer taps that are used in the Agilent 89441A can be determined according to the following equation [41]:

$$Taps = \left[(L-1)\cdot(points/symbols)\right]+1 \tag{7.33}$$

where L is the FFE filter length. For a symbol-spaced equalizer, one point per symbol can be used. The main tap of the FFE filter is located at $(L-1)/2$ up to a setting of 31-taps, and at the 15th tap up to 75 taps. From 76 to 99 taps, the main tap is located at $L/5$, as shown in the Figure 7.24 example. For longer FIR filters, the center tap is selected closer to the beginning of the filter in order to accommodate multipath measurements.

In order to measure the MER and the EVM, the following parameters have to be set on the Agilent 89441A instrument:

- Demodulation format– the QAM mode
  - Digital demodulation (QPSK–16-QAM)
  - Video demodulation (64-QAM–256-QAM)
- Nominal symbol rate
- Measurement filter – Root raised cosine filter[1]

[1] The combination of a root-raised cosine filter in the Agilent 89441A with a root-raised cosine in the CM transmitter yields in an overall raised cosine response that matches the reference filter.

- Reference filter – Raised Cosine
- Roll-off factor – the α parameter
- Enable the adaptive equalizer and setup its length (number of symbols)
- QAM channel frequency and channel bandwidth
- Select data result length (N) – should be much larger than the QAM constellation size
- Set to continuous sweep mode

The MER of the tested QAM transmitter (MER_T) can be estimated using the following relation:

$$10^{-MER_T/10} = 10^{-MER_M/10} - 10^{-MER_I/10} \tag{7.34}$$

where MER_M and MER_I are the measured MER of the QAM transmitter and of the Agilent 89441A instrument, respectively. For example, the measured 256-QAM MER in Figure 7.24 is 37.845-dB, while the calibrated instrument MER is 42-dB. Thus, the corrected 256-QAM MER is 39.95-dB. Once the MER or the EVM parameters have been measured for a given QAM transmitter, they can be used in a similar way to estimate the MER or EVM of an unknown QAM receiver.

7.12 BER of M-ary QAM Signals in AWGN Channel

It can be shown that rectangular M-ary QAM constellations in which $M = 2^k$ for an even k are equivalent to two-phase amplitude modulation (PAM) constellations, each having $L = \sqrt{M} = 2^{k/2}$ constellation points on each of the QAM carriers [35]. Thus, the probability of error for M-ary QAM signals in AWGN channel is easily determined from the probability of error for PAM signals. Recalling that L-ary PAM signals are represented geometrically by one-dimensional constellation points located at ±d, ±3d,..., ±(L-1)d, where the Euclidean distance between adjacent points is 2d. The average symbol energy of the L-ary PAM constellation is given by

$$E_s = \left[\frac{L^2 - 1}{3}\right] \cdot d^2 \tag{7.35}$$

Let us assume an AWGN channel with zero mean and variance $\sigma^2_n = N_0/2$, where N_0 is the noise spectral density and all the PAM amplitude levels are equally likely. The probability of error for the L-ary PAM is the probability that the noise magnitude exceeds half the dis-

tance between adjacent levels (d). The exception is for the two outer levels ± $(L-1)\cdot d$, where an error can occur only in one direction. Thus, it can be shown that P_L is given by

$$P_L = 2\left[1-\frac{1}{L}\right]Q\left[\sqrt{\frac{6E_s}{(L^2-1)N_0}}\right] \tag{7.36}$$

where Q(∘) is defined as

$$Q(x) = \frac{1}{\sqrt{2\pi}}\int_x^{\infty} e^{-u^2/2}du = \frac{1}{2}erfc\left(\frac{x}{\sqrt{2}}\right), \tag{7.37}$$

where erfc(x) is the well-known complementary error function. Recalling that the relationship between the energy per symbol to the energy per bit is $E_s = E_b\cdot\log_2(L)$, the uncoded BER for L-ary PAM signals assuming Gray coding is given by

$$P_b^{PAM} = \frac{2}{\log_2 L}\left[1-L^{-1}\right]\cdot Q\left[\sqrt{\frac{6(\log_2 L)E_s}{(L^2-1)N_0}}\right] \tag{7.38}$$

Following Proakis's approach, the probability of error for the M-ary QAM signal can be determined from the probability of error for the PAM signals, since one can demodulate the PAM signals on each of the quadrature components of the receiver. Thus, the probability for a correct decision for an M-ary QAM constellation is given by

$$P_c = \left[1-P_{\sqrt{M}}\right]^2 \tag{7.39}$$

where $P_{\sqrt{M}}$ is the probability of error of √M-ary PAM constellations with 50% of the average power in each of the QAM carriers. Thus, the probability of symbol error for the M-ary QAM constellation is given by

$$P_{QAM} = 1-\left[1-P_{\sqrt{M}}\right]^2 = 2P_{\sqrt{M}} - P_{\sqrt{M}}^2 \tag{7.40}$$

where $P_{\sqrt{M}}$, has been adjusted for M-ary QAM, and is given by

$$P_{\sqrt{M}} = 2\left[1-M^{-1/2}\right]\cdot Q\left[\sqrt{\frac{3E_s}{(M-1)N_0}}\right] \tag{7.41}$$

If $P_{\sqrt{M}} \ll 1$, then Equation (7.40) can be approximated by

$$P_{QAM} \approx 2P_{\sqrt{M}} = 4\left[1 - M^{-1/2}\right] \cdot Q\left[\sqrt{\frac{3E_s}{(M-1)N_0}}\right] \tag{7.42}$$

Assuming Gray coding, the uncoded M-ary QAM BER for rectangular constellations is given by

$$P_b^{QAM} = \frac{4}{\log_2 M}\left[1 - M^{-1/2}\right] \cdot Q\left[\sqrt{\frac{6(\log_2 \sqrt{M})E_s}{(M-1)N_0}}\right] \tag{7.43}$$

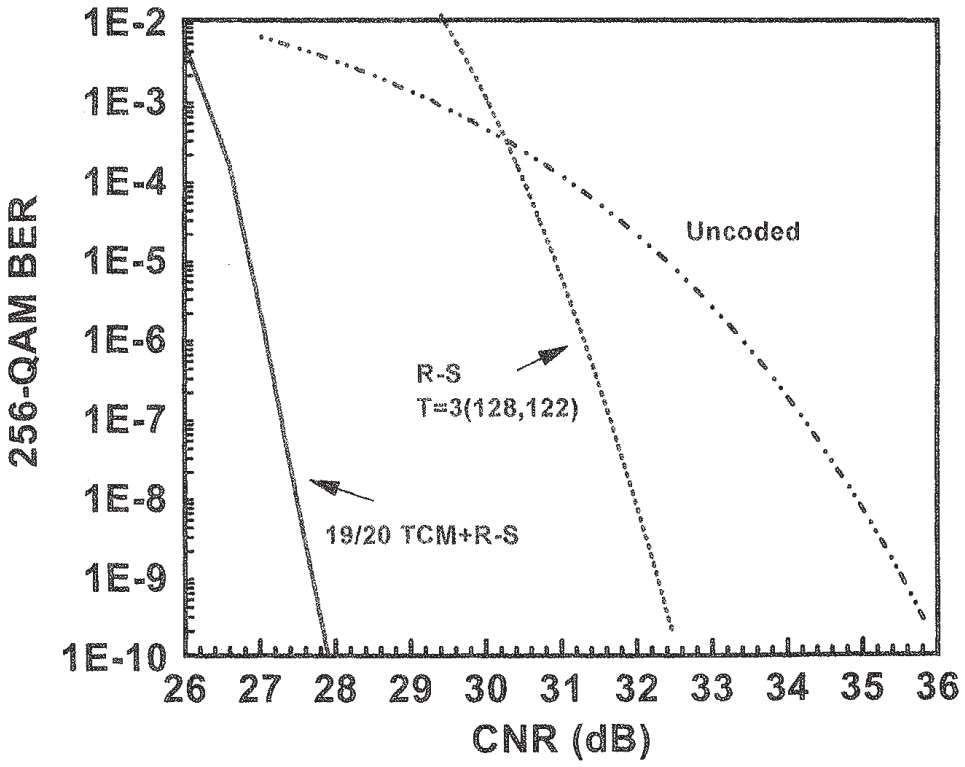


Figure 7.25 Theoretical 256-QAM uncoded, R-S T=3 (128,122) coded, and 19/20 TCM+R-S coded BER versus the CNR (in dB) for AWGN channel.

To calculate the coded R-S 64-QAM or 256-QAM BER, substitute Equation (7.43) into Equation (7.1) for the R-S symbol error rate. Figure 7.25 shows, for example, the theoretical 256-QAM uncoded, R-S T = 3 (128,122) coded, and 19/20 TCM and R-S T = 3 (128,122) coded BER versus the CNR, assuming the presence of only AWGN. It was assumed in Figure 7.25 that the channel bandwidth is equal to the symbol rate bandwidth, which means that the CNR is equivalent to E_s/N_0. Notice that the concatenated R-S T = 3 (128,122) with 19/20 rate TCM reduces the required CNR by more than 7-dB at BER of 10^{-9}.

The transmission parameters for 64-QAM and 256-QAM modulation formats, which are based on DOCSIS 1.1 protocol [1] and ITU-T J.83B standard [42], are summarized in Table 7.3. Notice the particular values that are used for the downstream symbol rate for both 64-QAM and 256-QAM. In order to understand where these values came from, one needs to understand some historical background. Many cable TV headends receive their analog and digital video feed from various satellite transponders, which are operating at QPSK modulation with an information rate of 26.97035 Mb/s (See Appendix C). Thus, to convert the incoming multiplexed video stream into 64-QAM, one needs to match the channel information rate. Thus, the symbol rate for 64-QAM signals can be calculated as follows:

$$\left[26.97035Mb/s\cdot\left(\frac{128}{122}\right)\cdot\left(\frac{15}{14}\right)\cdot\left(\frac{53{,}802}{53{,}760}\right)\right]/6 = 5.056941 - Mbaud \tag{7.44}$$

where we have taken into account the FEC overhead as well as the MPEG sync bytes. For a 256-QAM modulation, there are no satellite transponders that are transmitting at an information rate of 38.8107 Mb/s. However, the Grand Alliance, which initially developed the standard for digital HDTV, has selected its information rate such two HDTV channels can fit exactly into a single 256-QAM channel. Thus, the symbol rate for 256-QAM modulation format can be calculated as follows:

$$\left[38.8107Mb/s\cdot\left(\frac{128}{122}\right)\cdot\left(\frac{20}{19}\right)\cdot\left(\frac{78{,}888}{78{,}848}\right)\right]/8 = 5.360537 - Mbaud \tag{7.45}$$

In comparison, Table 7.4 shows the corresponding ITU-T J.83 Annex A standard for 64-QAM and 256-QAM modulation formats. This standard has been developed for 8-MHz channel bandwidth, which is mostly used in European countries. Notice that the FEC coding approach in this standard has been to use R-S block code with a larger T = 8 rather than use R-S code with a shorter T concatenated with TCM. The advantage of the concatenated code in Annex B is the addition of about 2-dB coding gain at BER = $1\cdot10^{-9}$ compared with

Table 7.3 Downstream cable TV transmission parameters for 64-QAM and 256-QAM modulation formats based on ITU-T J.83 Annex B standard [41].

PARAMETER	256-QAM	64-QAM
Channel bandwidth	6-MHz	6-MHz
Total symbol rate	5.360537 MBaud	5.056941 MBaud
Total channel bit rate	42.884 Mb/s	30.341644 Mb/s
Information rate (includes MPEG sync bytes)	38.8107 Mb/s	26.97035 Mb/s
Bits per symbol	8 bits	6 bits
R-S coding	T = 3 (128,122)	T = 3 (128,122)
TCM coding	19/20 rate	14/15 rate
FEC sync overhead	78,888/78,848 (40-bit sync word)	53,802/53,760 (42-bit sync word)
Interleaver depth	I = 128, J = 1	I = 8,16,32,64,128 J = 16,8,4,2,1
Roll-off factor	$\alpha = 0.12$	$\alpha = 0.18$
IF center frequency	44 or 43.75 MHz	44 or 43.75 MHz
Theoretical CNR (only AWGN at coded BER = $1 \cdot 10^{-9}$)	27.9-dB	21.8-dB

Table 7.4 Downstream 64/256-QAM transmission parameters based on ITU-T J.83 Annex A standard [41].

PARAMETER	256-QAM	64-QAM
Channel bandwidth	8-MHz	8-MHz
Total symbol rate	6.952 MBaud	6.952 MBaud
Total channel bit rate	55.616 Mb/s	41.712 Mb/s
Information rate (includes MPEG sync bytes)	50.981 Mb/s	38.236 Mb/s
Bits per symbol	8 bits	6 bits
R-S coding	T = 8 (204,188)	T=8 (204,188)
FEC sync overhead	188/187	188/187
Interleaver depth	I = 204, J = 1	I = 12, J = 17
Roll-off factor	$\alpha = 0.15$	$\alpha = 0.15$
IF center frequency	36.125 MHz	36.125 MHz
Theoretical CNR (only AWGN at coded BER = $1 \cdot 10^{-9}$)	29.9-dB	23.8-dB

Annex A for a Gaussian channel. The drawback is the more complex receiver design, and the need for a deeper convolutional interleaver in the presence of burst and impulse noise.

References

1. CableLabs *Data-Over-Cable Service Interface Specifications (DOCSIS)*, Radio Frequency Interface Specifications SP-RFIv1.10I-990311 (1999). See also http://www.cablemodem.com.
2. Digital Audio-Visual Council (DAVIC) 1.2 Specification Part 8, Lower Layer Protocols and Physical Interfaces, Revision 4.2 (1997).
3. IEEE 802.14a High-Capacity Physical Layer Specification, IEEE 802.14a Hi-Phy Task Group, Draft 1 (1999).
4. DVS-031, *Digital Video Transmission Standard for Cable Television*, Society for Cable Telecommunication Engineers (1998).
5. S. Lin and D. J. Catello, *Error-Correction Coding for Digital Communications*, Prentice Hall, Englewood Cliffs, New Jersey (1983).
6. J. L. Ramsey, "Realization of Optimum Interleavers," *IEEE Transactions on Information Theory* **IT16**, 338-345 (1970).
7. G. D. Forney, "Burst-Correcting Codes for the Classic Bursty Channel," *IEEE Transactions on Communication Technology* **COM19**, 772–781 (1971).
8. G. Ungerboeck, "Trellis-Coded Modulation with Redundant Signal Sets, Part I; Introduction," *IEEE Communication Magazine* **25**, 5–11 (1987).
9. G. Ungerboeck, "Trellis-Coded Modulation with Redundant Signal Sets, Part II; State of the art," *IEEE Communication Magazine* **25**, 12–21 (1987).
10. B. Sklar, *Digital Communications*, Prentice Hall, Englewood Cliffs, New Jersey (1988).
11. G. D. Forney, Jr., "The Viterbi Algorithm," *Proceedings of IEEE*, 268–278 (1973).
12. A. J. Viterbi, "Error Bounds for Convolutional Codes and Asymptotically Optimum Decoding Algorithm," *IEEE Transactions on Information Theory*, **IT-13**, 260–269 (1967).
13. L. H. Charles Lee, *Convolutional Coding: Fundamentals and Applications*, Artech House, Boston (1997).
14. H. Nyquist, "Certain Topics of Telegraph Transmission Theory," *Transactions of American Institute of Electrical Engineers* **47**, 617–644 (1928).
15. H. Graham, "Modulator Having Direct Digital Synthesis for Broadband RF Transmission," U.S. Patent Number 5,412,352, May (1995).
16. H. T. Nicholas III, H. Samueli, "A 150-MHz Direct Digital Frequency Synthesizer in 1.25-μm CMOS with –90-dBc Spurious Performance," *IEEE Journal of Solid State Circuits*, **26**, 1959-1969 (1991).

17. B. Daneshrad and H. Samueli, "A Carrier and Timing Recovery Technique for QAM Transmission on Digital Subscriber Loops," *Technical Digest of International Conference on Communications*, Geneva, Switzerland, 1804–1808 (1993).
18. M. Kolber, "DSP for Analog Engineers," *General Instrument Journal*, 29–37 (1999).
19. H. Samueli and C. P. Reames "System for, and Method of, Processing Quadrature Amplitude Modulated Signals," U.S. Patent Number 5,754,591, May (1998).
20. B. C. Wong and H. Samueli, "A 200 MHz All-Digital QAM Modulator and Demodulator in 1.2-μm CMOS for Digital Radio Applications," *IEEE Journal of Solid State Circuits* **26**, 1970–1979 (1991).
21. R. W. Lucky, "Automatic Equalization for Digital Communications," *Bell System Technical Journal* **44**, 547–588 (1965).
22. R. W. Lucky and H. R. Rudin, "An Automatic Equalizer for General Purpose Communication Channels," *Bell System Technical Journal* **46**, 2179 (1967).
23. R. W. Lucky, J. Salz, and E. J. Weldon Jr., *Principles of Data Communication*, McGraw-Hill, New York (1968).
24. E. A. Lee and D. G. Messerschmitt, *Digital Communication*, 2nd Ed., Kluwer Academic Publishers (1996).
25. B. Widrow, J. M. McCool, M. G. Larimore, and C. R. Johnson Jr., "Stationary and Non-stationary Learning Characteristics of the LMS Adaptive Filter," *Proceedings of the IEEE* **64**, 1151–1162 (1976).
26. S. Haykin, "Adaptive Filter Theory," Prentice Hall, Second Edition (1991).
27. S. U. H. Qureshi, "Adaptive Equalization," *Proceedings of the IEEE* **73**, 1349–1387 (1985).
28. D. D. Falconer and L. Ljung, "Application of Fast Kalman Estimation to Adaptive Equalization," *IEEE Transactions on Communications*, **COM-26**, 1439–1446 (1978).
29. Y. Sato, "A Method of Self-Recovering Equalization for Multilevel Amplitude Modulation," *IEEE Transactions on Communications*, **COM-23**, 679–682 (1975).
30. D. N. Godard, "Self-Recovering Equalization and Carrier Tracking in Two-Dimensional Data Communication Systems," *IEEE Transactions on Communications* **COM-28**, 1867–1875 (1980).
31. D. Hatzinakos and C. L. Nikias, "Blind Equalization Using a Tricepstrum-Based Algorithm," *IEEE Transactions on Communications*, **COM-39**, 669–682 (1991).
32. L. Tong, G. Xu, and T. Kailath, "Blind Identification and Equalization Based on Second-Order Statistics," *IEEE Transactions on Information Theory*, **IT-40**, 340–349 (1994).
33. J. A. C. Bingham, *The Theory and Practice of Modem Design*, J. Wiley & Sons, New York (1988).
34. A. J. Rustako, L. J. Greenstein, R. S. Roman, and A. A. M. Saleh, "Using Times-Four Carrier Recovery in M-QAM Digital Radio Receivers," *IEEE Journal of Selected Areas on Communications*, **SAC-5**, 524–533 (1987).

35. J. G. Proakis, *Digital Communications*, 3rd Ed., McGraw-Hill, New York (1995).
36. J. G. Proakis, P. R. Drouilhet Jr., and R. Price, "Performance of Coherent Detection Systems Using Decision-Directed Channel Measurement," *IEEE Transactions on Communication Systems*, **CS-12**, 54–63 (1964).
37. I. Horikawa, T. Murase, and Y. Saito, "Design and Performance of 200 Mbits/s 16-QAM Digital Radio System," *IEEE Transactions on Communications*, **COM-27**, 1953–1958 (1979).
38. K. H. Mueller and M. Muller, "Timing Recovery in Digital Synchronous Data Receivers," *IEEE Transactions on Communications*, **COM-24**, 516–531 (1976).
39. B. Daneshrad, and H. Samueli, "A Carrier and Timing Recovery Technique for QAM Transmission on Digital Subscriber Loops," Technical Digest of *IEEE International Conference on Communications*, 1804–1808 (1993).
40. W. Webb and L. Hanzo, *Modern Quadrature Amplitude Modulation: Principles and Applications for Fixed and Wireless Communications*, IEEE Press, New York (1995).
41. HP 89440/AGILENT 89441A Operator's Guide, Hewlett-Packard Co. (1995).
42. Telecommunication Standardization Sector of International Telecommunication Union (ITU-T) Recommendation J.83: Digital Multi-Programme Systems for Television, Sound and Data Services for Cable Distribution (4/97).

CHAPTER 8

SUBSCRIBER HOME TERMINALS

In this chapter we shall discuss the architecture and performance of the most important subscriber home terminals that are currently employed in HFC networks, namely, digital set-top boxes (STBs) and cable modems (CMs). Chapter 8 will start with a brief overview of the basic building blocks of a digital STB with a detailed discussion on each of the building blocks in the following sections. In Section 8.2 the operating principles of the RF cable TV tuner are reviewed, while in Section 8.3 the operation and coding scheme of the out-of-band (OOB) receiver are reviewed. Section 8.4 will discuss the building blocks and operation of the upstream QAM transmitter based on what was learned in Chapter 7 on RF QAM modems. After the QAM signal has been demodulated, the demultiplexing and decoding of the MPEG video and audio streams are discussed in Section 8.5. One of the key building blocks of the digital STB is the conditional access and control block, which is discussed in Section 8.6. Another important STB building block is the processing and display of video images and graphics content on the TV screen to enable the viewing of the different STB applications, which is reviewed in Section 8.7. The requirements of the STB hardware resources such as its central processing unit (CPU) and memory are reviewed in Section 8.8. Section 8.9 will introduce the architecture of an advanced digital STB platform with a built-in DOCSIS CM. The last section will review the different transmission impairments of 64/256-QAM signals over HFC networks such as phase noise, multipath echoes, burst noise, and AM hum modulation. Understanding these impairments enables one to develop a link budget for the digital STB operating in a cable TV network.

8.1 Digital Set-Top Box Building Blocks

As was discussed in Chapter 1, the interactive digital STB acts as a broadband gateway to the home to enable the delivery of existing analog cable TV channels, MPEG-2 compressed audio and video channels using different TV-based interactive applications, and Internet-based applications [1–3]. (See Chapter 12.) Figure 8.1 shows a simplified block diagram of an interactive digital STB for use in HFC networks [4], which consists of four main sections. The RF front-end of the digital STB consists of an A/B switch, diplex filter, RF cable TV tuner, and an OOB tuner. The A/B switch is designed to switch between two possible input ports to the STB. The diplex filter, as we learned in Section 2.4.2, provides the necessary isolation, which is typically better than 65-dB, between the downstream and the upstream

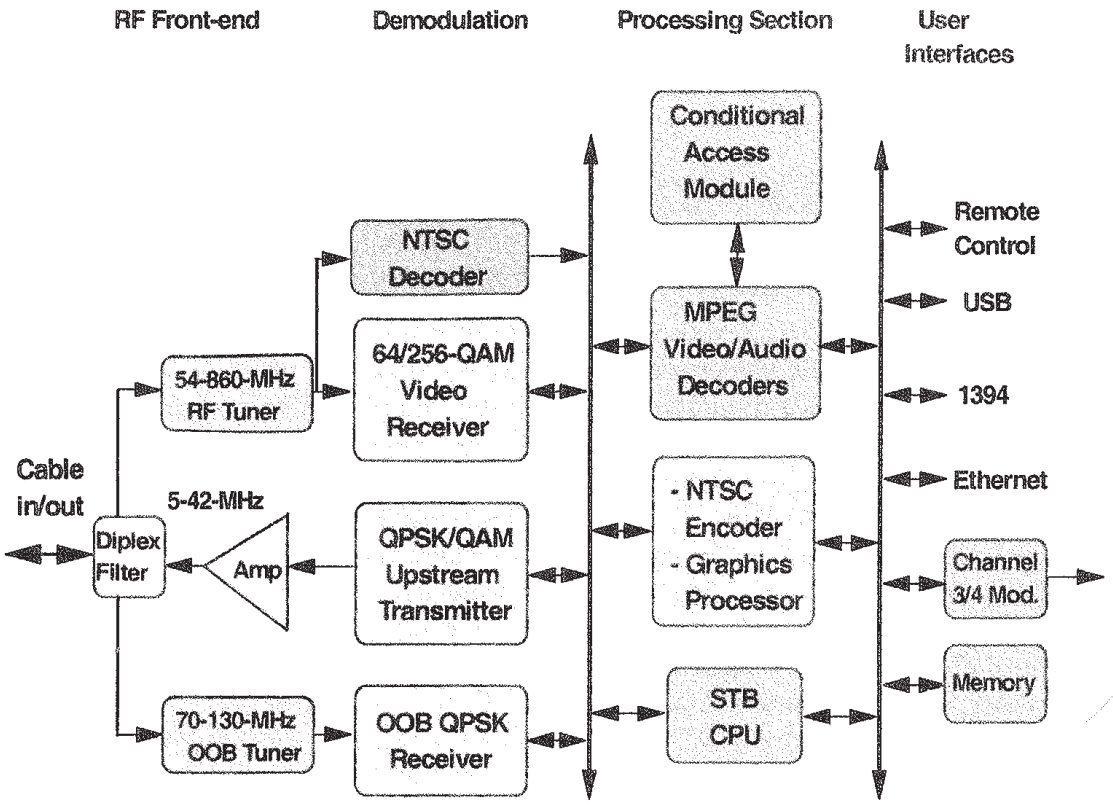


Figure 8.1 Simplified block diagram of an interactive digital set-top box. After Ref. [3] (© 1999 IEEE).

portions of the cable TV RF spectrum. The downstream cable TV tuner is discussed in Sections 8.2 and 8.3. The second section of the digital STB consists of a 64/256-QAM receiver based on the ITU–T J.83 Annex A/B standard, an OOB QPSK receiver, an upstream QPSK/QAM RF transmitter, and an NTSC decoder. The central section of the digital STB has a variety of processing capabilities, depending on the type of multimedia information. It consists of a conditional access module or a security processor, an MPEG transport stream demultiplexer and decoder, an NTSC encoder, a graphics processor, a high-performance CPU, and different types of memory modules such as flash, read-only memory (ROM), and synchronous-dynamic-random-access memory (SDRAM). The back section of the digital STB platform provides different types of output interfaces for the multimedia information including an RF channel 3 or 4 NTSC modulator, composite video and audio outputs, a universal serial bus (USB), an IEEE 1394 or FireWire [5], a 10-base-T Ethernet, and a telephone modem. The operating principles and performance requirements of each of these building blocks are presented in the following sections. The performance requirements

of most of these building blocks have been addressed by the following two standard organizations:

(A) The digital-video subcommittee (DVS) of the Society of Cable Telecommunication Engineers (SCTE)

(B) CableLabs OpenCable specification, which often refers to some of the DVS documents.

The various relevant documents of both DVS and OpenCable will be referenced throughout this chapter.

8.2 Cable TV RF Tuner

The STB's cable TV RF tuner is designed to downconvert the received RF cable TV channel, which may be either AM-VSB or QAM channel format, to an intermediate frequency (IF). If the downconverted signal is an M-ary QAM signal, then it is sent to the QAM receiver in the STB. If the downconverted signal is an AM-VSB channel, it is demodulated by the NTSC demodulator and then decoded by the NTSC decoder to a baseband video stream. The operating principle of cable TV tuners is based on the superheterodyne detection process, which was invented by E. H. Armstrong during World War I [6]. Cable TV tuners can be divided into two main types, namely, single and dual-conversion tuners. Dual-

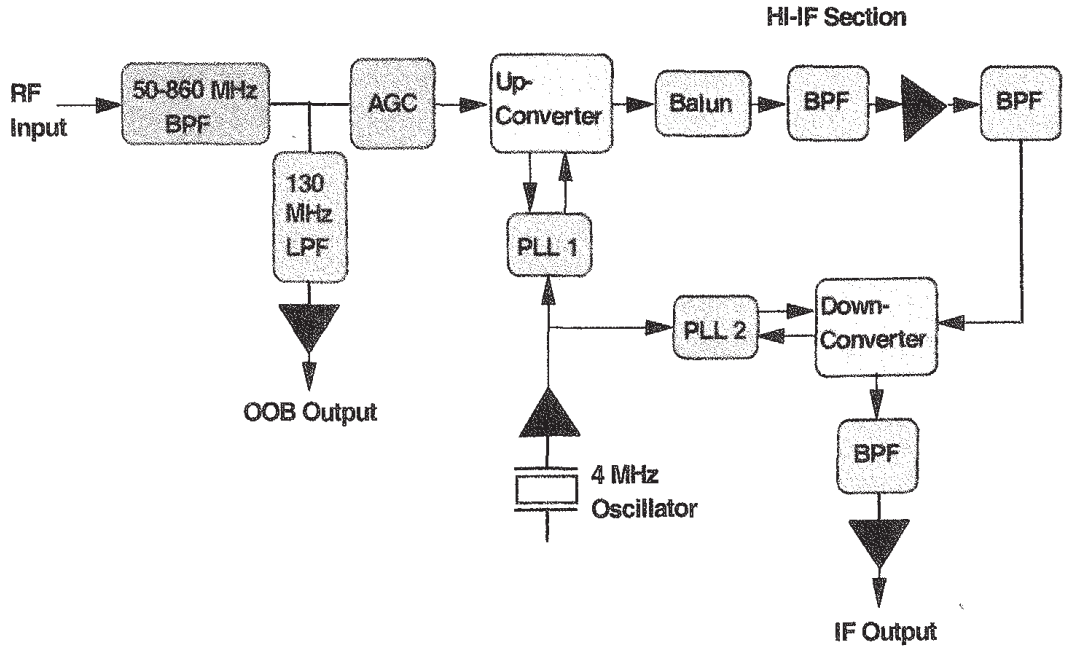


Figure 8.2 Simplified block diagram of a dual-conversion cable TV tuner. After Ref. [7].

conversion tuners, which have two frequency conversion stages between the input and output ports, are typically used in digital STBs in order to achieve the spurious and nonlinear distortion performance necessary for robust operation in an HFC network [7]. Figure 8.2 shows a block diagram of a typical dual-conversion superheterodyne cable TV tuner. The dual-conversion tuner can be divided into three main sections as follows: (A) upconverter section, (B) high-IF section, and (C) downconverter section. In the upconverter section, the input AM-VSB or M-QAM signals from 54-MHz to 860-MHz are first upconverted to a fixed IF, which is the sum of the first synthesized phase-locked loop (PLL) frequency and the tuned channel visual carrier (f_{in}). The first synthesized PLL frequency is obtained by taking the difference between the first local oscillator (LO) frequency (f_{LO}) and the tuned channel visual carrier. The subscriber, using an infrared remote control, selects the tuned channel frequency. The first LO frequency, which is typically between 1.1-GHz and 2-GHz, is selected such that the frequency difference between f_{LO} and the tuned channel visual carrier is above the input signal range. Part of the input RF signal is split before the first upconversion stage in the tuner, then filtered by 130-MHz low-pass filter (LPF), and amplified for the OOB receiver. The operation of the OOB receiver is discussed in the next section. In addition, a DC or low-frequency (< 15-MHz) control signal is used to select the proper port of the A/B switch. Note that the upconverter section essentially determines the noise figure (NF) and distortion performance of the tuner as well as the phase noise degradation of the signal.

Bipolar semiconductor technology was traditionally used for low cost synthesized PLL circuits. However, the wireless industry has generated a large market for very low-power synthesizers using bipolar complementary metal oxide semiconductor (BiCMOS) ICs having power consumption of less than 100-mW. Furthermore, replacing two synthesized PLLs using bipolar ICs with one dual-synthesizer BiCMOS IC lowers the power consumption even further with additional cost benefits.

In the high-IF section of the tuner, a balun transformer is typically used to connect directly between the unbalanced transmission line (coaxial cable) input to the tuner and the balanced load at the tuner output [8]. Using balun transformers eliminates potential problems from unbalanced-to-balanced operation and possible impedance mismatches, which may cause ringing, ghosting, and unwanted radiation. The fixed frequency IF signal is then filtered by a 6-MHz BPF, and amplified before it is downconverted by the second stage to a 44-MHz center frequency.

The traditional narrow-band high-frequency amplifier design uses an air-coil between the supply and the collector, which is often hand inserted in the tuner. New tuner designs use a quarter-wavelength transmission line to eliminate the need for the air-coil. Using both voltage feedback and constant base current-source-emitter resistors helps to achieve a noise figure performance of less than 2.5 dB with a low-cost bipolar transistor [7].

In practice, the high-IF section is typically implemented using ceramic BPFs. The ceramic filters use high dielectric materials to realize their small size with the required frequency response [9]. Although these filters cannot easily achieve the desired image attenuation in a

single device, a pair of ceramic filters with an amplifier in between can achieve the required response. In fact, better than 0.5-dB frequency flatness over a 6-MHz channel bandwidth was achieved in General Instrument's dual-conversion tuner using ceramic filters [7]. Each filter has a typical image rejection of 40 dB, a 1-dB bandwidth of 35-MHz, and an insertion loss of 1.5 dB.

The third section of the tuner downconverts the high frequency IF signal to a fixed 44-MHz frequency. In practice, both the upconverter and downconverter sections of the cable TV tuner are implemented using Gallium-Arsenite (GaAs) integrated circuits, requiring only 5 V [10]. This approach simplifies the cable TV tuner design, improves its reliability, and reduces the cost. Section 8.10.1 discusses the tuner characteristics and performance requirements such as phase noise and noise figure in a digital STB for robust QAM transmission.

8.3 Out-of-Band (OOB) Receiver

An active OOB data channel provides continuous communication from the cable TV headend to the digital STB at the subscriber's home via the cable TV HFC distribution network. The digital STB typically remains powered up even when it is in the "off" state. The OOB channel remains active independent of the tuned TV channel, whether the received channel is analog or digital and whether the digital STB box is turned "on" or "off." Thus, whenever the digital STB is connected to the coaxial cable and AC power, the OOB channel is active for downstream communication.

There are two standards, which are currently being used in STB, for the transmission of the OOB signals. The OOB transmission standards are specified in SCTE DVS-167 [11] and SCTE DVS-178 [12] documents. DVS-167 specifies the following two transmission rates: (I) 1.544-Mb/s for grade A, and (II) 3.088-Mb/s for grade B (optional). The OOB transmission rate according to DVS-178 is 2.048-Mb/s. This information rate is nominally divided into two parts as follows: (1) 1.544-Mb/s is used for the addressable data stream, application program downloads, program guides, and future services not yet conceived, and (2) 0.461-Mb/s is reserved for future applications.

In general, any service directly linked to an individual MPEG service or MPEG transport stream, which is sometimes called transport multiplex, is carried in-band within the specific multiplex. Global applications, those requiring continuous communications, or those services available simultaneously with any of the available television services, are carried in the OOB channel. At the cable TV headend, the desired parts of each input data stream, which originated from various sources, are multiplexed into a 1.544-Mb/s MPEG-2 transport stream for output. Then, null MPEG packets are added to this stream to pad it up to the transmitted stream rate of 2.005-Mb/s. The MPEG transport stream is then QPSK modulated, error encoded, and upconverted to an RF frequency in the 70-MHz to 130-MHz band.

Table 8.1 Out-of-band cable TV transmission specifications according SCTE DVS-178 standard.

Parameter Name	Specifications
Transport Protocol:	MPEG-2 transport stream (MPEG-TS) compliant
Modulation:	QPSK, differential coding for 90°-phase invariance
Symbol Rate:	1.024-MBaud
Symbol Size:	2 bits per symbol
Channel Spacing (BW):	1.8-MHz
Transmission Frequency Band:	71 to 129-MHz
Carrier Center Frequency:	75.25[1] MHz ± 0.01%
Data Rate:	2.048-Mb/s ± 0.01%
Forward Error Correction:	96,94 Reed-Solomon block code, T = 1, 8-bit symbols
FEC Framing:	Locked to MPEG-TS, two FEC blocks per MPEG packet
Interleaving:	Convolutional (96,8)
Nominal Information Rate:	2.005-Mb/s (132.8 b/s margin)
Frequency Response:	Raised cosine filter, $\alpha = 0.5$ (receiver only)

As was explained in Section 8.2, the 70–130 MHz frequency band is split at the front end of the RF tuner and directed to the OOB receiver. Earlier practice has assumed one of several default frequencies such as 75.25-MHz or 72.75-MHz, in order to allow the QPSK receiver to downconvert to a secondary IF equal to the symbol rate. The current digital STB practice has an agile OOB receiver that can tune to any RF frequency in the 70- to 130-MHz band. As with the downstream QAM receiver, the received IF is oversampled, typically four times, separated into "I" and "Q" components, and Nyquist filtered to produce a complex baseband data stream. Then, a simple symbol-spaced feedforward and feedback equalizer with typically two to four taps is used to remove the ISI generated by the presence of various impairments such as multipath echoes over the cable TV network. The FEC scheme for the OOB channel, which is similar to downstream QAM channels, is composed of four layers as follows: (A) frame synchronization, (B) de-interleaving, (C) Reed-Solomon (R-S) decoding, and (D) de-randomization. Table 8.1 summarizes the physical attributes of the OOB chan-

[1] Other possible OOB carrier center frequencies are 72.75 MHz and 104.2 MHz.

nel, which is commonly used in the cable TV industry [12]. The OOB FEC scheme according to the DVS-178 standard is described in more detail in the following sections.

8.3.1 OOB Randomizer

The randomization of the MPEG-2 transport stream in the OOB receiver is similar to the randomization done in the QAM receiver. The randomizer circuit performs exclusive-OR operation on the input MPEG transport sequence with the randomizer's pseudorandom number (PN) generator output sequence. The randomization frame consists of two MPEG packets with the randomizer PN generator reset at the start of every second MPEG-TS packet. MPEG-TS sync bytes are inverted on alternate packets to improve receiver synchronization performance. The randomizer is a 13-bit counter implemented as a linear feedback shift register (LFSR) as shown in Figure 8.3. Binary arithmetic and taps are placed at the output of stages 13, 11, 10, and 1. Stages 2 through 9 are loaded with a seed value of "0." The corresponding generating polynomial is defined as

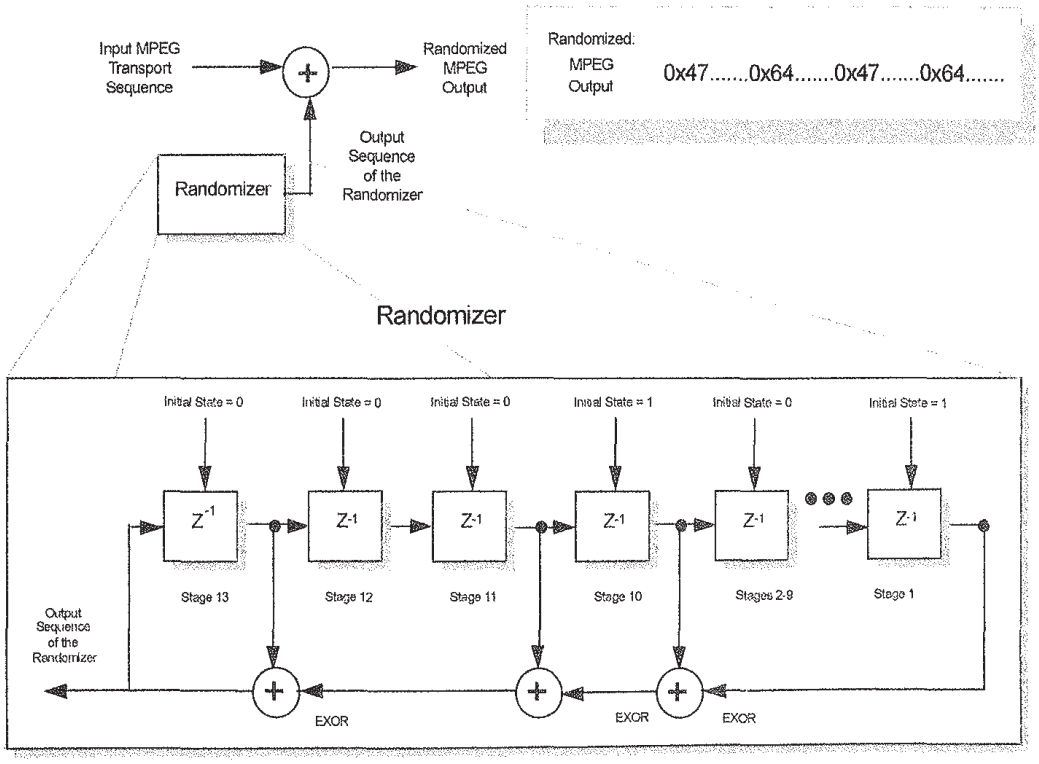


Figure 8.3 Block diagram of OOB randomizer. After Ref. [12].

$$g(X) = X^{13} + X^{11} + X^{10} + X + 1 \tag{8.1}$$

The same circuit is used for de-randomizing the received MPEG-2 transport stream packets. The sync symbol of the first MPEG-TS packet in a frame remains 0x47 after randomization because the first randomizer output byte after reset is "0x00." The second MPEG-2 sync byte is changed by the randomizer but will be returned to the MPEG-TS standard 0x47 by the de-randomizer at the receive site.

8.3.2 OOB Reed-Solomon Coding

The forward error correction (FEC) code in the OOB transmission system is a Reed-Solomon (R-S) block code [13]. No convolutional coding is required for the relatively robust QPSK transmission on cable TV networks. The R-S code is T = 1 (96,94) over GF(256), which is capable of one symbol error correction every R-S block of 96 symbols. The GF(256) is constructed based on the following primitive polynomial over GF(2):

$$p(X) = X^8 + X^4 + X^3 + X^2 + 1 \tag{8.2}$$

and the generating polynomial for the R-S code is defined as

$$g(X) = (X - \alpha)(X - \alpha^2) = X^2 + \alpha^{26}X + \alpha^3 \tag{8.3}$$

where α is a primitive element in GF(256). The OOB FEC frame consists of two R-S blocks with two parity symbols in each R-S block, which equals one MPEG transport packet.

Mapping from FEC frame to MPEG-TS packets is done as follows: the first 94 bytes are unaltered and used directly as received. The next two bytes are the parity bytes obtained from the R-S polynomial calculation. Two blocks of 96 bytes are sent for every 188-byte MPEG packet received. The FEC frame is reset at the start of each MPEG transport stream packet.

8.3.3 OOB Interleaver

Interleaving the coded R-S symbols before transmission and de-interleaving after the reception causes multiple burst errors that occur during transmission to be spread out in time, and thus to be handled by the receiver as if they were random errors. Separating the R-S symbols in time enables the random error-correcting R-S code to be useful in a bursty-noise environment. Using a convolutional interleaver with a depth of I = 8 symbols, the R-S T = 1 (96,94) decoder can correct an error burst of 8 symbols, which corresponds to a burst noise protection of 32 μsec. Interleaving is synchronized to the R-S blocks, and thus to MPEG-2

transport stream packets. MPEG-2 transport stream sync bytes always pass through commutator branch 1 of the interleaver and hence are not delayed through the interleaver.

8.3.4 OOB QPSK Mapping

The OOB modulator uses a differential encoding scheme to resolve the 90° phase ambiguity in the detection of the QPSK signal at the demodulator. The OOB QPSK demodulator should be capable of handling both forms of differential coding as listed in Table 8.2. Also, a means of selecting the appropriate form of decoding for the user's system must be present in the QPSK demodulator.

Table 8.2 Differential Coding Scheme for OOB QPSK Signal.

I Data	Q Data	Default Carrier Phase Changes	Alternate Carrier Phase Changes
0	0	No Change	No Change
0	1	–90° CW	+90° CW
1	0	+90° CW	–90° CW
1	1	180°	180°

8.4 RF QAM Transceiver

The RF QAM transceiver in the digital STB consists of a downstream QAM receiver and an upstream QPSK/QAM burst transmitter. The design and operation of the QAM receiver was already discussed in Chapter 7. The upstream RF transmitter in either the digital STB or CM enable subscribers via the cable TV network to transmit data packets to the CMTS or other burst receivers, which are located at the cable TV headend. The discussion here will focus on the upstream burst transmitter in the STB. RF upstream transmission requirements of CMs will be discussed in Chapter 11 when the physical layer of DOCSIS protocol is explained [14]. Figure 8.4 shows a simplified block diagram of an RF upstream QAM transmitter. For most applications, the data generated at the subscriber's home must be transmitted in short packets. The small asynchronous transfer mode (ATM) protocol cell structure is well suited for this application [15]. The input data packets to be transmitted are first placed in a small burst first-in-first-out (FIFO) buffer (not shown in Figure 8.4) in order to de-couple the input rate from the transmission data rate. In other word, the FIFO buffer allows the data packets to be input while a burst is actively being transmitted. The FEC coding scheme that follows the FIFO buffer consists of a randomization layer and an R-S coding layer, which provide the necessary coding gain for the AWGN channel for combating burst noise (see the discussion in following sections).

Before we discuss the preamble prepend block, let us introduce the burst packet format. For network connectivity reasons, it is convenient to transmit the data packet to the headend using an ATM packet [15]. Table 8.3 shows the upstream packet format according to the SCTE DVS-178 standard [12]. Each ATM packet is concatenated with a 28-bit unique word (UW), a one-byte packet sequence counter, and eight R-S parity bytes. The 28-bit UW, which can be written as (I, Q), is used to identify the start of the data packet for robust sync detection by the return-path receiver. The packet sequence byte consists of a message number (three bits), and a sequence number (five bits). The message number is used to associate upstream cells with a particular protocol data unit (PDU). It is incremented every time the first cell of a new PDU is sent. The sequence number, which has a field length of five bits, is used to identify the order of the cells within a PDU. It starts at zero for each new message number and is used by the headend return-path demodulator to detect missing cells for the RF modem report-backs. The preamble, which is composed of a UW and a packet sequence number, is added to each FEC-encoded ATM packet by the preamble prepend block shown in Figure 8.4. Similar to the downstream QAM receiver, the return-path transmitter also uses differential encoding to enable phase invariant reception at the cable TV headend. Two

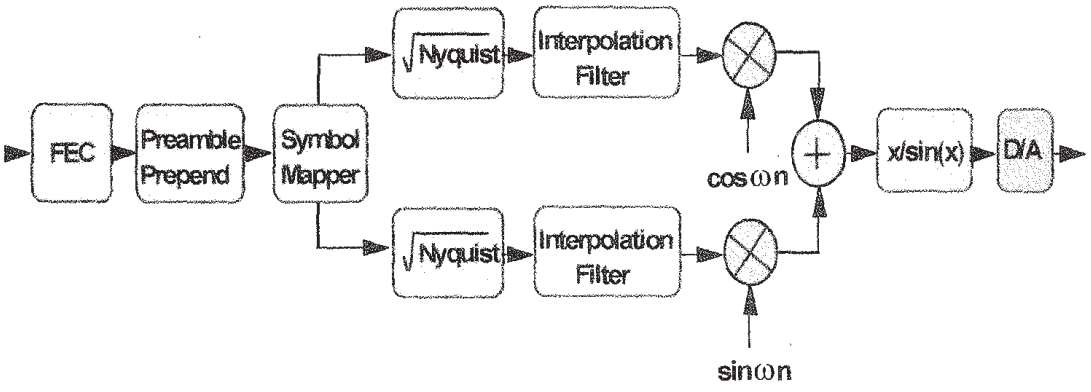


Figure 8.4 Block diagram of an upstream QAM burst transmitter.

Table 8.3 Packet format for an upstream transmitter in a digital set-top box.

Parameter	Specification
Unique Word	28 bits (1100 1100 1100 1100 1100 1100 0000)
Packet Sequence	1 byte
ATM Data	53 bytes
R-S Parity	8 bytes

modes of differential decoding can be defined (see Table 7.5) to accommodate different system local oscillators. The output data from the differential encoder feeds the Nyquist pulse-shaping filters, which are implemented using SRRC filters with a roll-off factor of 25% or 50% ($\alpha = 0.25$ or 0.5). For robust upstream transmission, particularly at high symbol rates (> 1-Mbaud), the amplitude ripple of the filter within the passband as well as the maximum attenuation of the stopband ripple needs to meet particular specifications. For example, the in-band amplitude ripple is specified to be within ± 0.3-dB and stopband attenuation greater than 30-dB according to DOCSIS 1.1 protocol [14]. Interpolation filters are used after the SRRC filters to increase the sampling rate of the baseband signal up to the symbol rate. Then, the output from the interpolation filters is multiplied by the quadrature oscillators using for example DDFS [16]. As was discussed in Section 7.4, an x/sin(x) correction filter is applied to the digitally shaped data burst before it is converted to an analog waveform using for example a 10-bit D/A converter. Table 8.4 summarizes the upstream transmitter specifications according to SCTE DVS-178 and DVS-167 standards. The DVS-178 and DVS-167 specifications represent upstream differentially encoded QPSK transmitters in digital STBs from General Instrument and Scientific Atlanta, respectively. Notice that both

Table 8.4 Upstream RF transmitter parameters for a digital STB.

Parameter Name	DVS-178 Specification	DVS-167 Specification
Modulation Type	Differentially-Encoded QPSK	Differentially-Encoded QPSK
Access Scheme	Polling and ALOHA (programmable)	TDMA
Data Transmission Rate	256 kb/s	256 kb/s (grade A) 1.544 Mb/s (grade B) 3.088 Mb/s (grade C)
Bits per Symbol	2	2
Channel Spacing	192-kHz	200-kHz, 1 MHz, 2-MHz
Transmit Filter Shape	SRRC, $\alpha = 0.5$	SRRC, $\alpha = 0.3$
FEC Code	R-S T = 4 (62,54)	R-S T = 3 (59,53)
RF Output Power Range	+24 dBmV to +60 dBmV	+25 dBmV to +53 dBmV
Spurious Output Level (Idle state)	< –30 dBmV (in-band), <–65 dBmV (out-of-band)	> 30 dB (out-of-band)
Frequency Range	8 to 40-MHz	8 to 26.5 MHz

upstream transmitters according to DVS-167 and DVS-178 do not utilize the full 35-MHz upstream band. The latest advanced digital STB from Motorola/General Instrument, which is called DCT5000+, provides significantly higher upstream symbol rates according to DOCSIS 1.1 [14]. In fact, the DOCSIS 1.1 protocol, which will be discussed in more detail in Chapter 11, specifies upstream symbol rates up to 2.56-Mbaud using 16-QAM format, and an upstream frequency up to 42-MHz.

8.4.1 RF Upstream FEC

A block code FEC is used to allow both correction of some transmission errors and detection of packets that cannot be corrected. For many applications, upstream packets that cannot be corrected can be retransmitted. Block or convolutional interleaving is not appropriate since their function is to spread out error bursts over many FEC blocks. These upstream transmissions often consist of a single FEC block. The upstream FEC in the digital STB transmitter consists of a R-S code and a randomizer, and it is described in the next two subsections. Note that this upstream FEC is different than the upstream FEC for CMs as specified by DOCSIS 1.0/1.1 (see Section 11.3.1).

8.4.1.1. Upstream R-S Coding

The FEC code in the return-path transmission link is a R-S T = 4 (62,54) code over the GF(256) field. Each R-S symbol consists of eight bits. This FEC code is capable of correcting four symbol errors for R-S block of 62 symbols. The following primitive polynomial over GF(256) is used:

$$p(X) = X^8 + X^7 + X^2 + X + 1 \tag{8.4}$$

The generating polynomial for this FEC code is

$$g(X) = (X-\alpha^{120})(X-\alpha^{121})(X-\alpha^{122})(X-\alpha^{123})(X-\alpha^{124})(X-\alpha^{125})(X-\alpha^{126})(X-\alpha^{127}) \tag{8.5}$$

where α is a primitive element in GF (256). The encoding circuit is efficiently implemented via shift registers using arithmetic over GF (256).

8.4.1.2 Upstream Randomizer

At the R-S encoder, each packet is fed through the randomizing circuit to maintain the balance between the ones and zeros within the bit stream. The randomizer circuit uses a pseudorandom number (PN) generator, which employs a 13-bit shift register. Taking the exclusive-OR of the input bit stream with the PN sequence output generates the randomized bit stream. Figure 8.5 shows the upstream randomizer structure using linear shift regis-

ters. Taps are located at the output of stages 1,3,4, and 13 of the shift register. Stages 1 to 5 of the shift register are always initialized to zero for each packet. Stages 6–13 are initialized

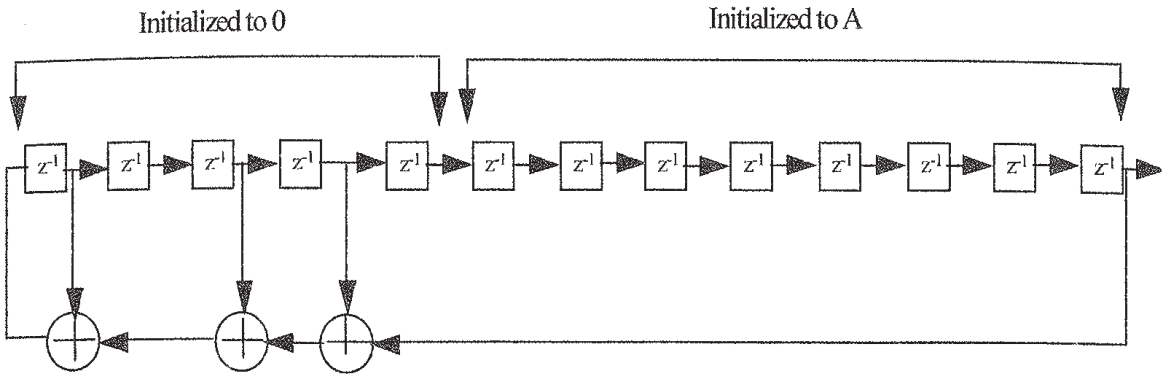


Figure 8.5 Randomizer structure for the upstream transmitter. After Ref. [12].

to a programmable value. The 13-bit default value for this initialization is 0xAA (0 0000 1010 1010), with the most significant bit shifted out first. The corresponding generating polynomial is defined as

$$g(X) = X^{13} + X^4 + X^3 + X + 1 \tag{8.6}$$

8.5 MPEG Video/Audio Demultiplexer and Decoder

The arriving MPEG-TS, which is sometimes called transport multiplex, to the STB consists of many different PESs, representing the different video and audio services. Each packet consists of 184 bytes of payload and 4 bytes of overhead. The transport header consists of a sync byte for packet delineation, a priority bit for congestion control, an ID for packet identification, scrambling control bits, an error indicator, and a continuity counter for packet-loss detection. The task of the MPEG processor is to demultiplex the MPEG-TS to the specific MPEG elementary stream according to the MPEG-2 service map, which identifies the program ID (PID), program type, and all other components that are associated with that service.

Each of the selected MPEG-2 video/audio and AC-3 audio programs is then decoded and processed. The MPEG processor also can utilize the main microprocessor in the STB for other functions such as decoding various MPEG formats. The MPEG-2 demultiplexer and decoder reconstruct the TV frames from the compressed MPEG-2 video, decompressing the "I" frame and using the "P" frame motion vectors to reconstruct the frame. The decoder/

Table 8.5 Baseband video performance parameters of OpenCable STB [2].

CHARACTERISTICS	SPECIFICATION
Video Standard	NTSC composite, EIA-563
Signal Level (composite video)	1.0 volt peak-to-peak, sync tip (–40 IRE) to reference white (100 IRE) ±10%
Long Time Distortion (Bounce)	± 1%, settle in less than 1 second
Field Time Distortion	± 4%
Line Time Distortion	± 2%
Short Time Distortion	± 6% (Rising and/or Falling)
Chrominance-to-Luminance Gain Inequality	≤ ±10 %
Chrominance to Luminance Delay	± 150 ns maximum
Frequency Response for Baseband Video Output	–2 to +2 dB, 0-kHz to 3.7 MHz
Terminal Contribution to Output Frequency Response for RF Output	–1 to +1 dB, 0 kHz to 3.75 MHz
Luminance Non-Linearity	5% p-p max.
Chrominance Nonlinear Phase Distortion	± 5°
Chrominance Nonlinear Gain Distortion	± 2%
Chrominance/Luminance Intermodulation	± 3%
Differential Gain (over 10% to 90% APL range)	10% p-p max. for RF modulated output; 5% p-p max. for baseband video output
Differential Phase (over 10% to 90% APL range)	10° p-p max. for RF modulated output 5° p-p max. for baseband video output
920 kHz Beat	–52 dBc
Video Signal-to-Noise Ratio (over the full input tuning range stated in "signal level" above)	53 dB for RF modulated video with a digital input signal and 48 dB with AM input signal at 0-dBmV. 57 dB for baseband video output with a digital input signal and 49 dB with AM input signal at 0-dBmV

CHARACTERISTICS	SPECIFICATION
Baseband Video Output Impedance	75 ohms ± 10%
Baseband Video Output Return Loss	≥ 16 dB across video bandwidth

decompressor predicts motion of the "B" frames and then reconstructs the "B" frames by applying the difference motion vectors that were developed by the MPEG-2 encoder at the video source. The decoder/decompressor receives 27-Mb/s (or 38-Mb/s for 256-QAM) multiplex by parsing the MPEG-2 transport stream syntax, and performing the video decompression process. It provides the digital video as described in Interface for Digital Component Video Signals in 525-line and 625-line Television Systems, CCIR 656 [17].

The MPEG-TS demultiplexer typically implements 32 PID filters to process transactions, messages, control and access communications, multicast data, video, audio, DOCSIS data, and other data traffic. Data traffic can be delivered to the filters via the OOB receiver or the RF tuner. The PID filters will have the ability to be addressed individually through the network address or be configured as a group address and respond to multicast address messages. The baseband video performance parameters of OpenCable STBs are summarized in Table 8.5.

An important and interesting application is the delivery of a 3D video program from the STB to the TV. The 3D video program can be derived and reconstructed at the STB from a 2D MPEG-2 video program stream enhanced by 3D information, which is carried as associated private data in the MPEG-2 data stream. This 3D service application can be viewed, for example, on a standard NTSC monitor, an HDTV monitor using IR synchronized eyeglasses, or in the future, direct 3D display systems.

8.5.1 VBI Retriever and Decoder

As we learned in Section 2.1.1, closed-caption information is carried on line 21, field 1 and/or field 2, of the vertical blanking interval (VBI) of an analog NTSC signal as mandated by the FCC. Closed captions, which are program-related data as defined in the EIA-608 standard, are given priority over other data, which may be carried on line 21[18]. The closed-caption format as defined in EIA-608 can be extended from lines 10 to 21 to support extended data services. The digital STB has a VBI data retriever to decode data from analog and digital video services. For digital video services, the VBI lines are constructed from the MPEG-2 transport streams using the defined extension to the picture user data syntax as defined in DVS-053 [19]. The STB receives and retrieves multicast IP data packets delivered over the VBI using the North American basic Teletext standard (NABTS) packet protocol, which is defined in EIA-516 [20]. For analog VBI pass-through and digital VBI reconstruction, the STB is reading or reconstructing data (captioning, text, HTML data, etc.) on all available lines (i.e., lines 10 through 20, plus

line 21). In analog pass-through mode, all lines are passed simultaneously. EIA-516 specifies the transmission of 36 bytes NABTS packet (including sync bytes) per NTSC VBI horizontal line. Table 8.6 summarizes the effective VBI data rates for 1 and 11 VBI lines.

Table 8.6 Effective VBI data rates for one and eleven VBI lines.

Characteristic	Specification
Horizontal Scan Line Refresh Rate	1/60th second
Aggregate Bit Rate	36 bytes x 8 bits per byte x 60 lines per second = 17,280 b/s
Maximum Allowable Overhead	39.9 %
Minimum Effective Throughput Required	17,280 b/s x (1–0.399) = 10, 380 b/s per line
Minimum Total Throughput for 11 VBI Lines	10,380 b/s per line x 11 lines = 114.2 kb/s

8.6 Conditional Access and Control

Conditional access or security has a primary importance for existing and new STB applications [1]. There is an increasing need to protect the transmitted information in a multiuser cable TV network from unauthorized use. Stories of unauthorized users or "hackers" breaking into various restricted networks are continuously in the news. Millions of STBs currently operating in the U.S. running multiple applications further exacerbate this problem. To address this problem, a variety of security methods and systems can be implemented, depending on the value of the information that needs to be protected. For example, point-to-point applications over cable TV network such as video-on-demand (VOD) and IP telephony are highly personalized applications with limited resale value in the network. Thus, minimum-security level is typically required for point-to-point applications. In contrast, point-to-multipoint applications, which are sometimes called broadcast applications, such as broadcast sporting events, have a potentially lucrative opportunity due to their high demand. Thus, there is a need to implement a high-level security system in order to make financially impractical the theft of services. Before we can discuss the basic concepts of access control and authorization, let us briefly review the basic digital encryption and decryption methods that are currently used in digital communication systems.

8.6.1 Digital Encryption/Decryption Basics

Digital encryption is the primary method to obscure information under the control of one or more secret keys. Unencrypted information is called *clear* or *plaintext*, while encrypted

information is called *ciphertext* [21, 22]. Block encryption always operates on a given size of block data such as 64, 128, 256, or more bits. Stream encryption, which is used to encrypt/decrypt high-speed and/or high-volume data, operates on the data a single bit at a time, typically through the generation of a keystream.

Let us denote plaintext message as M and a ciphertext message as C. K is called a key if it uniquely determines a one-to-one mapping, which is called the encryption function, from M to C. This definition can be written as

$$C = E_K(M) \tag{8.7}$$

The process of applying the encryption transformation is simply called encryption of message M. The reverse process is called decryption of ciphertext message C to obtain M. The term cryptosystem defines a complete system with encryption-decryption algorithms, and with all possible plaintexts, ciphertexts, and keys. There are two generic types of cryptosystem: symmetric-key (or secret-key), and public-key. In symmetric-key cryptography, the same secret key is used for both encryption and decryption. The most popular symmetric-key cryptosystem, which was developed by IBM in the middle 1970s and has been a federal standard since 1976, is called data encryption standard (DES).

In a public-key cryptosystem, each user has a public key, which becomes public, and a private key, which remains secret. All communication between the sender and the receiver is done using only public keys. Thus, it is no longer necessary to trust the security of the communication system. The transmitted encrypted message can be decrypted only with the secret key, which is known only to the recipient. The most popular public-key cryptosystem is called Rivest-Shamir-Adleman (RSA), which was named after its inventors [23].

The RSA key generation algorithm works as follows: generate two large prime numbers, each roughly the same size, say p and q, and compute their product $n = p \cdot q$ and $\phi = (p-1)(q-1)$. N is called the *modulus*. Choose a number e, $1 < e < \phi$, such that e is relatively prime to ϕ. Find another number d such that $(ed-1)$ is divisible by ϕ. The public key is the pair (n, e), while pair (n, d) is the secret key. The numbers p and q should be destroyed or kept secret. The security of the RSA algorithm is based on the assumption that it is difficult to obtain the private key d from the public key (n, e). To use the RSA public-key encryption, the sender creates a ciphertext C using the relation $C = M^e \bmod(n)$, where the message is M, and the recipient public key is (n, e). To decrypt, the decrypt the message from the sender uses the relation $M = C^d \bmod(n)$. Since only the recipient knows d, only the recipient can decrypt this message. Generally speaking, the larger the RSA modulus, the greater the security, but the longer it takes to decrypt. Thus, the size of the RSA modulus should fit one's security needs. Another valuable use of public-key encryption is called authentication or digital signatures. Using a hash function, the digital signature generates a message authentication code (MAC), which reflects the authenticity of the message. The MAC is encrypted using a secret key. This allows any public user to decrypt the message using a public key and confirm the authenticity of the message by confirming the MAC.

The DES algorithm is a Feistel cipher that operates on a plaintext block size of 64 bits to produce a ciphertext block of the same size [22]. The effective size of the secret key is 56 bits (eight bits can be used as parity bits, producing a 64-bit input key size). Thus, the number of possible keys is simply $256 \cong 7.2 \cdot 10^{16}$. Recently, a DES cracking machine was used to recover a DES key in 56 hours. Thus, with rapidly increasing computation power of modern day desktop PCs, 56-bit keys are becoming vulnerable to exhaustive search and thus may not be secure enough for some applications. To increase the security of the DES algorithm, the plaintext message can be encrypted multiple times, typically by cascading multiple block ciphers or stages, where each stage does not need to have independent keys. For example, triple encryption sometimes called triple DES can be written mathematically as

$$C = E_{K_3}\left\{E_{K_2}\left[E_{K_1}(M)\right]\right\} \tag{8.8}$$

where E_K denotes a block cipher with key K, and K_1, K_2, and K_3 are three secret keys, which may be independent. The case with $K_1 = K_3$ is often called two-key triple encryption.

8.6.2 Access Control Basics

As shown in Figure 8.1, the digital STB has an embedded security system. The task of the security system can be divided into two parts: access control and decryption. The term conditional access refers to providing authorization to subscribers to view only the digital STB services that they paid for. The conditional access system technology of General Instrument is called DigiCipher® II. The conditional access control is specified through the following components:

- The entitlement control message (ECM) defines particular program access requirements, and is primarily managed through a tiering structure with secret key delivery. The encrypted program keys are delivered in the ECM stream. The ECM is typically transmitted in the downstream in-band 64/256-QAM channels.
- The entitlement management message (EMM) defines the access or authorization rights for a given digital STB, which is processed in the security processor. The EMM is typically being transmitted in the OOB channel.

Both ECM and EMM are usually used with the previously discussed encryption methods, namely, either public-key or symmetric-key encryption, to control the distribution of the key used to encrypt the protected information. The access to a given encrypted service can be done in two ways: (A) direct delivery of the service key to decrypt the encrypted service, and (B) tiered structure coupled with encrypted key delivery.

As we discussed before, with millions of subscribers and with many services used by each user, the problem of direct-key delivery becomes very complicated. To achieve a significant

reduction in the number of keys without loss of security, a tiered structure delivery is used. Improved security is achieved by changing the service keys many times per second. Specific bits are designated in the EMM for each service in order for tiered delivery to work. It should be pointed out that the entitlement specification in the EMM is very efficient compared with direct delivery, requiring a change by only one bit per tier.

When the STB is tuned to a particular program, it receives an ECM that is associated with that service and compares the tiers contained in the ECM with those stored in the STB from the previously received EMM. The previously delivered EMM has the list of all the entitlements purchased by or granted to the subscriber as well as a group key. A group key is a limited duration secret key that can be used to decrypt services from a given tier. If the EMM stored in the STB has one or more tier bits that are also in the received ECM, the STB is authorized to use the group key. If the ECM does not contain tier bits that are stored in the STB EMM, then the STB is not authorized and can't use the group key.

8.6.3 Renewable Security

The embedded security system in the digital STB can also be a disadvantage. The 1996 Telecom Act Order 98-116 mandated the availability of digital STB at retail outlets with a renewable and replaceable security system in order to "accelerate private sector deployment of STB." Such a removable security system is called a point-of-deployment (POD) module, and the digital STB is called the host. The advantage of the renewable security system is the availability of digital STB at retail electronic stores, which is portable across many different HFC networks and cable operators. Thus, when moving from one cable system to another, the consumer can replace only the POD module and not its digital STB. Without the POD module, the digital STB can only receive channels in the clear, namely, unencrypted services. The next-generation of digital STBs, which are named OpenCable set-top terminals, are required to be compliant with OpenCable specifications [2, 24-25].

Let us briefly review the system architecture of the OpenCable STB and POD module. Figure 8.6 shows a block diagram of the OpenCable front-end host with the POD module. When the input signal is an MPEG video stream, it is demodulated by the in-band 64/256-QAM receiver, and then fed to the conditional access processor in the POD module. The authorization rights information for the received MPEG stream, namely, the EMM, is demodulated by the OOB demodulator and processed in the POD module. The OOB processing unit in the POD module provides FEC coding for the OOB receiver as well as program-identification (PID) filtering for the selected stream. The host remains tuned to the OOB channel in order to continuously received in-band services. If the subscriber is authorized for the tuned service, then the POD module decrypts the requested MPEG stream, and it is demultiplexed and decoded in the host as shown in Figure 8.6. To protect the transmission of the MPEG stream across the interface between the POD module and the host, OpenCable copy protection (CP) is used [26]. If the requested MPEG stream isn't authorized or the POD module is removed, the output of the QAM receiver is directly routed to the MPEG transport stream demultiplexer. Then, a message may appear on the subscriber's TV moni-

tor, saying that the host is not authorized for the requested service. Nonencrypted digital services are transmitted through the POD module to the MPEG demultiplexer. When the input signal is a clear analog channel, it is routed through the NTSC demodulator and the VBI decoder.

For upstream communications, the data packets are routed through the POD CPU to the OOB processing unit to the upstream burst transmitter as shown in Figure 8.6.

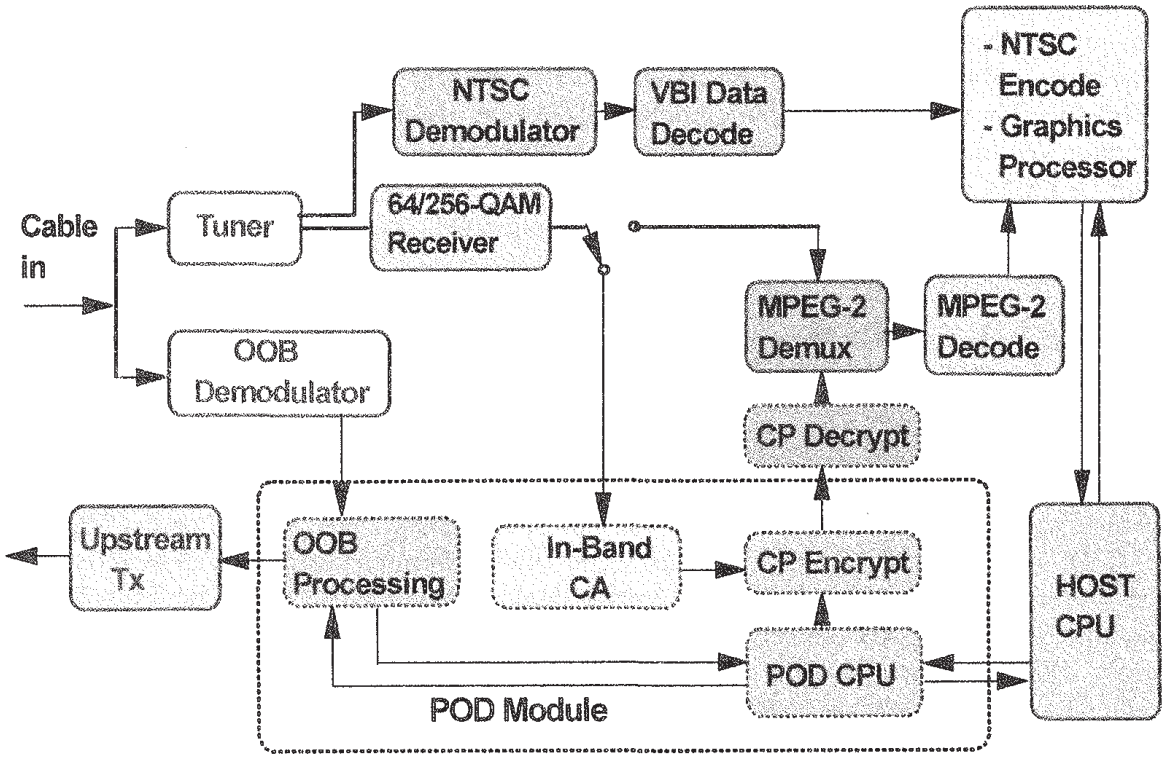


Figure 8.6 Block diagram of OpenCable Host with POD module for bidirectional cable plants. After Ref. [2].

8.7 Graphics Processor

There are various STB applications such as Web browsing and electronic program guide (EPG) that require the display of graphics content and video images on the TV monitor. The graphics processor, which sometimes is integrated in a single IC with the NTSC composite video encoder, is required to provide high-quality anti-aliased text with real-time two-dimensional (2D) and three-dimensional (3D) graphics effects, which can be incorporated

with on-screen video images. Let us first review basic 2D/3D graphics concepts and methods before discussing the on-screen video and 2D/3D graphics rendering requirements in advanced digital STBs.

8.7.1 Basic 3D Graphics Concepts and Techniques

Before discussing the various techniques to map and display 3D graphics objects on a TV monitor, let us first explain the challenges in mapping a high-resolution color-separated graphics display (24-bits) to a 16-bit modulated TV channel. In particular, graphics content is digital with progressive scan format, has no TV synchronization signal, and can exist in various resolutions such as 600 x 400, etc. To properly display the graphics image on the TV monitor, the following functions are required:

- Video color conversion: The first step is to convert the digital red-green-blue (RGB) pixel data to digital video components, namely, *Y*, *U*, and *V*. Then, the color information has to be reduced to 16-bit in a 4:2:2 format.
- Interlacing: The progressive-scan graphics content must be interlaced before it can be displayed on a TV monitor.
- Anti-flicker filter: An artifact associated with the interlacing process is the flickering of the displayed image on the TV monitor. An adaptive 2-tap/3-tap anti-flicker filter can be used with other video enhancements to produce a high-quality display.
- Overscan compensation: Since the display area on a TV monitor is smaller than that on a graphics monitor, a portion of the displayed graphics may not be visible. The process in which the graphics content is contracted to accommodate the TV monitor's visible area is called overscan compensation.
- NTSC encoding: The encoding process consists of converting the flicker-filtered digital graphics data (*YUV*) to an analog composite NTSC waveform using a 9-bit A/D converter.

Let us now discuss the basics for 3D graphics [27]. The recent explosive growth in consumer appetite for 3D games and other virtual-reality applications has required the STB to deliver high-quality 3D texture-mapped images approaching photo-realism. Generally speaking, the implementation of 3D graphics can be divided into three distinct steps. The first step is called the scene manager, which may be integrated with a particular application, and is responsible for providing an internal presentation of the virtual scene to be imaged. The scene description is done using an internal database of virtual objects, what materials objects are made of, and how the scene is lit. The second step is the geometry processing including light modeling, which provides geometrical transformation of 3D objects onto 2D screen coordinates. The third process is called rendering or rasterization, which provides near photo-realistic scenic details to the 3D graphics objects, depending on its texture, light, viewing angle, and background [27]. Since rendering is a very pixel-intensive operation that

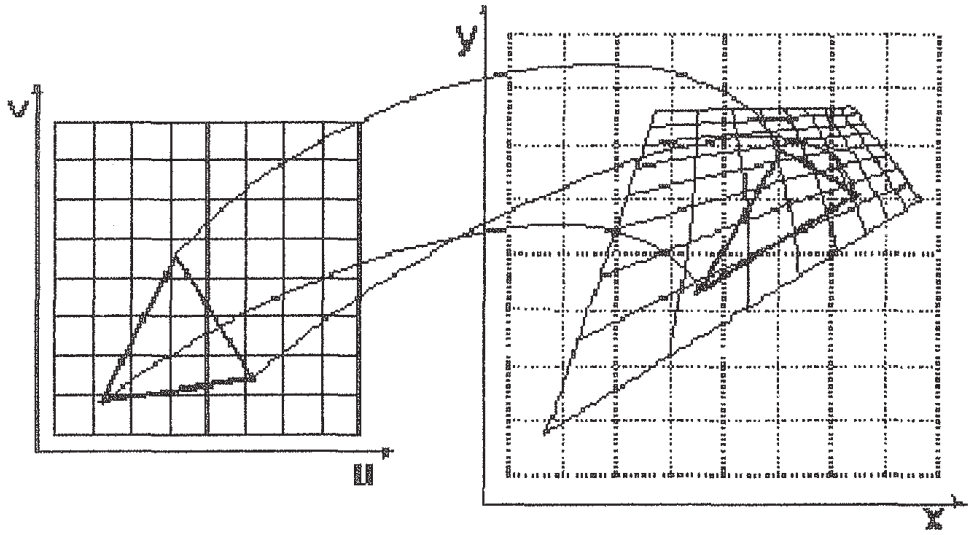


Figure 8.7 Triangle shape mapping from 2D geometry onto a 3D surface.

may be limited by the graphics hardware capabilities, let us briefly review its features. Texture mapping is by far the most important feature of a rendering engine because it provides realistic details to 3D objects without complicating the object's geometry. Without such texturing, mapping of complex 3D objects would be significantly more complicated since it would require the use of thousands of polygons to depict these objects. From a historical perspective, texture mapping has enabled the PC industry to embrace the use of 3D graphics.

Polygon mesh is the most common form to approximately represent a surface of an object. Texture on a polygon is generated by mapping a 2D texture pattern on each pixel of the polygon. Since polygons are rendered in perspective, it is important that texture be mapped in perspective as well. However, when an object is receded into the distance, texture is distorted, requiring texture perspective correction. Texture distortion can be minimized, for example, by reducing the size of the textured object. Perspective correction, which involves computational intensive operations of each pixel of the textured object, is necessary for photo-realistic 3D graphics.

There are several qualitative levels of texture mapping, depending on the complexity of the texture mapping logic. The simplest method is called point sampling, where the nearest texture element is mapped onto the corresponding pixel on the screen. Only one texture element is used for each pixel during the mapping. However, because of storage constraints, texture patterns are stored in a finite resolution, which may appear blocky on the screen from a close viewpoint. Another visual artifact of point-sampled images is that they scintillate or sparkle when the objects move. There are several anti-aliasing filtering techniques that can be applied to reduce this effect. In these techniques, multiple texture elements are filtered to derive a single texture element, which is mapped onto a pixel on the screen,

resulting in a higher-quality image. Filtering really means weighted averaging of adjacent pixels (the more averaging the greater computing cost). For example, in the bilinear filtered texture method, the four nearest texture elements are bilinearly interpolated to determine the final texture element value, which is mapped onto a single pixel on the screen. This method smoothes out the blockiness caused by the point-sampled images, resulting in enhanced image quality. The drawback of this method is that it does not eliminate the "sparkling" artifact created by the point sampling method, thus requiring the use of more advanced texture techniques.

Another type of texture mapping visual artifact is depth aliasing, which occurs when objects that are further from the viewpoint appear smaller on the screen with less detail than closer objects. As the object moves further from the viewpoint, the texture image becomes more compressed when mapped onto a smaller object. To eliminate the depth-aliasing artifact, a *MIP-mapping* technique is used[2]. A MIP-map is a series of prefiltered, prescaled texture patterns. The original texture map is reduced by 1/4 (averaging every four pixels) for the next level of detail (LOD), and stored as the second MIP-map in memory. This MIP-map is further reduced by 1/4 to produce the third MIP-map for LOD. This process is repeated until the texture pattern is reduced to a 1x1 map. Then, the appropriate MIP-map is selected, depending on the distance of the object from the viewpoint. MIP-mapped textures reduce sparkling artifacts and appear to be more 3D realistic. However, the MIP-mapping introduces a visual artifact when the object is moving away or towards the viewer. The object jumps from one LOD to the next one whenever the MIP-map boundary is crossed. This artifact can be corrected using the *trilinear MIP-mapping* technique.

Retrieval of stored texture information in a dedicated graphics memory is one of the main factors that determine the performance of a 3D graphics engine. Typically, the application only stores the required texture for a particular scene in the dedicated graphics memory. Other unused texture information is generally stored in the STB memory such as SDRAM, and it is transferred over to the graphics memory using a dedicated 32-bit or 16-bit wide bus. To increase access to graphics memory, particularly for computationally intensive techniques such as the trilinear MIP-mapping, on-chip cache is used.

One of the important aspects of conveying depth perception to the viewer is the use of hidden surface removal. For example, in a scene where a house is covered by trees, the portion of the covered house has to be removed to convey realistic depth effects. The two common techniques for hidden surface removal are called *polygon sorting* and *Z-buffering* techniques. In the polygon sorting technique, the system CPU sorts the objects, either back-to-front or front-to-back, before being rendered into the frame buffer. The closer object overwrites the distant object if there is overlap between the two. The main drawback of this technique is its suitability for moving objects and accurately rendering objects that are interpenetrated. In the Z-buffering technique, the Z (depth) value of each pixel is stored, and the rendering engine compares its depth value with the previously rendered pixel for the same X-Y location. If the object is closer to the viewer, the graphics processor overwrites the

[2] MIP is derived from the Latin phrase *multum in parvo*, which means many in one.

previously rendered object in the same frame buffer. The advantage of the Z-buffering technique is relieving the CPU from sorting objects for hidden surface removal. In addition, it works well with moving objects, and renders accurately interpenetrating objects. The main drawback is the high system memory requirement. In practice, polygon sorting has been abandoned and Z-buffering is mainly used.

Another artifact, which degrades the quality of a 3D image, is called aliasing. Aliasing along the edges of an object, which results from high contrast between colors of adjacent pixels, causes visual anomalies such as stair stepping, scintillation, and break-up of solid lines to dotted lines. Polygon or edge anti-aliasing techniques remove such artifacts, resulting in enhanced image quality, and add realism to a scene. There are several anti-aliasing techniques that use the average area concept. In the *alpha blending* technique, which is a low-cost implementation of this concept, the percentage of a covered pixel by any polygon along an edge is calculated and used to blend its color with the already rendered pixels. Polygons are rendered from back to front. This technique improves the sharpness of jagged polygon edges and displayed text, is simple to implement, and does not require extra memory. The drawback of this technique is that the background color can bleed through the 3D object in front along the interior edges. Other techniques such as sub-pixel anti-aliasing with Z-buffering produce high quality, accurately rendered 3D objects.

An important feature of rendering objects such as water or glass is transparency or translucency. To create the effect of translucency, a 3D object is assigned an α value (0 to 1) that determines how much can be seen through it to whatever is behind it. A completely opaque object has $\alpha = 0$, while a translucent object has $\alpha = 1$. Translucency can also be used to gradually blend two adjacent LODs of an object, which is called LOD morphing. This feature is particularly useful for rendering moving objects in motion-driven scenes. In order to do alpha blending, the system needs an alpha channel. Each pixel consists of RGB color components, usually 24-bits, and the α component with an additional 8 bits, specifying how the pixel's colors should be merged with another pixel when the two are overlaid, one on top of the other.

Another interesting feature of rendered objects is called fogging. Fogging, which is a form of alpha blending, is used to create atmospheric effects such as low visibility conditions in flight-simulation games. With fog, distant objects can be rendered with fewer details, improving rendering speed. Fog is simulated by attenuating the color of an object with the fog color as a function of distance, where more distant objects appear less visible. Two techniques to implement fogging are called per-vertex (linear) fogging, and per-pixel (nonlinear) fogging. In the per-vertex technique, the fog value at the polygon vertices is interpolated to determine the fog factor at each pixel within the polygon. Realistic fogging is achieved as long as the polygons are small. Unnatural fogging is obtained with large polygons. However, the per-pixel fogging technique works well with large objects since fogging is a nonlinear function of the object's distance from the viewpoint.

8.7.2 On-Screen Video and 2D/3D Graphics Rendering Requirements

In an advanced digital STB, video and graphics rendering are required to be overlaid on TV screen backgrounds, which may consist of real-time video (analog or digital), graphics, or Internet web pages, blended with MPEG-2 decompressed displays, providing full-rate frame grabbing with scaling. The STB is required to render graphics-in-video, video-in-graphics, browser-in-video, video-in-browser, video-in-video, whether such video is still-frame or motion video.

As we learned in the previous section, a high-performance graphics processor, particularly for 3D display applications, requires the use of a low-latency, high-throughput data interface to its main memory. Accelerated graphics port (AGP), which was developed by Intel to be used with PCI bus, can provide real data throughput up to 1Gb/s.

Various applications in the future may require the delivery of 3D video to be displayed on a standard TV or HDTV monitor. One way to accomplish this task is to reconstruct the 3D-video program at the STB from a 2D MPEG-2 video program stream enhanced by 3D information, which is carried as associated private data in the MPEG-2 data stream. The various 3D programs can be viewed on a standard NTSC or HDTV set, using, for example, IR synchronized eyeglasses. It is expected that in the near future direct 3D display monitors will be available without the need for special eyeglasses.

The processing required for this application is described as follows, and is shown in Figure 8.7. The MPEG-2 stream with 3D information encoded in private user data is input to the MPEG-2 decoder, whereby such decoder outputs a 2D RGB image as a texture map to be input to the graphics processor; it is able to extract the private user data for input to the applications processor. The applications processor derives four outputs from the private user data input: (1) raw 3D data; (2) processed 3D data; (3) polygon data for input to the graphics processor; and (4) eyeglass shutter synchronization signals as input to the IR blaster for IR transmission to the IR synchronized eyeglasses. The first two (i.e., raw 3D data and processed 3D data) of these four data signals must be routed onto a 1394 link for use by external 3D receiver/display devices. Video/graphics is rendered in five planes:

- Background texture
- Media plane (MPEG-2 video)
- Graphics plane
- Cursor (minimum 16 x 16)
- Scaleable video-in-graphics plane

It should be pointed out that the display resolution rendering and digitizing modes must match and blend with the different resolutions to support animation; frame capture; transparent, opaque, and translucent partial or full-screen overlays on analog or digital video; per-

pixel alpha blending; high-speed blitting; and display size scaling. Blitting means copying a large array of bits from one part of the STB's memory to another part, particularly when the memory is being used to determine what is shown on a display screen. The graphics processor in the STB should be able to scale graphics images as needed where the graphic images are designed for a different pixel aspect ratio.

The graphics plane can operate in various color modes such as

- 16-color indexed with color look-up table
- 256-color indexed with color look-up table
- 16-bit RGB/YUV (24-bit desired), 32-bit for α-blending
- Programmable graphics plane with respect to spatial size, screen position, and memory map location.

The important features of the video-in-graphics plane include its full scalability to any arbitrary size, and its capturing to memory. These features allow the analog, MPEG, or HD format, decoded digital video service to be scaled and captured to memory for display in a window within the graphics plane. The video-in-graphics plane will have the capability to be placed either above or below the graphics plane.

The alpha blending and chroma key modes for the graphics plane for each color mode can be supported, for example, as follows:

- 16-color indexed look-up table with reserved chroma key index
- 256-color indexed look-up table with reserved chroma key index
- 32,768-color RGB with chroma key bit (5:6:5:1)
- 4,096-color RGB with 4-bit alpha channel (4:4:4:4)
- 16-color indexed look-up table with 8-bit alpha

It should be pointed out that to get true color, one needs to use 24–32 bits per pixel.

The combination of pixel blitter with alpha blending allows one fast scrolling with graphical block moves, where all color modes can be supported with dedicated pixel color and pattern filling. Furthermore, pixel blitting supports nonrectangular shape instantiation[3], including the same alpha blending capabilities defined previously. Text blitter with antialiased font capabilities can be supported, for example, with dedicated text blitting hardware, and provide two-color (one bit per pixel) or four-color (two bits per pixel) font text instantiation.

The STB can also deliver a reconstructed ATV/HDTV signal in its original format with graphic additions, and ATV/HDTV signal with graphics, which has been converted to a NTSC formatted signal. The required hardware and firmware implementation features include:

[3] Instantiation means producing a more defined version of some object by replacing variables with values (or other variables).

- The contents of the color map need to be modifiable under software control.
- The graphics display resolution should be configurable to match the MPEG-2 resolutions supported by the STB.
- The STB should have hardware acceleration for pixel blitter and text blitter transfers.
- Graphics rendering should be blended with the MPEG-2 decompressed display;
- Graphics rendering and display should be double-buffered for smooth animation.

8.8 CPU and Memory

8.8.1 Set-Top Box CPU

As we learned in the previous sections, the digital STB has various processors to perform the various functions such as MPEG-2 video decoding, AC-3 audio decoding, decryption and access control, and graphics. The main CPU in the digital STB, which is separated from the other processors, is responsible for handling the overall management of the STB and the various applications. This includes the real-time operating system (RTOS), application program interfaces (APIs), resident and special applications downloads and execution, arithmetic and logical operations, DSP algorithm acceleration, imaging, and 2D/3D graphics. In order for the main CPU to execute in a timely fashion the numerous instructions it receives from the RTOS and various applications, it must be high-performance with sufficient memory and have appropriate memory bus architecture. Such a CPU is, for example, a 64-bit superscalar million instructions per second (MIPS)-based microprocessor with reduced instruction set computer (RISC) architecture, operating at a clock frequency of 200-MHz or more [28]. Superscalar microprocessor refers to a microprocessor architecture that enables more than one instruction to be executed per clock cycle. The MIPS term refers only to the CPU speed, while real applications are generally limited by other factors, such as input/output (I/O) speed. Nearly all microprocessors, including the Pentium, PowerPC, Alpha, and SPARC microprocessors, are superscalar. Table 8.7 summarizes typical characteristic specifications of the main CPU processing capabilities.

The main CPU, which provides the flexibility to download new functions and applications, also supports a series of system hardware and software interrupts that can be dynamically prioritized, and provides a hardware timing function to supply programmable timing with a 1-ms resolution. Additional CPU features may include 5-volt tolerant I/O, per set instruction and data cache locking, power down wait instruction feature, and DSP multiply-add and three-operand multiply capability. Future advanced digital STB designs are migrating toward higher integration implementations, including more advanced microprocessor(s) utilizing 0.25-μm or smaller CMOS technology, five layer, with supply voltage of 3.3V or less. Furthermore, it is possible that a truly integrated advanced digital STB will be able to integrate the functionality of the various processors with the main CPU on a single chip.

Table 8.7 Processing capabilities for the Set-Top Box CPU microprocessor.

Characteristic	Specification
Instruction Set	MIPS IV instruction set
Address / Data Word Width	32, 64, or 128 bits as required to support features
CPU Clock Frequency	≥ 200 MHz
Superscalar Instruction Issue Rate	Integer + floating point
Integer/Floating Point	2.7/2.5
MIPS	233 minimum
Instruction/Data Cache	16-kB/16-kB
Set Associativity	Two-way
Write Policy	Write-back, write-through
Minimum System Memory Interface Bandwidth	Determined by STB manufacturer for sufficient support and render services
Upper Limit of Memory Frequency	> 87 MHz
Typical Power Consumption at 3.3 V	< 3 watts

8.8.2 Set-Top Box Memory

The digital STB uses four different types of memory modules for various purposes. The four types of memory modules are (A) random access memory (RAM), (B) read only memory (ROM), (C) synchronous dynamic RAM (SDRAM), and (D) flash memory. Let us briefly review the characteristics of each type of memory module. RAM, which is used in many electronic devices, is for temporary storage of data, which can be randomly accessed by the CPU and other processors for various tasks. When the power is disconnected, all data stored in RAM is lost. This is the reason why RAM is called volatile memory. In contrast, ROM is typically used to store specific STB codes (under particular conditions) such as self-diagnostics and navigational instructions.

Another type of volatile memory is SDRAM [29]. The use of SDRAM in digital STBs is designed to partially fulfill the increased demand by the main CPU for higher data rate transfers than conventional DRAM technology can provide. Synchronous DRAM technology combines recent industry advances in fast DRAM architecture with high-speed interface and miniature packaging technologies. The core of SDRAM memory is a standard DRAM with the important addition of synchronous control logic. By synchronizing all address, data, and control signals with a single system clock, SDRAM technology enhances performance, simplifies design, and provides faster data transfer. For example, one 1Mx16 SDRAM can replace four 256Kx16 page-mode DRAMs and provide the 135-200-Mbyte/sec data access

required for MPEG-II television (NTSC and PAL) applications. SDRAM is typically used for graphics rendering and on-screen video and graphics display.

Flash memory modules are reprogrammable modules that retain their content after the power source is removed or disconnected. Thus, flash memory is called nonvolatile memory. Generally speaking, flash memory offers lower cost and higher performance than other competitive memory modules. Flash memory is a solid-state reliable module with no mechanical parts. Flash memory is based on a technology similar to electrically erasable programmable read only memory (EEPROM), but unlike EEPROM, flash is more scalable and cost effective. With production densities of up to 8 MB, flash memory modules are used in applications where moderate amounts of nonvolatile storage are desired such as STBs, PCs, digital cameras, and cellular phones. When the STB first powers up, the firmware typically is loaded from flash to DRAM, and it is executed in DRAM. Slower flash memory access times, compared to processors or other system components, have pushed set-top designers to this boot and download scheme.

Generally speaking, there are two system architectural methods to achieve the required memory bandwidth [30]. In the distributed method, which is also the more conventional one, the required memory module is typically attached to the processor performing a specific function such as 3D graphics. This approach works well if the memory can be easily partitioned and there are no problems with memory granularity. However, the increasing integration of the various functions in the digital STB has motivated the use of the unified memory architecture (UMA) method. In the UMA method, the same block memory can be effectively shared among the various processors. For example, the SDRAM memory is shared among MPEG-2 decompression, on-screen graphics, and other applications. However, the SDRAM memory sharing allocation process can provide priority to the MPEG video/audio decoding when competing against graphics or application uses, since it requires the most continuous use of SDRAM for buffering functions.

The different memory modules are needed in the STB to support the following software and/or firmware activities:

- MPEG-2 decompression
- Resident device drivers, utilities, RTOS kernel
- Graphics
- Resident applications
- Downloaded applications
- CM processing

Table 8.8 shows an example of the different memory module sizes in a digital STB that are needed for the various functions described. The STB design needs to support a hardware memory manager for memory protection of application processes and the operating kernel, and to provide a flat address space for user processes. The STB typically uses a secure, nonvolatile random access FLASH memory for essential information storage such as video channel maps,

authorization tables, and OOB channel assignments. The contents of the Flash memory can be downloadable via the HFC network. A minimum of 4-kB nonvolatile memory is typically reserved for subscriber messaging.

Table 8.8 Different types of memory modules for advanced digital STB.

Characteristic	Specification	Description
RAM	8 MB	CPU, applications
ROM	2 MB	Boot strap and navigational diagnostics
SDRAM	8 MB	Shared with graphics and MPEG-2 decode, and on-screen display
FLASH	8 MB	Code download, booting

8.9 Advanced Set-Top Box with Built-in DOCSIS Cable Modem

The digital STB that we have discussed so far provides basic and interactive TV-based applications. However, it does not allow the subscriber to get a high-speed Internet access through the cable TV network. To get an Internet access, the subscriber needs a CM. An advanced digital STB combines the functionality and features of an interactive digital STB and a CM. Figure 8.8 shows a simplified block diagram of an advanced digital STB with a built-in DOCSIS CM [31]. Note that the advanced STB has three RF tuners as follows: (I) 54–860-MHz RF tuner for NTSC/MPEG video reception, (II) 54–860-MHz RF tuner for simultaneous Internet access through the DOCSIS CM, and (III) 70–130-MHz RF tuner for the OOB channel. The DOCSIS modem is essentially an RF QAM transceiver operating according to DOCSIS 1.0/1.1 protocols [14]. The DOCSIS protocol, which defines both the physical (PHY) layer and the media-access-control (MAC) layer, will be discussed in detail in Chapter 11. Currently, the basic transmission and MPEG video processing with limited graphics capabilities are integrated into a single chip, which is available today using 0.25-μm CMOS technology. With 0.18-μm CMOS technology, most of the building blocks of the advanced digital STB (excluding the analog-front-end and DRAM) shown in Figure 8.8 can be integrated into a single IC. The advanced digital STB represents a key technology platform for the cable TV operators to significantly increase their revenue base over the currently installed digital STBs. Consequently, the digital STB software architecture as well as the various TV-based and Internet-based interactive applications will be addressed in detail in Chapter 12.

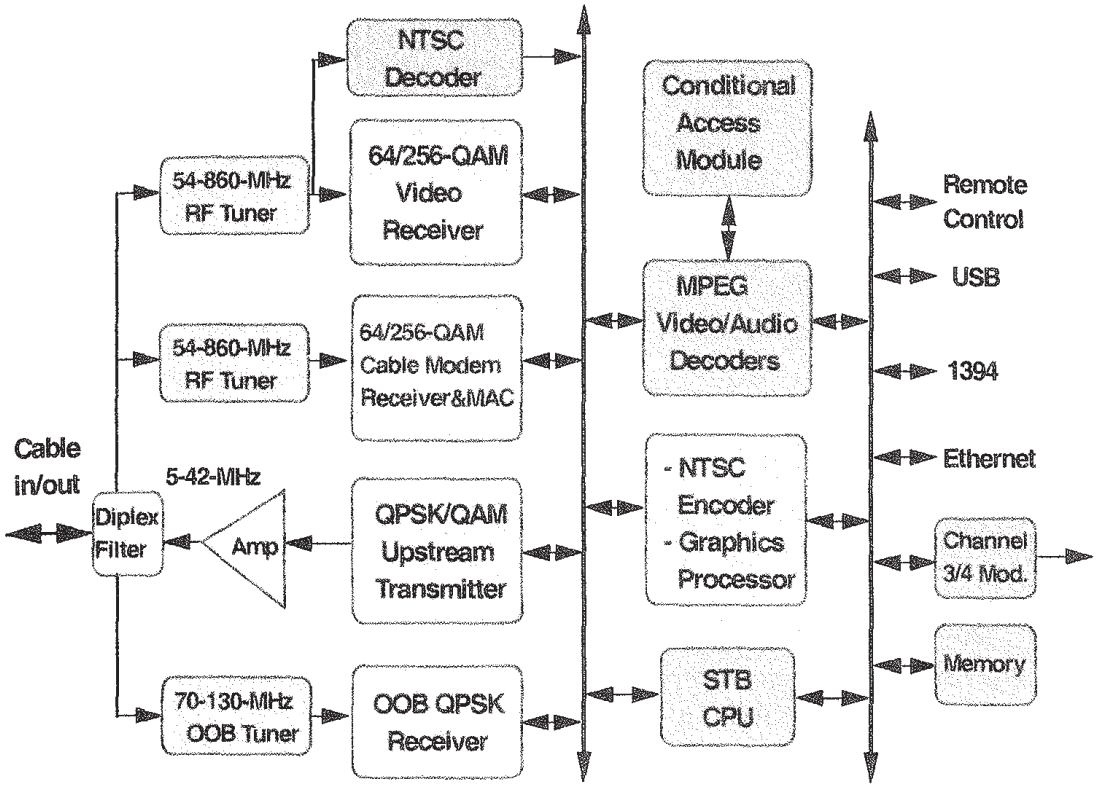


Figure 8.8 Block diagram of an advanced digital set-top box with a built-in DOCSIS modem. After Ref. [3] (© 1999 IEEE).

8.10 M-QAM Transmission Impairments in HFC Networks

The downstream transmission performance of a digital STB or CM in HFC networks can be divided into two class categories as (I) nonlinear distortions induced by lightwave impairment effects, and (II) electronic impairment effects. Chapters 9 and 10 discuss in detail the different types of lightwave effects, including single and multiple wavelength effects over cable TV networks without and with EDFAs, respectively. Generally speaking, the electronic impairment mechanisms, which are discussed in this section, also can be divided into three different groups: (A) electronic implementation impairments, (B) cable TV headend impairments, and (C) cable TV network transmission impairments. Before we discuss the impairment mechanisms caused by the cable TV network, let us briefly review type A and B impairments.

It is well known that the actual hardware implementation of the digital STB design can significantly affect not only the on-screen analog/digital and graphics display and audio output, but also the interaction of the subscriber with the different applications. Rather than discussing overall STB implementation issues, let us focus on the implementation losses of the front-end of the STB, including the QAM receiver, which are essential for robust operation. The implementation losses of RF and IF front-end of the STB are

- RF tuner noise figure (NF)
- RF tuner phase noise
- RF tuner nonlinear distortions
- A/B switch
- SAW filter
- QAM receiver

The generated 64/256-QAM channels at the cable TV headend also can be impaired before they are transmitted over HFC network. These impairments include

- QAM modulator modulation error ratio (MER)
- QAM channel up-converter phase noise
- Adjacent channel spurious noise.

Finally, the electronic impairments in cable TV networks can be divided as follows:

- Additive white Gaussian noise (AWGN)
- Multipath electrical echoes and group delay
- In-band QAM amplitude variations
- Phase noise
- Burst and impulse noise
- AM hum modulation
- Nonlinear distortions (CSO, CTB, XMOD)

The characteristics and impact of the nonlinear distortions, particularly their bursty behavior, on the downstream QAM receiver are discussed as part of the transmission impairments in lightwave systems in Section 9.2. The discussion and results that are presented in this section will focus on a downstream QAM receiver operating according to ITU-T J.83 Annex B specifications [32].

8.10.1 Set-Top Box Front-End Losses

Figure 8.9 shows a simplified block diagram for the RF input signal path through the front-end of the digital STB to the QAM receiver with the assumed signal gain or loss through

each block. The RF tuner and IF amplifier are assumed, for example, to have a worst-case NF of 9.5 dB and 10 dB, respectively. In addition, the NF of the A/B switch and SAW filter is assumed to be equal to their loss. The overall worst-case NF of the STB is obtained using Equation (2.4). This yields an overall worst case NF of 13 dB for the STB. With 13-dB worst case NF, the thermal noise floor for 256-QAM channel (i.e., 5.36-MHz noise bandwidth) is −44.96-dBmV. As the RF input signal level is reduced below its nominal level, the 256-QAM implementation loss caused by the 13 dB NF of the STB is increased. Let us introduce the concept of an implementation loss (IL) for a receiver. The IL of a receiver caused by a given impairment can be defined as [33]

$$IL(dB) = SNR_{in} - SNR_{theory} \tag{8.9}$$

where SNR_{theory} is the theoretical input SNR of an ideal receiver without the impairment at a given BER, and SNR_{in} is the resultant input SNR of the actual receiver with the impairment at the same BER, which can be calculated as follows:

$$SNR_{in}(dB) = -10 \cdot \log\left[10^{-SNR_{theory}/10} - 10^{-SNR_{imp}/10}\right] \tag{8.10}$$

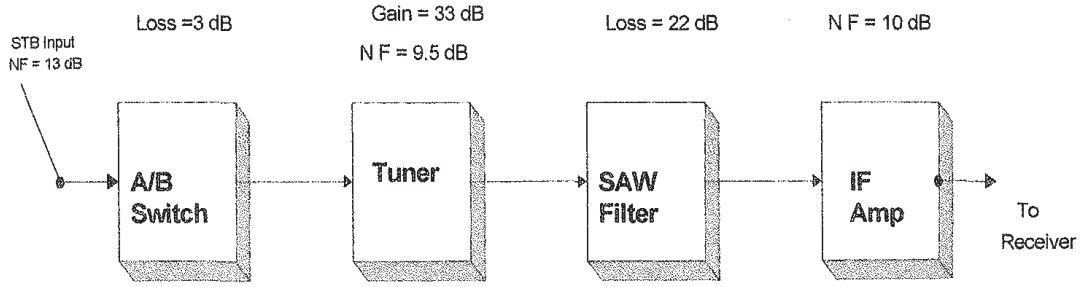


Figure 8.9 Simplified block diagram of an RF input signal path through the front-end of a digital STB.

Table 8.9 NF-related 256-QAM implementation loss at different RF input signal levels.

RF Input Signal Level	SNR due to NF	256-QAM Implementation Loss
−5 dBmV	40 dB	0.28 dB
−10 dBmV	35 dB	0.94 dB
−13 dBmV	32 dB	2.14 dB
−15 dBmV	30 dB	4.16 dB

where SNR_{imp} is the equivalent input SNR for Gaussian noise that would degrade the QAM receiver the same as the impairment, and it is typically measured by an RF spectrum analyzer. For example, the SNR caused by the NF of the STB is 30-dB at an RF input level of −15 dBmV (Table 8.9), and the theoretical SNR for 256-QAM at BER = $1 \cdot 10^{-10}$ is 27.9 dB (Table 7.3). Substituting these values in Equation (8.10) yields SNR_{in} = 32.06 dB. When the NF impairment is added, the input AWGN must be reduced in order to maintain the same BER. Therefore, the implementation loss is 32.06 dB − 27.9 dB = 4.16 dB. The RF tuner also generates its own phase noise and nonlinear distortions. The worst-case single-sideband (SSB) phase noise of a typical dual-conversion tuner as a function of the frequency offset from the QAM carrier is shown in Figure 8.10. Notice that the phase noise behavior of the RF tuner drops approximately as $1/f^2$ up to about 1 kHz. From 1 kHz up to 100 kHz, the SSB phase noise drops as $1/f^3$. Furthermore, as the RF tuner warms up, its phase noise characteristic changes nonlinearly with frequency. Consequently, it is recommended to specify the phase noise requirement of the RF tuner at room temperature and

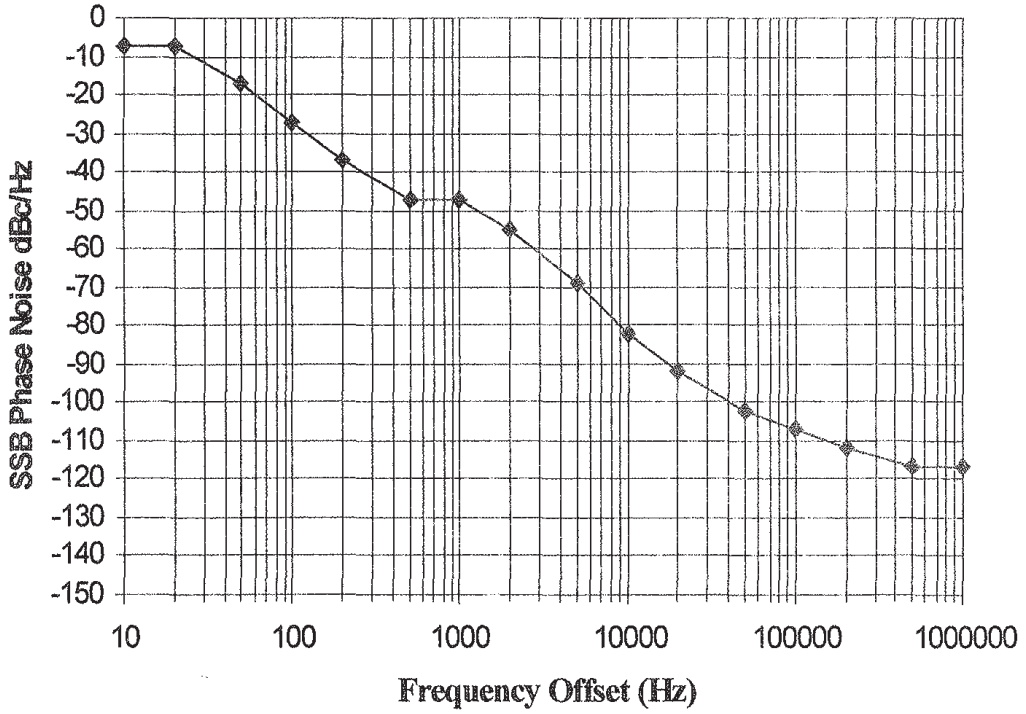


Figure 8.10 Measured single-sideband (SSB) phase noise versus the frequency offset from the carrier for a typical dual-conversion RF tuner.

Table 8.10 Typical characteristics of a dual-conversion cable TV tuner.

Characteristics	Typical Value
RF Input Level Range (AM video)	0 dBmV to +15 dBmV
Noise Figure (NF)	9 dB
Frequency Response Flatness (in 6-MHz)	0.5 dB
Conversion Gain	33 dB
Phase Noise at 10 kHz offset	–85 dBc/Hz
CSO Distortion	≤ –60 dBc
CTB Distortion	≤ –65 dBc
Cross-Modulation Distortion	≤ –60 dBc
Output Return Loss	≥ 10 dB
Image Rejection	≥ 64 dB
Input Return Loss	≥ 5 dB
Isolation	≥ 70 dB

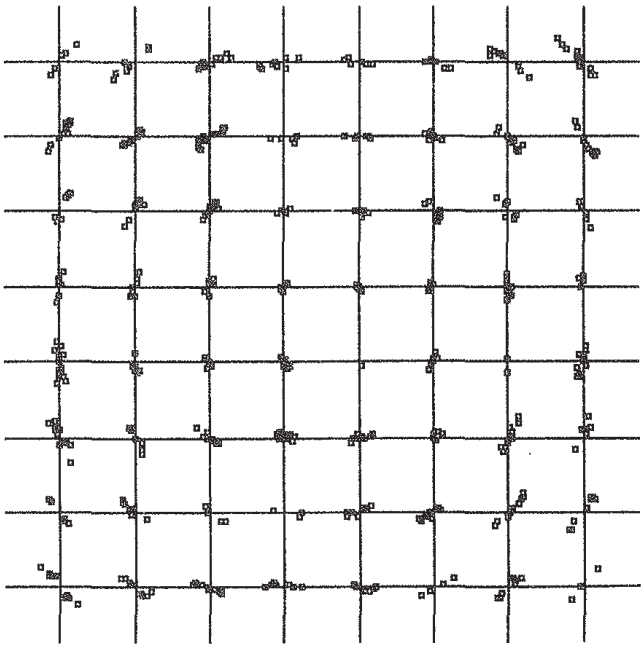


Figure 8.11 The effect of phase noise on a 64-QAM constellation.

at the maximum operating temperature at various offset frequencies. The recommended worst-case SSB phase noise specifications at room temperature of RF tuner are typically –78 dBc/Hz and –85 dBc/Hz at 10 kHz offset for 64-QAM and 256-QAM modulations, respectively. The rationale for these specifications can be explained as follows. The amount of phase noise that the QAM receiver "sees" is determined by the RF tuner phase noise,

external phase noise, and its carrier-recovery loop. The carrier-recovery loop in the QAM receiver acts as a high-pass filter to the phase noise generated by the tuner. Thus, the total phase noise at the QAM receiver is obtained by the numerical integration of the SSB phase noise under the curve shown in Figure 8.10 and filtered by the receiver carrier recovery loop. This value can be converted into the total RMS phase noise jitter (in radians), which is given by [33, 34]:

$$\phi_{RMS} = \left[\frac{2\pi}{360}\right]\sqrt{P_t} \tag{8.11}$$

where P_t is the total integrated power. Table 8.10 summarizes the typical characteristics of a dual-conversion tuner for a digital STB. The effect of phase noise on a 64-QAM constellation is shown in Figure 8.11. The outer constellation points are smeared the most, while the center constellation points remain almost unchanged. From a practical perspective, it is also important that the generated nonlinear distortions by the RF tuner are sufficiently small, and sufficient isolation (≥ 70-dB) exists between downstream and upstream transmission.

8.10.2 QAM Transmitter Losses

In addition to front-end losses at the digital STB, the generated RF QAM signal at the cable TV headend is not an ideal QAM signal. In Section 7.9.2, we explained the concept of equalized MER for a QAM transmitter. The measured SNR of the QAM modulator needs to be corrected for the departure of the HP89441A instrument from an ideal receiver according to Equation (7.33). As we learned in Section 7.6.2, the SAW filter reduces spurious noise, which is out of the QAM channel. To translate the generated QAM channel at a 44-MHz IF to the desired RF channel frequency, an upconverter unit is typically used. Adjacent channel interference (ACI) is generated when multiple QAM channels are contiguously stacked one next to the other. Since the carrier level of the various QAM channels across the cable TV frequency plan can be different by as much as 10-dB or more, the measured QAM SNR will be further reduced because of the ACI effect. In addition, the upconverter unit has its own SSB phase noise, which will be transmitted downstream to the digital STB or CM receiver. If the upconverter is overdriven by the 44-MHz IF signal, it can result in compression of the digitally modulated carrier, resulting in a data/packet loss.

8.10.3 Additive White Gaussian Noise (AWGN)

Once the SNR of the QAM modulator has been measured, the performance of the downstream QAM receiver in the digital STB or CM needs to be measured first in a back-to-back configuration in the presence of a Gaussian noise. Figure 8.12 shows an example of the measured and calculated 256-QAM coded BER (ITU-T J.83 Annex B) versus E_S/N_o (in dB) for a Gaussian channel. The RF input signal level to the QAM receiver was 0 dBmV.

Pseudorandom bit sequence (PRBS) $2^{23}-1$ data and the clock signals are typically used for this measurement. As we learned in Chapter 7, the ITU-T J.83 Annex B FEC consists of a 16-state trellis- coded modulation (TCM) at a rate of 19/20 concatenated with R-S T = 8 (128,122) code. The transmitted symbol rate is 5.36094 MBaud. The measured 256-QAM CNR (= E_s/N_0) has been corrected for the departure of the QAM modulator from an ideal modulator. For example, assuming 42-dB MER for the QAM modulator, the corrected 256-QAM CNR in a 5.36-MHz receiver noise bandwidth (= transmitted symbol rate) is 28.8-dB at BER = $1 \cdot 10^{-9}$. This results in about 1-dB implementation loss for the QAM receiver.

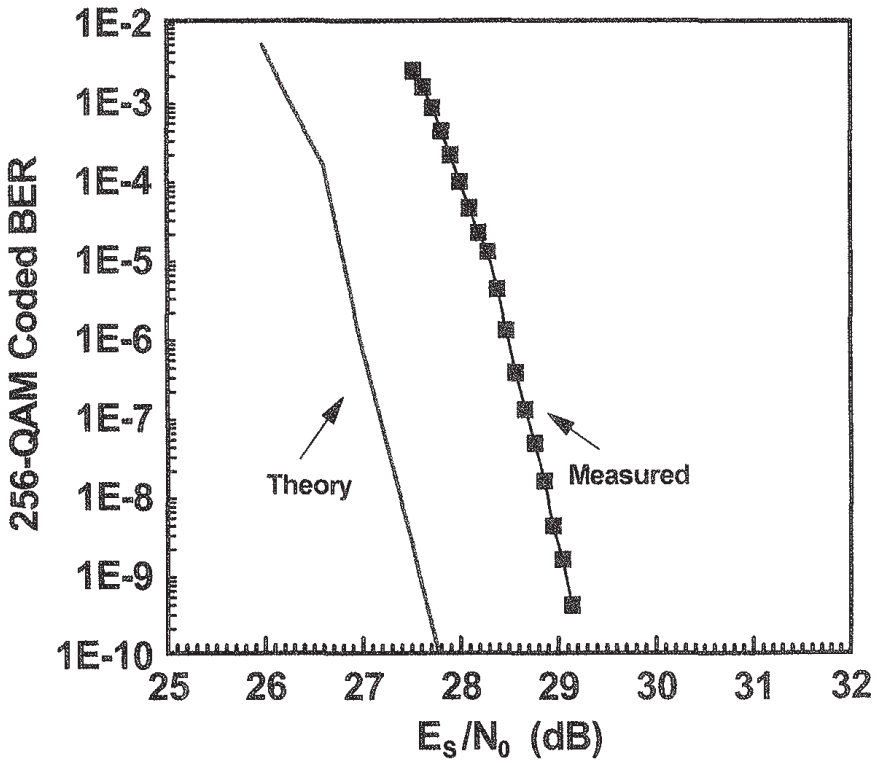


Figure 8.12 Measured and calculated 256-QAM BER as a function of the CNR, assuming only AWGN and RF input power level of 0-dBmV.

8.10.4 Multipath Reflections

Multipath microreflections in the coaxial portion of the HFC network can significantly degrade the CNR of the QAM channel. Static multipath reflections can be generated in a lab using, for example, an Agilent 11759A dynamic ghost simulator, which can generate single

or multiple echoes with a specified magnitude, time delay, and phase relative to the transmitted signal. It is often more convenient and simple to analyze the adaptive equalizer (AE) behavior in the presence of a single dominant echo rather than multiple echoes. Figure 8.13 shows an example of the measured echo magnitude for a transmitted 256-QAM signal as a function of the echo time delay in microseconds. The data was obtained by setting the 256-QAM SNR to 30-dB for a single echo with 180° phase relative to the transmitted signal. Then, the echo magnitude was increased from –50-dBc until QAM carrier acquisition could not be achieved.

The QAM receiver used in this measurement features a 32-tap symbol-spaced equalizer (8 FFE taps and 24 DFE taps) with decision-directed adaptation. One of the FFE taps is typically used as the center tap, leaving 7 FFE taps for leading echoes and 24 DFE taps for lagging echoes. Since the modulation symbol duration is approximately 186.55 ns, the theoretical total range of the AE is –1.3 μs to +4.48-μs. For time delays up to 4.0 μ s, the ITU-T J.83B receiver can equalize lagging echoes with a relative magnitude up to –10 dBc. For delays up to 4.5 μs, lagging echoes with magnitude of –30 dBc can be equalized. Echoes with time-delays greater than 4.5 μs cannot be equalized, and thus behave like noise. This result demonstrates that the AE can "handle" any single echo with magnitude up to –10 dBc almost independently of the echo's time delay within its range. From a practical point of view, the dashed line (Fig. 8.13) can be used as an echo magnitude specification that can that can be reliably handled by the tested QAM receiver at various delays.

There are various models such as the IEEE 802.14 HFC channel model [35] and the DOCSIS 1.1 model [14], which specify the echo magnitude and time delay for an HFC network. Generally speaking, the multipath behavior of a cable TV network can vary widely from one area to another. These two multipath models may represent two extremes, and are shown here only for comparison. As we learned in Chapter 2, the DOCSIS 1.0 model assumes only a single dominant reflection with a specified maximum echo magnitude at each time delay interval. In contrast, the IEEE 802.14 model allows for one or more discrete

Table 8.11 Multipath echo profile according to the IEEE 802 HFC model. After Ref. [35].

Echo Time Delay	Total Echo Magnitude (Downstream)	Total Echo Magnitude (Upstream)
0 to 0.2 μs	–11 dBc	–10 dBc
0.2 to 0.4 μs	–14 dBc	–12 dBc
0.4 to 0.8 μs	–17 dBc	–14 dBc
0.8 to 1.2 μs	–23-dBc	–18 dBc
1.2 to 2.5 μs	–32 dBc	–24 dBc
2.5 to 5 μs	–40 dBc	–30 dBc
5 to 15 μs	None	–35 dBc
> 15 μs	None	None

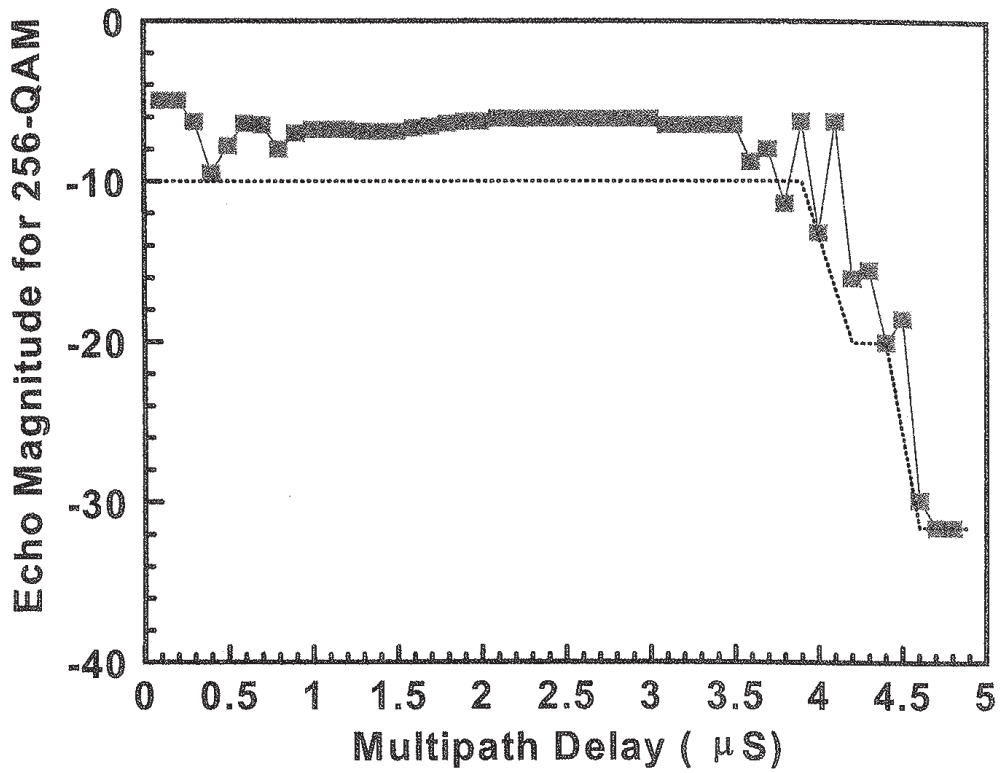


Figure 8.13 The measured echo magnitude relative to the transmitted 256-QAM signal (in dBc) as a function of the multipath time delay (μs).

reflections within each time interval, where the echo magnitude is randomly distributed within each time interval. Table 8.11 shows, for example, the maximum downstream and upstream echoes' magnitude for each time interval according to the IEEE 802 model. Specifying the echo magnitude at the maximum of the time-delay interval produces the largest GDV. But, it does not necessarily have the worse effect on the transmitted signal. It turns out that breaking the magnitude of a single echo into multiple echoes within the time-delay interval lowers the GDV, but actually has a worse effect on the transmitted signal because of a higher peak-to-RMS ratio for combining multiple echoes compared with a single echo.

The effect of multipath echoes on the transmitted QAM signal also can be analyzed using the DFE and FFE tap values within the time delay range of the AE. Figure 8.14 shows an example of a histogram of the tap values for a symbol-spaced AE with eight DFE taps and eight FFE taps in the presence of a –14-dBc echo with a time-delay of 1.2 μs relative to the received 64-QAM signal [36]. Since the ITU-T J.83 Annex B receiver was operating in the 64-QAM mode, the corresponding tap spacing is 0.1978 μs. One of the FFE taps is designated as the center tap (zero time-delay), which has been set to an arbitrary value of +10 dB.

The other seven FFE and eight DFE taps are available for echo cancellation. In order to cancel the effect of the multipath echo, the adaptation algorithm has set the sixth DFE tap weight to –14 dBc relative to the center tap. This indicates that there is an echo with a –14 dBc magnitude and time delay of 1.2 μs. The fifth tap, which is located at time delay of 1.0 μs, is also activated at about –25 dBc. However, the possibility of a second echo with a time delay of 1.0 μs is very low since the magnitude of the seventh tap is quite low. Thus, it probably means that the single echo is actually occurring between the fifth and sixth taps, or between time delays of 1.0 and 1.2 μs, but closer to 1.2 μs. Notice that most of the other taps are also partially activated, which could be due to the presence of very weak echoes, or there may be a slight tilt in the channel. In practice, the Agilent 89441A instrument provides a frequency response display that is calculated as the Fourier transform of the tap values (see Figure 7.16).

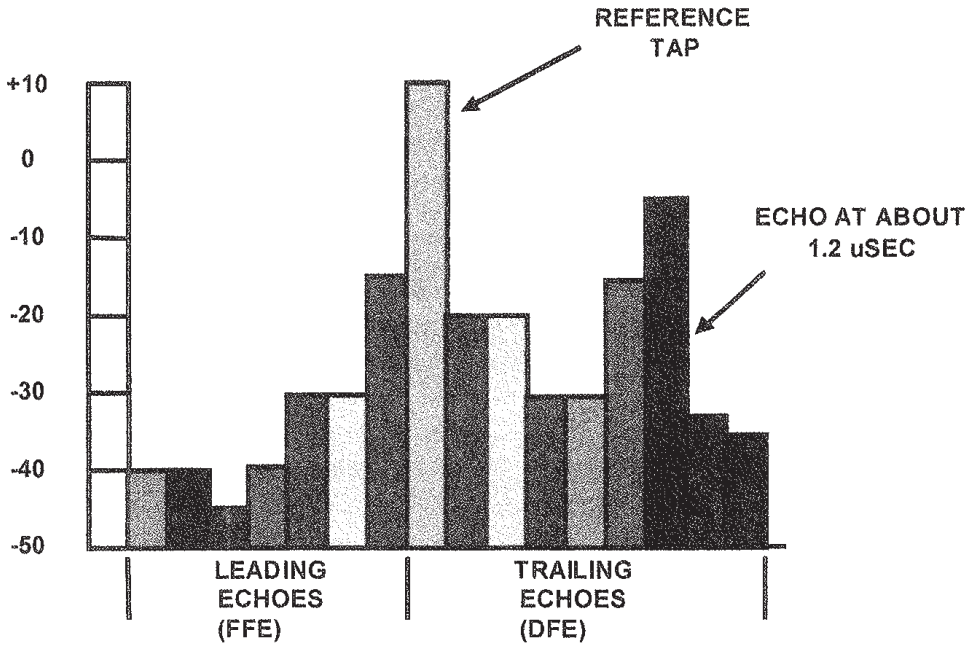


Figure 8.14 Tap weights for an adaptive equalizer in the presence of a –14-dBc echo at about 1.2-μs time-delay. After Ref. [36].

8.10.5 Amplitude and Group Delay Variations

The amplitude and the group delay (GD) of the transmitted downstream and upstream QAM channel can significantly vary across within its bandwidth and also across the cable TV frequency spectrum because of multipath reflections and poor frequency response. The in-

band amplitude variation, which often is called amplitude ripple, is specified to be no more than 3-dB for downstream 64/256-QAM channels according to DOCSIS 1.1 [14]. However, there is no specification for the QAM channel amplitude variation across the cable TV frequency plan. Cable operators typically like to balance the QAM channel amplitude across the frequency plan and limit the amplitude slope to less than 10 dB. For upstream transmission, the maximum amplitude ripple is specified to be 0.5-dB per MHz according to the DOCSIS 1.1 specifications [14].

As we learned in Section 2.8, the group delay variation (GDV) is related to the magnitude and time delay of the multipath echoes. The downstream GDV, which is typically generated by the diplex filters in active coaxial components in the HFC network and an improper network alignment, is specified to be no more than 75-ns within the transmitted QAM channel. The upstream GDV is specified per 1-MHz of channel bandwidth because the channel bandwidth is not fixed, but is allowed to vary within specific steps. For example, the maximum upstream GDV is specified to be 200-ns/MHz across the upstream band (5–42 MHz) according to the DOCSIS 1.1 specifications [14].

8.10.6 Burst and Impulse Noise

As we learned in Chapter 2, burst and impulse noise, particularly on the return path portion of the HFC network, constitute another important degradation mechanism. The frequency of occurrence of burst noise longer than 1-μs can vary significantly from one cable TV network to another. Generally speaking, although such bursts occur only a handful of times in a 24-hour period, changing HFC network conditions can generate relatively long duration bursts (>10-μs) at a much higher rate. For example, the IEEE802.14 HFC model specifies the following assumptions for burst noise [35]:

- Burst events are Poisson distributed with a downstream rate of one burst per minute, and an upstream burst of one per ten seconds
- Each burst of the event is amplitude modulated with zero-mean Gaussian noise in 1 MHz RF bandwidth (0.5-MHz lowpass baseband noise) with standard deviation equal to 1/4 of carrier amplitude
- The carrier frequency of each event is selected from a uniform distribution between 5-MHz and 15-MHz
- Each burst event has the same amplitude, where the amplitude of each event is selected from a sawtooth distribution, which is zero at 0-Vrms and is peaked at 1-Vrms (= 60 dBmV across 75 ohms)
- With multiple bursts per event, the duration of each burst is selected from a uniform distribution between 1-μs and 30-μs. With a single burst, the burst length is exponentially distributed with a mean of 30-μs.
- The space between a burst and the following burst (if there is another in the event) is selected from a sawtooth distribution peaked at 10-μs and down to zero at 130-μs.

To understand the downstream transmission degradation of QAM channels in the presence of burst noise, let us look at the following test result. The operating point of a 256-QAM receiver was set for a sufficiently high CNR (i.e., error-free transmission), say 35-dB, in the presence of a Gaussian noise. Then, a pulse generator was fed to a doubly balanced mixer, which was used to gate the Gaussian noise during the burst pulse, thus reducing the 256-QAM CNR. During the burst event, the QAM CNR was sufficiently reduced to corrupt the 256-QAM constellation, thus preventing the QAM receiver from reacquiring the QAM carrier. The gated burst noise signal was combined with the 256-QAM modulator output at IF, and upconverted to RF before it was fed to the QAM receiver. The measured burst noise duration was adjusted until uncorrectable errors were observed at BER $\leq 1 \cdot 10^{-6}$. This coded BER level is typically selected since it is approximately the threshold of visibility (TOV) for transmitted digital video and because it also allows one to collect a good error statistics for a reliable measurement. Figure 8.15 shows the measured duration of the gated burst noise at a coded BER $\leq 1 \cdot 10^{-6}$ as a function of the interleaver depth (J) at a 10 Hz burst noise repetition rate. The case of $I = 128$, $J = 1$ interleaver/deinterleaver combination, which is specified by DOCSIS 1.1, has a theoretical burst-noise protection value of 66-μs. There are two important issues, which are apparent in Figure 8.15. First, the measured burst noise erasure

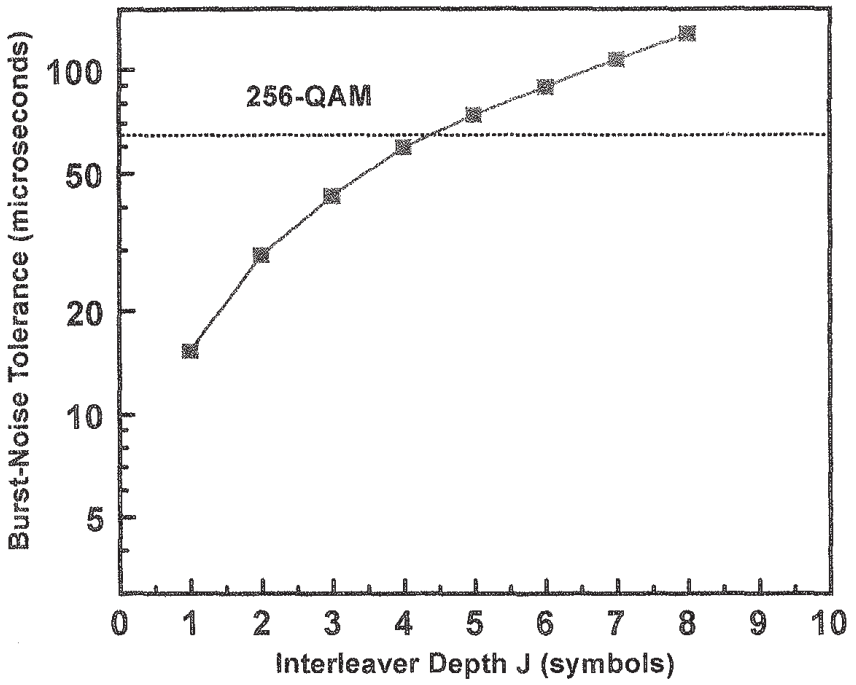


Figure 8.15 Burst-noise tolerance duration of 256-QAM receiver at BER $\leq 1 \cdot 10^{-6}$ versus the interleaver depth (symbols).

for $I = 128$, $J = 1$ interleaver mode is significantly below the theoretical value for 256-QAM transmission. This is because the analog front end of the QAM receiver, particularly the RF tuner, adds phase noise and nonlinear distortions, further degrading the QAM receiver performance. Second, a downstream receiver operating in 256-QAM mode is significantly more sensitive to the burst noise rate than in the 64-QAM mode as expected. Thus, in order to achieve the theoretical burst noise tolerance of 66-μs, the $I = 128$, $J = 4$ interleaver needs to be used. The drawback is the additional cost of SRAM memory and added latency in the QAM receiver for robust transmission.

8.10.7 AM Hum Modulation

AM hum modulation, as explained in Section 2.5.4, is an amplitude distortion of the transmitted signal caused by the modulation of the signal by the power line sources at 60-Hz and 120-Hz. According to the FCC rules in Section 76.605, cable TV operators are required to keep the AM hum modulation at or below 3% peak-to-peak (0.26 dB amplitude reduction) of the transmitted QAM signal [37]. The shape of the AM hum modulation signal is actually trapezoidal with rise and fall times of about 0.25-ms. It should be pointed out that the QAM channel degradation increases very rapidly as the AM hum modulation increases above 3% peak-to-peak. The AM hum degradation can be mitigated, for example, by implementing a fast AGC loop within the QAM receiver, allowing the equalizer to track the QAM signal variations. Lab measurements have shown that the 256-QAM CNR can be degraded by more than 1-dB at an AM hum modulation of 5% peak-to-peak.

8.10.8 64/256-QAM System Link Budget

To specify the required operating conditions for the digital STB, one needs first to construct a system link budget based on all the various impairment types. The system link budget takes into account the simultaneous presence of all the different types of impairments over the cable TV network. To develop the link budget for the STB, one needs to calculate the associated implementation loss for each type of impairment on the transmitted 64/256-QAM channels. Table 8.12 summarizes, for example, OpenCable STB specification for downstream transmission of both AM-VSB video and 64/256-QAM signals [31]. The nominal relative carrier power levels for both the analog and digital signals are given in Table 8.13. These values are needed to determine the adjacent channel interference between the analog and digital signals. Note that these relative power levels must be within the absolute RF input power range of −15 dBmV to +15 dBmV for the digital signals.

Using this procedure, the required 256-QAM C/(N+I) versus the RF input level (in dBmV) to a digital STB was calculated in the presence of white Gaussian noise and multiple simultaneous impairments. In this example, 79 AM-VSB channels (55.25–547.25 MHz) with a CNR of 45 dB at RF input level of 0-dBmV, and thirty-three 256-QAM channels (553.25–751.25) were transmitted to the digital STB. The RF power ratio of the AM-VSB

channels to the 256-QAM channels was fixed at 5 dB. As the RF input power level is reduced below 0-dBmV, the required C/(N+I) for error-free transmission steadily increases from 34 dB in the presence of multiple simultaneous impairments. At an RF input level of –12 dBmV, the required C/(N+I) is 39 dB. The operating margin of the digital STB is defined as the difference between the C/(N+I) for the cable TV plant and the STB in the presence of multiple simultaneous impairments. Thus, the operating margin represents a safety margin for the cable TV operators to work with the required C/(N+I). The operating margin in the presence of the actual impairments is likely to vary from 0 dB to 5 dB, depending on the type of impairment and its magnitude. This means that the cable TV operator must continuously monitor and balance the magnitude of all of the impairments over its network. Failure to do so can easily reduce or even eliminate the STB operating margin, resulting in interrupted analog and digital services.

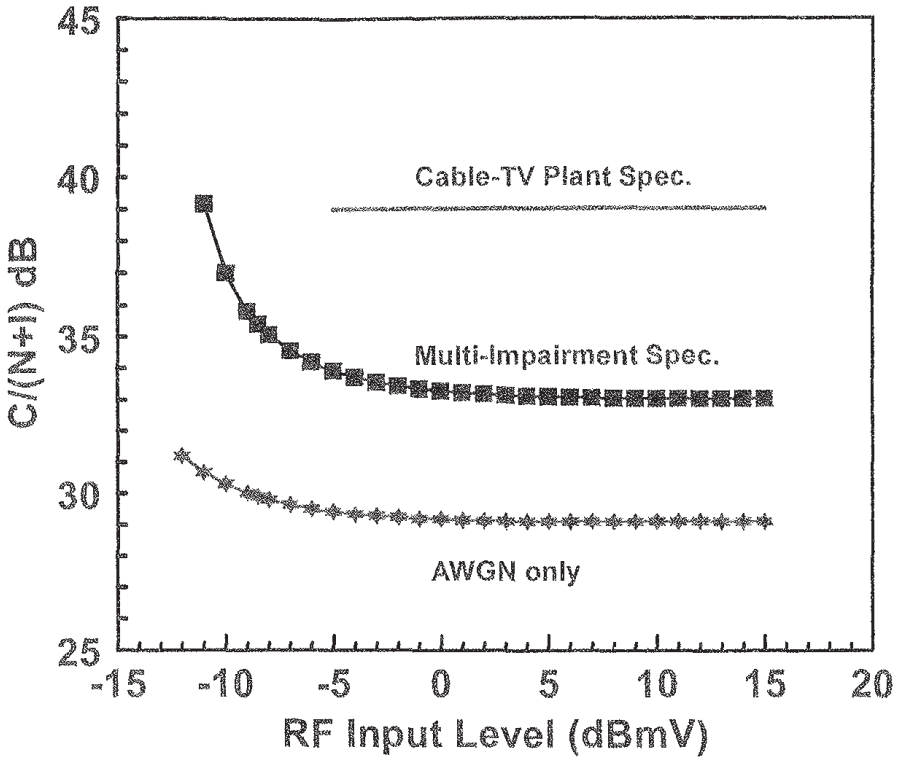


Figure 8.16 Calculated 256-QAM C/(N+I) in the presence of Gaussian noise and multiple impairments as a function of the RF input level to the STB. The solid line represents the assumed cable TV network specification.

Table 8.12 OpenCable downstream STB specification for 64/256-QAM transmission (0°–40° C). After Ref. [31].

CHARACTERISTICS	OpenCable STB Analog and 64/256-QAM SPECIFICATIONS
RF Input Channel Bandwidth	6 MHz
RF Frequency Range	54 MHz-860 MHz (IRC/HRC/standard frequency plans)
RF Input Signal Level Range	−15 dBmV to +15 dBmV for 64-QAM −12 dBmV to +15 dBmV for 256-QAM 0 to +15 dBmV for Analog visual carrier −10 to −17 dBmV for Analog aural carrier
RF Input Return Loss	≥ 6 dB (over full tuning range)
RF Input Impedance	75 ohm unbalanced
RF Bypass Isolation	≥ 60 dB (over full tuning range)
C/(N+I)[2] @ BER=$1 \cdot 10^{-9}$	≥ 33 dB for 256-QAM[3] ≥ 27 dB for 64-QAM[3]
CSO Distortions	≤ −60 dBc[4]
CTB Distortions	≤ −63 dBc[4]
Cross-Modulation Distortions	≤ −57 dBc[4]
Spurious Emissions (within the output channel 3/4 bandwidth)	≤ −60 dBc[4]
Spurious Emissions (outside the output channel)	≤ −10 dBc[4]
Phase Noise Tolerance[5]	≤−88 dBc/Hz @ 10 kHz offset
In-Band Amplitude Ripple Tolerance	≤ 5 dB (peak-to-peak) for digital channels ≤ 4 dB (peak-to-peak) for analog channels
Burst Noise Duration	Not longer than 25 μsec at10 Hz repetition rate
CW Interference	Included in C/(N+I)

[2] C/(N+I) includes the simultaneous presence of all impairments in the 6-MHz channel bandwidth.
[3] Channel loading assumptions: at least 110 AM-VSB channels with CNR = 43 dB, and at least 20 QAM channels at RF input level of −10 dBmV.
[4] Channel loading assumptions: at least 110 AM-VSB video channels at RF input level of +15 dBmV, and at least 20 QAM channels at RF input level of +5 dBmV.

[5] The phase noise tolerance specification is for a phase noise generated by the cable TV network relative to the center of the QAM signal band, excluding the contribution of the tuner in the set-top box.

CHARACTERISTICS	OpenCable STB Analog and 64/256-QAM SPECIFICATIONS
Multipath Reflections (One dominant echo with maximum specified magnitude relative to the primary QAM channel)	–10 dBc at time-delay ≤ 0.5 μsec –15 dBc at time-delay ≤ 1 μsec –20 dBc at time-delay ≤ 1.5 μsec –30 dBc at time-delay < 5.0 μsec –35 dBc at time-delay ≥ 5 μsec
Group Delay Variation Tolerance	≤ 0.25 μsecond across the 6-MHz channel
AM Hum Modulation	Not greater than 3% (p-p)
Adjacent Channel Interference	≤ 10 dBc between QAM channels
Conversion isolation (RF input to channel 3/4 RF output)	≥ 65 dB

Table 8.13 Nominal and range of the relative carrier power levels for the transmitted analog and digital signals to the digital set-top box. After Ref. [31].

Channel Type	Nominal and Range of the Relative Carrier Power Level
Analog Channel	0 dBc (reference level)
Downstream OOB Channel	–8 ± 5 dBc
Downstream 64-QAM Channel	–10 ± 2 dBc
Downstream 256-QAM Channel	–5 ± 2 dBc

References

1. R. K. Jurgen, *Digital Consumer Electronics Handbook*, McGraw-Hill, New York, 1997.
2. CableLabs, *OpenCable Set-top Terminal CORE Functional Requirements for Bi-directional Cable*, CFR-OCS-BDC-INTC03-00818 (2000).
3. W. S. Ciciora, "Inside the Set-Top Box," *IEEE Spectrum Magazine*, April, 70–75 (1995).

4. H. Samueli, "Broadband Communications ICs: Enabling High-Bandwidth Connectivity in the Home and Office," *IEEE International Solid-State Circuits Conference Proceedings*, paper MA 1.3 (1999).
5. IEEE, IEEE Standard for High Performance Serial Bus, IEEE 1394–1995 (1996).
6. Information on Edwin H. Armstrong can be found in the Web site: http://www.world.std.com/~jlr/doom/armstrng.htm.
7. M. Waight, "Wireless Industry Opens Doors for Cable," *NCTA Technical Papers* (1996).
8. P. Putman, *Question of Balance: A Look at Voltage Current, Video, Cables and Where the Balun Fits In*, Intertec Publishing (1999).
9. D. Agahi, "Monolithic Ceramic Block Combline Bandpass Filters," *RF Design*, March, 35–41 (1989).
10. N. Scheinberg, "A GaAs Up Converter Integrated Circuit for a Double Conversion Cable TV "STB" Tuner," *IEEE Journal of Solid-State Circuits*, **29**, No. 6, June, 688–692 (1994).
11. DVS-167, *Digital Broadband Delivery System: Out-Of-Band Transport*, Society of Cable Telecommunications Engineers (1998).
12. DVS-178, *Cable System Out-Of-Band Specifications*, Society of Cable Telecommunications Engineers (1998).
13. S. Lin and D. J. Costello Jr., *Error Control Coding: Fundamentals and Applications*, Prentice-Hall, Englewood Cliffs, N.J. (1983).
14. CableLabs, *Data-Over-Cable Service Interface Specifications: Radio Frequency Interface Specification* SP-RFIv1.1-I01-990311 (1999).
15. The ATM Forum, *ATM User-Network Interface (UNI) Specification Version 3.1*, Prentice-Hall PTR (1995).
16. H. T. Nicholas III and H. Samueli, "A 150-MHz Direct Digital frequency Synthesizer in 1.25-μm CMOS with -90-dBc Spurious Performance," *IEEE Journal of Solid State Circuits* **26**, 1959–1969 (1991).
17. International Radio Consultative Committee (CCIR) Recommendation 656, *Interface For Digital Component Video Signals in 525-Line and 625-Line Television Systems* (1994).
18. EIA-608, Recommended Practice for Line 21 Data Service, Electronic Industries Association (1994).
19. DVS-053, *Standard for Carriage of NTSC VBI Data in Cable Digital Transport Streams*, Society of Cable Telecommunications Engineers (1998).
20. EIA-516, *Joint EIA/CVCC Recommended Practice for Teletext: North American Basic Teletext Specification (NABTS)*, Electronic Industries Association (1998).
21. D. R. Stinson, *Cryptography Theory and Practice*, CRC Press, Boca Raton, Florida (1995).
22. A. J. Menezes, P. C. Van Oorschot, and S. A. Vanstone, *Handbook of Applied Cryptography*, CRC Press (1997).
23. RSA Labs, *Frequently Asked Questions About Today Cryptography 4.0* (1998).

24. CableLabs, *OpenCable Host-POD Interface Specification*, IS-POD-131-WD01-991008 (1999).
25. CableLabs, *OpenCable Set-top Terminal CORE Functional Requirements for Unidirectional Cable*, CFR-OCS-UDC-WD04-991015 (1999).
26. CableLabs, *OpenCable POD Copy Protection System*, IS-POD-CP-WD02-991027 (1999).
27. See for example A. B. Tucker Jr., Editor-in-chief, *The Computer Science and Engineering Handbook*, CRC Press (1997).
28. For details on RISC microprocessors see http://developer.intel.com/design/strong/sapps.html.
29. For technical discussion on SDRAM see http://www.chips.ibm.com/products/memory/sdramart/sdramart.html.
30. J. Mitchell, "Minimizing Memory Cost in Set-top Boxes," *NCTA Technical Papers*, 57–64 (1996).
31. CableLabs, *OpenCable Set-top Terminal with DOCSIS Modem CORE Functional requirements for Bidirectional Cable* (1999).
32. ITU-T Recommendation J.83 Annex B, Digital Multi-program Systems for Television Sound and Data Services for Cable Distribution, April (1997).
33. M. Kolber, "Predict Phase-Noise Effects in Digital Communications Systems," *Microwaves and RF Magazine* **9**, 59–70 (1999).
34. D. Barker, "The Effects of Phase Noise on Higher-Order QAM Systems," *Communication Systems Design* **10**, 35–42 (1999).
35. T. Kolze, "Proposed HFC Channel Model," General Instrument IEEE802.14 contribution, IEEE 802.14-96/196, Enschede, Netherlands (1996).
36. M. Kolber and M. Ryba, "Measuring Multipath in the Wireless Cable Environment," *RF Design Magazine* **2**, 52–74 (1999).
37. FCC Code of Federal Regulations, Title 47, Part 76, Section 605, Subpart K, Technical Standards, Cable Television Service (1997).

CHAPTER 9

TRANSMISSION IMPAIRMENTS IN WDM MULTICHANNEL AM/QAM LIGHTWAVE SYSTEMS

In general, one can categorize the different subcarrier multiplexed (SCM) multichannel AM/QAM video lightwave transmission systems into four main groups as follows:

1. DM laser transmitter-based systems operating around 1310-nm
2. EM laser transmitter-based systems operating around 1319-nm
3. EM laser transmitter-based systems operating around 1550-nm
4. DM laser transmitter-based systems operating around 1550-nm

There are many technical and economic design considerations that determine which laser transmitter system one should select to address the access network needs. The purpose of this chapter is to explain the theoretical models for the different lightwave impairment mechanisms, and how the performance of such systems operating at both single and multiple wavelengths are degraded. The degradation mechanisms for EDFA-based WDM SCM multichannel lightwave systems are discussed in Chapter 10. The reasons for partition will become clear later when we discuss the evolution of the current HFC network architecture toward dense-wavelength-division-multiplexed (DWDM) architecture. The main lightwave degradation mechanisms are:

(A) Clipping-induced impulse noise
(B) Bursty nonlinear distortions
(C) Multiple optical reflections
(D) Dispersion-induced distortions
(E) Stimulated Brillouin scattering (SBS)
(F) Self-phase modulation (SPM)
(G) Stimulated Raman scattering (SRS)
(H) Cross-phase modulation (XPM)
(I) Polarization-dependent distortions

Each of these impairment mechanisms is discussed in detail in the following sections.

9.1 Clipping-Induced Nonlinear Distortions

Recently, there have been many studies on QAM channel degradation due to the loading of the AM-VSB video channels at the laser transmitter [1–5]. It has been shown experimentally by Maeda, et al., [1] that the bit error rate (BER) of a transmitted 16-QAM channel is significantly degraded at the optical receiver when transmitting multiple (e.g., >40) AM-VSB video channels. A BER floor is formed, caused by the "clipping" behavior of the laser transmitter. Figure 9.1 shows the clipped output modulated waveform from the ideal laser L-I curve. This phenomenon occurs when the instantaneous voltages of each of the loaded AM-VSB signals add up to temporarily drive the laser diode below its threshold, thus clipping the transmitted modulated signal [5, 6]. The clipping noise can be observed on electrical spectrum analyzer by setting the center frequency to the QAM channel, resolution and video bandwidth each to their maximum (3-MHz), and frequency span to zero. In this

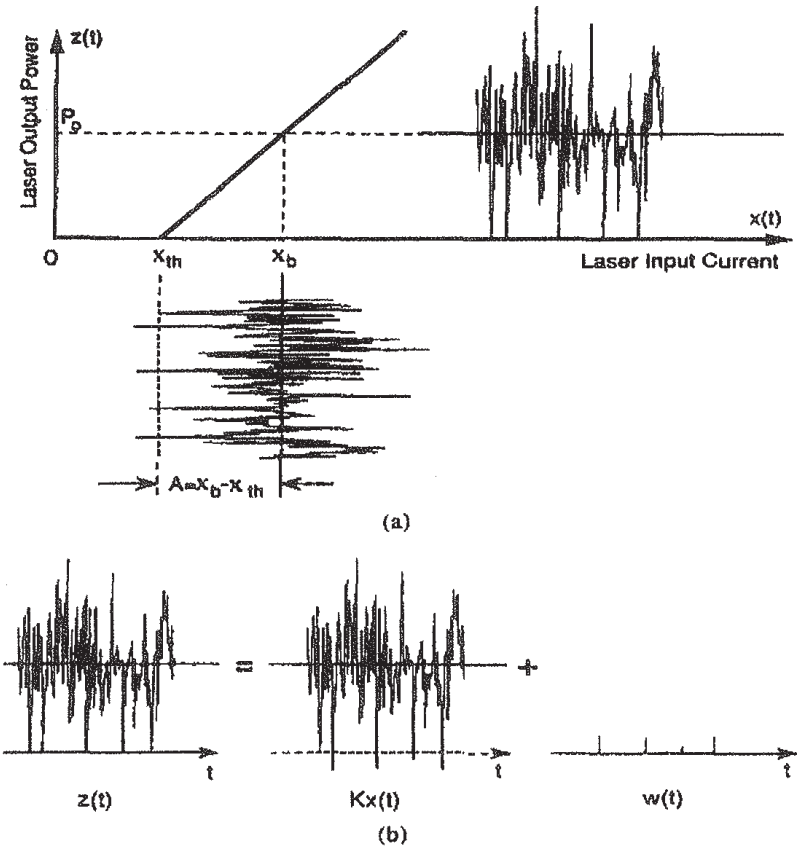


Figure 9.1 (a) Laser clipping noise at the biased input point (X_b) of the laser L-I curve; (b) laser output decomposed as a sum of the attenuated input signal and noise. After Ref. [6] (© 1995 IEEE).

way, the spectrum analyzer is used as a bandpass filter, and the observation of the clipping impulse events in a given time period is controlled by the sweep time of the spectrum analyzer [3].

9.1.1 Asymptotic Statistical Properties of Clipping Noise

In order to understand the model for the BER of M-ary QAM channels, which will be discussed in the Section 9.1.2, let us briefly review the asymptotic statistical properties of clipping-induced impulse noise. We note that the laser transmitter is essentially a memoryless device over the cable TV frequency range. Thus, the laser clipping problem shown in Fig. 9.1(a) is essentially equivalent to the A-level crossing problem discussed by Mazo [6]. Let us consider the signal x(t) to be a stationary zero-mean Gaussian process that models the composite input signal of multiple subcarrier signals. Using Bussgang's theorem, the laser output signal z(t) can be written as

$$z(t) = K \cdot x(t) + w(t) \tag{9.1}$$

where w(t) is the clipping noise and K is chosen so that x(t) and z(t) are uncorrelated. Thus, multiplying both sides of Equation (9.1) by x(t) and taking the expectation value, K is given by

$$K = -\frac{E[x \cdot w]}{E[x^2]} = -\frac{1}{\sigma A\sqrt{\pi}} \int_A^{\infty} x(x+w)\exp[-x^2/2\sigma^2]dx \tag{9.2}$$

Based on these assumptions, we can write the following three asymptotic statistical properties of clipping noise.

1. The sequence of upcrossing epochs of a high-level A by input signal x(t) asymptotically becomes a Poisson process. Based on a paper by Rice [7], the expected rate of upward crossing of level $A > 0$ by a stationary zero-mean Gaussian process x(t) is given by

$$\lambda_A = \frac{1}{2\pi}\frac{\dot{\sigma}}{\sigma}\exp[-A^2/2\sigma^2] \tag{9.3}$$

where $A = x_b - x_{th}$, as shown in Figure 9.1(a),

$$\sigma^2 = E[x^2(t)] \tag{9.4}$$

is the power variance of Gaussian process $x(t)$, and $d[\sigma^2]/dt$ is the variance of the first derivative of $x(t)$. Furthermore, if the spectrum of $x(t)$ is flat over a band of frequencies $[f_1, f_2]$, then according to Rice [7] we have

$$\left[\frac{d\sigma/dt}{\sigma}\right]^2 = (2\pi)^2 \frac{f_2^3 - f_1^3}{3(f_2 - f_1)} \tag{9.5}$$

and

$$\lambda_A = \left[\frac{f_2^3 - f_1^3}{f_2 - f_1}\right]^{1/2} \exp[-A^2/2\sigma^2] \tag{9.6}$$

2. The probability density function (pdf) of the time intervals between an upcrossing and a downcrossing (e.g., clipping intervals) asymptotically becomes a Rayleigh distribution. Denoting the time interval length as τ, the pdf is given by [6]

$$p(\tau) = \frac{\pi}{2}\frac{\tau}{\bar{\tau}^2}\exp[-\frac{\pi}{4}(\frac{\tau}{\bar{\tau}})^2] \tag{9.7}$$

for $\tau \geq 0$, where $\bar{\tau}$ is the average clipping time interval. The clipping rate is related to average clipping interval by

$$\lambda_A \bar{\tau} = \Pr ob\{x(t) > A\} = \frac{1}{\sigma\sqrt{2\pi}}\int_A^\infty dx \exp[-x^2/2\sigma^2] = \frac{1}{2}erfc(\frac{A}{\sigma\sqrt{2}}) \tag{9.8}$$

where erfc(•) is the complementary error function.

3. The shape of the clipping process between any upcrossing and downcrossing, that is, the shape of w(t) over the clipping interval τ, asymptotically becomes a parabolic arc,

$$f(t) = \frac{1}{2}\ddot{x}(t)[t^2 - \frac{1}{4}\tau^2] \tag{9.9}$$

for $|t| < \tau/2$, and $f(t) = 0$ otherwise.

Based on these asymptotically statistical properties, the clipping-noise waveform can be modeled as a random Poisson pulse train

$$w(t) = \sum_{k=-\infty}^{k=\infty} p(t - t_k; \tau_k) \tag{9.10}$$

with $p(t)$ denoting the parabolic arc given by Equation (9.9), t_k denoting the Poisson clipping times, and τ_k denoting the Rayleigh distributed-clipping intervals.

Another useful relationship, which we will use in the next section, is the area under $f(t)$ which is given by

$$A_\tau = \left[\frac{\dot{\sigma}}{\sigma}\right]^2 \frac{A\tau^3}{12} \tag{9.11}$$

where dσ/dt is given by Equation (9.5).

9.1.2 BER of M-ary QAM Channels Due to Clipping Noise

Now we are ready to discuss the BER performance of M-ary QAM channels in the presence of asymptotic clipping impulse noise and additive white Gaussian noise. The analytical model for M-ary QAM transmission system is shown in Figure 9.2.

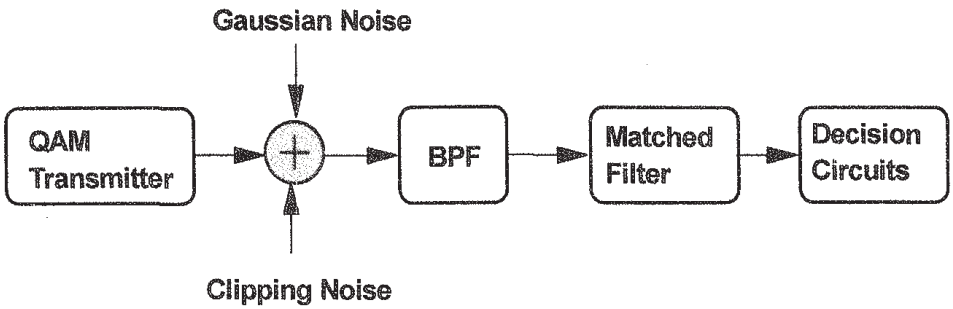


Figure 9.2 Analytical model of an M-ary QAM system in the presence of clipping-induced impulse noise and Gaussian noise (BPF = bandpass filter). After Ref. [6] (© 1995 IEEE).

According to work by Middleton [7], the first-order characteristic function of the clipping noise can be written as:

$$\Psi_I(\xi;t) = \exp(\lambda_A \int_0^\infty \int_0^\infty g(\tau, A_\tau) dA_\tau d\tau \int_{-\infty}^\infty d\alpha \{\exp[j\xi y(t-\alpha;\tau)] - 1\}) \tag{9.12}$$

where $g(\tau, A_\tau)$ is the joint probability function of the random variables τ and A_τ, and $y(t; \tau)$ is the impulse noise output of the QAM receiver, which is given by the convolution of the following terms:

$$y(t;\tau) = p(t;\tau) \otimes h_{BPF}(t) \otimes h_M(t) \tag{9.13}$$

where h_{BPF} and h_M are impulse responses of the bandpass filter (BPF) and matched filter, respectively. Using the Fourier transform on Equation (9.13), the QAM receiver output power is then given by

$$\langle y^2 \rangle = \int_{-\infty}^{\infty} S_p(f) |H_{BPF}(f)|^2 |H_M(f)|^2 df \tag{9.14}$$

where $S_p(f)$ is the power spectral density of the clipping noise, and H_{BPF} and H_M are the Fourier transform functions for the BPF and matched filter, respectively.

To simplify Equation (9.12), let us make the following assumptions:

(A) The average clipping duration interval τ is much smaller than the symbol duration T_s (= 1/B) of M-ary QAM signal in the frequency band of interest. The clipping pulse train can be approximated by

$$w(t) \cong \sum_{k=-\infty}^{k=\infty} A_\tau \delta(t - t_k) \tag{9.15}$$

(B) We assume that the BPF at the QAM receiver is an ideal BPF and the impulse noise power spectral density is flat across the filter band. Thus, Equation (9.13) becomes

$$y(t; \tau) = A_\tau h_M(t) \tag{9.16}$$

With these assumptions, Equation (9.12) simplifies to

$$\Psi_I(\xi) = \exp\left(\lambda_A \int_0^{\infty} g(A_\tau) dA_\tau \int_{-\infty}^{\infty} \{\exp[jA_\tau \xi h_M(t-\tau)] - 1\} d\alpha \right) \tag{9.17}$$

For M-ary QAM channel, the impulse response of the matched filter $h_M(t)$ is either $(2/T_s)^{1/2}$ $\cos(\omega_c t)$ or $(2/T_s)^{1/2}$ $\sin(\omega_c t)$ for $0 \le t \le T_s$ and 0 otherwise for either the I or the Q channel. Substituting $h_M(t)$ in Equation (9.17) and letting $t = T_s$, we obtain the following relation:

$$\Psi_I(\xi) = \exp\{\gamma \int_0^{\infty} [J_0(\xi A_\tau \sqrt{2/T_s}) - 1] g(A_\tau) dA_\tau\} = e^{-\gamma} \exp\{\gamma \langle J_0[\xi A_\tau \sqrt{2/T_s}] \rangle\} \tag{9.18}$$

where $\gamma = \lambda_A t_s$ is sometimes referred to as the clipping or impulsive index, that is, the clipping noise during one symbol interval, $J_0(\bullet)$ is the zero-order first-kind Bessel function, and $\langle \bullet \rangle$ is the expectation value of the function inside the brackets.

Expanding J_0 in power series of γ, and assuming a small probability for clipping ($\gamma << 1$), Equation (9.18) can be further simplified to

$$\Psi_I(\xi) \cong 1 - \gamma + \gamma \cdot [1 + \frac{\gamma C_4 \xi^4}{4^3} \cdot \exp(-\xi^2 \langle A_\tau^2 \rangle / 2T_s) - \frac{\gamma^2 C_6 \xi^6}{2 \cdot 4^3 (3!)^2} \exp(-\xi^2 \langle A_\tau^2 \rangle / 2T_s)] \cdot \exp(-\xi^2 \langle A_\tau^2 \rangle / 2T_s) \tag{9.19}$$

where terms with ξ^8 or higher order have been neglected, and C_4 and C_6 are given by the following equations:

$$C_4 = 72\left\langle A_\tau^2 \right\rangle^2 / T_s^2$$
$$C_6 = 7 \cdot 12^3 \left\langle A_\tau^2 \right\rangle^3 / T_s^3 \tag{9.20}$$

The $1-\gamma$ represents the probability of no clipping during one symbol interval, while the last term represents the probability that clipping occurred in the same symbol interval.

Since the additive Gaussian noise and the clipping noise are statistically independent, the total characteristic function can be written as

$$\Psi_{I+G}(\xi) = \Psi_I(\xi)\Psi_G(\xi) = \left[1-\gamma+\gamma\left\{1+\frac{\gamma C_4 \xi^4}{4^3} e^{-\frac{\xi^2\sigma_I^2}{2\gamma}} - \frac{\gamma^2 C_6 \xi^6}{2\cdot 4^3 (3!)^2} e^{-\frac{\xi^2\sigma_I^2}{2\gamma}}\right\} e^{-\frac{\xi^2\sigma_I^2}{2\gamma}}\right] e^{-\frac{\xi^2\sigma_G^2}{2}} \tag{9.21}$$

where the Gaussian noise variance is σ^2_G, and is given by

$$\sigma_G^2 = B\cdot\left[N_{th}^2 + 2qI_r + RIN\cdot I_r^2\right] \tag{9.22}$$

where N_{th} is the optical receiver noise equivalent current, q is the electronic charge, I_r is the receiver photocurrent, and *RIN* is the laser transmitter relative-intensity noise.

The clipping noise variance is given by

$$\sigma_I^2 = \left\langle y^2 \right\rangle = \lambda_A \left\langle A_\tau^2 \right\rangle = \gamma \left\langle A_\tau^2 \right\rangle / T_s \tag{9.23}$$

The pdf of the total noise (clipping + Gaussian) at the QAM receiver output can be obtained by taking the Fourier transform of Equation (9.21):

$$P_{I+G}(n) = \frac{1-\gamma}{\sqrt{2\pi}\sigma_G} e^{-\frac{n^2}{2\sigma_G^2}} + \gamma\left[\frac{\phi^{(0)}(n/\sigma_{\gamma 1})}{\sigma_{\gamma 1}} + \frac{\gamma C_4 \phi^{(4)}(n/\sigma_{\gamma 2})}{4^3\sigma_{\gamma 2}^5} + \frac{\gamma^2 C_6 \phi^{(6)}(n/\sigma_{\gamma 3})}{4^3(3!)^2\sigma_{\gamma 3}^7}\right] \tag{9.24}$$

where

$$\sigma_{\gamma i}^2 = \sigma_G^2 + i\sigma_I^2/\gamma = \sigma_G^2\left[1 + i/\gamma G\right] \tag{9.25}$$

i = 1,2,3, G is the Gaussian noise to clipping noise variance ratio, and

(9.26)

$$\phi^{(k)}(z) = (-1)^k H_k(z) \frac{e^{-z^2/2}}{\sqrt{2\pi}}$$

where $H_k(z)$ are the Hermite polynomials.

We now can use Equation (9.24) to obtain the probability of error of M-ary QAM channels in the presence of impulsive clipping noise. Assuming independent I and Q channels and Gray coding, the average bit-error probability (BER) at the output of a coherent receiver is given by

$$P_e = \frac{2}{\log_2 M}(1 - M^{-1/2}) \int_{d_{\min}/2}^{\infty} P_{I+G}(n) dn \tag{9.27}$$

where $d_{\min}$ is the minimum distance between adjacent states of M-ary QAM constellation and is given by

$$d_{\min} = 2\sqrt{\frac{3T_s P_{av}}{(M-1)}} \tag{9.28}$$

where P_{av} is the average power per symbol. Using Equation (9.24) in Equation (9.27), carrying out the integration, and applying Equation (9.28), the BER is given by

$$P_e^{I+G} = \frac{2(1-\gamma)}{\log_2 M}\left[1 - M^{-1/2}\right] erfc\left(\sqrt{\frac{3SNR_G}{2(M-1)}}\right) + \frac{2\gamma(1-M^{-1/2})}{\log_2 M}\left[erfc(\frac{\Delta_1}{\sqrt{2}}) - \frac{9\gamma\phi^{(3)}(\Delta_2)}{4(2+\gamma G)^2} - \frac{21\gamma^2\phi^{(5)}(\Delta_3)}{4(3+\gamma G)^3}\right] \tag{9.29}$$

where

$$\Delta_i = \frac{d_{\min}}{2\sigma_{yi}} = \sqrt{\frac{3SNR_G}{(M-1)(1+i/\gamma G)}} \tag{9.30}$$

i = 1,2,3, and SNR_G is the ratio of average energy per information symbol to the Gaussian noise variance of M-ary QAM signal. The first term in Equation (9.29) represents the BER of the M-ary QAM channel due to Gaussian noise, while the second term represents the BER due to clipping noise. Notice from this equation that the BER behavior is mainly affected by three independent parameters: SNR_G, G, and γ. We will see some examples in the next section for these parameters.

The BER model of the transmitted M-ary QAM channels, which was discussed so far, assumes a single-level clipping for directly modulated laser transmitters. However, this model underestimates the clipping noise in externally modulated laser-transmitter-based

transmission systems. The transfer function of the externally modulated laser transmitter can be expanded to a two-level clipping model, in which single-level clipping is a special case [9]. The generalized two-level clipping model for the BER is similar to the model discussed here. It turns out that the first-order approximation to the BER of the transmitted M-ary QAM channels in externally modulated-based systems is twice that of directly modulated-based systems under the same operating conditions. Furthermore, if one clipping level is more than 10% larger than the other clipping level, the two-level clipping model can be closely approximated by the single-level clipping model.

9.1.3 Comparison to Experimental Results

In recent years, many experiments were done to explain the effect of clipping-induced impulse noise on the BER performance of M-ary QAM channels. Maeda, et al., [1] was the first to measure the effect of BER degradation of the 16-QAM channel due to the clipping noise from 42 simulated analog cable TV channels using directly modulated DFB laser transmitter operating at 1310-nm. The AM modulation index per channel was 5% and 6% at

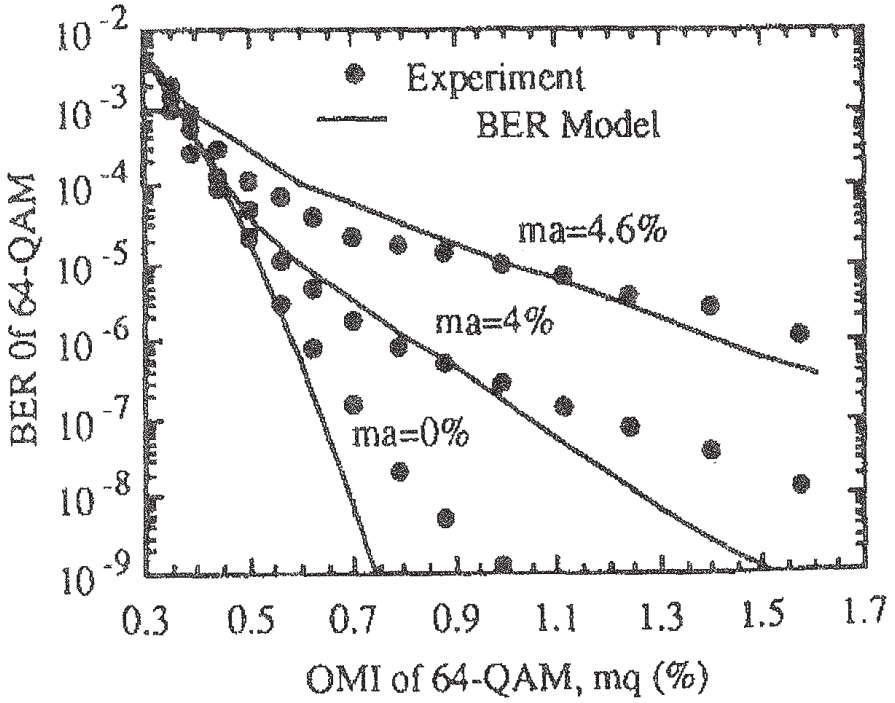


Figure 9.3 Measured and calculated 64-QAM BER as a function of the 64-QAM modulation index at AM modulation indices of 0%, 4%, and 4.6% for a directly modulated lightwave system. After Ref. [8] (© 1995 IEEE).

an optical received power of –1-dBm, and the 16-QAM channel was centered at 601.25-MHz. The calculated BER of the 16-QAM channel was based on Middleton's class A noise model, assuming that the impulsive index is equivalent to the probability of clipping. This assumption it turns out significantly underestimates the impulsive index, resulting in lower BER curves than the measured data. Thus, the validity of the calculated results was questioned. Other authors have obtained good agreement with Middleton's class A model [8–10]. Pham [10], for example, used a directly modulated 1550-nm DFB laser transmitter, which operated at a very large AM modulation index (5–6%) per channel, and thus probably contributed an additional amount of nonlinear distortion in the QAM channel band.

Using the Section 9.1.2 model of the BER of the QAM channel due to clipping-induced impulse noise, Q. Shi [8] calculated the BER of the 64-QAM channel based on the Lu, et al.[3] experimental results. Figure 9.3 shows the calculated and measured 64-QAM BER versus the 64-QAM optical modulation index (OMI) at AM modulation indices of 0%, 4%, and 4.6%. Sixty simulated AM channels (55.25 – 493.25-MHz), according to the US NTSC frequency plan, were transmitted with a single 64-QAM channel centered at 601.25-MHz using a directly modulated DFB laser transmitter. The AM CNR was 52-dB with CSO and CTB distortions less than –60-dBc. Figure 9.3 indicates that a good agreement between the

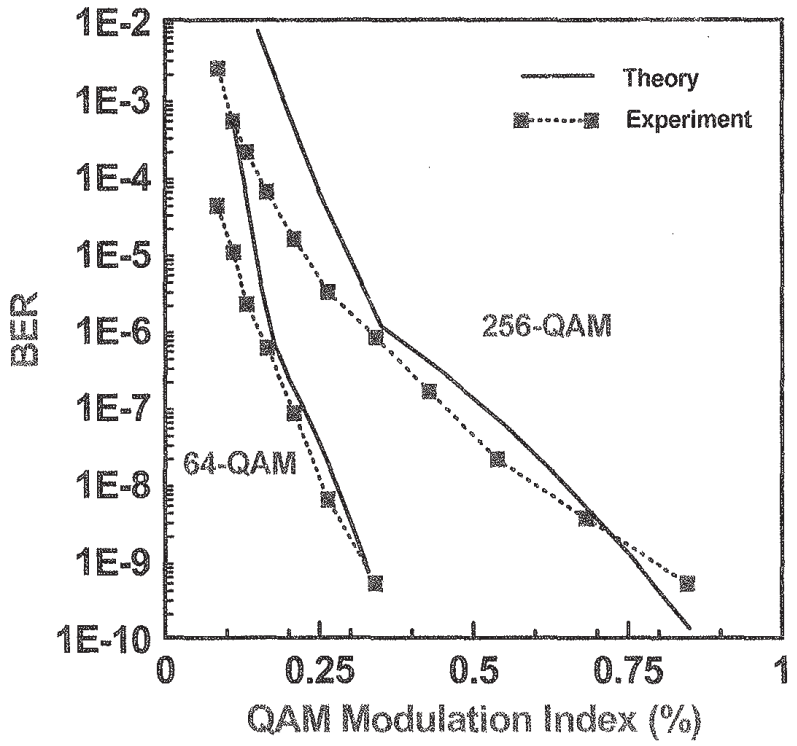


Figure 9.4 Measured and calculated uncoded 64-QAM and 256-QAM BER versus the QAM modulation index for an externally modulated 1550-nm lightwave system with 79 AM channels. After Ref. [4] (© 1995 IEEE).

Table 9.1 The parameters used to calculate the 64/256-QAM BER result in Figure 9.4

Parameter Name	Value
AM CNR	53.66 dB
AM Modulation Index	3 %
QAM Symbol Rate	5 Mbaud
Clipping Index (γ)	$5.3 \cdot 10^{-5}$
G (clipping-to-Gaussian-noise variance ratio)	32.6 dB
Laser Relative-Intensity Noise (RIN_L)	–164 dBc/Hz
Optical Receiver Responsivity	0.85 A/W
Receiver Noise Equivalent Current	$7\text{-pA/(Hz)}^{0.5}$
Received Optical Power	0 dBm
QAM Channel Bandwidth	6 MHz

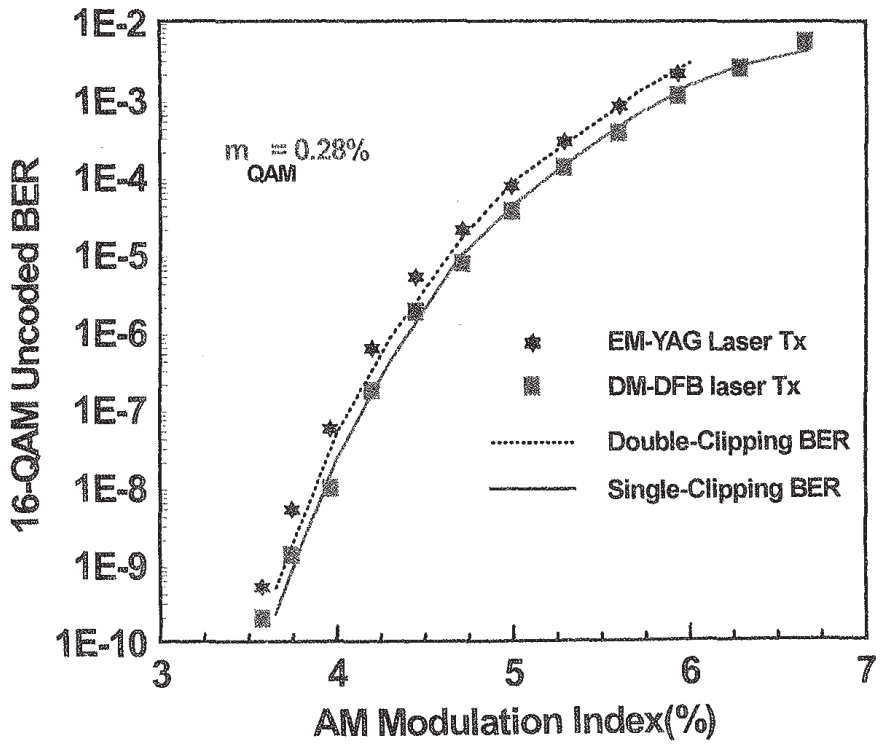


Figure 9.5 Measured (symbols) and calculated (lines) 16-QAM BER versus the AM modulation index for a hybrid 61AM/16-QAM transmission system using a 1310-nm directly modulated DFB laser transmitter and a 1319-nm externally modulated YAG laser transmitter. After Ref. [9] (© 1998 IEEE).

experimental results and the BER model presented in Section 9.1.2 was obtained. Furthermore, the BER of the QAM channel is significantly degraded as the AM modulation index is increased.

An additional comparison between the measured and calculated uncoded 64-QAM and 256-QAM BER versus the QAM modulation index for an externally modulated 1550-nm lightwave transmission system is shown in Figure 9.4. In this experiment, 79 simulated AM channels (55.25–547.25-MHz) along with four QAM channels, which were centered above the AM channels band, were transmitted over 50-km of SMF. The AM CNR was 53.6-dB with CSO and CTB distortions less than –65-dBc. The experimental results are also in good agreement with the calculated 64/256-QAM BER. Table 9.1 lists the parameters used to calculate the uncoded 64/256-QAM BER result in Figure 9.4. The average 64-QAM signal power level relative to the AM signal can be also found from Figure 9.4. Consider, for example, BER = 10^{-8} and AM modulation index (m_A) of 4%. Then, the calculated 64-QAM modulation index (m_{QAM}) is 1.25%. This corresponds to 20·log (1.25/4) ≅ –10 dBc, whereas the experimental result is – 8 dBc (m_{QAM} = 1.53%).

To further understand the difference between the single-level clipping and the double-level clipping BER models, consider the next result. Shi and Ovadia [9] have compared the calculated BER of 16-QAM channel operating at QAM modulation index of 0.28% in the presence of 61 simulated AM channels using the single-level clipping and the double-level clipping models based on the Ovadia, et al., [2] experimental results. The 16-QAM channel was operating at 5-Mbaud and was centered at 539.25-MHz. Figure 9.5 shows the measured and calculated uncoded 16-QAM BER versus the AM modulation index for a 1310-nm directly modulated DFB laser-transmitter-based system and a 1319-nm externally modulated YAG laser-transmitter-based system. The measured BER results are in excellent agreement with the calculated results. As expected, the 16-QAM BER increases dramatically with the AM modulation index. This result also confirms the assumption that the 16-QAM BER in an externally modulated transmission system is approximately twice that of a directly modulated transmission system operating at the same AM and QAM modulation indices.

It should be pointed out that symmetric double-clipping events have been taken into account. It has been shown [9] that the BER of QAM signals in the presence of double-clipping events, to the first-order approximation, is twice the BER from single-level clipping events under the same conditions.

9.1.4 BER of QAM Channel Due to "Dynamic Clipping" Noise

So far, we have discussed the BER of a QAM channel, which was "statically" clipping by the nonlinear transfer function of a laser diode or an optical modulator. In Section 9.1.2, we assumed that the laser diode can be modeled as an ideal memoryless device; that is, the laser output voltage responds instantaneously to changes in its input current. Recent measurements have shown that this is not the case. Figure 9.6 shows, for example, the normalized time dependence of the laser output (solid line) signal after being pulse modulated [11]. The

dashed line shows the input pulse. Notice the significant turn-on delay, which is the difference between the output and input signals and typically varies from 0.3- to 0.5-ns, in addition to the frequency oscillations. This experimental result supports the explanation that dynamic clipping generates frequency-dependent nonlinear distortions that are different from those generated by static clipping. The observed frequency oscillations correspond to the laser resonance frequency. Anderson and Crosby [11] have calculated the uncoded 64-QAM BER as a function of the QAM channel center frequency and compared it with their experimental results. The clipping distortion is modeled as the difference between the clipped output and input signals. This difference can be approximated by a Poisson sequence of random parabolic pulses with a Rayleigh distribution for the pulse width τ. The laser diode is assumed to have a turn-on time delay $\Delta\tau$ independent of τ, after which the laser diode turns on immediately. Neglecting the frequency oscillations, the clipping impulse is approximated as a truncated parabola. Figure 9.7 shows the measured and calculated (solid lines) uncoded 64-QAM BER as a function of the QAM channel center fre-

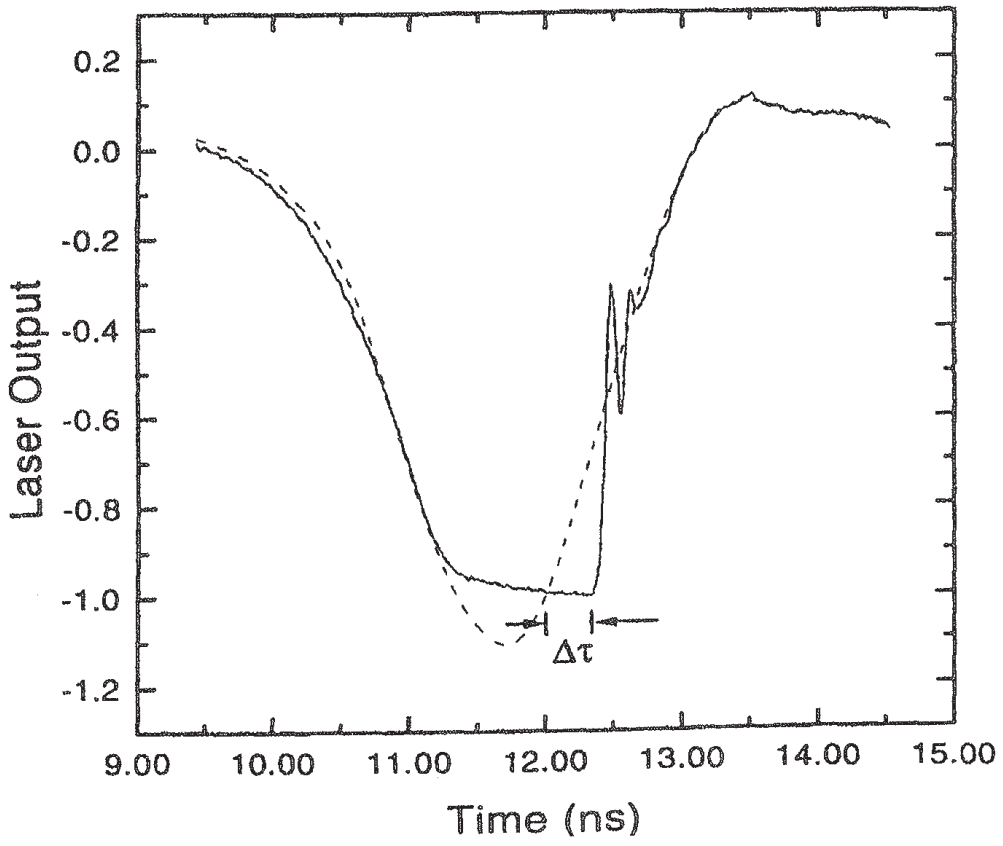


Figure 9.6 Normalized time dependence of the laser output (solid line) after being pulse modulated, showing the turn-on delay. The dashed line shows the input pulse. After Ref. [14] (© 1996 IEEE).

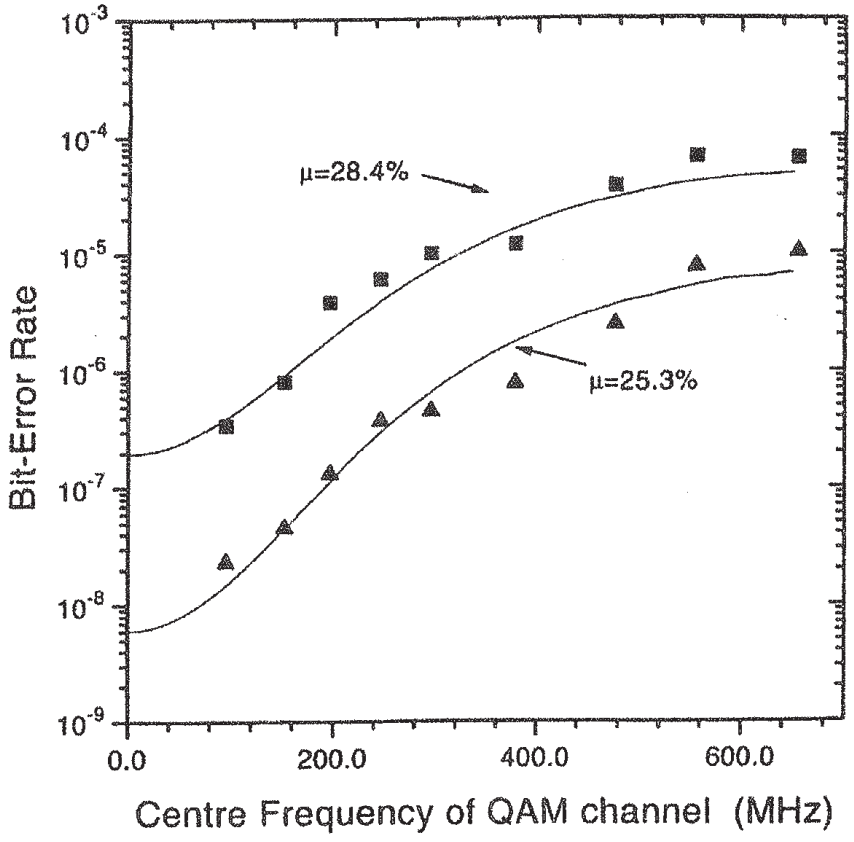


Figure 9.7 The measured and calculated (solid lines) of 64-QAM BER versus the QAM channel center frequency at a total RMS modulation index of 25.3% (triangles) and 28.4% (squares). After Ref. [11] (© 1996 IEEE).

quency for total RMS modulation indices of 28.4% (squares) and 25.3% (triangles), assuming 0.4-ns turn-on delay. Sixty-three simulated AM channels (55.25–555.25 MHz) with a single 64-QAM channel were used to directly modulate a DFB laser transmitter. The 64-QAM channel to the AM channel power ratio was −10 dBc. The 64-QAM channel was operating at 6.25-Mbaud. The BER was calculated based on the stated assumptions, and it is in good agreement with the experimental results. Notice that the observed uncoded BER at 600-MHz is degraded by approximately three orders of magnitude compared with the BER at 50-MHz.

9.1.5 Clipping Noise Reduction Methods

There are various methods, which have been proposed and demonstrated recently, to improve the transmission performance of SCM AM/QAM systems. Several recent works have

introduced the concept of a preclipping circuit to compensate for the statically clipped laser diode [12–15]. In this method [12], the multiplexed AM-VSB signal is preclipped by a limiter in order to avoid below-threshold operation of the laser diode. Then, a bandpass filter is applied to the preclipped signals, since they contain various distortions over a wide frequency band. The filtered and preclipped signals are multiplexed with the digital signals before they are used to drive the laser diode. Since the QAM modulation index is much lower than that of the AM modulation index, the multiplexed preclipped signals do not momentarily drive the laser diode below the threshold. Thus, the QAM channels are transmitted without clipping distortion-induced degradation. This method provides an AM CNR improvement of 1.3-dB.

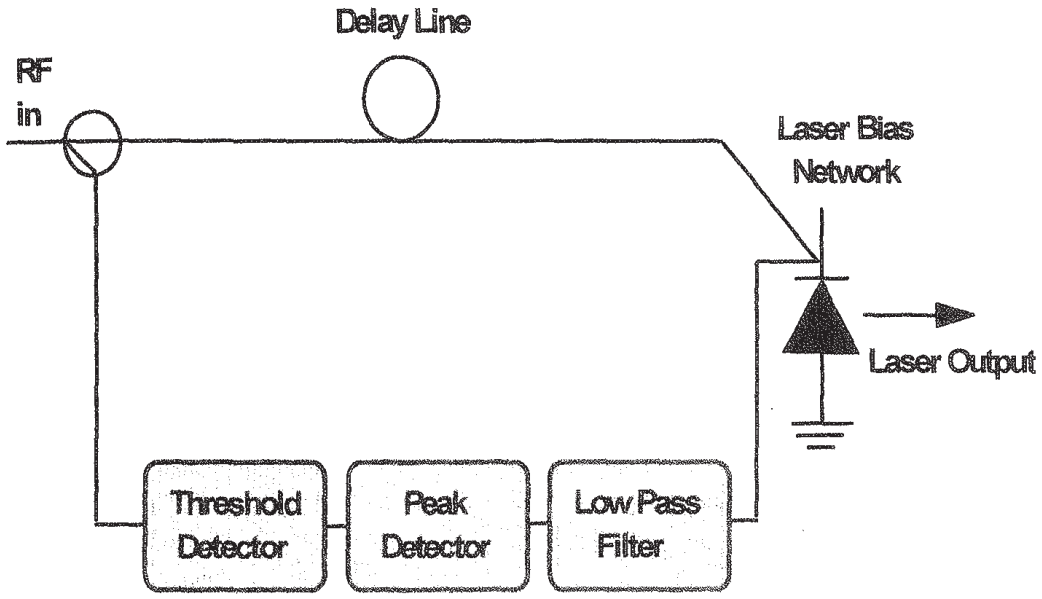


Figure 9.8 Block diagram of the clipping-reduction circuit. After Ref. [12] (© 1995 IEEE).

Another preclipping method [13] uses a bandstop filter instead of a low-pass filter. The bandwidth of the stopband filter spans all the transmitted QAM channels, such that the filter will cut off the preclipping noise in this band. Thus, the preclipped waveform is altered much less than for the low-pass filter case since the bandwidth of the stopband filter is typically much larger. For a stopband of 200-MHz with the preclipping method, the authors calculated that the 64-QAM BER is reduced by more than three orders of magnitude at a QAM modulation index of 0.5% for a directly modulated transmission system with 65 AM channels and one 64-QAM channel centered at 600-MHz. Furthermore, this approach also

applies to other frequency plans, where for example, the QAM channels are located between the AM channels. In this case, the low-pass filter in the preclipping method cannot be used.

Another intrinsically different approach from the preclipping methods to reduce the clipping distortions before the laser diode is shown in Figure 9.8 [14]. In this approach, part of the RF input signal is split and delayed. The clipping-reduction circuit allows the clipping events to be detected, amplified, shaped, and then fed forward to the DFB laser. The laser bias current is then increased momentarily by this current pulse in coincidence with the clipping event. Thus, this scheme permits an increase in the total RMS modulation index in the SCM lightwave system without increasing the magnitude of the clipping distortions. Using this approach, the authors were able to increase the AM CNR by more than 1.5-dB without further degradation of the CSO and CTB distortions for their 80 AM channel transmission system operating at an AM modulation index of 4% per channel. The clipping reduction circuit reduces the required the 64-QAM SNR at BER of 10^{-8} by about 14-dB.

Another approach conceptually similar to the one shown in Figure 9.8 to reduce the clipping distortions is called a dissymmetrization scheme [15]. The difference between the dissymmetrization and the clipping reduction circuits is that the peak detector in Figure 9.8 is replaced by a short-time hold circuit, and an inverting amplifier is added after the low-pass filter before the split signal is recombined with the delayed portion of the RF input signal to drive the DFB laser. The dissymmetrization scheme allows the clipping waveform of the multiplexed AM signal below a given threshold to be detected, low-pass filtered, amplified, and inverted. This signal, which is called the dissymmetrization signal, is then added to the delayed SCM signal to obtain the dissymmetrized SCM signal to drive the laser. The purpose of the short-time hold circuit is to reduce the pulse width variations before the low-pass filtering such that the amplitude of the dissymmetrized signal does not depend on the width of the clipped waveform. The author was able to improve the RMS modulation index by up to 5-dB for an SCM lightwave system operating in the 200–600-MHz band using a 1550-nm directly modulated DFB laser transmitter.

9.2 Bursty Nonlinear Distortions

As we learned in Section 2.5, when AM-VSB video channels are transmitted through a nonlinear device such as a laser transmitter, second-order distortions, namely, $f_i \pm f_2$ type where f_1 and f_2 are two AM channel frequencies, and the third-order distortions, namely, $f_1 \pm f_2 \pm f_3$, are generated. Due to the temporal properties of modulated AM-VSB signals, the CSO/CTB distortions are typically time-varying distortions, which generate burst errors in a hybrid SCM AM/QAM lightwave system. As expected, the burst errors degrade the BER performance of the transmitted QAM channels in the lightwave link [16].

To understand the effect of the bursty behavior of the nonlinear distortions, the following experiment was constructed. Seventy-nine modulated AM-VSB channels were combined with two 256-QAM channels, operating at 40.5-Mb/s at RF frequencies of 571.25-MHz and 643.5-MHz to directly modulate a 1310-nm DFB laser transmitter. A broadband AWGN

source was used in the QAM link for BER-SNR measurements. After transmission through 10.6-km of an SMF, the combined signal was detected at an optical power of 0-dBm at the cable-TV receiver. The AM CNR was 51.8-dB with an average CSO distortion of –56.8-dBc, and a CTB distortion of –60-dBc in the QAM channel band centered at 571.25-MHz. It turns out that the CSO distortion located at 572.5-MHz is the dominant nonlinear distortion in the QAM band centered at 571.25-MHz. The DFB laser transmitter was operating at an AM modulation index of 3.5% per channel with a clipping index $\gamma \approx 4 \cdot 10^{-4}$. As we will see later, CTB distortion is typically the dominant distortion in the QAM band for EM laser transmitter-based lightwave systems. Figure 9.9 shows typical 100-μs time traces of the average (trace A) and peak (trace B) CSO distortion at 572.5-MHz on a spectrum analyzer (SA) in a zero-span mode [16]. In this mode, the SA acts as a sampling oscilloscope. The SA trigger was set to be 30-dB below the 256-QAM carrier and to start the sweep for any event of the peak CSO distortion, which is above the solid line. The 30-

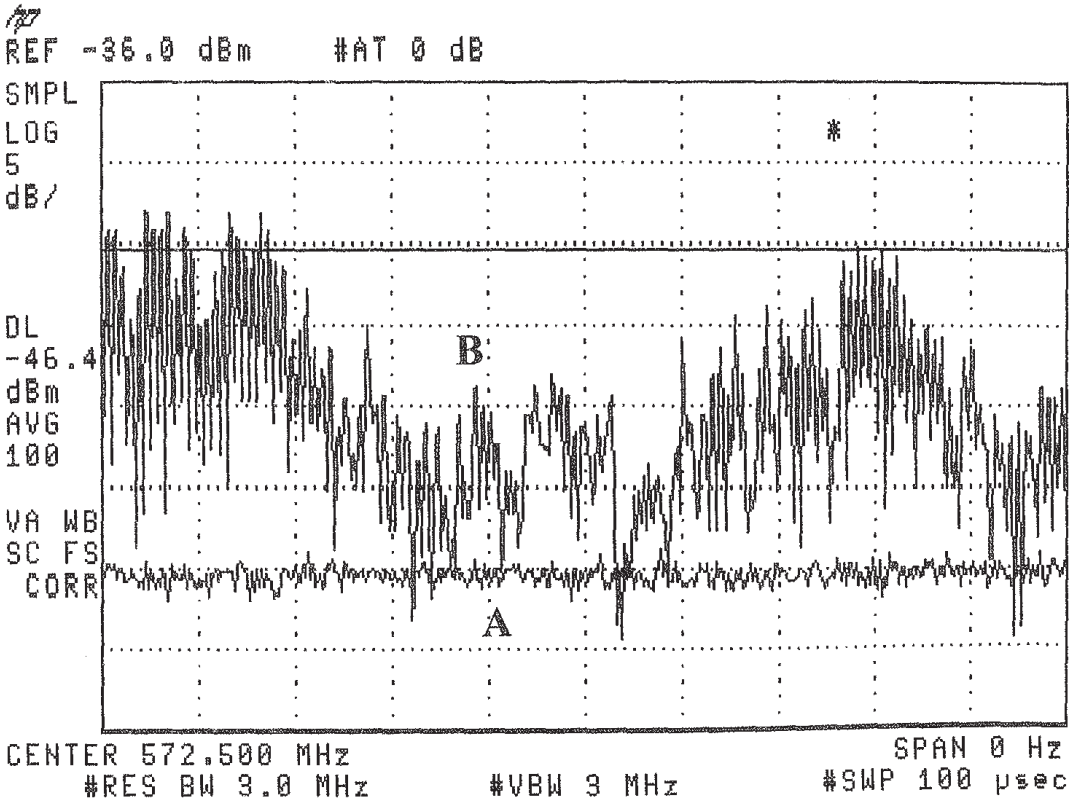


Figure 9.9 Typical 100-μs traces of the average (trace A) and peak (trace B) CSO distortions at 572.5-MHz on a spectrum analyzer in zero span mode. The solid horizontal line is the single sweep trigger for the peak CSO distortion. After Ref. [16] (© 1998 IEEE).

dB 256-QAM CNR corresponds to a coded BER = 1.5 x 10^{-9} in the presence of AWGN. Thus, the trigger line represents the threshold level for impulses with higher amplitudes that would degrade the coded BER above 10^{-9}.

The observed bursty behavior of the peak CSO distortion, which has non-Gaussian statistics, can be explained as follows. Unlike CW carriers from a multitone generator, the peak envelope power of the modulated AM-VSB video signals can vary by as much as 18-dB, depending on the picture content [17]. Furthermore, the synchronization pulses of the AM-VSB channels may temporarily align with each other, causing the corresponding video carriers to be at their maximum power at the same time, resulting in increased CSO/CTB distortions. Thus, the use of CW carriers to simulate modulated video carriers does not accurately represent the time dependence of the peak CSO/CTB distortions.

The use of CW carriers instead of modulated video carriers also affects the laser clipping distortion. In particular, the automatic-gain control (AGC) circuitry in the DM-DFB laser transmitter will maintain the average RF power at a fixed level. Under these conditions, the AGC circuitry reduces the AM modulation indices of the CW carriers by a factor of $\sqrt{\delta}$ ($\delta \approx$

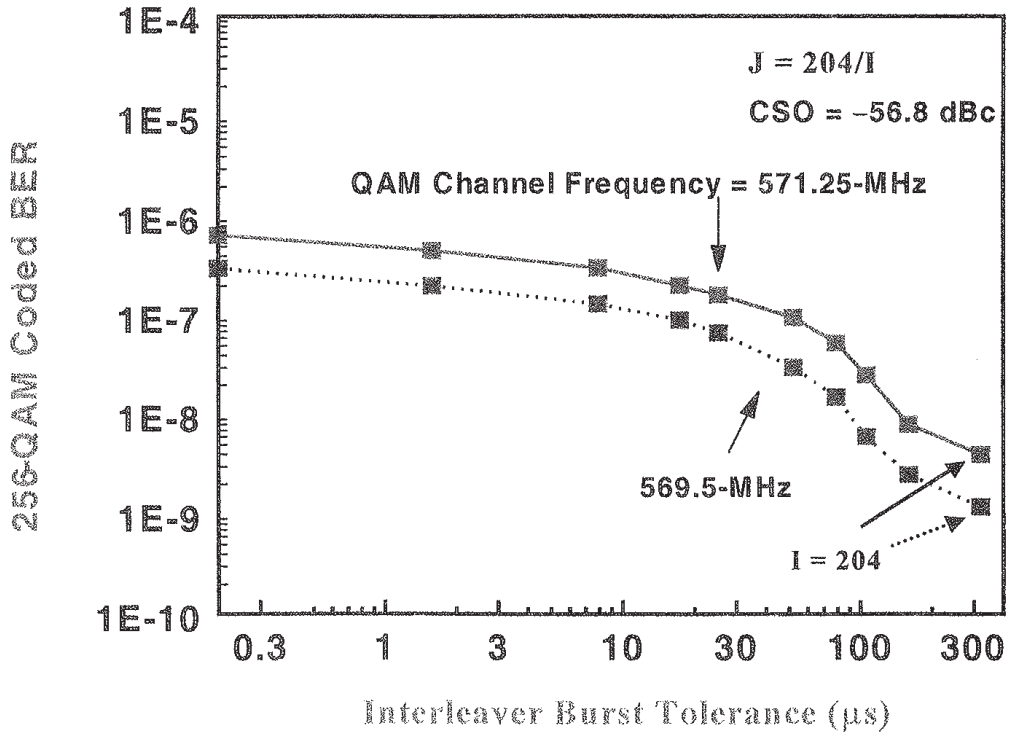


Figure 9.10 Measured 256-QAM coded BER versus the interleaver burst length tolerance with and without QAM channel frequency offset at QAM SNR of 30-dB and CSO distortion of –56.8-dBc. After Ref. [16] (© 1998 IEEE).

0.46), and the corresponding CNR is lowered by a factor of δ (about 3.4-dB) compared with modulated video carriers, resulting in a reduced nonlinear distortion [18].

In order to combat the generated burst errors, a variable convolutional interleaver in the QAM modem, with a depth of up to I = 204 symbols and with J = 204/I symbols, was used with the R-S code [19]. Interleaving the R-S symbols before transmission and deinterleaving them after reception evenly disperses the burst errors in time, and thus the QAM receiver can handle them as if they were random errors. It can be shown that the maximum burst noise tolerance, which is provided by the interleaver and deinterleaver combination, is given by [16]

$$\tau = \frac{(J \cdot I + 1) \cdot T}{R_{RS}} \left[\frac{I}{N} \right] \tag{9.31}$$

where I and J are the interleaver parameters, N = 204 symbols is the R-S block size, R_{RS} is the transmitted R-S symbol rate, and T = 8 symbols. Figure 9.10 shows the measured

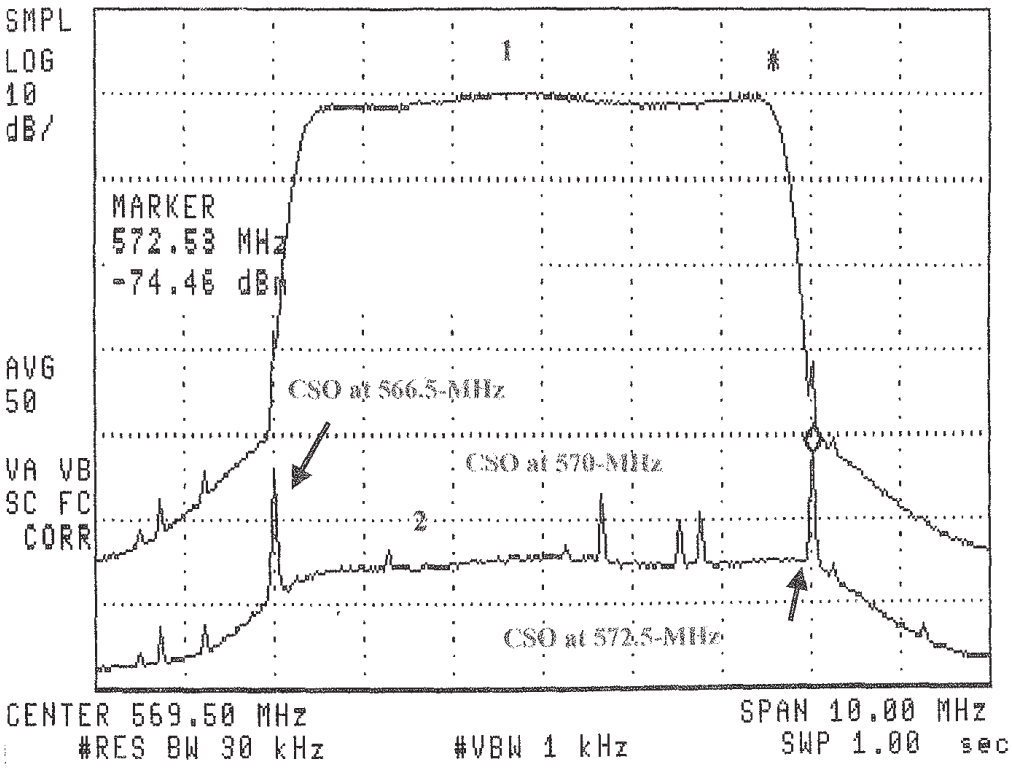


Figure 9.11 The RF spectrum with (trace 1) and without (trace 2) the transmitted 256-QAM channel centered at 569.5-MHz. After Ref. [16] (© 1998 IEEE).

256-QAM coded BER versus the interleaver burst tolerance $\tau(\mu s)$ for QAM channel center frequencies of 571.25-MHz and 569.5-MHz. The 256-QAM SNR was set to 30-dB, corresponding to a coded BER= 1.5×10^{-9} with no AM channel loading. Since the interleaver with I x J = 204 symbols was used, increasing I according to Equation (9.31) results in increasing the burst tolerance of the QAM receiver as shown in Figure 9.10. For the I = 204, J = 1 interleaver mode, the nearly four times reduction in the 256-QAM BER is obtained by the QAM channel frequency offset alone. For a burst duration of 30-μs or less, the 256-QAM coded BER slowly decreases as the interleaver depth is increased, since the average observed burst length is still larger than the maximum burst tolerance of the interleaver/de-interleaver combination. However, as the interleaver burst tolerance becomes significantly larger (≥ 3X) than a burst duration of about 30-μs, most of the generated burst errors are effectively corrected by the interleaver, resulting in a steeper reduction in the coded BER. In fact, the 256-QAM coded BER is reduced by more than two orders of magnitude compared with the no-interleaver case.

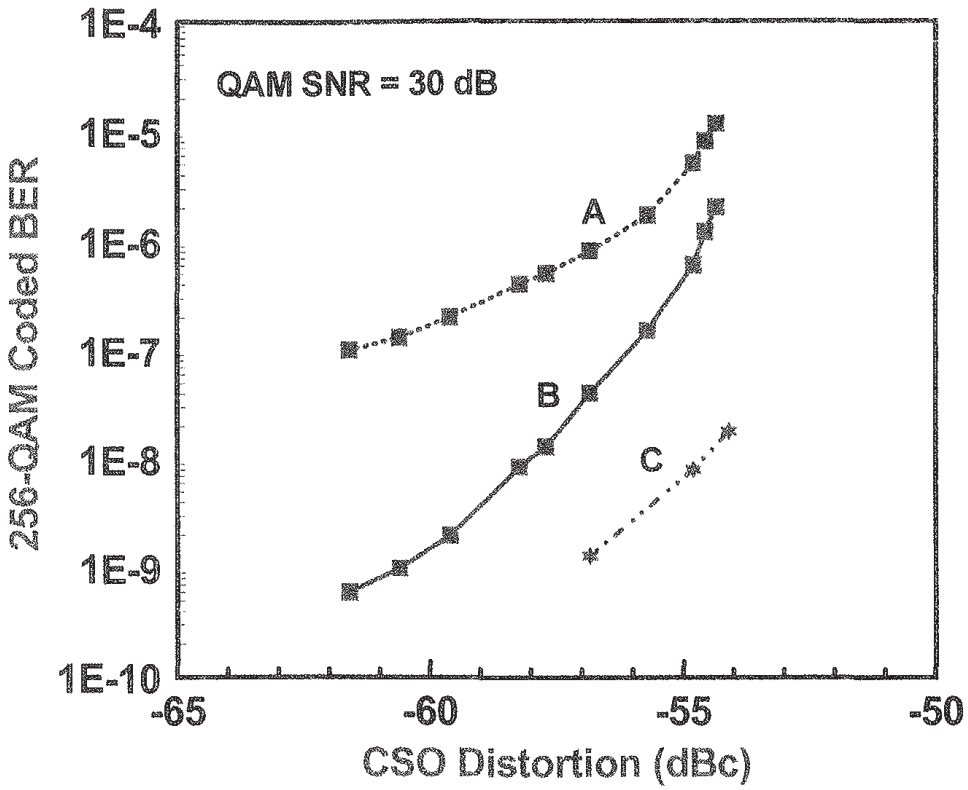


Figure 9.12 The 256-QAM coded BER versus the CSO distortion at 572.5-MHz for (A) no interleaver, (B) I = 68, J = 3 interleaver, and (C) downshifted QAM channel centered at 569.5-MHz and I = 204, J =1 interleaver. After Ref. [16] (© 1998 IEEE).

Examination of the RF spectrum of the transmitted QAM channel centered at 569.5-MHz with the CSO and CTB distortions provides further insight. Shifting the QAM channel frequency down to 569.5-MHz, the dominant CSO distortions at 572.5-MHz and at 566.5-MHz are now located outside the downshifted QAM channel band as shown in Figure 9.11 (trace 2). The other nonlinear distortions in the downshifted QAM band, namely, the CSO distortion at 570-MHz and the CTB distortion at 571.25-MHz, have smaller magnitudes relative to the QAM carrier. If the CTB distortion becomes the dominant distortion in the QAM band, then, a 3-MHz downshift of the QAM channel frequency to 568.25-MHz is required to improve the coded BER. Thus, the 256-QAM coded BER is reduced by more than 500 times to nearly error free using the $I = 204$, $J = 1$ interleaver with QAM channel frequency offset compared with the no-interleaver and QAM channel frequency offset case. The fixed QAM frequency offset method can easily be applied for multiple contiguous QAM channels, where the dominant CSO and CTB distortions will fall in the small gaps between the QAM channels.

Does the interleaver in the QAM receiver work as well at other CSO distortion levels?

To answer this question, the AM modulation index per channel at the laser transmitter was changed while keeping the power ratio between the QAM and the AM-VSB channels constant. Figure 9.12 shows the 256-QAM coded BER as a function of the relative magnitude of the CSO distortion located at a frequency of 572.5-MHz for the following three cases: (A) no interleaver, (B) the $I = 68$, $J = 3$ interleaver, and (C) a downshifted QAM channel to 569.5-MHz with a 30-dB SNR and $I = 204$, $J = 1$ interleaver. Notice that the $I = 68$, $J = 3$ interleaver works best at CSO distortion levels less than –60-dBc. At higher CSO distortion levels, the interleaver is being overwhelmed with burst errors, resulting in BER performance that approaches the no-interleaver case. Consequently, using the $I = 204$, $J = 1$ interleaver with a QAM channel frequency offset can provide robust transmission even in the presence of large CSO distortions (> –55-dBc).

9.3 Multiple Optical Reflections

It is known that multiple optical reflections in optical fiber link degrade the performance of SCM multichannel AM-VSB/QAM video transmission systems due to two or more discontinuities in the index of refraction and a Rayleigh backscattering effect in long fibers [20–25]. The laser transmitter's phase noise fluctuations are converted to intensity noise by interferometric phase-to-intensity noise conversion from multiple reflection points along the fiber link. The effect of multiple discrete optical reflections on the transmission performance of lightwave systems can be minimized using angled polished connectors (APC), fusion splices, and high-return loss fiber-optic components.

Rayleigh scattering is due to microscopic inhomogeneities in the fiber index of refraction along the optical transmission path, which presents a fundamental limitation that cannot be ignored even in a relatively short optical fiber length (≈ 10-km).

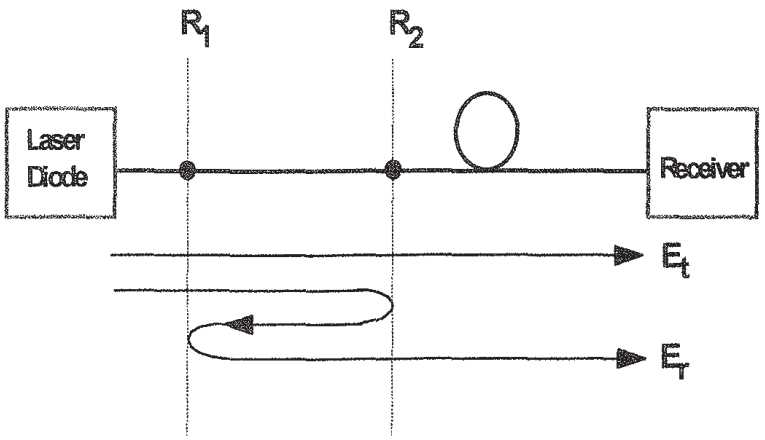


Figure 9.13 Interference intensity noise generated from the interference between the double-Rayleigh backscattered light and the directly propagating light.

Double-Rayleigh backscattering (DRB) is due to the interference between the main propagating optical beam and the doubly reflected optical beam between two adjacent microreflectors (R_1 and R_2) along the fiber as shown in Figure 9.13 [20]. The system impact of the interferometric phase-to-intensity conversion due to DRB and laser RIN will be analyzed first [21]. Then, the effect on the transmitted AM and QAM channels in an SCM multichannel AM/QAM lightwave system will be discussed.

9.3.1 Interferometric Noise Due to DRB

The interference noise between two or more discrete optical reflections is sometimes called interference intensity noise (IIN). For two discrete reflectors, the IIN is proportional to the equivalent reflectance,

$$R_{eq}^2 = P_{12}\eta_{12}R_1R_2 \tag{9.32}$$

where P_{12} is the polarization coupling between reflectors 1 and 2 with reflectance R_1 and R_2, respectively; η_{12} is the fiber loss.

To model the effect of DRB, let us assume that a single fiber with length L is made up of N ($N \to \infty$) equal discrete microreflectors ($L = N \cdot \Delta x$), which reflect light incoherently [20].

Each microreflector has a loss of $\eta = \exp(-\alpha\Delta x)$ where Δx is the differential fiber length, and a reflectivity $R = S\alpha_s\Delta x$, where S is the fraction of the scattered light that is captured by the fiber, and α_s the proportion of the signal scattered per unit length. The N microreflectors form a total of $N(N-1)/2$ Fabry-Perot etalons with a total equivalent reflectance given by

$$R_{eq}^2(N) = \sum_{i=1}^{N-1}\sum_{j=i+1}^{N} P_{ij}R_iR_j\eta_{ij} = PR^2\cdot\frac{\eta}{(1-\eta)^2}\left[N(1-\eta)-(1-\eta^N)\right] \tag{9.33}$$

where P_{ij} is the polarization coupling between the microreflectors i and j. To get the right side result of Equation (9.33), it was assumed that all of the microreflectors have the same reflectivity R, polarization coupling P, and equal spacing between adjacent microreflectors. To show the interaction between the fiber and discrete reflections, Equation (9.33) can be written in the following recursive form:

$$R_{eq}^2(N+1) = R_{eq}^2(N) + R_{N+1}R_{in}(N) \tag{9.34}$$

where the last term represents the increased noise due to the interaction between the added reflector and the original group, whose total reflectance is given by

$$R_{in}^2(N) = PR\left[\frac{1-\eta^N}{1-\eta}\right] \tag{9.35}$$

where, as before, equal spacing between adjacent microreflectors was assumed, and the same reflectivity R and polarization coupling.

Equations (9.34) and (9.35) can be further reduced if one assumes $P = 0.5$ since Rayleigh scattering is randomly polarized. The insertion loss of the micro-reflector is given by:

$$R_{in}^2(L) = \frac{S\alpha_s}{4\alpha}\left(1-e^{-\alpha L}\right) \tag{9.36}$$

$$R_{eq}^2(L) = \frac{1}{2}\left[\frac{S\alpha_s}{\alpha}\right]^2\left(\alpha L-1+e^{-\alpha L}\right) \tag{9.37}$$

where η was approximated as,

$$\eta \approx 1-\alpha\cdot\Delta x \tag{9.38}$$

For a typical 1310-nm single-mode fiber, $S = 0.0015$ and $\alpha = \alpha_S = 0.081$ nepers/km.

9.3.2 Laser RIN Due to Multiple Discrete Optical Reflections

Consider the case of a laser diode operating under CW conditions, where the emitted optical field can be written as

$$E_i(t) = A\exp(i\omega_0 t + \phi(t)) \tag{9.39}$$

where ω_0 is the laser center frequency and ϕ (t) is the laser random phase noise. The light intensity according to Figure 9.13, in which the directly propagating field $(\alpha_1\alpha_2)^{1/2}E_i(t)$ and the doubly reflected light with the same polarization $\alpha_1(\alpha_1\alpha_2R_1R_2)^{1/2}E_i(t-\tau)$ interfere at the optical receiver, is given by

$$I(t) = \left|\sqrt{\alpha}E(t) + R\sqrt{\alpha}E(t-\tau)\right|^2 \cong \alpha|A|^2\left[1+\rho(t,\tau)\right] \tag{9.40}$$

where R is the effective reflection coefficient given by $R = \alpha_1(R_1R_2)^{1/2}$, R_1 and R_2 are the intensity reflection coefficients of the two fiber-optic connectors, $\alpha = \alpha_1\alpha_2\alpha_1$, α_1 and α_2 are optical attenuation coefficients between the connectors and between the second connector and the receiver, respectively, τ is the time delay between the direct and doubly reflected light, and $\rho(t,\tau)$ is given by

$$\rho(t,\tau) = 2R\cdot\cos[\omega_0\tau + \phi(t) - \phi(t-\tau)] \tag{9.41}$$

Thus, ρ contains the interference component of the light intensity I(t). The autocorrelation function of the power spectral density of $\rho(t,\tau)$ is given by

$$S_\rho(t,\tau) = \left\langle \rho(t',\tau)\rho(t'+t,\tau)\right\rangle = 4R^2\left\langle \cos[\omega_0\tau + \theta(t',\tau)]\cdot\cos[\omega_0\tau + \theta(t+t',\tau)]\right\rangle \tag{9.42}$$

The random variable $\theta(t, \tau) = \phi(t) - \phi(t-\tau)$ is normally distributed with $\sigma^2 = 2\pi\tau\cdot\Delta\nu$, where $\Delta\nu$ is the 3-dB Lorentzian linewidth of the laser diode.

It can be shown that the autocorrelation function is given by

$$S_\rho(t,\tau) = 2R^2\begin{Bmatrix} e^{-2\pi\tau\Delta\nu}\cdot[1+\cos(2\omega_0\tau)], & |t|>\tau \\ e^{-2\pi\Delta\nu\cdot|t|}\cdot[1+\cos(2\omega_0\tau)e^{-4\pi\Delta\nu\cdot(\tau-|t|)}], & |t|<\tau \end{Bmatrix} \tag{9.43}$$

The single-sided noise power spectral density is obtained by taking the Fourier transform of Equation (9.43) and subtracting the DC term,

$$RIN(f) = 4R^2\left[1+\left[\frac{-\sin(\gamma f)}{\pi f}\right]e^{-\gamma\Delta\nu}\cos(2\omega_0\tau)\right]+$$

$$\frac{4R^2}{\pi}\left[\frac{\Delta\nu}{f^2+(\Delta\nu)^2}\right]\cdot\left\{1-e^{-\gamma\Delta\nu}\left[\cos(\gamma f)-\frac{f}{\Delta\nu}\sin(\gamma f)\right]-\cos(2\omega_0\tau)\left[e^{-2\gamma\Delta\nu}-e^{-\gamma\Delta\nu}[\cos(\gamma f)+f\sin(\gamma f)/\Delta\nu]\right]\right\} \tag{9.44}$$

where $\gamma = 2\pi\tau$. From Equation (9.44) we can see that the maximum conversion of phase noise to intensity noise occurs when the main propagating light beam interferes in quadrature with the doubly reflected light beam, that is, $\omega_0\tau = (n \pm 1/2)\pi$. This result is given by [22]

$$RIN(f) = \frac{4R_1R_2}{\pi}\left[\frac{\Delta\nu}{f^2+\Delta\nu^2}\right]\cdot\left\{1+e^{-4\pi\tau\Delta\nu}-2e^{-2\pi\tau\Delta\nu}\cos(2\pi f\tau)\right\} \tag{9.45}$$

where R_1 and R_2 are the effective reflectivities of two fiber connectors, $\Delta\nu$ is the 3-dB Lorentzian linewidth of the laser transmitter, f is the frequency, and τ is the time delay between the direct and the doubly reflected light. When $2\pi\Delta\nu\tau << 1$, Equation (9.45) becomes $16\pi R^2\Delta\nu\tau\cdot 2\text{sinc}^2(f\tau)$, which is the limit of small phase fluctuations, and the maximum RIN is proportional to the laser linewidth. In the incoherent interference limit, where $2\pi\Delta\nu\tau >> 1$, Equation (9.45) becomes $(4R^2/\pi)[\Delta\nu/(\Delta\nu^2+f^2)]$. When the laser linewidth is very narrow such as for YAG lasers, the effect of this interferometric RIN becomes negligible for both of these limits. In contrast, the modulated linewidth of the DM-DFB laser transmitter is broad ($\Delta\nu$ > 1GHz), and the interferometric RIN is significantly increased in the presence of high multiple optical reflections (R > –40-dB) due to bad optical connectors. Sections 9.3.3 and 9.3.4 discuss the effect of multiple optical reflections on both the AM-VSB and QAM channels.

9.3.3 Multiple Reflections Effect on AM-VSB Channels

In a typical transmission link, the sources of optical reflections are fiber-optic splices, connectors, and couplers. Figure 9.14 shows a typical multichannel SCM hybrid AM/QAM lightwave transmission system with a frequency-allocation plan [23]. Sixty-one simulated AM channels are combined with a single 16-QAM signal centered at 539.25-MHz to directly modulate either a 1310-nm DFB laser transmitter or a 1319-nm EM-YAG laser transmitter. An additive white Gaussian noise (WGN) source is used for the measurement of BER versus SNR for the QAM channel. Multiple discrete optical reflections are generated by placing two variable back reflectors (VBRs) with a double-loop polarization controller in a 4.4-km of lightwave link as shown in Figure 9.14. The polarization controller is typically used to maximize the phase-to-intensity conversion [21]. The optical isolation between the VBRs and each of the laser transmitters is better than 50 dB. In this measure-

ment, FC/APC SMF connectors (return loss < –60 dB) were used to minimize an additional interferometric noise.

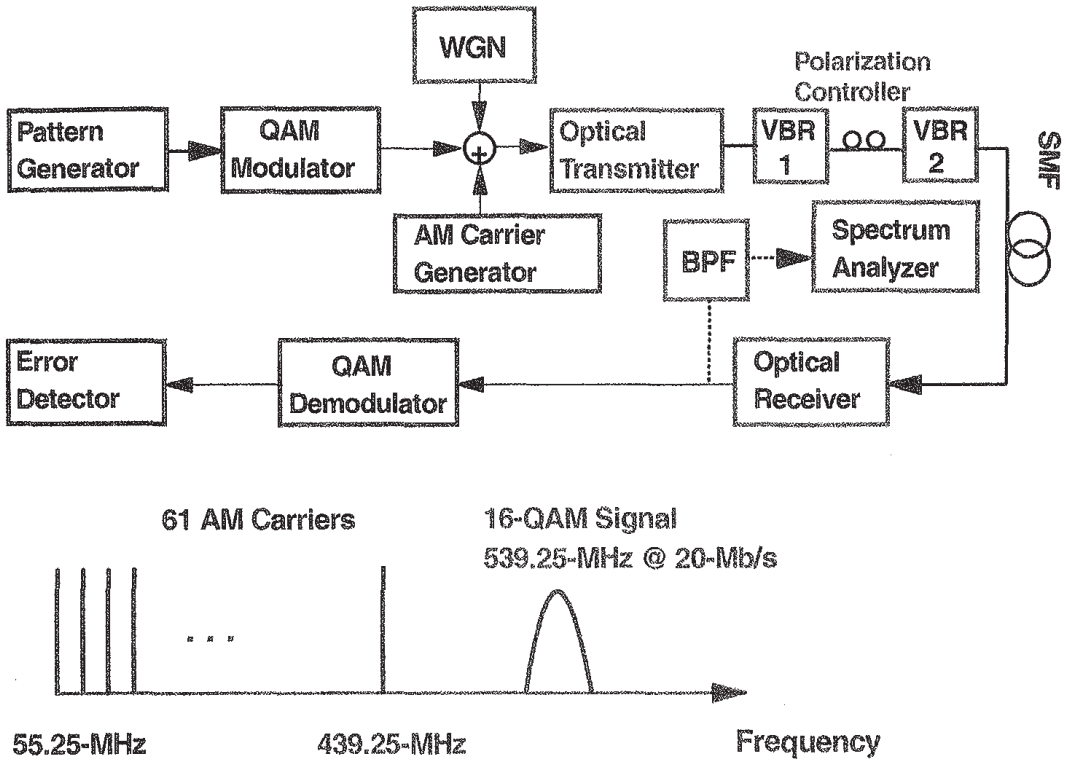


Figure 9.14 Typical experimental setup and frequency-allocation plan. After Ref. [23] (©1994 IEEE).

To provide a fair comparison between the 1310-nm-based laser transmitters, a two-part experiment was conducted [23]. First, the AM modulation index of the DFB laser transmitter was reduced from 4.2% per channel (manufacturer specified optimum value) to 3.3% in order to minimize the clipping-induced impulse noise effect on the BER of the 16-QAM channel. Figure 9.15 shows the AM CNR as a function of the reflection level at channel frequencies of 55.25-MHz, 205-MHz, and 439.25-MHz in lightwave systems using a 1310-nm DM-DFB laser transmitter and a 1319-nm EM-YAG laser transmitter operating at an AM modulation index of 3.3% per channel. Notice that the 53-dB AM CNR drops rapidly for reflection levels greater than –50-dB. At a reflection level of –14-dB, the resultant CNR is only about 20-dB as shown in Figure 9.15. In contrast, the 55-dB AM CNR is reflection independent for the same AM modulation index using the EM-YAG laser transmitter.

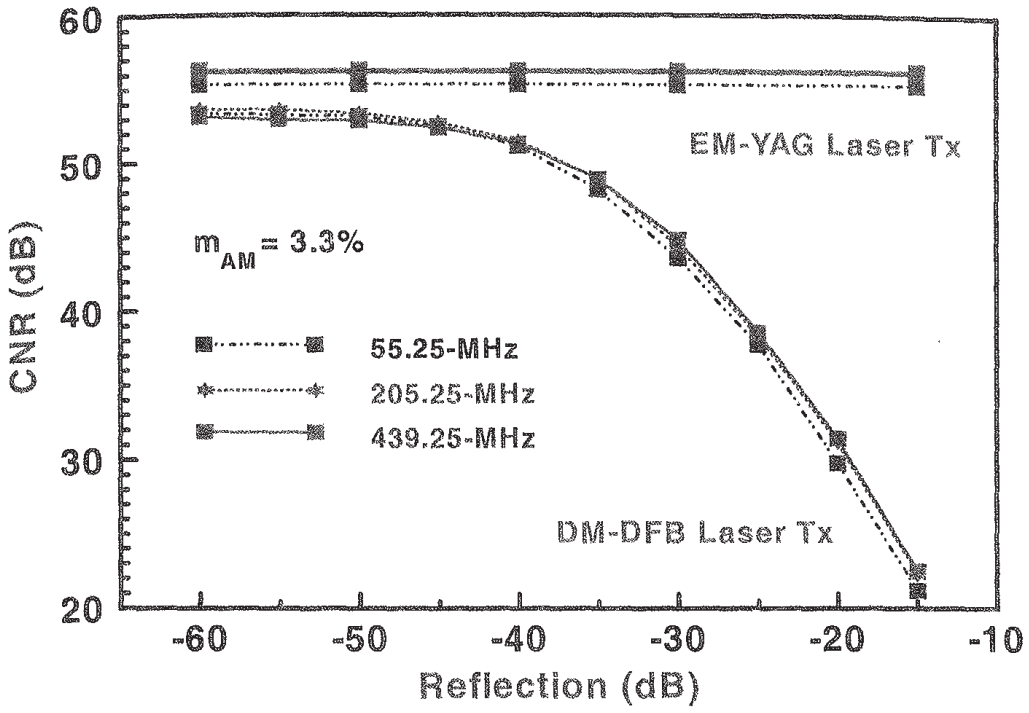


Figure 9.15 CNR versus the reflection level for a directly modulated 1310-nm DFB laser transmitter and a 1319-nm externally modulated YAG laser transmitter operating at an AM modulation index of 3.3% per channel. After Ref. [23] (© 1994 IEEE).

The AM CNR degradation due to optical reflections for the DM-DFB laser transmitter-based systems can be explained as follows: When the AM modulation index per channel is reduced to 3.3%, the interferometric intensity noise (IIN) becomes the dominant noise source. The effective backscatter coefficient of the 4.4-km long SMF is –35.9-dB, compared with the theoretical value of –30 dB for an infinite-length fiber. The IIN is generated from two sources, namely, multiple discrete reflections between the two VBRs and from the fiber's Rayleigh backscatter interacting with those discrete reflections. Thus, an infinite number of "optical cavities" are formed that degrade the lightwave system's performance in the same manner as do cavities formed by discrete reflections. The CNR degradation due to multiple optical reflections in a 1550-nm EM-DFB laser transmitter-based system is different than both previous cases. Figure 9.16 shows, for example, the AM CNR as a function of the reflection level for a 79 AM channel SCM lightwave system. All of the channels were transmitted over a 10.8-km of SMF using a 1550-nm EM-DFB laser transmitter operating at an AM modulation index of 3.2% per channel [24]. This result demonstrates two important new features. First, the CNR of the AM channels exhibits a strong frequency-dependent degradation. Channel 2 (= 55.25 MHz) degrades the most, while channel 79 (= 547.25 MHz) degrades the least. Second, the magnitude of the AM CNR degradation at a given

AM frequency is larger than that of a 1319-nm externally modulated YAG laser transmitter-based SCM system, but less than that of a 1310-nm directly modulated DFB laser-transmitter-based SCM system.

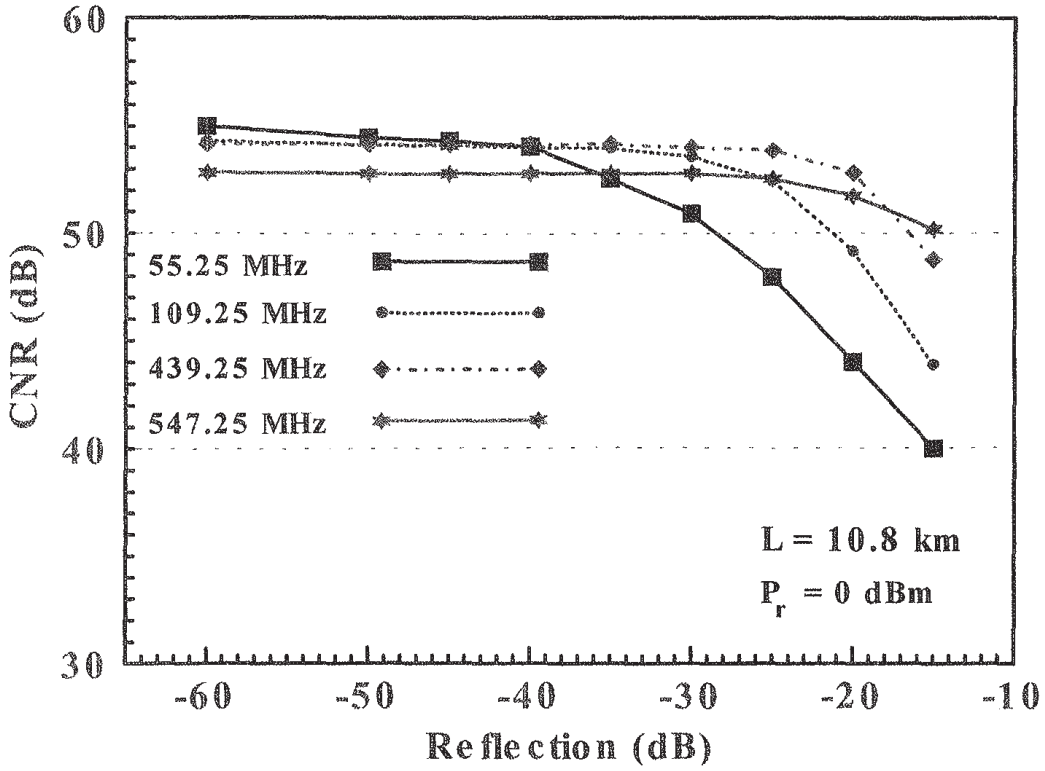


Figure 9.16 CNR versus the reflection level for a 79 AM channel SCM lightwave system using a 1550-nm externally modulated laser. After Ref. [24] (© 1995 IEE).

To understand the AM CNR degradation results, recall from Chapter 5 that the CNR at the optical receiver for an AM-VSB system can be written as

$$CNR = \frac{(m_a I_r)^2}{2B\left[2qI_r + N_r^2 + RIN \cdot I_r^2\right]} \tag{9.46}$$

where m_a is the AM modulation index per channel, I_r is the receiver photocurrent, B is the noise video bandwidth (= 4 MHz), q is the electronic charge, N_r is the receiver noise equivalent current, and RIN is the total relative-intensity-noise in the link. In addition, we recall that the worst-case RIN caused by multiple reflections is given by Equation (9.45). Let us

examine the following two interesting cases. For a very narrow linewidth laser such as the EM-YAG laser transmitter ($\Delta\nu < 10$ kHz), Equation (9.45) is reduced to $(16/\pi)R_1R_2\Delta\nu\cdot\tau^2$, which does not have a frequency dependence. The very low RIN as a result of the narrow linewidth does not degrade the observed AM CNR. In contrast, Equation (9.45) is reduced to $(4/\pi)\ R_1R_2/\Delta\nu$ for a broad modulated linewidth ($\Delta\nu > 1$ GHz) as is the case for a DM-DFB laser transmitter. The high RIN (RIN = −130 dBc/Hz at −15 dB reflection) reduces significantly the observed CNR without frequency dependence. In the intermediate case such as for the EM-DFB laser transmitter ($\Delta\nu = 1$ MHz), the RIN generated from multiple reflections has strong frequency dependence, particularly at the lower cable-TV frequencies based on Equation (9.45).

9.3.4 Multiple Reflections Effect on the QAM Channels

The effect of multiple optical reflections on the QAM channel is even more dramatic [23].

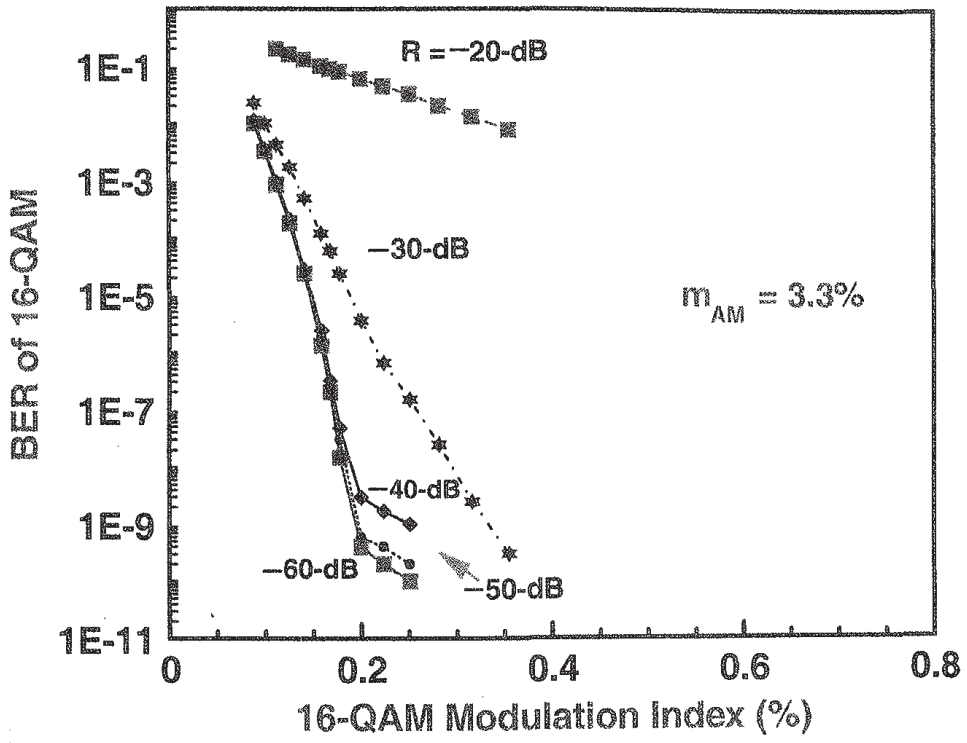


Figure 9.17 16-QAM BER versus the QAM modulation index at reflection levels of −20-dB, −30 dB, −40 dB, −50 dB, and −60 dB for a directly modulated 1310-nm DFB laser transmitter. After Ref. [23] (© 1994 IEEE).

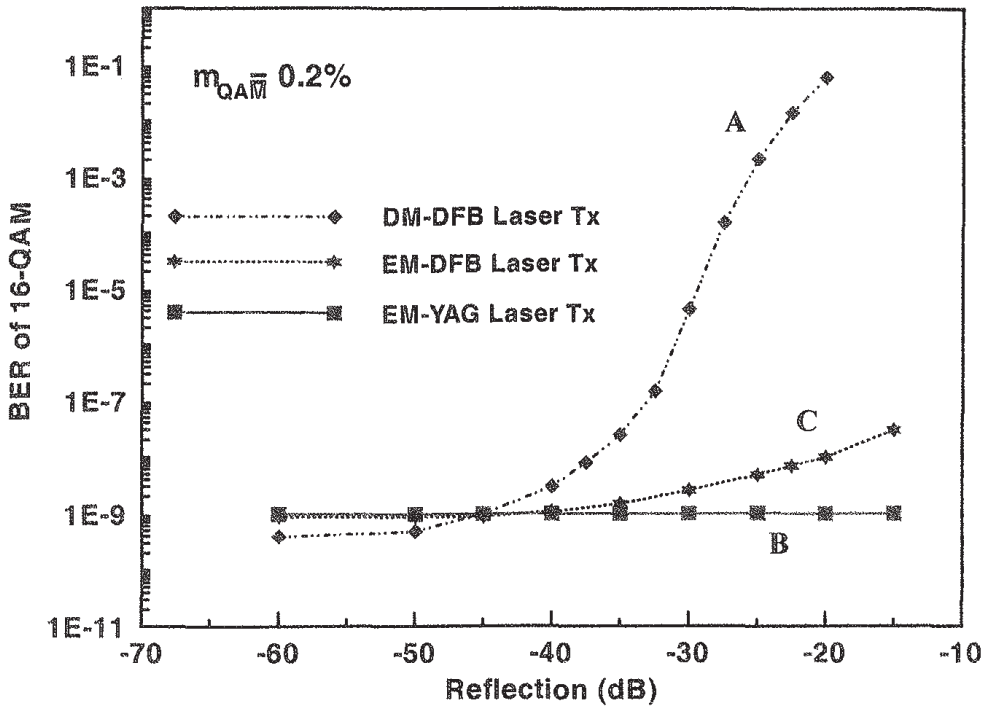


Figure 9.18 16-QAM BER versus the reflection level at 0.2% QAM modulation index for (A) a 1310-nm directly modulated DFB laser transmitter with AM modulation index of 3.3% per channel, (B) a 1319-nm externally modulated YAG laser transmitter at the same AM modulation index, and (C) a 1550-nm externally modulated DFB laser transmitter with AM modulation index of 3.2% per channel. After Ref. [24] (© 1995 IEE).

Figure 9.17 shows, for example, the 16-QAM uncoded BER as a function of the QAM modulation index with an AM modulation index of 3.3% at reflection levels from –60 dB to –20 dB (on both VBRs) for a DM-DFB laser transmitter-based lightwave system. At a –60 dB reflection level, the 16-QAM BER shows only a small impairment due to the clipping-induced impulse noise. As the reflection level is increased to –40-dB, the 16-QAM BER is increased from 10^{-10} to 10^{-9} for a 0.22% QAM modulation index. The 16-QAM BER is significantly increased to 10^{-6} at a reflection level of –30-dB. In fact, one needs twice the QAM modulation index at a reflection level of –30-dB compared with the –60-dB reflection level case to achieve the same 16-QAM BER of 10^{-9}. At a reflection level of –20-dB or higher, the 16-QAM BER is unacceptably high.

In the case of the EM-YAG laser transmitter-based system, the 16-QAM BER is independent of the reflection level, even for high reflections (> –15-dB). It has been argued in a

previous study that the AM video signal and the interference noise are highly correlated [25]. Under standard CNR measurement, when the video carrier is turned off, the noise is also effectively turned off, resulting in no measurable degradation. However, the QAM results support the interpretation that the EM-YAG laser transmitter has a negligible amount of phase noise to be converted to intensity noise, resulting in immunity to even high reflection levels [25]. Only a small 16-QAM SNR degradation (≈ 0.7 dB) is observed for the 1550-nm EM-DFB laser transmitter-based system. The comparison of the QAM BER degradation caused by multiple optical reflections among the different laser transmitters is illustrated in Figure 9.18. The 256-QAM coded BER versus the reflection levels at a QAM modulation index of 0.8% is shown for the following three cases:

(A) DM-DFB laser transmitter with an AM modulation index of 3.3%,
(B) EM-YAG laser transmitter with an AM modulation index of 3.6%, and
(C) 1550-nm EM-DFB laser transmitter with an AM modulation index of 3.2%.

Consequently, the 1319-nm EM-YAG laser-transmitter-based lightwave system has the best immunity to multiple optical reflections for both the AM and the QAM channels.

9.4 Dispersion-Induced Nonlinear Distortions

When a DM-DFB laser transmitter operating at 1550-nm is used in an AM/QAM video light wave link, the laser frequency chirp interacts with the fiber chromatic dispersion to produce nonlinear distortions [26–28]. The fiber chromatic dispersion, which is caused by the wavelength dependence of the index of refraction, is about 17-ps/mn-km at 1550-nm for a standard SMF. As we learned in Section 3.3.2, the gain saturation effect in the DFB laser diode is responsible for its optical frequency chirping. When a DFB laser is amplitude modulated, dynamic wavelength or frequency changes are produced. Because of the fiber dispersion, different wavelengths propagate with different group velocities through the fiber.

A closed-form analytical expression can be obtained by solving the rate equations for the DFB laser using frequency-domain analysis [26, 28]. However, a simpler and more intuitive time-domain analysis will be presented here [27]. Assuming a directly modulated DFB laser by only two RF subcarriers, the injected optical power to the fiber can be written as

$$P_{in}(t) = P_0 + P_0 m\left[\sin(\Omega_1 t + \phi_1) + \sin(\Omega_2 t + \phi_2)\right] \tag{9.47}$$

where P_0 is the average transmitted optical power, m is the modulation index of each subcarrier, and Ω_i and ϕ_i (i = 1, 2) are the frequencies and phases of the two subcarriers, respectively. The transmitted optical power through the fiber can be written as

$$P_t(t) = \alpha \cdot \frac{d(t - \Delta\tau_g)}{dt} P_{in}\left[t - \Delta\tau_g(I)\right] \tag{9.48}$$

where α is the fiber attenuation and $\Delta\tau_g(I)$ is the group delay variation due to the fiber dispersion, which depends on the driving current of the DFB laser. Consequently, $\Delta\tau_g(I)$ is given by the following equation:

$$\Delta\tau_g(I) = D \cdot L \cdot \Delta\lambda(t) \cong D \cdot L \cdot \frac{d\lambda}{df}\frac{df}{dI} I(t) = -\frac{\lambda^2}{c} D \cdot L \cdot \frac{df}{dI} I(t) \tag{9.49}$$

where D is the fiber dispersion, L is the fiber span, and df/dI represents the frequency chirp of the DFB laser. The DFB laser driving current can be written as

$$I(t) = I_{\max}\left[\sin(\Omega_1 t + \varphi_1) + \sin(\Omega_2 t + \varphi_2)\right] \tag{9.50}$$

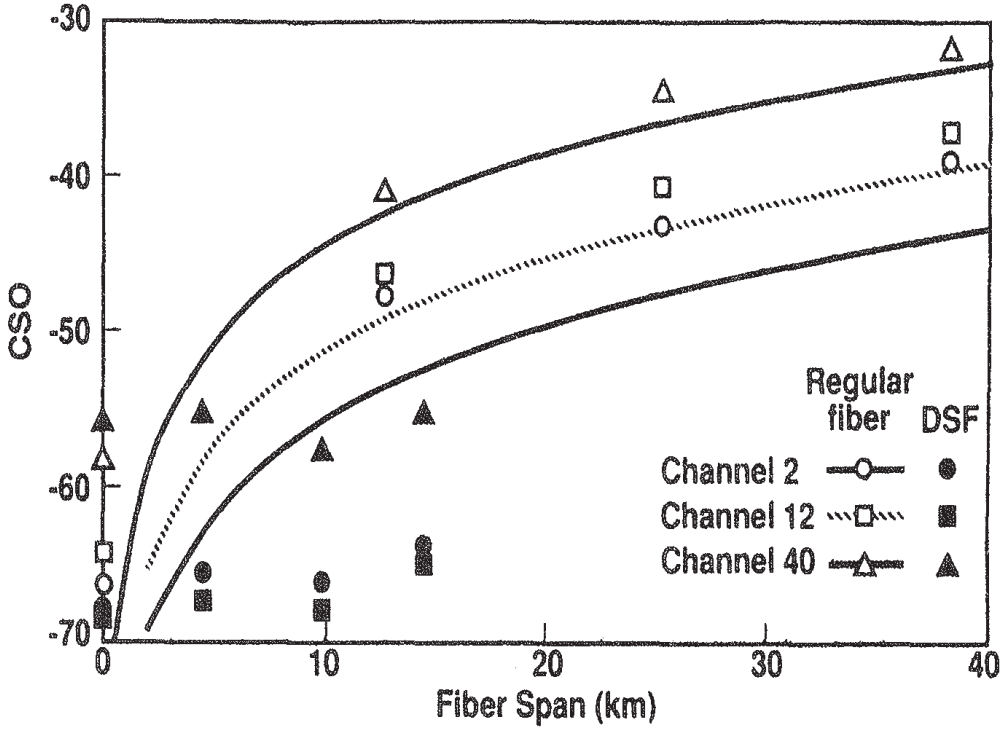


Figure 9.19 Measured (symbols) and calculated (lines) CSO distortion at channel 2, 12, and 40 versus the fiber span for a standard SMF and DSF using a DM-DFB laser transmitter with a chirp of 720-MHz/mA. After Ref. [27] (© 1991 IEEE).

The second term in Equation (9.48) represents the power-level compression or expansion after transmission through the fiber. The last term in Equation (9.48) can be expanded as

$$P_{in}(t-\Delta\tau_g) = P_{in}(t) - \Delta\tau_g \cdot \frac{dP_{in}}{dt} \tag{9.51}$$

where higher orders have been neglected. Substituting Equations (9.49), (9.50), and (9.51) into Equation (9.48), the second-order intermodulation distortion products relative to the subcarrier are given by

$$IM_2 / C = \left[D \cdot L \cdot I_{\max} \left(\frac{\lambda^2}{c} \right) \frac{df}{dI} \right]^2 \cdot (\Omega_1 + \Omega_2)^2 \tag{9.52}$$

For a multichannel video transmission system, the CSO distortions are obtained by multiplying Equation (9.52) by the CSO product counts, N_{CSO}, and replacing $\Omega_1 + \Omega_2$ by the CSO distortion frequency Ω_d as follows:

$$CSO = N_{CSO} \left[D \cdot L \cdot I_{\max} \left(\frac{\lambda^2}{c} \right) \frac{df}{dI} \right]^2 \cdot \Omega_d^2 \tag{9.53}$$

Notice that the CSO distortion is proportional to the square of the distortion frequency, the frequency chirp, the laser driving current, and the fiber dispersion.

Figure 9.19 shows the measured and calculated CSO distortion at channels 2, 12, and 40 versus the fiber span for a 42 AM video channel system using a DM-DFB laser transmitter with a frequency chirp of 720-MHz/mA in both a standard SMF and a dispersion-shifted fiber[1] (DSF) [26]. Notice that an acceptable level of CSO distortion (< –62-dBc) limits the fiber length to only a few kilometers in a standard SMF. This is the primary reason why DM-DFB laser transmitters operating at 1550-nm cannot be used for long-distance transmission over a standard SMF.

There are two main options to overcome this limitation. The first option is to use an EM-DFB laser transmitter operating at 1550-nm, which has a negligible residual frequency chirp from the $LiNbO_3$ MZ modulator. The other option is to use dispersion-compensating fibers or chirped-fiber gratings to compensate for the fiber dispersion and reduce the nonlinear distortions to acceptable levels.

[1] For a dispersion-shifted fiber, the zero-dispersion point is shifted from about 1310-nm to 1550-nm.

9.5 Optical Fiber Nonlinear Effects

In order to achieve longer transmission distances or to provide more fiber splits, higher optical power needs to be launched into the optical fiber. This has been accomplished by the recent development of high-power 1550-nm laser transmitters and high-power in-line EDFAs with output powers as high as +27-dBm. However, the various nonlinear effects in an optical fiber limit the upper bound of the injected optical power in HFC or DWDM access networks. The nonlinear fiber-optic effects can be divided into single-wavelength effects and multiple-wavelength effects. The single-wavelength fiber nonlinearities include the stimulated Brillouin scattering (SBS) effect and self- and external-phase modulation (SPM and EPM) effects, while the multiwavelength nonlinearities include the stimulated Raman scattering (SRS) and cross phase-modulation (XPM) effects.

9.5.1 Stimulated Brillouin Scattering Effect

The SBS effect converts the transmitted optical signal in the fiber to a backward-scattered signal, and thus limits the maximum optical power that can be launched into the SMF. Consider a refractive index grating in the fiber, which is formed by acoustic (sound) waves that are traveling at a velocity of approximately 6-km/s. For a Bragg grating, the grating period is $\Lambda = \lambda/2n = 1.55\text{-}\mu m/2x1.5 \cong 0.516\text{-}\mu m$. The grating scattering is stimulated by the injected optical power in the fiber. In order to conserve energy and momentum, an acoustic phonon is generated at a frequency of 6-km/s/0.516-μm = 11.6-GHz lower than the 1.55-μm incident light for the directly reflected beam. This is known as the Brillouin-Stokes frequency shift. Therefore, the SBS process generates a backward-propagating light beam at a lower frequency than the 1.55-μm incident beam. At low incident optical power levels, the scattering cross section is sufficiently small so that one can neglect the optical power losses. However, above the so-called SBS power threshold, the optical power of the backward-scattered signal increases exponentially when the incident power is increased, leading to significant optical power losses. Based on Smith's condition [29], the SBS power threshold is defined when the backward-scattered power is equal to the injected power, which for a uniform fiber is given by [30]

$$P_{th} = \frac{21\alpha \cdot A_{eff}}{(1-e^{\alpha L})g_0}\left[\frac{\Delta\nu_B \otimes \Delta\nu_L}{\Delta\nu_B}\right] \tag{9.54}$$

where A_{eff} is the effective fiber core area, α is the fiber loss coefficient, L is the total fiber length, and g_0 is the peak Brillouin gain and is given by

$$g_0 = \frac{2\pi K n^7 \cdot p_{12}^2}{c\lambda^2 \cdot \rho_0 V_a \cdot \Delta\nu_B} \tag{9.55}$$

where n is the fiber refractive index, ρ_o is the material density, V_a is the acoustic velocity, p_{12} is the elasto-optic coefficient, and $0.5 < K < 1$ accounts for the optical field polarization. The operator $\otimes$ denotes the convolution of $\Delta\nu_L$, which is the laser linewidth, and $\Delta\nu_B$, which is the spontaneous Brillouin linewidth of the fiber in which the Brillouin gain can be accumulated along the fiber length. For Gaussian profiles, the convolved linewidth is $(\Delta\nu_L^2 + \Delta\nu_B^2)^{1/2}$, while for Lorentzian profiles, the convolved linewidth is $\Delta\nu_L + \Delta\nu_B$. For silica- based fibers, the Brillouin gain bandwidth is about 20-MHz at 1550-nm. Equations (9.54) and (9.55) indicate that the SBS threshold is directly proportional to $\Delta\nu_B$. For a standard SMF, $g_0 = 2\text{x}10^{-9}$ cm/W, and the SBS threshold without modulation is approximately 6-dBm (4-mW) at 1550-nm and 9-dBm (8-mW) at 1310-nm. In addition to the dependence of the SBS threshold on the fiber type and uniformity along its length, the SBS threshold depends on the specific optical system requirements such as modulation format, symbol rate, and modulation type (i.e., direct or external). The effects of SBS on the CNR performance of SCM lightwave system can be demonstrated through the following experimental result shown in Figure 9.20 [31]. The AM and the scattered optical power were measured as a function of the injected optical power in the fiber using a 1550-nm EM-DFB laser transmitter. Forty-two AM-VSB channels with an optical modulation index of 4% per channel were transmitted over 13-km of dispersion-shifted fiber. As injected optical power

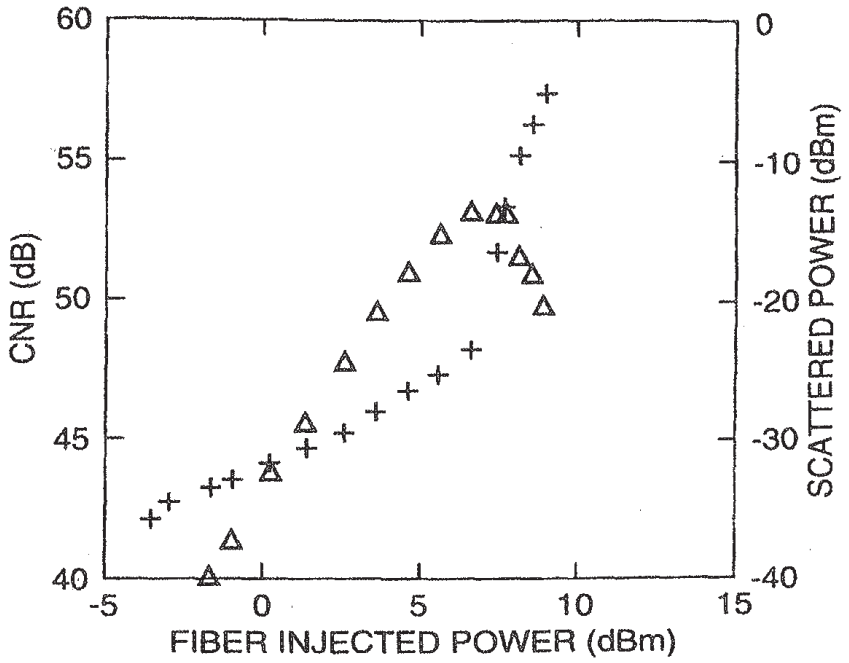


Figure 9.20 Measured CNR (Δ) and the scattered optical power (+) versus the fiber injected power (in dBm). After Ref. [31] (© 1992 IEEE).

is increased above +6-dBm, the SBS scattered power dramatically picks up and the AM CNR rapidly degrades. The SBS also induces CSO and CTB distortion degradations in externally modulated 1550-nm laser transmitters, which are typically used due to the chromatic dispersion degradation (see next section). Since the $\Delta\nu_B$, which is about 20-MHz at 1550-nm for silica fibers, is lower than the NTSC channel 2 frequency, most of the reflected power is frequency independent when the injected power is above the SBS threshold. The CSO and CTB distortions can be approximated by [32]

$$CSO(dB) = 10 \cdot \log\left\{ N_{CSO}\left[\frac{(1-\sigma)m}{4\sigma}\right]^2 \right\} \tag{9.56}$$

$$CTB(dB) = 10 \cdot \log\left\{ N_{CTB}\left[\frac{3(1-\sigma)m^2}{16\sigma}\right]^2 \right\} \tag{9.57}$$

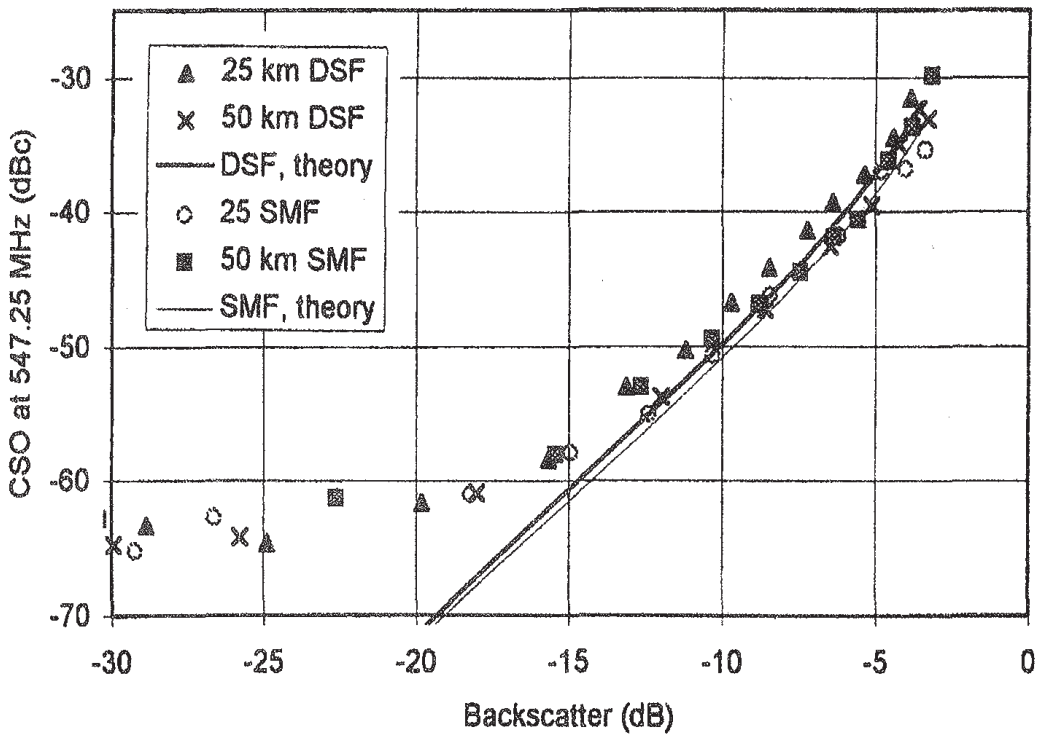


Figure 9.21 Measured (symbols) and predicted (lines) CSO distortion at 547.25-MHz caused by SBS in 25-km and 50-km of both a DSF and SMF. After Ref. [32] (© 1997 Optical Society of America).

where $\sigma = (1 - R_{BS}/0.85)/2$ is the fractional transmission coefficient for the SMF that was empirically estimated from the ratio of the backward-scattered power to the injected power (R_{BS}), m is the modulation index, and N_{CSO} and N_{CTB} are the CSO and CTB product counts, respectively. Figure 9.21 shows, for example, the measured and predicted CSO distortion at 547.25-MHz caused by SBS in 25-km and 50-km of a DSF and a standard SMF versus the backward-scattered power. To maintain the CSO distortion below –62-dBc, the backward-scattered power should be less than –20-dB, corresponding to a SBS threshold power of about 14-dBm, to achieve the necessary phase-modulation index. For a single-tone phase modulation, the increase in the SBS threshold is given by [33, 34]

$$\Delta P_{SBS}^{th}(\beta) = -10 \cdot \log\left[\max_{k\in\{0,1,..\}}\left\{J_k^2(\beta)\right\}\right] \tag{9.58}$$

The effect of SBS can be countered by two methods. In method A, a single tone with a phase modulation at a frequency above about twice the maximum channel frequency (≈1.8 GHz) is used to avoid additional distortions. The phase-modulation method is more effective in reducing the interferometric noise, but requires relatively high electrical powers

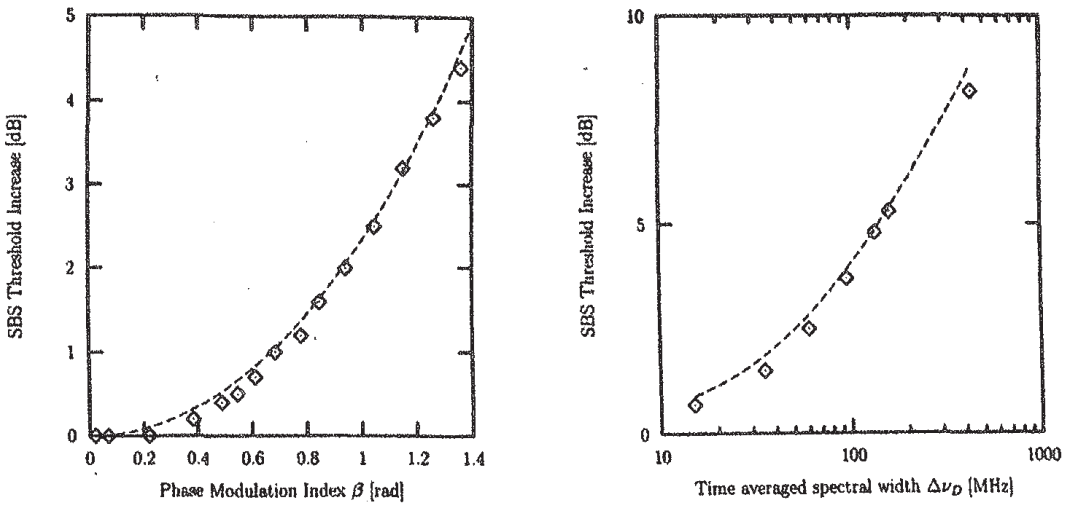


Figure 9.22 Measured (symbols) and calculated (dash lines) SBS threshold increase (dB) versus (A) the phase modulation index (β) using method 1, and (B) the time-averaged effective laser linewidth ($\Delta\nu_D$). After Ref. [33] (© 1994 IEEE).

Figure 9.22(A) shows the measured and calculated SBS threshold increase versus the phase modulation index (β). Using this method, the SBS threshold can be increased by about 10-dB, corresponding to optical injected power of +16-dBm (40-mW) at 1550-nm.

In method B, a low frequency dithering of the optical frequency of the laser transmitter is applied by modulating the laser bias current, resulting in a broader effective laser linewidth. Assuming a Lorentzian linewidth, the SBS threshold power increase can be obtained from Equation (9.47) and is approximated by

$$\Delta P_{SBS}^{th}(\Delta \nu_D) = 10 \cdot \log\left[1 + \frac{\Delta \nu_D}{\Delta \nu_B}\right] \tag{9.59}$$

Figure 9.22(B) shows the measured and calculated SBS threshold increase versus the time-averaged effective laser linewidth. This method can easily provide an SBS threshold above +20-dBm by allowing a frequency excursion above 1 GHz, and requires only a simple low-power laser current modulation. However, there are two possible limitations to this method. First, the package parasitics of high-power DFB lasers limit the maximum frequency of the modulating signal. Second, broadening the laser linewidth beyond 50-MHz may result in the CNR degradation of the transmitted AM channels.

9.5.2 Self- and External Phase-Modulation Effects

The self-phase-modulation (SPM) effect occurs due to the interaction between the fiber's chromatic dispersion and the modulated optical spectrum of the propagating signal in the fiber. Second- and third-order nonlinear distortions of either a DM-DFB or an EM laser transmitter are generated when high-power (below the Brillouin threshold) optical signals are transmitted through a dispersive nonlinear optical fiber [35–37]. The SPM effect is so named since the lightwave signal propagating through the fiber modulates its own phase.

An analytical solution to the SPM induced by CSO and CTB distortions can be obtained using the wave envelope equation in a lossy, dispersive, and nonlinear medium as follows:

$$\frac{\partial A}{\partial z} + \beta_1 \frac{\partial A}{\partial t} - \frac{i}{2}\beta_2 \frac{\partial^2 A}{\partial t^2} + \alpha A = -ikn_2|A|^2 A \tag{9.60}$$

where α is the fiber loss coefficient, β is the propagation constant, $\beta_1 = d\beta/d\omega = 1/v_g^1$ is the first-order dispersion coefficient, $\beta_2 = d^2\beta/d\omega^2$ is the second-order dispersion coefficient, n_2 is the nonlinear refractive index of the fiber; $n = n_o + n_2|A|^2$, where n_o is the fiber refractive index at low optical power, and $A(z, t)$ is the envelope of the propagating electric field represented by

$$A(z,t) = \sqrt{x(z,t)}\exp[iy(z,t)] \tag{9.61}$$

where the electric field is propagating along the z-axis. Substituting Equation (9.61) into Equation (9.60), and requiring that both the intensity modulation information $x(z, t)$ and the phase modulation information $y(z, t)$ are real quantities, the following equations for the intensity and phase are obtained:

$$\frac{\partial x}{\partial z} + \beta_1 \frac{\partial x}{\partial t} = -\beta_2 \left[\frac{\partial x}{\partial t}\frac{\partial y}{\partial t} + x\frac{\partial^2 y}{\partial t^2} \right] - 2\alpha x \tag{9.62}$$

$$\frac{\partial y}{\partial z} + \beta_1 \frac{\partial y}{\partial t} = \frac{\beta_2}{8x^2}\left[-\left(\frac{\partial x}{\partial t}\right)^2 + 2x\frac{\partial^2 x}{\partial t^2} - 4x^2\left(\frac{\partial y}{\partial t}\right)^2 \right] - kn_2 x \tag{9.63}$$

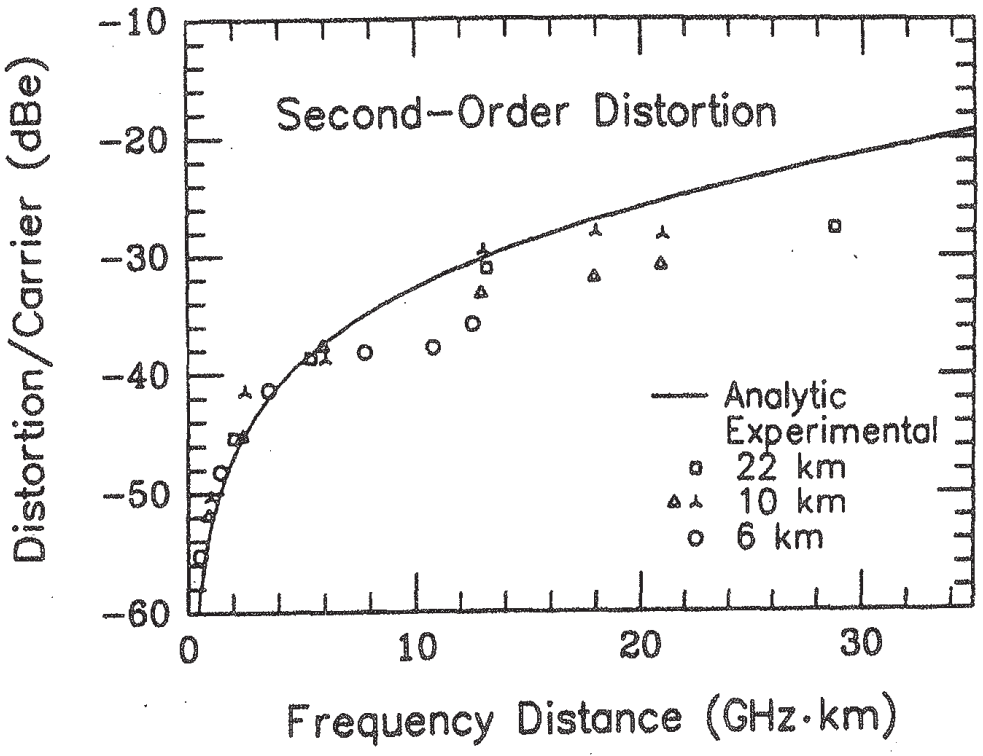


Figure 9.23 Measured second-order distortion due to SPM for a directly modulated DFB laser transmitter with 20-GHz chirp versus the frequency distance product. The solid line is the analytical solution for dual-tone input. After Ref. [36] (© 1991 IEEE).

At the fiber input ($z = 0$), the light intensity and phase are given by

$$x(0,t) = P_0\left[1 + m\sum_{i=1}^{N}\cos(\Omega_i t + \phi_i)\right] \tag{9.64}$$

$$y(0,t) = \gamma m\int_0^t dt'\sum_{i=1}^{N}\cos(\Omega_i t' + \phi_i) \tag{9.65}$$

$$y(0,t) = \beta\sum_{i=1}^{N}\cos(\Omega_i t' + \phi_i) \tag{9.66}$$

where P_0 is the average optical power of the optical signal, m is the modulation index per channel, Ω_i is the subcarrier frequency, and N is the number of cable TV channels. Equation (9.65) applies to a DM-DFB laser transmitter, where $\gamma = G(I_b - I_{th})$ is the laser-chirp parameter (GHz/mA), and I_b and I_{th} are the bias and threshold currents of the DFB laser, respectively. Equation (9.66) applies to an EM-DFB laser transmitter, where β is the phase-modulation index. Substituting Equations (9.64) and (9.65) into the intensity and phase equations (9.62 and 9.63), and after lengthy manipulations, the SPM-induced CSO distortion (CTB distortion is much smaller) is given by [36]

$$CSO_{SPM}(\Omega) = N_{CSO}\left[\frac{mP_0}{2A_{eff}}\left(\frac{L - L_{eff}}{\alpha}\right)\beta_2 k n_2 \Omega^2\right]^2 \tag{9.67}$$

where $\beta_2 = -D\lambda^2/2\pi c$, D is the dispersion coefficient of the fiber (17-ps/nm·km at 1550-nm), A_{eff} is the effective fiber core area, α is the fiber loss coefficient, $L_{eff} = (1 - e^{-\alpha L})/\alpha$ is the effective interaction length, and N_{CSO} is the CSO product count. Figure 9.23 shows the measured and calculated second-order distortion due to SPM for a DM-DFB laser transmitter with 20-GHz frequency chirp versus the frequency distance product for a standard SMF. Since the resulting CTB distortion caused by SPM was more than 30-dB smaller than the CSO distortion, it is neglected here. Figure 9.23 result clearly demonstrates that CSO distortions produced by the SPM effect using a DM-DFB laser transmitter operating at 1550-nm will limit the transmission distance to less than 10-km.

There are three main solutions to the SPM-induced CSO distortions, and they are as follows: (A) using an EM laser transmitter, which has a very low frequency chirp; (B) using a DSF; and (C) compensating for the fiber optic dispersion. Method A is the most widely used in the U.S. since it allows the use of a standard SMF. The other methods are usually more expensive to implement since they require either the installation of a new type of fiber-

optic cables (instead of the standard installed cables) or using complex fiber optic components to compensate for the fiber dispersion.

The specific magnitude of the resultant CSO distortion is determined by the complex interplay of the SPM, the fiber length dispersion, and the sign of the phase-modulation index caused by the external modulator's residual chirp. Desem [37] has shown that the SPM contribution to the CSO distortion could be equal but opposite in sign to the CSO due to its initial phase modulation. Consequently, a total cancellation of the CSO distortion at a particular distance can be achieved. For fiber-optic links around 100-km, the phase modulation caused by the optical modulator's residual chirp is typically not a problem.

A related effect to the SPM is the external phase modulation (EPM) [38]. As previously explained, a high SBS threshold is achieved by applying a high phase-modulation index (β) in the integrated MZI and phase modulator for an EM laser transmitter. The EPM effect is the conversion of this external phase modulation to intensity modulation that interacts with the nonlinear dispersive optical fiber. The EPM effect generates CSO distortions in addition to the SPM effect, and thus needs to be carefully analyzed to correctly predict the resulting CSO distortions, particularly at long distances. For further discussions on EPM and SPM effects in optical links with cascaded EDFAs, see Section 10.1.5.

9.5.3 Stimulated Raman Scattering Effect

As we learned in Chapter 1, wavelength-division multiplexers and demultiplexers are used in HFC networks in order to deliver a mixture of broadcast and narrowcast services to the subscriber's home. The downstream and upstream DWDM architecture for cable TV networks will be discussed in Chapter 10. The analysis in this section concentrates on the crosstalk between two or more high-power WDM channels or wavelengths due to the stimulated Raman scattering (SRS) effect. In SCM WDM lightwave systems, each WDM wavelength is modulated by its own RF subcarrier frequencies.

Let us first consider the simple case of two WDM channels, where each wavelength is modulated by M RF subcarriers [39]. Then, the launch optical power to the fiber is given by

$$P_j(t)|_{z=0} = P_0\left[1+\sum_{i=1}^{M} m\cos(\Omega_i t+\theta_{ji})\right] \tag{9.68}$$

where j = p, s represents the pump (shorter λ) and signal (longer λ) wavelengths, respectively. It is assumed that both wavelengths have the same average optical power P_0, and are modulated with the same set of RF subcarrier frequencies Ω_i, which have the same optical modulation index, m, but random phases θ_{pi} and θ_{si}.

A given SRS interaction is proportional to $g_{ps}P_pP_s$, where g_{ps} is the Raman efficiency between the pump wavelength with power P_p and signal wavelength with power P_s. Substitut-

ing P_s and P_p from Equation (9.68), the total SRS crosstalk from RF subcarrier i at the pump wavelength is composed of the following three terms:

1. $mg_{ps}P_0^2\cos(\Omega_i t + \theta_{pi})$ – This term is due to the SRS interaction between RF subcarrier i at the pump wavelength and the signal wavelength; this is just the optical power loss, $mg_{ps}P_0^2$, of RF subcarrier i.
2. $mg_{ps}P_0^2\cdot\cos(\Omega_i t + \theta_{si})$ – This term is due to the SRS interaction between the pump wavelength and the RF subcarrier i in the signal wavelength. This is the most important SRS crosstalk term in SCM WDM lightwave systems.
3. $(M/8)^{1/2}\, m^2\cdot g_{ps}P_0^2$ – This term is due to the SRS interaction between the RF subcarriers in the pump and signal wavelengths. This term is about one order of magnitude smaller than the first two terms, and thus can be neglected.

It should be pointed out that the SRS interactions between the pump and signal wavelengths cause only DC optical power loss or gain, and thus do not contribute to the SRS crosstalk at the subcarrier frequencies.

An analytical solution to the SRS crosstalk can be obtained by solving the following equations for the pump and signal wavelength in an optical fiber [40]

$$\frac{\partial P_s}{\partial z}+\frac{1}{v_{gs}}\frac{\partial P_s}{\partial t}=(g_{ps}P_p-\alpha)P_s \tag{9.69a}$$

$$\frac{\partial P_p}{\partial z}+\frac{1}{v_{gp}}\frac{\partial P_p}{\partial t}=(-g_{ps}P_s-\alpha)P_p \tag{9.69b}$$

where V_{gs} and V_{gp} are the group velocities of the transmitted light at the signal and pump wavelengths, respectively, and it is assumed that both channels have the same fiber-loss coefficient, α. An analytical solution to Equations (9.69a, 9.69b) is obtained by assuming that the SRS interaction is in the linear regime. The electrical crosstalk level suffered by subcarrier i in the signal or pump wavelength due to SRS is given by

$$XT_i^{sp}=\frac{\left(2g_{ps}P_0\right)^2\left[\left(\frac{\alpha L_{eff}}{2}\right)^2+e^{-\alpha L}\sin^2\left(d_{ps}\Omega_i L/2\right)\right]}{\left[\alpha^2+(d_{ps}\Omega_i)^2\right]\left[1\pm 2g_{ps}P_0L_{eff}\right]^2} \tag{9.70}$$

where $d_{ps} = |1/V_{gp} - 1/V_{gs}|$ is the group velocity mismatch between the pump and the signal wavelengths, L is the fiber length, L_{eff} is the effective fiber length. The right-hand side term

in the denominator (Equation 9.70), where + is for the signal channel and – is for the pump channel, is attributed to the subcarrier loss or gain due to the SRS interaction. With $d_{ps} = 0$, the SRS crosstalk is independent of the subcarrier frequency. Figure 9.24 shows the calculated electrical SRS crosstalk level for two WDM channels with 20-km of a standard SMF at 1300-nm, and at increasing channel spacings from 2- to 16-nm. An effective fiber core area of 50-μm^2 and an optical fiber loss of 0.4-dB/km were assumed. This result demonstrates that crosstalk levels can easily exceed –62 dBc as required for robust AM-VSB transmission even for modest input optical power levels per WDM channel (< +10-dBm). The SRS crosstalk is significantly increased with the number of WDM channels and the optical input power per channel. For example, SRS crosstalk level of –60 dBc is obtained for 4 WDM channels with 4-nm spacing, 20-km of standard SMF, and with optical input power of 0-dBm.

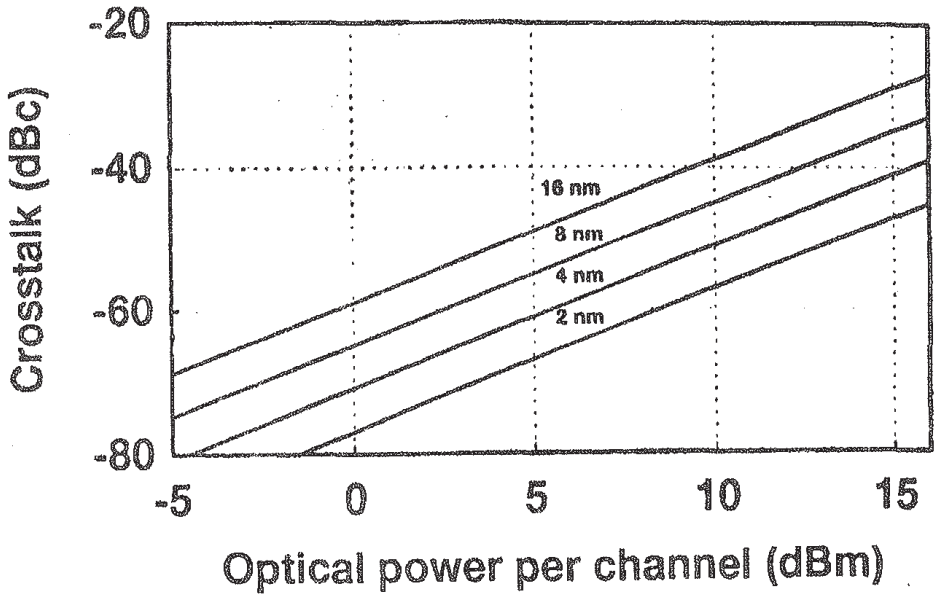


Figure 9.24 Calculated SRS crosstalk level (electrical) versus the input optical power per WDM channel at 1300-nm with two WDM channels and 20-km of standard SMF. The crosstalk dependency for channel spacings of 2-nm, 4-nm, 8-nm, and 16-nm are shown. After Ref. [36] (© 1995 IEEE).

For WDM SCM lightwave systems operating at 1550-nm, the SRS crosstalk is generally lower than in the zero-dispersion case, but it depends on the RF subcarrier frequency. In particular, the SRS crosstalk is lower at higher subcarrier frequencies (≥ 400-MHz) because

the fiber dispersion is significant and can cause walkoff between RF subcarriers at different optical wavelengths.

9.5.4 Cross Phase-Modulation Effect

In a WDM SCM system, the fiber nonlinearities lead to crosstalk between subcarriers on different wavelengths. Due to the fiber dispersion at 1550-nm, the phase of the transmitted signals is converted to intensity modulation leading to the so-called cross-phase modulation (XPM) induced crosstalk [41, 42]. Let us assume two optical waves with the same polarization propagating in a SMF, and let A_1(z, t) and A_2(z, t) be the slowly varying field envelope of each wave, with $\lambda_1 > \lambda_2$. Assuming the slowly varying envelope approximation, the XPM is described in terms of the coupled equations as follows [43]:

$$\begin{aligned} \frac{\partial A_1}{\partial z} + \frac{1}{v_{g1}}\frac{\partial A_1}{\partial t} &= \left[-2j\gamma P_2 - \alpha/2\right]A_1 \\ \frac{\partial A_2}{\partial z} + \frac{1}{v_{g2}}\frac{\partial A_2}{\partial t} &= \left[-2j\gamma P_1 - \alpha/2\right]A_2 \end{aligned} \tag{9.71}$$

where v_{gi} (i = 1, 2) are the group velocities for wave 1 and 2, γ is the nonlinearity coefficient, and α is the absorption coefficient. The normalized XPM crosstalk at λ_1 is given by [43]

$$XT_{XPM_1} = \frac{-2\ddot{\beta}_1\Omega^2\gamma P_c}{\left(\alpha - j\Omega d_{12}\right)^2}\left\{\left[e^{-\alpha L}\cos(\Omega d_{12}L) - 1 + \alpha L\right] + j\left[e^{-\alpha L}\sin(\Omega d_{12}L) - \Omega d_{12}L\right]\right\} \tag{9.72}$$

where β_1 is the phase constant of wave 1, Ω is the RF modulation frequency, P_c is the average optical power, $d_{12} = (1/v_{g1} - 1/v_{g2})$ is the walkoff parameter between wave 1 and 2, and L is the fiber length. A similar expression for the XPM crosstalk at λ_2 can be easily obtained by changing $d_{12} \rightarrow d_{21}$, $\beta_1 \rightarrow \beta_2$. Notice that the XPM-induced crosstalk at both λ_1 and λ_2 have the same sign. In contrast, the SRS-induced crosstalk at λ_1 is 180° out of phase with the SRS-induced crosstalk at λ_2. This is because shorter wavelengths provide gain for the longer wavelengths through the SRS interaction. Thus, subcarriers at λ_1 acquire SRS crosstalk through gain, while subcarriers at λ_2 acquire SRS crosstalk through depletion. The total observed crosstalk is the combination of the SRS-induced and the XPM-induced intensity modulations. The SRS-induced crosstalk and the XPM-induced crosstalk are in phase for λ_1, but out of phase for λ_2. Figure 9.25 shows the measured and calculated total crosstalk versus the modulation frequency at λ_1 = 1546-nm, where λ_2 = 1542-nm, P_c = 17-dBm, and L = 25-km [43]. The crosstalk is dominated by the XPM effect. The solid line

represents the calculated total crosstalk, while the dashed lines represent the SRS and XPM crosstalk contributions. At low modulation frequencies or large $\Delta\lambda = |\lambda_1 - \lambda_2|$, the crosstalk is dominated by the SRS effect, and at high modulation frequencies or small $\Delta\lambda$, the crosstalk is dominated by the XPM effect. At λ_1 and at modulation frequency of about 600-MHz, the SRS-induced crosstalk is added in phase with the XPM-induced crosstalk, increasing the total crosstalk (XPM + SRS) by about 20-dB compared with their out-of-phase crosstalk contributions.

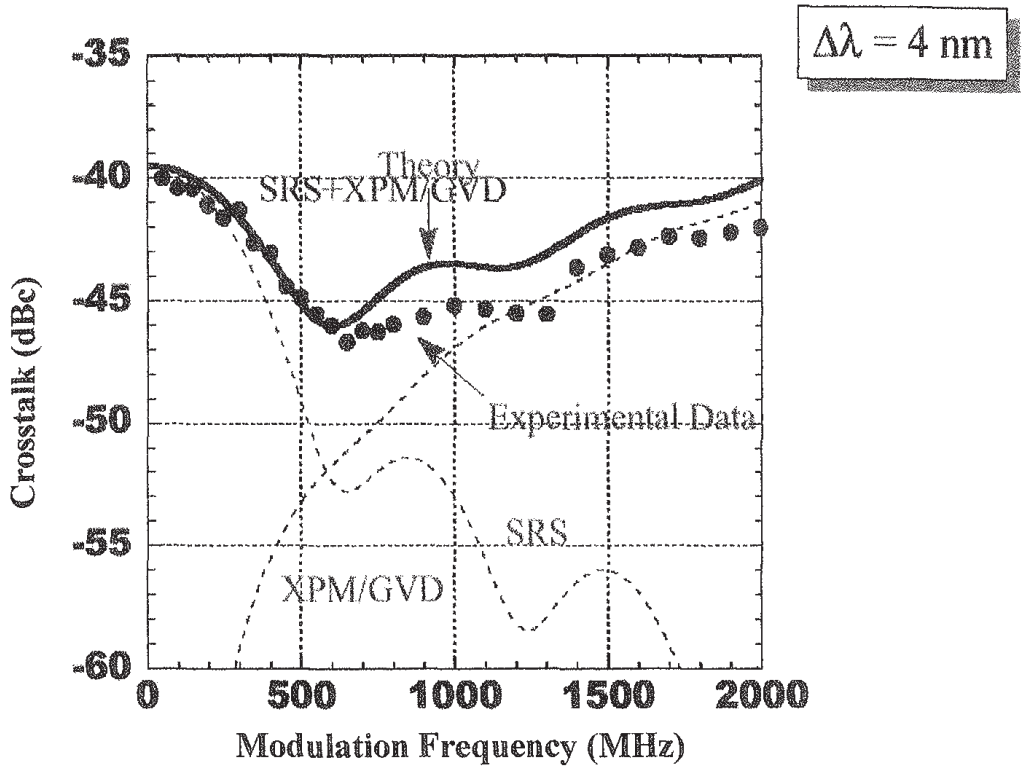


Figure 9.25 Measured (solid circles) and calculated (lines) crosstalk level versus the modulation frequency at λ_1 for $\Delta\lambda$ = 4-nm, P_c = 17-dBm, and L = 25-km. The solid line represents the total crosstalk level from both SRS and XPM. After Ref. [43] (© 2000, IEEE).

9.6 Polarization-Dependent Distortion Effects

In the polarization-dependent distortion effects, which were first reported in 1992 [44–46], the magnitude of the CSO or CTB distortion levels depends on either the polarization of the

input light beam to the fiber, or to the optical isolator, or to cascaded in-line EDFAs. The polarization-induced nonlinear distortions in cascaded EDFAs will be explained in Section 10.1.5, when the performance of AM video trunking links is discussed.

Optical isolators, as was explained in Section 3.1 on the DFB laser module, are passive, nonreciprocal optical devices based on the Faraday effect. Birefringent optical crystals with a thickness of about 5-mm are typically used. Optical isolators can be divided into two groups: isolators with an optical isolation that are either sensitive or insensitive to the input polarization state. The type-A isolator separates the input port from the backward-reflected light. In a type-B isolator, the effective numerical aperture of the reflected light is much higher than that of the input port. The mechanism of the polarization-induced distortion in

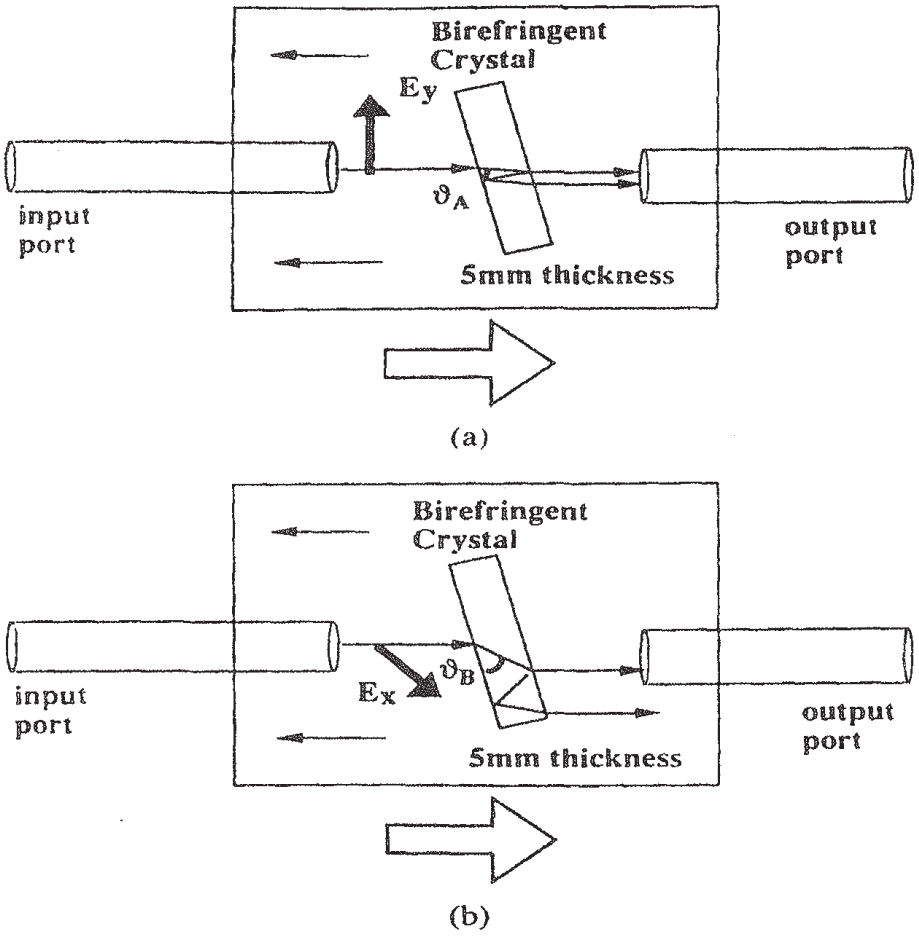


Figure 9.26 Mechanism of the polarization-dependent distortion in optical isolators when (a) multiple optical reflections are injected into the output port and (b) multiple optical reflections are not injected to the output port. After Ref. [45] (© 1994 IEEE).

optical isolators is illustrated in Figure 9.26. The birefringent crystal is typically rotated by a small angle relative to the input light beam to avoid specular reflection at the front facet of the crystal. Some of the multiple optical reflections are transmitted through the back facet of the birefringent crystal, depending on the orientation of the input beam's electric field. A Birefringent crystal has two optical axes, which are typically referred to as the "slow" and "fast" axes with corresponding refractive indices. θ_A and θ_B denote the refraction angles at the front facet of the birefringent crystal for the two input light polarization states, respectively. For a vertically polarized light (smaller refraction angle), the main propagating beam as well as some of the reflected beams are coupled into the output port of the fiber as shown in Figure 9.25(a). The doubly reflected beam (higher order reflections are neglected) will be relatively delayed compared to the main propagating beam, and thus generates interferometric interference, as we learned in Section 9.1.2. For DM-DFB laser transmitters, the interaction between the laser frequency chirp with polarization-induced multiple optical reflections

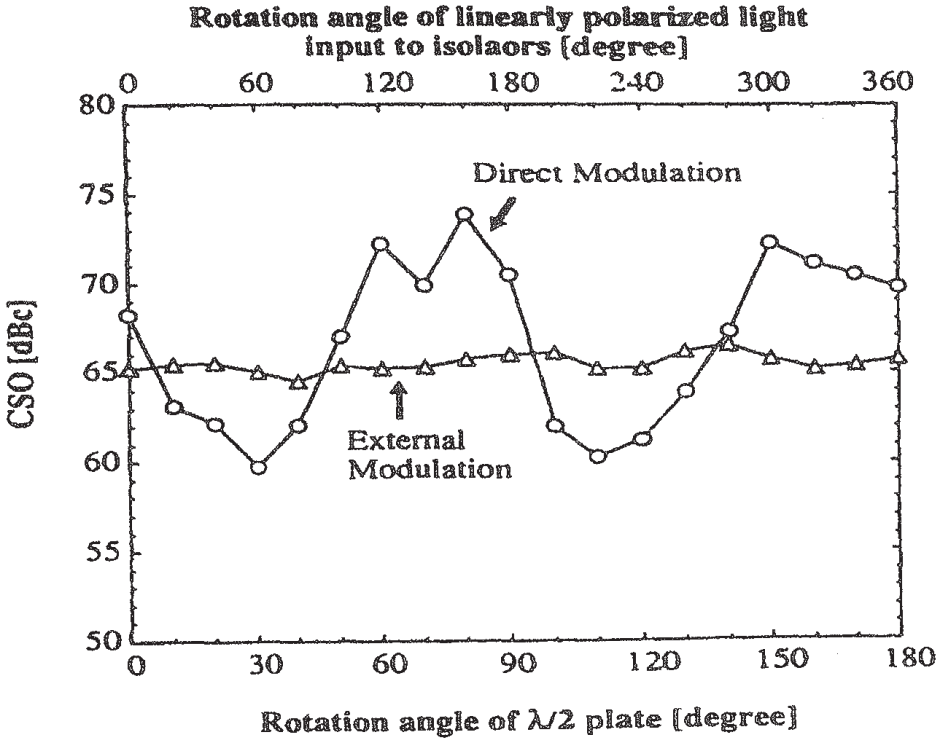


Figure 9.27 measured CSO distortions versus the rotation angle of λ/2 plate for type-A isolator using a direct-modulation scheme (circles) and an external-modulation scheme (triangles). After Ref. [45] (© 1994 IEEE).

will generate nonlinear distortions, mainly CSO distortions. In contrast, for the horizontally polarized light (larger refraction angle), only the main propagating beam is coupled into the output port of the fiber as shown in Figure 9.26(b). This type of polarization-induced nonlinear distortion can be avoided by using EM laser transmitters.

To understand the performance differences between using a direct modulation and external modulation of a laser transmitter, let us examine the following result. Figure 9.27 shows the measured CSO distortions versus the rotation angle of linearly polarized light into a type-A isolator under both a direct-modulation scheme (circles) and an external-modulation scheme (triangles). Notice that while the CSO distortion changes by only a few decibels, the CSO distortion varies by almost 15-dB. Kikushima, et al. [45] have also reported that the CSO distortion levels induced by SBS effect can vary by about 5–7 dB, depending on the polarization state of the input light in a fiber optic link. This is attributed to a factor of two higher Brillouin gain when linearly polarized light is input compared with circularly polarized light [47]. The degradation issues in the transmission of AM/QAM video signals due to polarization-induced nonlinear distortions in cascaded EDFAs, which typically use many optical isolators, are discussed in more detail in Chapter 10 on AM video lightwave trunking links.

References

1. K. Maeda, H. Nakata, and K. Fujito, "Analysis of BER of 16QAM Signal in AM/16QAM Optical Transmission System," *Electronics Letters* **29**, 640–641 (1993).
2. S. Ovadia, L. Eskildsen, J. T. Sciarabba, C. Lin, and W. T. Anderson, "Bit-Error-Rate Impairment in Hybrid Multichannel AM-VSB/16-QAM Video Lightwave Transmission System," *IEEE Photonics Technology Letters* **7**, 869–871 (1994).
3. X. Lu, G. E. Bodeep, and T. E. Darcie, "Broadband AM-VSB/64-QAM Cable TV System over Hybrid Fiber/Coax Network," *IEEE Photonics Technology Letters* **7**, 330–332 (1994).
4. S. Ovadia, H. Dai, C. Lin, and W. T. Anderson, "Performance of Hybrid Multichannel AM/256-QAM Video Lightwave Transmission Systems," *IEEE Photonics Technology Letters* **7**, 1351–1353 (1995).
5. Q. Shi, "Asymptotic Clipping Noise Distribution and Its Impact on M-ary QAM Transmission over Optical Fiber," *IEEE Transaction on Communications* **43**, 2077–2084 (1995).
6. J. E. Mazo, "Asymptotic Distortion Spectrum of Clipped, DC-Biased Gaussian Noise," *IEEE Transactions on Communications* **40**, 1339–1344 (1992).
7. S. O. Rice, "Distribution of the Duration of Fades in Radio Transmission," *Bell System Technical Journal*, vol.**37**, 581–635 (1958).

8. Q. Shi, R. S. Burroughs, "Hybrid Multichannel Analog/Digital CATV Transmission Via Fiber Optic Link: Performance Limits and Trade Offs," *NCTA Technical Papers*, 182–193 (1994).
9. Q. Shi and S. Ovadia, "Effects of Clipping-Induced Impulse Noise in Externally Modulated Multichannel AM/M-QAM Video Transmission Systems," *IEEE Transactions on Communications* **46**, 1448–1450 (1998).
10. K. Pham, J. Conradi, G. Cormack, B. Thomas, and C. W. Anderson, "Impact of Noise and Nonlinear Distortion due to Clipping on the BER Performance of a 64-QAM Signal in Hybrid AM-VSB/QAM Optical Transmission System," *Journal of Lightwave Technology* **13**, 2197–2205 (1995).
11. T. Anderson and D. Crosby, "The Frequency Dependence of Clipping Induced Bit-Error rates in Subcarrier Multiplexed Systems," *IEEE Photonics Technology Letters* **8**, 1076–1078 (1996).
12. A. Kanazawa, M. Shibutani, and K. Emura, "Preclipping Method to Reduce Clipping-Induced Degradation in Hybrid Analog/Digital Subcarrier-Multiplexed Optical Transmission Systems," *IEEE Photonics Technology Letters* **7**, 1069–1071 (1995).
13. Q. Pan and R. J. Green, "Pre-Clipping AM/QAM Hybrid Lightwave Systems with Band-stop Filtering," *IEEE Photonics Technology Letters* **8**, 1079–1081 (1996).
14. C. Y. Kuo and S. Mukherjee, "Clipping Reduction for Improvement of Analog and Digital Performance Beyond Clipping Limit in Lightwave CATV Systems," OFC Post-deadline, paper PD18-1 (1996).
15. L. Pophillat, "Optical Modulation Depth Improvement in SCM Lightwave Systems Using a Dissymmetrization Scheme," *IEEE Photonics Technology Letters* **6**, 750–753 (1994).
16. S. Ovadia, "The Effect of Interleaver Depth and QAM Channel Frequency Offset on the Performance of Multichannel AM-VSB/256-QAM Video Lightwave Transmission Systems," *IEEE Photonics Technology Letters* **10**, 1174–1776 (1998).
17. G. Hutson, P. J. Shepherd, and W. S. J. Brice, *Colour Television Systems Principles, Engineering Practice and Applied Technology*, McGraw-Hill International (1990).
18. S. S. Wagner, T. E. Chapuran, and R. C. Menendez, "The Effect of Analog Video Modulation on Laser Clipping Noise in Video-Distribution Networks," *IEEE Photonics Technology Letters* **8**, 275–277 (1996).
19. B. Sklar, *Digital Communications Fundamentals and Applications*, PTR Prentice Hall (Englewood Cliffs, New Jersey, 1988).
20. A. F. Judy, "Generation of Interference Intensity Noise from Fiber Rayleigh Backscatter and Discrete Reflections," *OFC Technical Digest*, 1991, paper WL4, p. 110.
21. J. L. Gimlett and N. K. Cheung, "Effects of Phase-to-Intensity Noise Conversion by Multiple Reflections on Gigabit-per-Second DFB Laser Transmission Systems," *Journal of Lightwave Technology* **7**, 888 (1989).

22. W. I. Way et al., "Multiple-Reflection-Induced Intensity Noise Studies in a Lightwave System for Multichannel AM-VSB Television Signal Distribution," *IEEE Photonics Technology Letters* **2**, 360–362 (1990).
23. S. Ovadia, L. Eskildsen, C. Lin, and W. T. Anderson, "Multiple Optical Reflections in Hybrid AM/16-QAM Multichannel Video Lightwave Transmission System," *IEEE Photonics Technology Letters* **6**, 1261–1264 (1994).
24. S. Ovadia, L. Eskildsen, C. Lin, and W. T. Anderson, "Reflection-Dependence of CNR and 16-QAM BER in AM/QAM Video Lightwave Systems Using Two Different Externally-Modulated Laser Transmitters," *IEE Electronic Letters* **31**, 1277–1278 (1995).
25. T. E. Darcie, G. E. Bodeep, and A. M. Saleh, "Fiber-Reflection-Induced Impairments in Lightwave AM-VSB CATV Systems," *Journal of Lightwave Technology* **9**, 991 (1991).
26. E. E. Bergmann, C. Y. Kuo, and S. Y. Haung, "Dispersion-Induced Composite Second-Order Distortion at 1.5-μm," *IEEE Photonics Technology Letters* **3**, 59–61 (1991).
27. D. B. Crosby and G. J. Lampard, "Dispersion-Induced Limit on the Range of Octave Confined Optical SCM transmission System," *IEEE Photonics Technology Letters* **6**, 1043–1045 (1994).
28. C. Y. Kuo, "Fundamental Second-Order Nonlinear Distortions in Analog AM CATV Transport Systems Based on Single Frequency Semiconductor Lasers," *IEEE Journal of Lightwave Technology* **10**, 235–243 (1992).
29. R. G. Smith, "Optical Power Handling Capacity of Low-Loss Optical Fibers as Determined by Stimulated Raman and Brillouin Scattering," *Applied Optics* **11**, 2489–2494 (1972).
30. X. Mao, R. W. Tkach, A. R. Chraplyvy, R. M. Jopson, and R. M. Derosier, "Stimulated Brillouin Threshold Dependence on Fiber Type and Uniformity," *IEEE Photonics Technology Letters* **4**, 66–69 (1992).
31. X. P. Mao, G. E. Bodeep, R. W. Tkach, A. R. Chraplyvy, T. E. Darcie, and R. M. Derosier, "Brillouin Scattering in Externally-Modulated Lightwave AM-VSB CATV Transmission Systems," *IEEE Photonics Technology Letters* **4**, 287–289 (1992).
32. M. R. Philips and K. L. Sweeney, "Distortion by Stimulated Brillouin Scattering Effect in Analog Video Lightwave Systems," *OSA TOPS vol.12 System Technologies*, 182–185 (1997).
33. F. W. Willems, W. Muys, and J. S. Leong, "Simultaneous Suppression of Stimulated Brillouin Scattering and Interferometric Noise in Externally Modulated Lightwave AM-SCM Systems," *IEEE Photonics Technology Letters* **6**, 1476–1478 (1994).
34. F. W. Willems, J. C. van der Plaats, and W. Muys, "Harmonic Distortion Caused by Stimulated Brillouin Scattering Suppression in Externally Modulated Lightwave AM-CATV Systems," *IEE Electronics Letters* **30**, 343–345 (1994).
35. M. R. Phillips, T. E. Darcie, D. Marcuse, G. E. Bodeep, and N. J. Frigo, "Nonlinear Distortion Generated by Dispersive Transmission of Chirped Intensity-Modulated Signals," *IEEE Photonics Technology Letters* **3**, 481–483 (1991).

36. D. A. Atlas, "Fiber Induced Distortion and Phase Noise to Intensity Noise Conversion in Externally Modulated CATV Systems," *NCTA Technical Papers*, 289–293 (1996).
37. C. Desem, "Composite Second Order Distortion Due to Self-Phase Modulation in Externally Modulated Optical AM-SCM Systems Operating at 1550-nm," *IEE Electronics Letters* **30**, 2055–2056 (1994).
38. M. C. Wu, C. H. Wang, and W. I. Way, "CSO Distortions Due to the Combined Effects of Self- and External-Phase Modulations in Long Distance 1550-nm AM-CATV Systems," *IEEE Photonics Technology Letters* **11**, 718–720 (1999).
39. Z. Wang, A. Li, C. J. Mahon, G. Jacobsen, and E. Bodtker, "Performance Limitations Imposed by Stimulated Raman Scattering in Optical WDM SCM Video Distribution Systems," *IEEE Photonics Technology Letters* **7**, 1492–1494 (1995).
40. G. P. Agrawal, *Nonlinear Fiber Optics*, Chapter 8, Academic Press (New York, 1995).
41. T. K. Chiang, N. Kagi, M. E. Marhic, and L. Kazovsky, "Cross-Phase Modulation in Fiber Links with Multiple Optical Amplifiers and Dispersion Compensators," *Journal of Lightwave Technology* **14**, 249–260 (1996).
42. R. Hui, Y. Wang, K. Demarest, and C. Allen, "Frequency Response of Cross-Phase Modulation in Multispan WDM Optical Fiber Systems," *IEEE Photonics Technology Letters* **10**, 1271–1273 (1998).
43. F. S. Yang, M. E. Marhic, and L. G. Kazovsky, "Nonlinear Crosstalk and Two Countermeasures in SCM-WDM Optical Communication Systems," *Journal of Lightwave Technology* **18**, 512–520 (2000).
44. T. E. Darcie and C. D. Poole, "Polarization-Induced Performance Variables," *Communication Engineering and Design Magazine*, 50–58 (1992).
45. K. Kikushima, "Polarization Dependent Distortion Caused by Isolators in AM-SCM Video Transmission Systems," *IEEE Photonics Technology Letters* **5**, 578–580 (1993).
46. K. Kikushima, Ko-ichi Suto, H. Yoshinaga, and E. Yoneda, "Polarization Dependent Distortion in AM-SCM Video Transmission Systems," *Journal of Lightwave Technology* **12**, 650–657 (1994).
47. R. H. Stolen, "Polarization Effects in Fiber Raman and Brillouin Lasers," *IEEE Journal of Quantum Electronics* **QE-15**, 1157–1160 (1979).

CHAPTER 10

EDFA-BASED WDM MULTICHANNEL AM/QAM VIDEO LIGHTWAVE ACCESS NETWORKS

Chapter 9 dealt with the transmission impairments in WDM SCM lightwave systems operating over relatively short links (< 30-km). Consequently, these links do not require the use of in-line EDFAs. However, typical HFC access networks, particularly in densely populated urban areas, employ relatively long optical links (> 50-km) or require a large number of optical splits. Cable TV operators are responding to the increasingly high optical power demands by deploying high-power in-line optical amplifiers, particularly EDFAs, throughout their networks. To address these issues and to build on the lightwave transmission impairments discussion in Chapter 9, Section 10.1 starts with the current architecture in WDM multichannel AM/QAM video lightwave access networks using cascaded EDFAs. The transmission performance results in the presence of various lightwave degradation mechanisms in these networks with cascaded EDFAs such as nonlinear distortions, SPM, EPM, polarization effects, and gain tilt are reviewed for both AM-VSB and QAM channels. In Section 10.2 the problem with the current HFC networks is explained. This problem leads the current evolution of the HFC architecture toward two-way DWDM access networks. The architecture of a DWDM downstream network carrying analog/digital video channels, high-speed data, as well as IP telephony is reviewed in Section 10.3. The architecture of return-path DWDM network is also reviewed in Section 10.4, including both frequency-stacking and digitized return-path schemes.

10.1 Architecture and Performance of Multichannel AM-VSB/QAM Video Lightwave Networks

As we discussed in Chapter 9, in order to maintain an acceptable AM CNR, the optical power budget of a video lightwave system based on a 1310-nm DM-DFB laser transmitter is typically limited to 10-dB. This moderate power margin imposes an upper limit on the length of the optical link and the number of optical splits. As pointed out earlier, many applications such as long-distance super-trunking and broadband networks based on passive optical network architectures require a much higher power link budget than can be provided using a DM-DFB laser transmitter. Figure 10.1 shows, for example, an EDFA-based multiwavelength multichannel hybrid AM-QAM video lightwave transmission network, in which

the master cable TV headend is typically connected by primary self-healing fiber-optics rings to the primary headends or the hubs in a large metropolitan area [1]. A self-healing fiber-optic ring has at least one redundant fiber ring with automatic-protection switching, which switches the traffic when equipment or point-to-point failures occur along the ring. Ultra-high-capacity video trunking can be achieved by using high-density WDM multiplexers and demultiplexers with high-power cascaded EDFAs [2]. In the primary fiber ring, multiple wavelengths in the 1550-nm band are transmitted bidirectionally with each wavelength carrying a mixture of AM and digital video signals at both RF passbands, using 64/256-QAM modulation formats, and at baseband at various rates such as OC-48 and OC-192. The secondary rings are connecting the primary hubs to the secondary hubs or headends. Notice that in a secondary fiber ring, only a few wavelengths are demultiplexed and transmitted using 1550-nm laser transmitters and in-line EDFAs. At the secondary hubs, the 1550-nm based broadcast traffic can be switched to a 1310-nm based traffic for both narrowcasting and broadcasting services.

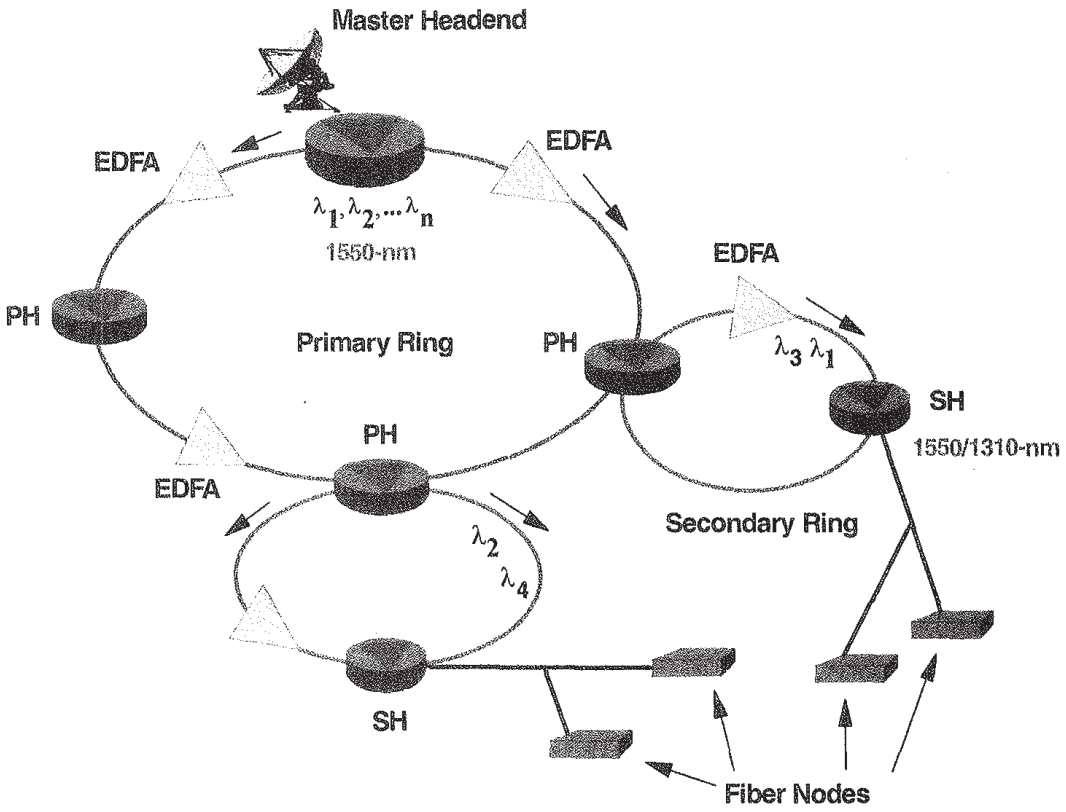


Figure 10.1 Multiwavelength and multichannel AM/QAM video lightwave trunking network using 1550-nm laser transmitters with cascaded EDFAs. PH = primary hub, SH = secondary hub. After Ref. [1] (© 1998 IEEE).

10.1.1 Multichannel AM/QAM Video Lightwave Trunking Systems

Recently, there have been many studies on the transport of only AM-VSB video signals in optically amplified 1550-nm lightwave systems [3–7]. The lightwave link performance has to overcome the transmission limitations imposed by SBS, SPM, clipping-induced impulse noise, and optical reflections. 1550-nm transmission systems using a DM-DFB laser transmitter, which were studied by Bulow, et al. [4], and Clesca, et al. [5], had an impressive optical power budget, partly due to the high laser-modulation index, with about 35 AM channels transmitted using a dispersion-shifted fiber (DSF). Muys, et al. [6] reported on 50 AM channel transmission using a 1550-nm EM-DFB laser transmitter with three cascaded 980-nm pumped EDFAs and a standard SMF. The advantage of such a system over the DM system is that the intermodulation distortions are essentially independent of the number of EDFAs used, since the EM laser transmitter generates virtually no frequency chirp, thereby preventing interaction with the fiber dispersion. Kuo, et al. [7] demonstrated the transmission of 80 AM channels with low CSO and CTB distortions over 100-km of a standard SMF. Using a differential detection scheme, which consisted of a pair of cable TV receivers followed by a broadband out-of-phase combiner, the authors showed that the AM CNR can be increased by 3-dB to at least 52.5-dB while maintaining a CSO distortion below –65-dBc over the AM-frequency band. A 120-km transmission of 79 simulated AM channels and four 64/256-QAM channels over a standard SMF with two cascaded EDFAs has been demonstrated by the authors [8].

Before reviewing the performance characteristics of a multichannel AM/QAM video lightwave trunking system, let us discuss the experimental setup, which is similar to the one shown in Figure 9.14 [8]. The lightwave link consisted of 120-km of a standard SMF with two in-line EDFAs as shown in Figure 10.2. The EM-DFB laser transmitter has built-in mechanisms for linearization and suppression of the SBS effect. The optical output from the laser transmitter was 15-dBm, and was 13-dBm from each in-line EDFA when operating in deep saturation. At

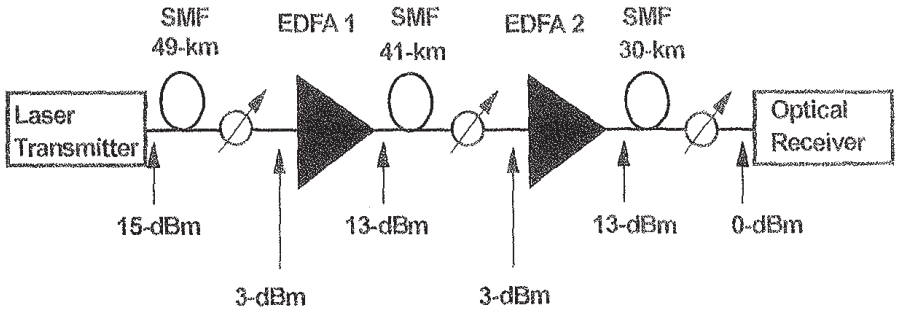


Figure 10.2 Block diagram of a 120-km lightwave transmission system experiment. After Ref. [8] (© 1996 IEEE).

the cable TV receiver, the composite video signal was detected and separated into analog and QAM channels using high/low-pass filters. The signal corresponding to each of the four QAM channels was downconverted to the IF frequency, demodulated, and then fed to an error detector for BER analysis.

10.1.2 Multichannel AM-VSB Video Lightwave Trunking Results

Performance of the multichannel AM-QAM video lightwave trunking system is first analyzed for SMF lengths up to 50-km without using the in-line EDFAs. The received optical power is set at 0-dBm using a variable optical attenuator. Figures 10.3 and 10.4 show the measured AM CNR with the CSO and CTB distortions (without the EDFAs) at an AM frequency of 295.25-MHz (channel 36) as a function of the AM modulation index per channel. At AM modulation index of 3.1% per channel, the worst-case measured CNR (channel 78) was 53.7-dB with CTB distortions less than –65-dBc and CSO distortions less than –70-dBc.

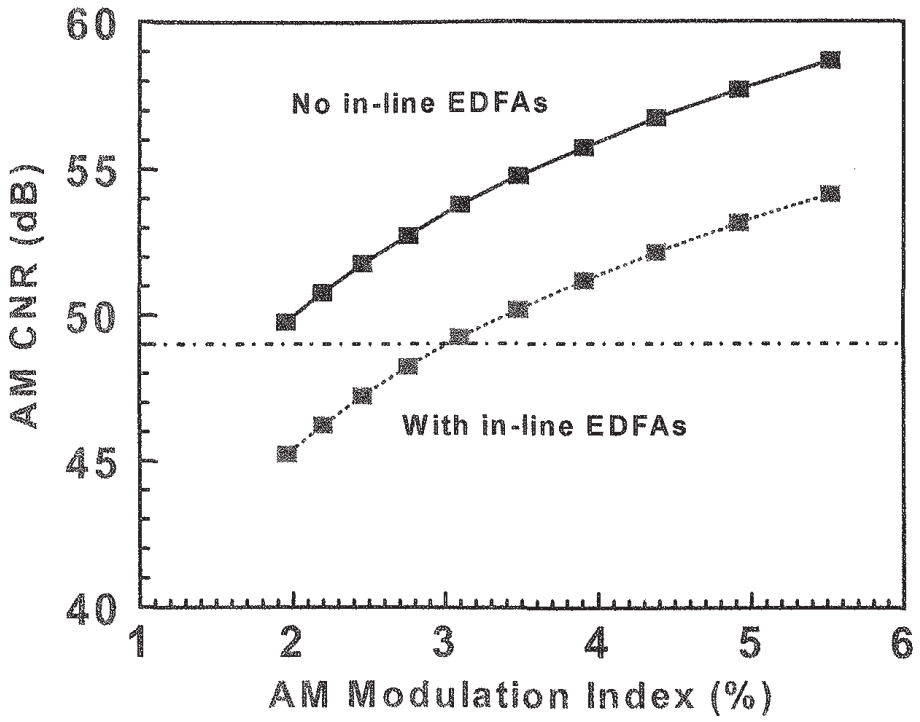


Figure 10.3 Measured AM CNR at frequency 295.25-MHz (channel 36) as a function of the AM modulation index with and without the in-line EDFAs. After Ref. [8] (© 1996 IEEE).

In order to select the proper operating point of the AM-QAM video lightwave trunking system with the cascaded EDFAs, the optical input power to each in-line EDFA needs to be deter-

mined. It is desirable to operate the EDFA in saturation to minimize the CNR penalty due to the amplifier's beat noise. With an optical power of 0-dBm at the receiver, the optimum optical input power of 3-dBm to each in-line EDFA is obtained by balancing the maximum possible AM CNR with the overall system link budget requirement. The AM CNR is increased by only 1-dB when the optical input power to the EDFA is increased from 3-dBm to 6-dBm, for example. Of course, the 1-dB addition to the AM CNR reduces the optical link budget by 3-dB. In contrast, some high-power in-line EDFAs, which have an NF greater than 5-dB, may require optical input power levels greater than 3-dBm [9]. This is due to the requirement from AM-QAM video lightwave trunking links to be able to transport at least 70 AM channels, each with a CNR greater than 50-dB, at a transmission distance of 100-km or more.

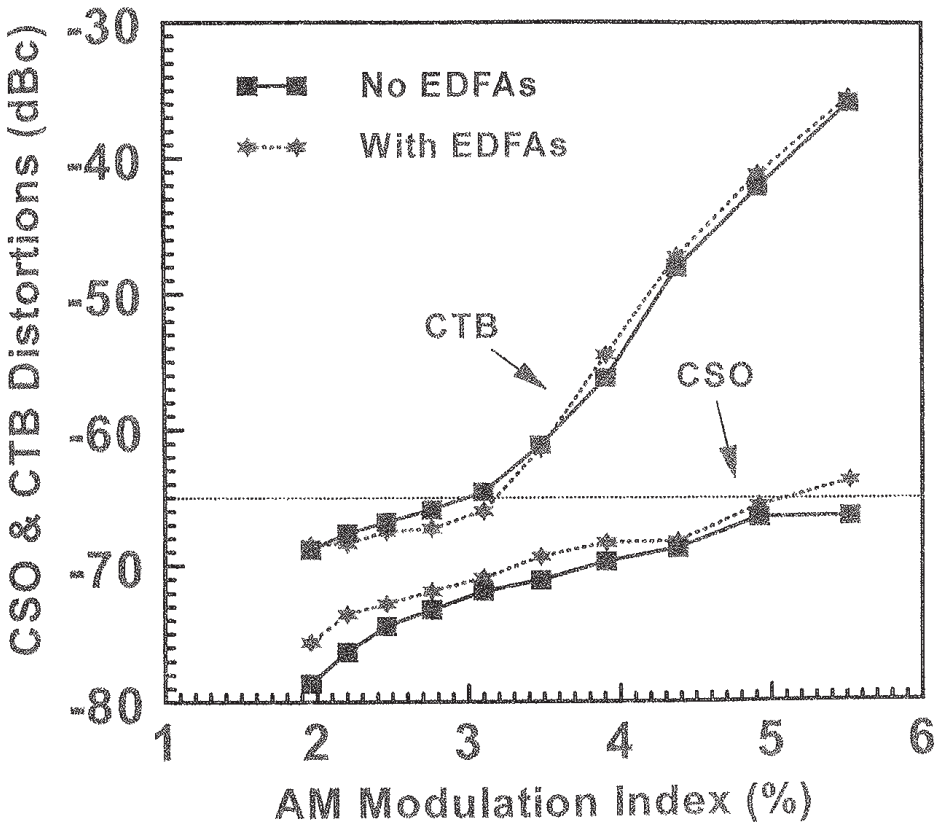


Figure 10.4 Measured CSO and CTB distortions versus the AM modulation index with and without the in-line EDFAs. After Ref. [8] (© 1996 IEEE).

The measured AM CNR with the CSO and CTB distortions at the AM frequency 547.25-MHz (channel 78) as a function of the AM modulation index per channel for an AM video trunking system with the cascaded EDFAs are shown in Figures 10.3 and 10.4. The optical input power to each in-line EDFA is set at 3 dBm, which is well above the input power for reaching the saturation point of these amplifiers. Notice that the measured AM CNR is decreased by about 4.5-dB caused by the addition of two in-line EDFAs at the optical input power level of 3-dBm. The transmitted AM CNR can be easily calculated using Equation (6.35). The measured CNR degradation is in good agreement with the calculated CNR penalty. Figure 10.4 shows that the use of in-line EDFAs has little effect on the CSO and CTB distortions for a single-wavelength operation. Furthermore, it suggests that degradation in the CSO and CTB distortions due to the residual chirp from the optical modulator in the 1550-nm EM-DFB laser transmitter is also negligible. The actual operating point of the transmitter is chosen by maximizing the AM CNR while maintaining distortion below acceptable levels. For example, according to Figures 10.3 and 10.4, the worst-case AM CNR at the AM frequency 547.25-MHz is 49.3-dB with CSO/CTB distortions less than –65-dBc at an AM modulation index of 3.1% per channel. Correspondingly, the optical power budget for this 120-km AM/256-QAM video lightwave link is 35-dB.

10.1.3 Multichannel AM-VSB/QAM Video Lightwave Trunking Results

The performance of 64/256-QAM digital channels is typically analyzed in terms of their uncoded BER. Figure 10.5 shows, for example, the measured BER of 64-QAM and 256-QAM channels as a function of the QAM SNR. The RF power of the 256-QAM channels was 12-dB below that of the AM channels. The solid lines in Figure 10.5 represent the theoretically predicted 64-QAM and 256-QAM BER (uncoded) versus the QAM SNR in a back-to-back configuration (no laser transmitter) with the assumptions of additive white Gaussian noise and Gray coding, included for comparison. While nearly error-free transmission was obtained for the 64-QAM channels, it is observed that a BER floor starts to emerge at around 35-dB SNR for 256-QAM channels, which were transmitted with the 79 AM channels at an AM modulation index of 3.1% per channel. This is likely due to the clipping-induced impulse noise and nonlinear distortion within the QAM band, which was generated by the AM channels operating at a much higher RF level [1, 10]. Although the BER performance can be improved by operating the 256-QAM channels at higher QAM signal levels, the increased QAM channel loading may cause the degradation of AM channel quality. The difference in transmission performance between the 64-QAM and the 256-QAM channels in the presence of 79 AM channels can also be illustrated using the QAM modulation index. Figure 10.6 shows the BER of the 64/256-QAM channels with and without the in-line EDFAs as a function of the QAM modulation index per channel. The QAM signal level for the transmission link with the in-line EDFAs to obtain an equal BER is found to be as much as 2.5-dB higher than the signal level without the in-line EDFAs. This is expected, of course, considering the added ASE noise from the in-line EDFAs. However, no other QAM channel impairment due to the amplifiers is observed under

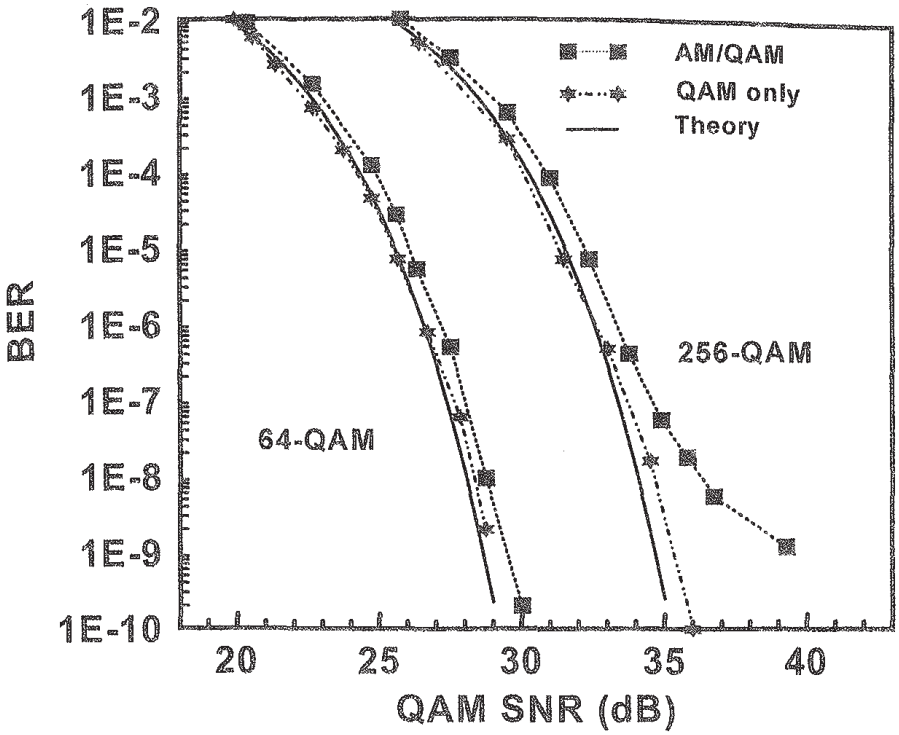


Figure 10.5 Measured uncoded BER of the 64-QAM and 256-QAM channels with and without the AM channels. The theoretical performance for only the 64-QAM and 256-QAM channels is also shown for comparison. After Ref. [8] (© 1996 IEEE).

the set operating condition. Figure 10.6 also indicates that at uncoded BER of 10^{-9}, the 256-QAM channels require almost three times the QAM modulation index of the 64-QAM channels operating at the same low BER. As the QAM modulation level increases from 64 to 256, the minimum distance between QAM clusters on the constellation map decreases, and thus the 256-QAM signals become more sensitive to intersymbol interference due to impulse noise and other impairments.

Do the transmitted 256-QAM channels affect the AM channels?
To answer this question, the AM CNR with the CSO and CTB distortions of the AM channels were measured as a function of the 256-QAM modulation index for the present system with four 256-QAM channels as shown in Figure 10.7. The AM modulation index remained fixed, while the QAM modulation index was increased up to 6% per channel. Notice that the AM CNR starts to deteriorate at a 256-QAM modulation index greater than about 2.5% per channel.

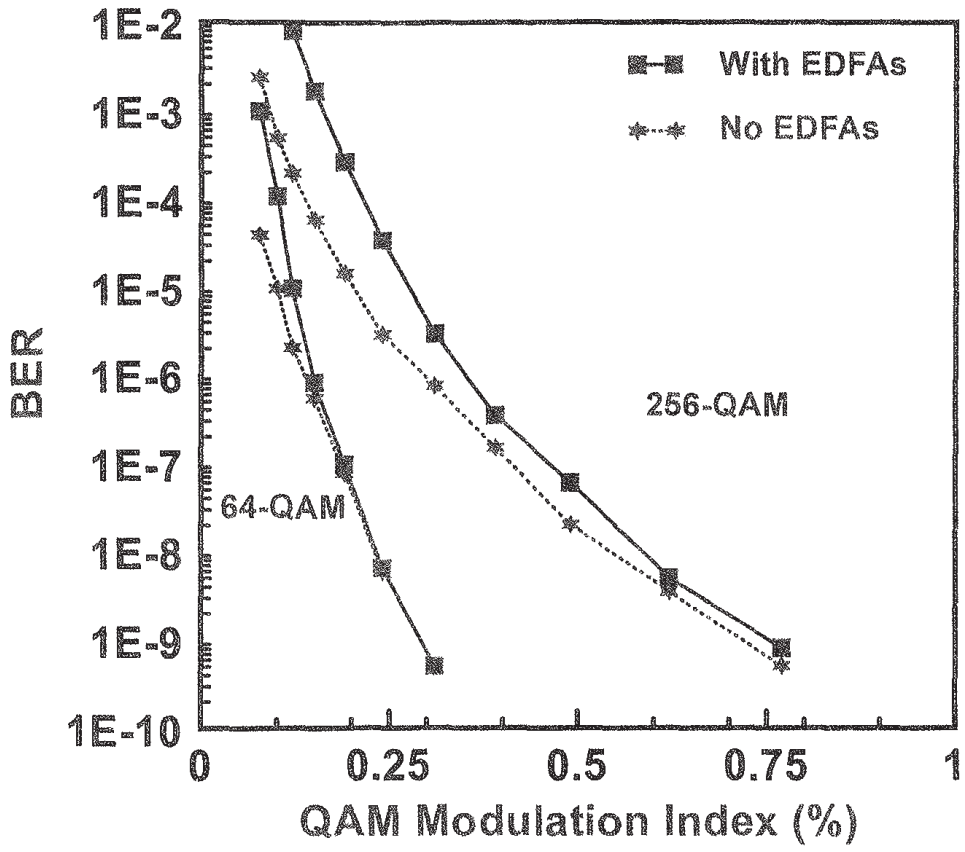


Figure 10.6 Measured uncoded BER of the transmitted 64-QAM and 256-QAM channels as a function of the QAM modulation index with and without the in-line EDFAs. After Ref. [8] (© 1996 IEEE).

Figure 10.8 shows the calculated AM CNR (without in-line EDFAs) versus the 256-QAM modulation index for a hybrid AM-QAM lightwave system with (A) 79 AM channels and four 256-QAM channels, (B) 79 AM channels and 33 QAM channels, and (C) 40 AM channels and 72 QAM channels. The model takes into account only the effect of the nonlinear clipping distortion at the laser transmitter [10]. As the QAM modulation index is increased, the four QAM channels behave like additional AM channels, increasing both the observed CSO and CTB distortions. Thus, the observed AM CNR degradation (Figure 10.6) is mainly due to the increased CSO and CTB distortions and not the additional clipping noise from the QAM channels. However, in a fully loaded hybrid AM-QAM video transmission system [Figure 10.8, B], the AM CNR degradation due to clipping distortion from both the AM and QAM channels appears at about 3% 256-QAM modulation index per channel. The impact of the QAM channels on the

AM CNR is best demonstrated by case (C), in which the number of AM channels is reduced by one-half, while the number of QAM channels doubles. Notice the steeper AM CNR degradation at the QAM modulation index of 3% due to the increased nonlinear clipping distor tion. These results demonstrate that even in a fully loaded hybrid AM/256-QAM video lightwave transmission system operating under normal conditions, the effect of the QAM channels on the AM channels is essentially negligible. By using an FEC scheme, such as ITU-T J.83 Annex A, which provides a 4.8-dB coding gain at BER of 10^{-9}, the nonlinear distortion effect on the AM channels is reduced since the 256-QAM signal levels can be kept relatively low compared to the AM signals (≈ –6-dBc).

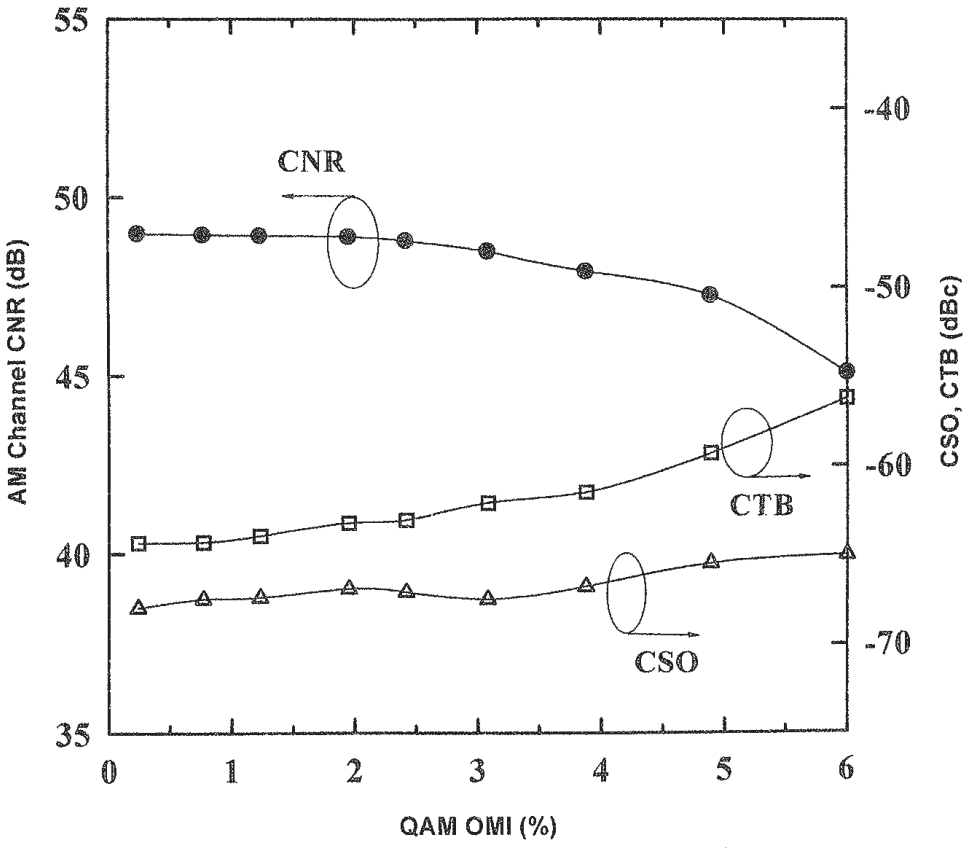


Figure 10.7 Measured AM CNR (solid circles) and CSO (triangles) and CTB (squares) distortions as a function of the 256-QAM modulation index. After Ref. [8] (© 1996 IEEE).

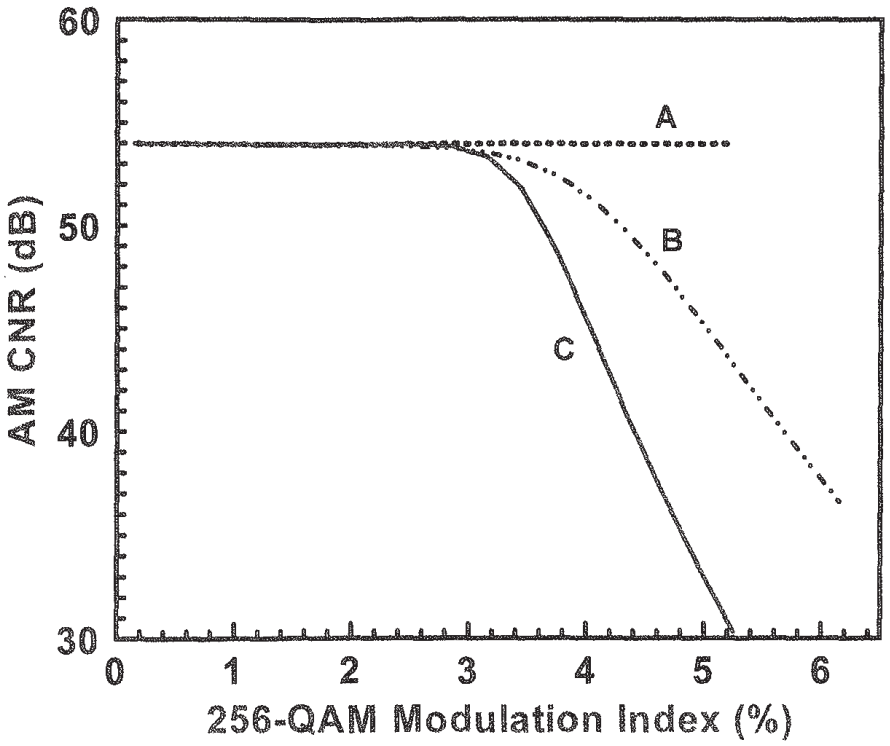


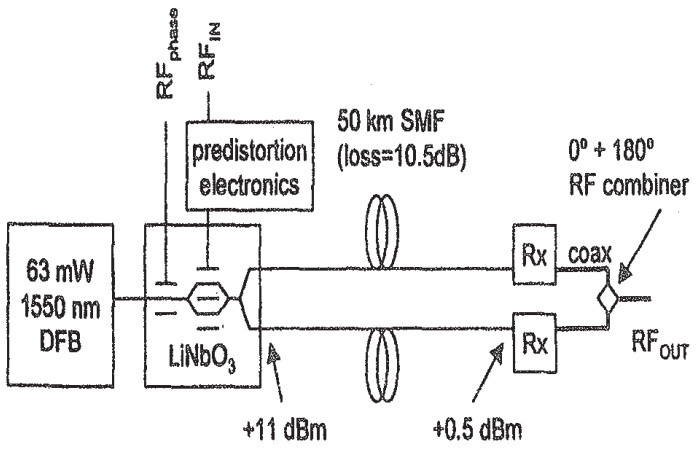
Figure 10.8 Calculated AM CNR versus the 256-QAM modulation index for a hybrid AM/256-QAM video system with (A) 79 AM with 4 QAM channels, (B) 79 AM with 33 QAM channels, and (C) 40 AM with 72 QAM channels.

10.1.4 Differential Detection in AM-VSB Video Trunking Systems

As explained previously, multichannel AM-VSB video trunking links typically use EM-DFB laser transmitters operating at 1550-nm for a long-distance transmission (≥ 100-km). However, the noise built up in the cascaded EDFAs and the nonlinear optical fiber effects, such as SPM and EPM, limit the maximum achievable AM CNR with an acceptable level of CSO and CTB distortions as measured at the cable TV receiver. One of the techniques to improve the AM CNR without degrading the CSO and CTB distortions is called the differential detection method [7, 11]. Figure 10.9 shows the differential detection scheme in a 50-km multichannel AM transmission system using a 1550-nm EM-DFB laser transmitter.

As we learned in Chapter 4, under the proper biasing condition, a dual-output $LiNbO_3$ MZ

intensity modulator produces two signals with the same intensity, but 180° out of phase with each other. Using two optical receivers at the other end of the fiber, the RF outputs are combined in phase as shown in Figure 10.9. If the total fiber span of the two links is less than $(c/n \cdot \Omega)$, where c/n is the speed of light in the fiber and Ω is the highest RF frequency, then the RF carriers are added coherently, increasing by 6-dB. However, the noise is added incoherently, increasing by 3-dB. Thus, the resultant CNR is increased by only 3-dB. The CSO and CTB distortions are canceled in the combined RF signal. Figure 10.10 shows the measured AM CNR versus the AM channel frequency after 100-km of standard SMF with two cascaded EDFAs using (a) a single receiver and (b) dual receivers. Below about 300 MHz, the AM CNR is improved by about 3-dB as expected. However, above 300-MHz, the AM CNR is improved by as much as 4.5-dB. This additional improvement of 1.5-dB in the AM CNR at high cable-TV frequencies is due to the cancellation in the phase-to-amplitude noise, which is correlated. According to Piehler et al., the differential detection scheme also reduced the measured CSO distortion, which was induced by dispersion and SPM, by as much as 20-dB compared with the same link using a single receiver [11]. Figure 10.10 (b) shows the measured AM CNR versus the channel frequency for 80 AM video channels, which were transmitted over 100-km of standard SMF at a low phase-modulation index ($\beta \leq 3$).



NTSC channel	CNR (dB)	CSO (dBc	CTB (dBc)
2	55.0	-76.6	-72.8
13	56.0	-84.5	-73.8
40	55.8	-79.5	-71.7
61	55.6	-77.3	-71.2
78	56.2	-75.9	-76.8

Figure 10.9 Differential detection scheme in a 50-km multichannel AM transmission system using a 1550-nm EM-DFB laser transmitter. The measured CNR, CSO, and CTB distortions are shown in the table. After Ref. [7] (© 1996 Optical Society of America).

Thus, the advantage of the differential detection scheme, which is similar to the distortion cancellation by a push-pull amplifier, is to boost the AM CNR by 3-dB or more without

degrading the CSO and CTB distortions at long-distance lightwave links. However, two optical receivers and one RF combiner must be used on two separate fibers.

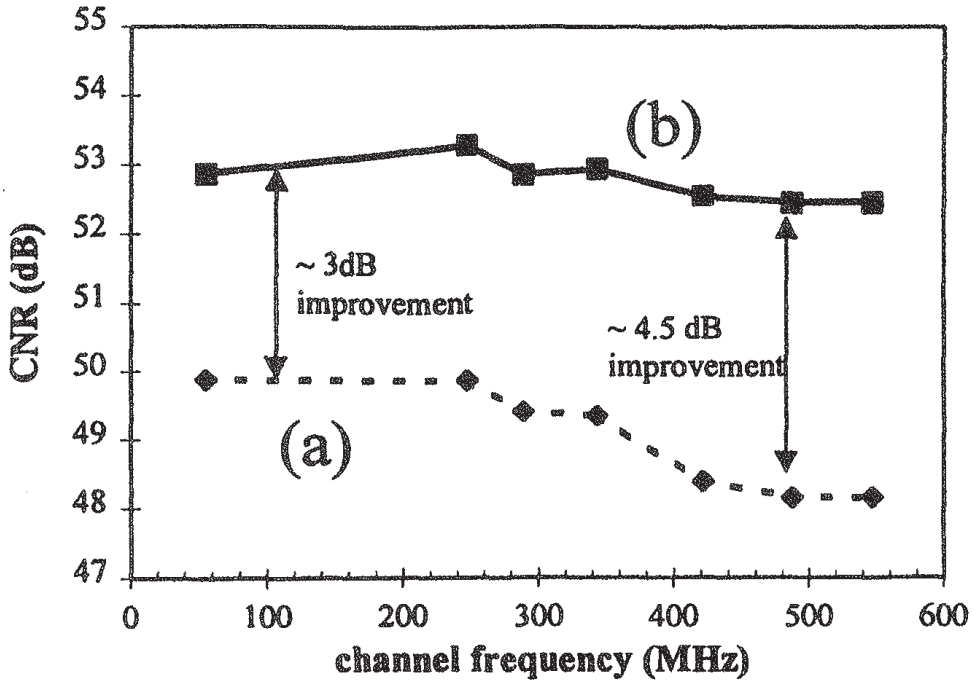


Figure 10.10 Measured AM CNR as a function of the AM channel frequency for 100-km optically amplified links with (a) single receiver, and (b) dual receivers with differential detection. After Ref. [7] (© 1996 Optical Society of America).

10.1.5 SPM and EPM Effects in AM Video Trunking Systems

As we learned in the previous chapter, CSO distortions induced by SPM and EPM effects degrade the performance of multichannel AM video links using 1550-nm EM-DFB laser transmitters. The impact of the SPM and EPM effects is particularly important when designing a long-distance (>100-km) AM video link with cascaded EDFAs. The CSO distortion can be still be approximated by Equation (9.67), where

$$\overline{z^2(L)} = (L - L_{eff})/\alpha \tag{10.1}$$

is replaced by

$$\overline{z^2(L)}+\left[1+e^{-\alpha L/N}\right]\cdot\sum_{i=1}^{N-1}\overline{z^2}\left[(N-i)\cdot L/N\right]$$

where N is the number of EDFAs, and L/N is the fiber span between adjacent EDFAs. Figure 10.11 shows the measured, numerically calculated, and analytical calculation of the CSO distortion at cable TV channel 78 (worst case) as a function of the total fiber span, assuming AM video transmission link with equal span EDFAs. The fiber span between adjacent EDFAs was 60-km with launch optical power to the EDFA of 12-dBm. The optical

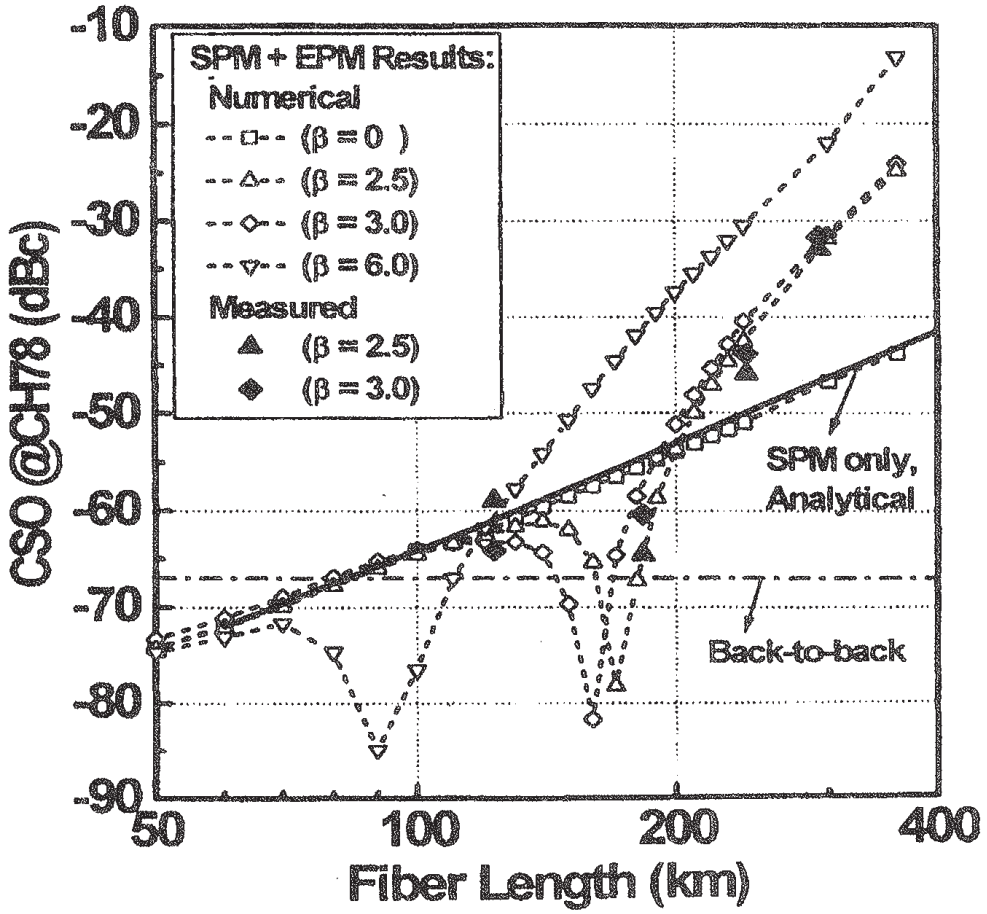


Figure 10.11 Measured, numerically calculated, and analytical CSO distortion at channel 78 as a function of the total fiber length in multichannel AM video trunking link, where the fiber span between adjacent EDFAs is 60-km, and with launched optical power at each EDFA of 12-dBm. After Ref. [12] (© 1999 IEEE).

modulation index per channel was 3% (78 AM channels) at operating wavelength of 1561.1-nm. A single-tone phase modulation at 1.9-GHz was used. The numerical calculations included both SPM- and EPM-induced CSO distortions and were based on a numerical solution to the envelope wave equations (Equations 9.62 and 9.63) using the split-step Fourier transform method. The accuracy of the numerical results was set to differ by less than 1-dB from the analytical results of the CSO distortion when the phase-modulation index was equal to 0 ($\beta = 0$).

Figure 10.11 indicates that when the phase-modulation index is relatively small ($\beta \leq 3$), and the total transmission distance is relatively short (e.g., < 120-km), the analytical results agree with the numerical and experimental results. At longer distances and/or larger phase-modulation index, the worst-case CSO distortion is determined by the combined effect of SPM and EPM. In other words, the predicted CSO distortion analysis based only on the SPM effect significantly underestimates the actual measured CSO distortion. Previous work on the SPM-induced CSO distortions was based on perturbation analysis of the envelope-wave equation and did not include the dependence of frequency, β, and L in the phase-modulation to intensity-modulation conversion, as well as carrier compression.

10.1.6 Polarization Effects in AM Video Trunking Systems

Large polarization-dependent CSO distortions can be generated in AM video trunking links with cascaded EDFAs, since each EDFA uses several optical isolators [13]. This is in spite of the fact that there may not be a measurable polarization-dependent distortion generated from a single EDFA. Figure 10.12 shows the measured CSO distortions versus the rotation angle of linearly polarized light input to cascaded EDFAs when (A) a direct-modulation scheme, and (B) an external-modulation scheme are adopted. The tested EDFAs use type B isolators for the input ports and type A isolators for the output ports. Notice that the CSO distortion degrades by more than 25-dB with 11-cascaded EDFAs compared with the no EDFA case under the direct-modulation scheme. In contrast, the CSO distortion varies by about 5-dB when the external-modulation scheme is used with a maximum extinction ratio. However, it should be pointed out that the input polarization state to the $LiNbO_3$ MZ modulator under the minimum insertion condition is different from that under the maximum extinction condition. As a result, the CSO distortion shows a large degradation (> 15-dB) with cascaded EDFAs as a function of the rotation angle of the linearly polarized light under external modulation.

The CSO distortion in multichannel AM/QAM video transmission link with cascaded EDFAs fluctuates with time. Figure 10.13 shows the measured CSO distortion with and with 11-cascaded EDFAs during a 20-minute period. This is due to the fact that the polarization state of the propagating light fluctuates within each EDFA, resulting in a fluctuating CSO distortion.

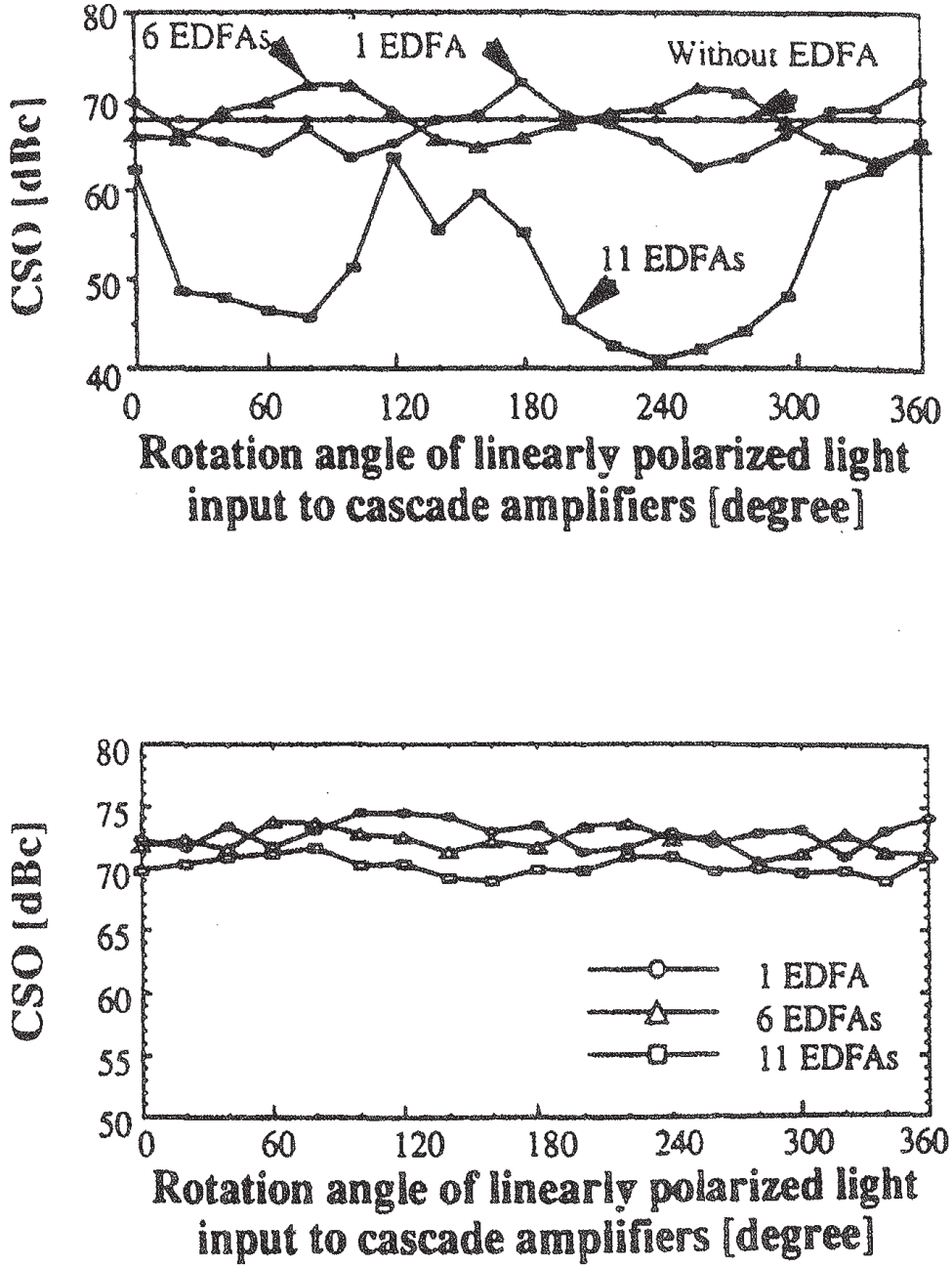


Figure 10.12 Measured CSO distortions versus the rotation angle of linearly polarized light input to cascaded type-γ EDFAs for (A) direct-modulation scheme (top), and (B) external-modulation scheme with maximum extinction ratio (bottom). After Ref. [13] (© 1994 IEEE).

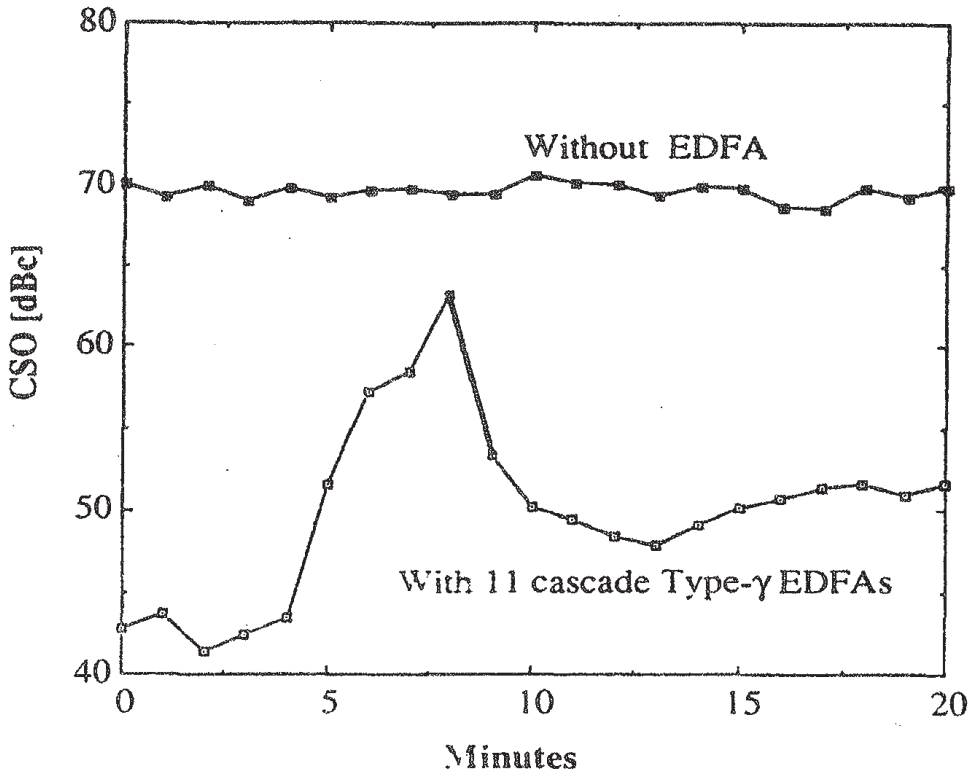


Figure 10.13 Measured CSO distortion level versus time with and without eleven cascaded EDFAs using direct modulation. After Ref. [13] (© 1994 IEEE).

10.1.7 Gain Tilt Distortion in AM Video Trunking Systems

A variation of the optical fiber amplifier gain with wavelength at a given optical input power level is called gain tilt. As we have learned in Chapter 6, EDFA can be used as a post amplifier in 1550-nm DM-DFB laser transmitter or as an in-line power amplifier to boost up the optical power. AM-VSB video lightwave trunking links using a 1310-nm DM-DFB laser transmitter with an in-line Praseodymium doped fiber amplifier (PDFA) are also included. In such laser transmitters, the wavelength-dependent gain of the EDFA interacts with the frequency chirping of the DM-DFB laser, primarily through the phase-to-intensity conversion, to enhance the CSO distortions [14–16]. Various authors have used both a simple and a rigorous analysis to explain the gain tilt distortion phenomenon. To derive an expression for the CSO distortion induced by gain tilt, let us follow the analysis of Clesca, et

al. [14]. It is assumed that a single CW carrier modulates the DFB laser current, and the EDFA input optical power and wavelength are given by

$$P_{in}(t) = P_0[1 + m\sin(2\pi ft)] \tag{10.3}$$

$$\lambda(t) = \lambda_0 - \Delta\lambda \cdot \sin(2\pi ft) \tag{10.4}$$

where P_0 is the average input optical power, m is the optical modulation index, f is the modulation frequency, λ_0 is the average signal wavelength, and $\Delta\lambda$ is the wavelength variation due to modulation. Notice that the input optical power and wavelength are in phase and 180° out of phase with the current modulation. Since the frequency scale of the EDFA gain dynamic is much smaller than the modulation frequency f, the EDFA gain can be expanded in a Taylor series as follows:

$$G[P_{in}(t), \lambda(t)] \cong G(P_0, \lambda_0) + \left[\frac{dG(P_0, \lambda)}{d\lambda}\right]_{\lambda_0} \cdot [\lambda(t) - \lambda_0] \tag{10.5}$$

where $dG/d\lambda$ at λ_0 is the EDFA gain tilt, namely, the wavelength-dependent gain as experienced by the modulated signal. Higher order terms have been neglected. The EDFA output power is simply the input optical power times the gain. Thus, using Equations (10.3), (10.4), and (10.5), the EDFA output power is given by

$$P_{out}(t) = P_{in}(t) \cdot G[P_{in}(t), \lambda(t)] \cong$$
$$G(P_0, \lambda_0) \cdot P_0 + G(P_0, \lambda_0) \cdot P_0 m\sin(2\pi ft) + \frac{1}{2}\left[\frac{dG(P_0, \lambda)}{d\lambda}\right]_{\lambda_0} \cdot \Delta\lambda m P_0 \cos(4\pi ft) \tag{10.6}$$

The ratio of the second-order harmonic distortion to the carrier (2HD/C) can easily be obtained from Equation (10.6). Recall from Chapter 2, to obtain the CSO distortion (relative to the carrier), one needs to multiply the 2HD/C by the CSO product count (N_{CSO}) and add 6-dB. Thus, the gain-tilt-induced CSO distortion expressed in dB is given by

$$CSO = 20 \cdot \log\left[\sqrt{N_{CSO}} \frac{\left[\frac{dG(P_0, \lambda)}{d\lambda}\right]_{\lambda_0} \cdot \Delta\lambda}{G(P_0, \lambda_0)}\right] \tag{10.7}$$

The CSO distortions can be improved or degraded, depending on the phase of the EDFA gain tilt distortions relative to the distortions generated by the DFB laser transmitter. Clesca, et al., [14] have measured CSO distortion degradations at the EDFA output for a

positive gain tilt, and CSO distortion improvement for a negative gain tilt. One way to avoid the CSO distortion induced by EDFA gain tilt is by using an externally modulated DFB laser transmitter (see Section 4.4.2).

10.2 The Problem with the Current HFC Networks

As we learned in Chapter 1, the broadband HFC networks with tree-and-branch architecture enabled robust transmission of the broadcast AM-VSB video channels through standard SMF to the multiple optical fiber nodes. In addition, cable TV operators were able to consolidate the deployment of headend equipment using fiber-optic rings to connect between the master headend and secondary headends or hubs in major metropolitan markets. Thus, cable TV operators were able to cut cost and further improve the quality and availability of the original broadcast services. The development of QAM modulators and low-cost QAM receivers with MPEG-2 digital video sources enabled the cable operators to offer tens of new digital video services along with the traditional AM-VSB channels. The rapid deployment of 750-MHz HFC networks also allowed the cable TV operators and some telecom services to provide competitive access to various businesses in major markets.

In the middle of the 1990s, the existing HFC network architecture started to evolve in a new direction. This evolution can be attributed to the following forces in the marketplace:

(A) An increased demand for high-speed data access in residential areas.
(B) The delivery of highly targeted interactive digital services.
(C) An increased competition from various telecommunication and DBS service operators.
(D) Improved cable TV network scalability with reduced life cycle cost.
(E) Improvements in fiber-optic technology and cable TV network management.

These requirements and market forces are demanding that the cable operators rethink their existing HFC network architecture. Fig. 10.12 shows, for example, the HFC network architecture used by the cable TV operators in a major metropolitan area. The signals from the master headend to the primary and secondary hubs are transmitted over SMF using 1550-nm externally modulated (EM) DFB laser transmitters. The composite signals are a mixture of traditional broadcast analog signals with MPEG compressed digital video. These hubs may house SONET equipment with the associated ADMs or some proprietary technology as well as modems, routers, and servers for high-speed data. The optical signals at 1550-nm are converted to RF signals and then back to optical signals for transmission to various optical-fiber nodes typically using 1310-nm DM-DFB laser transmitters.

The problem with this network architecture is that the secondary hubs had grown very rapidly to become very large facilities that are expensive to maintain since they house both passive and active systems. Another problem with this architecture is the upgrading cost of an existing one-way 450-MHz HFC network for premium video and data services. This is because it required not only additional installation of fiber-optic cables for two-way trans-

mission, but also architectural changes to the HFC network with additional equipment installations at the primary or secondary headends [17].

Recently, DWDM technology has emerged as the most significant and important option for the cable TV operators to solve their current bandwidth bottleneck in their HFC network architecture. The next section discusses the DWDM network architecture for both downstream and upstream transmission.

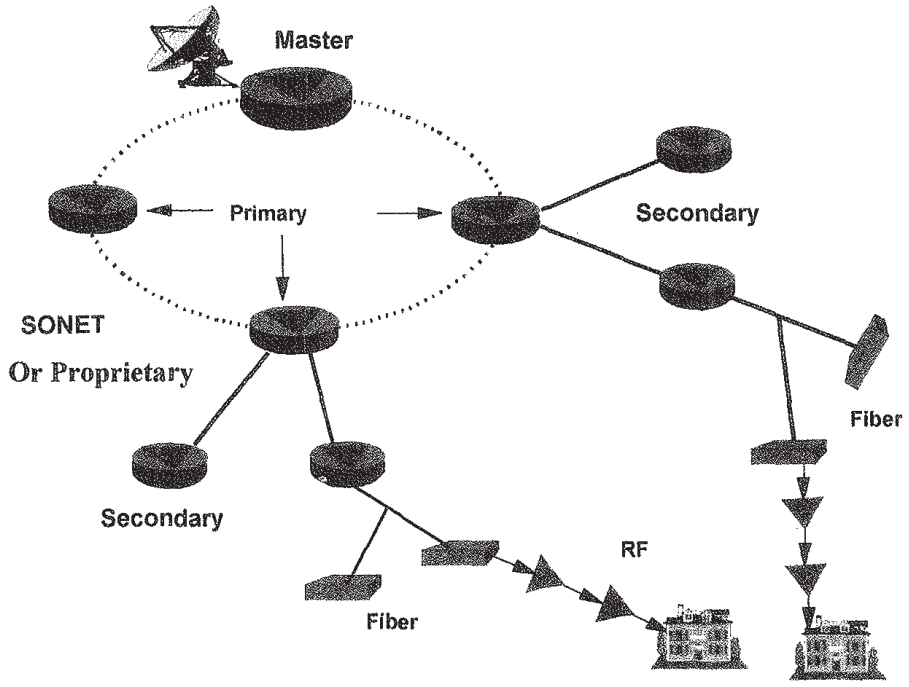


Figure 10.14 Conventional architecture of hybrid fiber/coax access network in a large metropolitan area.

10.3 Downstream DWDM Access Network Architecture

Simplified block diagrams of the downstream DWDM network architecture are shown in Figures 10.1 and 10.15 [18, 19]. The primary hubs are connected to the master headend, as shown in Figure 10.1, by self-healing primary fiber rings using SONET or some proprietary technology that can support bidirectional transmission. Up to 33 contiguous 64/256-QAM channels operating at RF center frequencies from 550-MHz to 750-MHz are loaded on each of the eight EM-DFB laser transmitters operating at International Telecommunication Union

(ITU) standard wavelengths in the primary hub. The ITU standard wavelength grid for fiber-optic telecommunication networks spans from 1520.25-nm to 1565.4961-nm with 100-GHz separation (i.e., about 0.8-nm) between adjacent wavelengths. Notice that each of the downstream DWDM laser-transmitters in Figure 10.15 may be loaded with different MPEG-2 video streams. The 1 x 8 multiplexed optical signal is transmitted to the primary or secondary hubs through, for example, 40-km of a conventional SMF. At the primary or secondary hubs, which are sometimes called optical transition nodes (OTN), the optical signal carrying the 64/256-QAM channels is amplified using an in-line EDFA with, for example, +17-dBm optical output power, and then optically 1 x 8 demultiplexed. The OTN, which is shown within the dotted line in Figure 10.15, consists of primarily passive optical components (see Section 3.2). Notice that only the EDFAs at the OTN require a temperature-controlled environment, which can be provided even at remote locations. The resultant optical signal can be multiplexed with typically 79 AM-VSB video channels, which are transmitted over a separate 40-km standard SMF using an EM-DFB laser transmitter with two different in-line EDFAs. Each primary hub can be connected to about five secondary hubs. From the secondary hubs, the optical signals can be transmitted to about 16 fiber nodes with each fiber node for every 1000–1200 homes passed. To further reduce cost, a 1 x 2 optical coupler can replace the 1 x 2 AM/QAM Mux at the OTN or secondary hub. The detected RF frequency spectrum at the output of the optical receiver is similar to the RF spectrum from a single-wavelength HFC network carrying both AM and QAM channels. There are three main advantages to this DWDM network architecture, as follows:

(A) Elimination of the need for an optical-to-RF-to-optical conversion at the primary or secondary hubs in order to deliver narrowcast video services.

(B) Increased network scalability and flexibility. Using, for example, dynamic wavelength allocation and/or add-drop wavelength multiplexing, new digital services can be added at one wavelength and/or remove at another wavelength in a specific serving area.

(C) Reduced operation, maintenance, and upgrade costs at the secondary hubs. This is possible since most of the downstream DWDM technology is optically passive, except for the EDFAs. Various cable TV operators anticipate about a 30% reduction in the cost of DWDM technology as well as 1550-nm laser transmitters in the next several years. In addition, only the EDFAs at the secondary hubs need a temperature-controlled environment.

Increased network flexibility enables cable TV operators to deliver the desired mix of narrowcast digital services and broadcast analog services to the targeted service area. For example, one of the main cable TV operators in the U.S. is planning to initially deploy one narrowcast laser transmitter per 10,000 homes passed, and incrementally add wavelength-specific laser transmitters as the subscribers' take rates increase [17]. At a take rate of 40% or more, it is expected that one dedicated narrowcast transmitter may be deployed for each 1000 homes passed in the network.

The disadvantages of this DWDM network architecture are as follows:

(A) Increased initial deployment cost at the secondary hub since the subscribers' take rates for narrowcast services may be below the break-even point for cable TV operators.

(B) Increased secondary-hub complexity as compared with the traditional HFC network architecture design.

As the DWDM network architecture becomes more mature with higher subscriber take rates for the premium digital services, the number of AM-VSB channels is expected to shrink to 30 channels or less, while the number of 64/256-QAM channels is expected to grow to more than 70 channels. In this case, a 1 x 4 AM/QAM mux can replace the 1 x 2 AM/QAM mux (Figure 10.15) to enable a wider mix of interactive digital services that are carried by different wavelength-specific WDM laser transmitters.

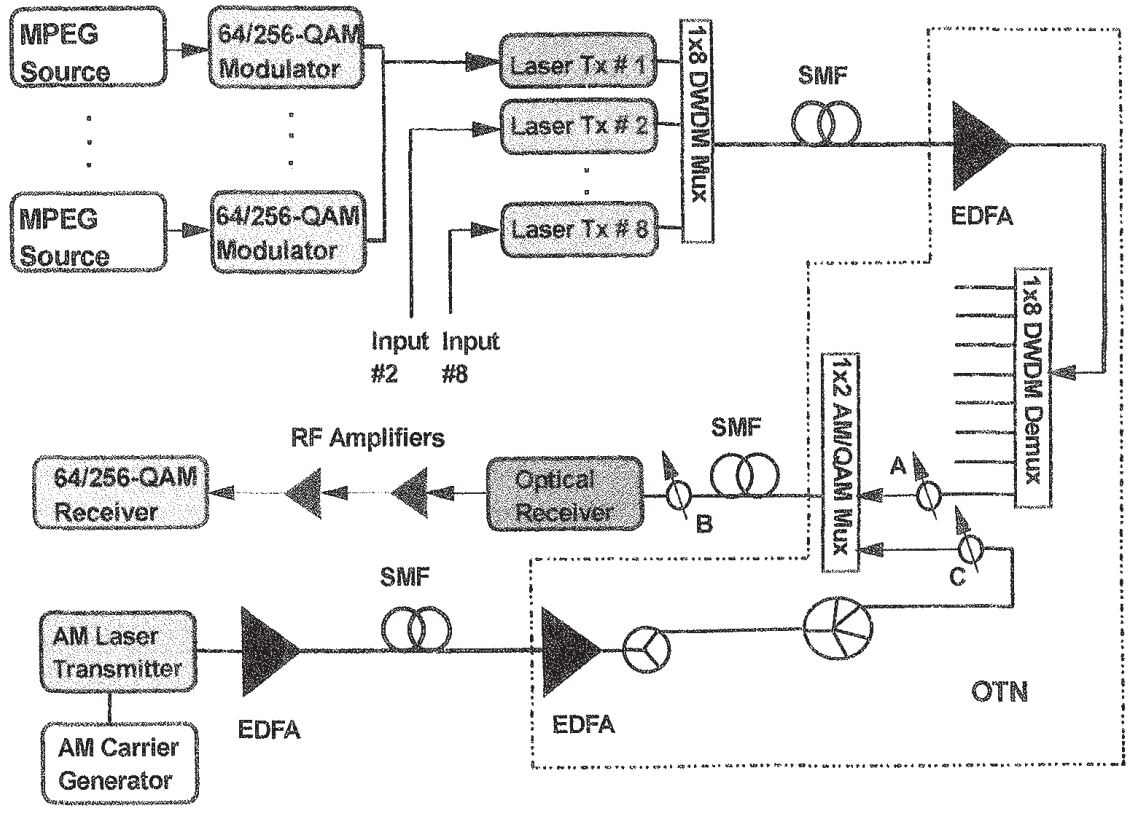


Figure 10.15 Basic downstream DWDM network architecture. The OTN is shown within the dotted line. After Ref. [19] (© 1999 IEEE).

10.4 Upstream DWDM Access Network Architecture

The return-path network architecture is also modified by the DWDM technology. Figure 10.16 shows a simplified block diagram of the upstream DWDM network architecture. It is assumed that each subscriber is connected to the closest fiber node through a coaxial cable plant. At the fiber node, a low-cost uncooled DFB laser transmitter operating at either a 1310-nm or a 1550-nm wavelength band will be used to transmit the high-speed data in the 5–42-MHz band to the secondary hub. These low-cost upstream laser transmitters typically have an optical link budget of 5-dB at 1550-nm or 7-dB at 1310-nm. The DWDM laser transmitters, which are located at the secondary or primary hubs, are typically operating in 1550-nm wavelength band with an optical link budget of 8-dB. Using a 1 x 4 DWDM multiplexer, the optical signal is transmitted, for example, through 40-km of a standard SMF to the primary hub. At the primary hub, the optical signal is amplified, for example, with a 13-dBm in-line EDFA, and optically demultiplexed to four different optical receivers as shown in Figure 10.16. Each cable subscriber can send high-speed data to the headend using a time-division-multiple access (TDMA) scheme according to the DOCSIS protocol standard [20]. Thus, the DWDM upstream network architecture with the TDMA scheme can provides at least four-fold traffic capacity over a standard HFC network architecture with TDMA. Two recently developed and field-deployed return-path technologies, namely, the frequency-stacking scheme (FSS) and the digitized return-path transport are reviewed in the following sections.

10.4.1 Frequency-Stacking Scheme

The demand for more upstream bandwidth from an increasingly larger number of cable subscribers generates additional pressure on the cable operators to provide larger return-path capacity and/or larger allocated bandwidth per subscriber. It turns out that the return-path network traffic capacity can be significantly expanded using the FSS in combination with TDM [18,19, 21]. Figure 10.16 shows an optimized upstream DWDM network architecture with FSS at both the secondary hub and fiber nodes. The FSS system typically consists of four main components as follows:

- Return-path upconverter, which is sometimes called frequency stacker, is a multistage phase-locked upconverter that translates the return-path frequency bands (5–42-MHz) to higher RF frequency bands. For example, Figure 10.17 shows the composite RF spectrum of four upconverted return-path frequency bands (5–42-MHz) using, for example, a Motorola FSS system. A reference pilot tone is generated at a frequency of 370-MHz in the FSS in order to synthesize the four-band stack. The pilot tone is transmitted along with the upconverted signal.
- High-performance return-path laser transmitter, typically an isolated DFB laser with TEC, with optical output power of 5-dBm or more. It should be pointed out that the la-

ser RIN is required to be sufficiently low for robust transmission.

- Block converter receiver, which is an optical receiver with wide dynamic range for power control of both the optical and the RF signals. The transmitted pilot tone is utilized in the block down-converter unit to synchronize the down-conversion process, thus removing any frequency offset errors.
- Block downconverter, which is sometimes called frequency destacker, is controlled by the locally generated pilot tone and is responsible for desynthesizing the composite RF spectrum into four separate return-path frequency bands. The composite RF signal is used to drive each of the DWDM upstream laser transmitters at the secondary hub.

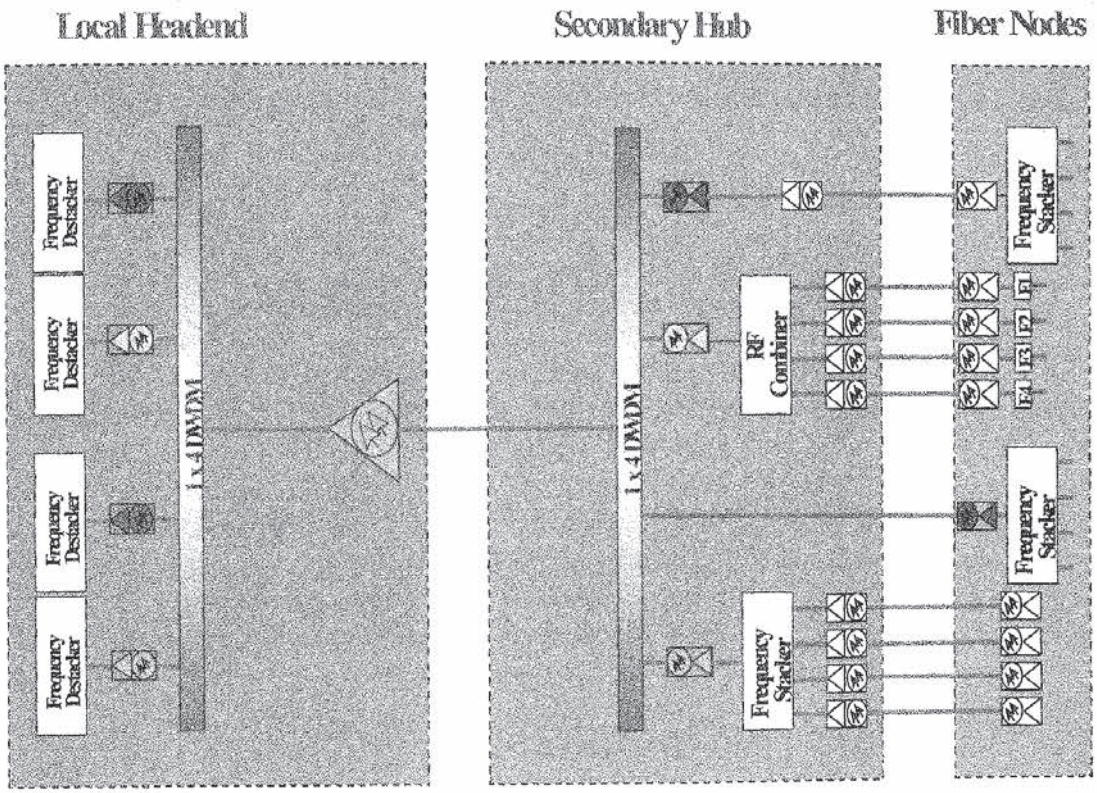


Figure 10.16 DWDM upstream network architecture with frequency stacking at both the fiber nodes and at the secondary hub. After Ref. [18].

The composite output RF signal from each optical receiver is transmitted to the block down-converter unit, which extracts the four separate 5–42-MHz upstream bands. Then, each of the high-speed data bands can be routed and transmitted to return-path burst receivers, and/

or other network control and management equipment. It should be pointed out that the FSS is best utilized at the optical fiber nodes instead of the secondary headends in the upstream DWDM network architecture.

Let us look more closely at the combined FSS/DWDM expansion process. A single shared traditional return-path 37-MHz segment provides 74-kHz bandwidth per home, assuming a 500-home-passed node, for example. The implementation of frequency stacking (4 band) increases the shared segment to 148-MHz, thereby increasing the return-path bandwidth per home to 296-kHz. The implementation of the combined scheme of frequency stacking and DWDM increases the return-path bandwidth segment to 32 times the return-path bandwidth segment, or 1184-MHz, thereby increasing the return bandwidth per home to 2.368-MHz. To meet subscribers' demands for more bandwidth beyond the 32 times bandwidth expansion factor, the cable operator can further reduce the number of homes passed for each optical fiber node.

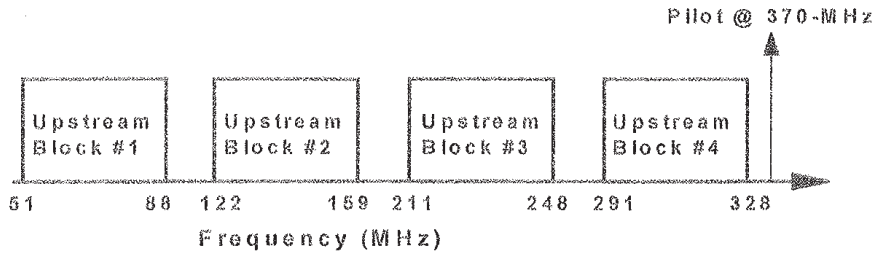


Figure 10.17 The composite RF spectrum of four upconverted upstream frequency blocks (5–42-MHz). After Ref. [19] (© 1999 IEEE).

10.4.2 Digital Return-Path Transport

There are two important factors that make the replacement of analog return-path transport with a digital technology desirable. These factors are a simplification of the reverse-path alignment, afforded by digital components, and a lowering of the return-path system cost [18]. These factors have been enabled by the continuous improvement in the digital component performance while their cost is declining, driven by high-volume applications. Figure 10.18 shows the basic element of a digital return-path in a DWDM network. The composite analog return-path waveform is converted to a sequence of digital words by an analog-to- digital converter (ADC) operating at a typical sampling rate of 100-MHz with 8–

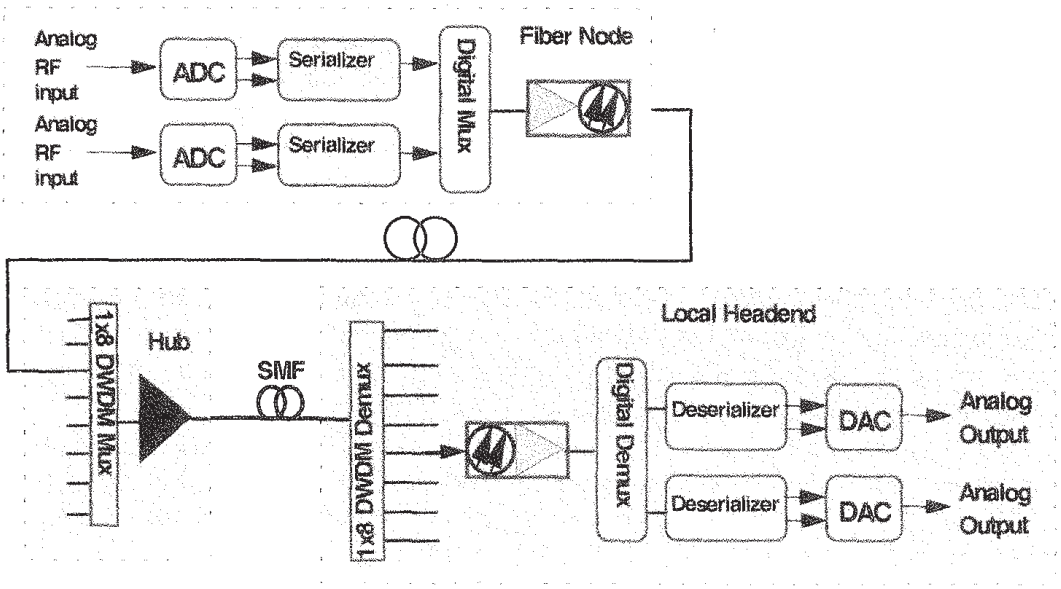


Fig. 10.18 Block diagram of digitized return path at the fiber node in DWDM network architecture. After Ref. [22] (© 2001 Optical Society of America).

12 bits of resolution. The parallel digital words are converted to a serial bit stream with the appropriate synchronization at the fiber node in order to recover the transmitted serial bit stream at the optical receiver output in the local headend. Using, for example, two 12-bit ADC (as shown in Fig. 10.18), which are currently being deployed by cable TV operators, the laser transmitter is modulated by an approximately 2.5-Gb/s TDM data stream (OC-48). The TDM data stream is optically multiplexed at the hub, and then demultiplexed at the local headend, where it is digitally demultiplexed and deserialized before it is presented to the digital-to-analog converter (DAC). The performance of the ADC is typically limited by its quantization noise, clipping noise, and distortions. Given the number of required resolution bits and the sampling frequency, the ADC noise density per unit bandwidth can be easily calculated from its SNR for a full-scale sine wave input. In analog fiber-optic links, the corresponding noise source is the laser RIN. The performance of various components, particularly laser transmitters, in return-path cable TV networks is typically characterized in terms of the noise-power ratio (NPR) curve. The NPR is simply the signal-to-noise plus the in-band clipping-and-distortion ratio. The NPR measurement loads the tested device with a Gaussian noise containing a notch at a test frequency. The depth of the notch is measured with respect to the noise power as is varied over the operating range of the tested device [22, 23]. The NPR curve is bound by Gaussian noise at low input signal levels and by clipping noise and distortions at high input signal levels relative to the optimum input level for a full-scale sine wave. The dynamic range (DR) of the component under test captures the range of

input levels between the Gaussian noise limit and the clipping-noise limit for which greater or equal to a specific NPR value can be obtained. Assuming a fully loaded return-path DWDM network, Table 10.1 shows the required NPRs and the corresponding DRs at the optical receiver output in the local headend using the FSS and digital return-path technologies with 10-bit and 12-bit ADCs and DACs [24]. The cumulative NPR of 37-dB is based on the following factors. Assuming a 64-QAM operation, one needs C/(N + I) of 27-dB for robust transmission. If four upstream bands are combined, one needs to add 6-dB to the cumulative NPR. An additional 4-dB are needed for operational margin to guarantee the 27-dB at the subscriber's home. The required large DR at the local headend is primarily attributed to two factors. First, the instantaneous magnitude of ingress noise and other interference cannot be controlled and can be relatively high. Second, STBs and CMs in the cable plant can acts as interferers, forcing upstream laser transmitters into clipping.

Several points can be drawn from Table 10.1. First, 12-bit digitized return-path technology at the fiber node provides the necessary NPR and DR at the local headend with about 2-dB margin over a 10-bit return-path technology. The return-path signals can be digitized at the secondary hubs (12-bits), and an uncooled 1310-nm DFB laser transmitter with a typical output power of 3-dBm can be used at the fiber node. Second, the 10-bit digitized return-path technology does not meet the necessary NPR and DR at the local headend. It should be pointed out that the required NPR and DR at the fiber node must be achieved over a wide operating-temperature range (–20°C to +65°C).

The digitization of the return-path with TDM in a DWDM network has a significant advantage over analog fiber links. When the return-path analog signals are digitized, the DWDM network becomes transparent to them. In other words, the digital return-path signal can be efficiently transmitted throughout the network without a noticeable degradation.

Table 10.1 Performance requirements for different return-path technologies. After Ref. [24].

Technology	NPR/DR (Node to SH)	NPR/DR (SH to PH)	Total NPR/DR (including RF)
DWDM (from fiber node)	40-dB/11-dB	42-dB/11-dB	37-dB/11-dB
DWDM+FSS (from fiber node)	38-dB/11-dB		37-dB/11-dB
DWDM+FSS (from SH)	42-dB/11-dB	42-dB/11-dB	37-dB/11-dB
Digitized at Node (12-bits)	38-dB/11-dB		37-dB/11-dB
Digitized at SH (12-bits)	40-dB/11-dB	42-dB/11-dB	37-dB/11-dB
Digitized at Node (10-bits)	36-dB/11-dB		Insufficient

Furthermore, digital signal-processing techniques can be used to minimize signal degradation before the ADC. Thus, the use of digital return-path technology in DWDM network architecture is very promising since it allows cable TV operators to reduce their network

upgrade costs while maintaining network transparency and flexibility. As the prices of the digital components continue to decline, driven down by high volumes, while their performance improves, the deployment of digital return-path technology becomes more and more attractive.

References

1. S. Ovadia and C. Lin, "Performance Characteristics and Applications of Hybrid Multichannel AM-VSB/M-QAM Video Lightwave Transmission Systems," *IEEE Journal of Lightwave Technology* **16**, 1171–1186 (1998).
2. C. Lin, K. P. Ho, H. Dai, S. K. Liaw, and H. Gysel, "High-Capacity Digital and Analog Video Trunking and Distribution Based on Hybrid WDM Systems," *OFC '97 Technical Digest*, paper ThS3.
3. W. I. Way, M. M. Choy, A. Yi-Yan, M. Andrejco, M. Saifi, and C. Lin, "Multichannel AM-VSB Television Signal Transmission Using an Erbium-Doped Optical Fiber Power Amplifier," *IEEE Photonics Technology Letters* **1**, 343–345 (1989).
4. H. Bulow, R. Fritschi, R. Heidemann, B. Junninger, H. G. Krimmel, and J. Otterbach, "Analog Video Distribution System with Three Cascaded 980 nm Single-Pumped EDFA's and 73 dB Power Budget," *IEEE Photonics Technology Letters* **4**, 1287–1289 (1992).
5. B. Clesca, P. Bousselet, J. Aug'e, J. P. Blondel, and H. F'evrier, "1480-nm Pumped Erbium-Doped Fiber Amplifiers with Optimized Noise Performance for AM-VSB Video Distribution Systems," *IEEE Photonics Technology Lett*ers **6**, 1318–1320 (1994).
6. W. Muys, J. C. van der Plaats, F. W. Willems, H. J. van Dijk, J. S. Leong, and A. M. J. Koonen, "A 50-Channel Externally Modulated AM-VSB Video Distribution System with Three Cascaded EDFA's Providing 50-dB Power Budget Over 30 km of Standard Single-Mode Fiber," *IEEE Photonics Technology Letters* **7**, 691–693 (1995).
7. C. Y. Kuo, D. Piehler, C. Gall, J. Kleefeld, A. Nilsson, and L. Middleton, "High-Performance Optically-Amplified 1550 nm Lightwave AM-VSB CATV Transport System," *OFC '96 Technical Digest* **2**, paper WN2.
8. H. Dai, S. Ovadia, and C. Lin, "Hybrid AM-VSB/M-QAM Multichannel Video Transmission Over 120-km of Standard Single-Mode Fiber with Er-Doped Optical Fiber Amplifiers," *IEEE Photonics Technology Letters* **8**, 1713–1715 (1996).
9. S. Ovadia, "CNR Limitations of Er-Doped Optical Fiber Amplifiers in AM-VSB Video Lightwave Trunking Systems," *IEEE Photonics Technology Letters* **9**, 1152–1154 (1997).

10. Q. Shi and S. Ovadia, "Effects of Clipping-Induced Impulse Noise in Externally Modulated Multichannel AM/QAM Video Transmission Systems," *IEEE Transactions on Communications* **46**, 1448–1450 (1998).
11. D. Piehler, J. Kleefeld, C. Gall, C. Y. Kou, A. Nilsson, and X. Zou, Technical Digest, Optical Amplifiers and their Applications, Monterey, paper SaB2 (1996).
12. M. C. Wu, C. H. Wang, and W. I. Way, "CSO Distortions Due to the Combined Effects of Self- and External-Phase Modulations in Long Distance 1550-nm AM-CATV Systems," *IEEE Photonics Technology Letters* **11**, 718–720 (1999).
13. K. Kikushima, Ko-ichi Suto, H. Yoshinaga, and E. Yoneda, "Polarization Dependent Distortion in AM-SCM Video Transmission Systems," *IEEE Journal of Lightwave Technology* **12**, 650–657 (1994).
14. B. Clesca, P. Bousselet, and L. Hamon, "Second-Order Distortion Improvements or Degradations Brought by Erbium-Doped Fiber Amplifiers in Analog Links Using Directly Modulated Lasers," *IEEE Photonics Technology Letters* **5**, 1029–1031 (1994).
15. C. Y. Kuo and E. E. Bergmann, "Second-Order Distortion and Electronic Compensation in Analog Links Containing Fiber Amplifiers," *IEEE Journal of Lightwave Technology* 10, 1751–1759 (1992).
16. J. Ohya, H. Sato, M. Mitsuda, T. Uno, and T. Fujita, "Second-Order Distortion of Amplified Intensity-Modulated Signals with Chirping in Erbium-Doped Fiber," *IEEE Journal of Lightwave Technology* **13**, 2129–2135 (1995).
17. O. Sniezko, "Video and Data Transmission in Evolving HFC Networks," OFC '98 Technical Digest, paper WE4 (1998).
18. O. Sniezko, "Reverse Path for Advanced Services – Architecture and Technology," *NCTA Technical Papers*, 11–30 (1999).
19. S. Ovadia, "Advanced Upstream CATV Access Technologies and Standards," *Digest of the IEEE/LEOS RF Photonics for CATV and HFC Systems*, 35–36 (1999).
20. CableLabs, *Data-Over-Cable Service Interface Specifications (DOCSIS): Radio Frequency Interface Specification*, SP-RFIv1.1-I03-991105 (1999).
21. T. Brophy, R. Howald, and C. Smith, "Bringing Together Headend Consolidation and High-Speed Data Traffic in HFC Architecture Design," *NCTA Technical Papers*, 189–204 (1999).
22. O. J. Sniezko and T. Werner, "Return-Path Active Components Test Methods and performance Requirements," Conference on Emerging Technologies Proceedings, 263–294 (1997).
23. L. West, "The Effect of Preamplifier Compression on Measured Noise Power Ratios," *IEEE Photonics Technology Letters* **12**, 924–926 (2000).
24. S. Ovadia, "Advanced Return-Path Cable TV Access Technologies," *OFC '01 Technical Digest* (2001).

CHAPTER 11

DATA-OVER-CABLE INTERFACE SPECIFCATIONS (DOCSIS) PROTOCOL

The data-over-cable interface specifications (DOCSIS) 1.1 standard is the primary protocol in the US for high-speed data transmission using CMs operating over HFC network. The purpose of this chapter is to explain the operation principles of the downstream and upstream physical (PHY) layer (Sections 11.2 and 11.3) as well as the *medium access control* (MAC) layer of the DOCSIS protocol. Sections 11.5 to 11.8 discuss the MAC layer format, features, and operation. In particular, quality of service and an upstream packet fragmentation are discussed in Section 11.8, and the interaction between the CM and the CM termination system (CMTS) is discussed in Section 11.9. In addition, the different random access and contention resolution methods are reviewed in Section 11.6.

11.1 DOCSIS Communication Protocol

The primary function of the CM system is to transparently transmit IP packets between the cable TV headend and the subscriber. The CM and CMTS operate as IP and logical-link-control (LLC) hosts as defined in the IEEE 802 standard [2] for communication over cable TV network. Figure 11.1 shows the defined DOCSIS protocol stack on the RF interface. The physical (PHY) layer consists of the *physical media dependent* (PMD) sublayer and the downstream *transmission convergence* (TC) sublayer. The data-link-layer (DLL) above the PHY layer consists of three sub-layers as follows: (A) medium-access-control (MAC) layer, (B) link security sublayer, and (C) logical link control (LLC) sublayer. The MAC defines the procedure and parameters in which the CM can interact with the CMTS in order to support various services on both downstream and upstream channels. The Link Security sublayer provides the necessary security for the transmitted IP packets [3]. The network layer protocol, which operates above the LCC sublayer, is IP version 4 and migrating to IP version 6 [4]. In the network layer, both the CM and CMTS must support *address resolution protocol* (ARP) over DIX link-layer framing [5,6]. Above the network layer, there are various network management and operation protocols including:

- Simple network management protocol (SNMP) for network management

- Trivial file transfer protocol (TFTP) is a file transfer protocol, which is used for downloading software and configuration information to a remote location [7]

- Dynamic host configuration protocol (DHCP), which is used to assign IP addresses and passing configuration information to hosts on a TCP/IP network [8]

- Time of Day Protocol, which is used to obtain the time of day.

Figure 11.2 shows the data forwarding through a CM and a CMTS. The data forwarding through the CMTS may be transparent bridging, or may employ network-layer forwarding (routing and IP switching). The data forwarding through the CM is link-layer transparent bridging. It should be pointed out that the data forwarding between the upstream and downstream channels within the MAC layer is different from a conventional local-area-network (LAN) forwarding because the upstream channels are point-to-point transmission on a shared media, while downstream channels are point-to-multipoint transmission on a shared media. In addition, the RF characteristics of upstream channels are significantly different from the downstream channels.

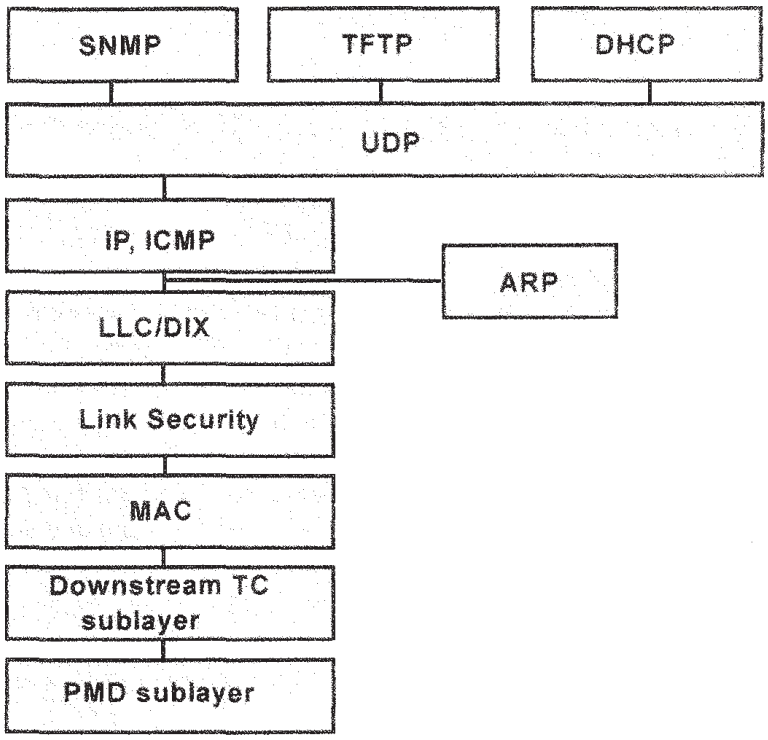


Figure 11.1 DOCSIS communication protocol stack on the RF interface. After Ref. [1].

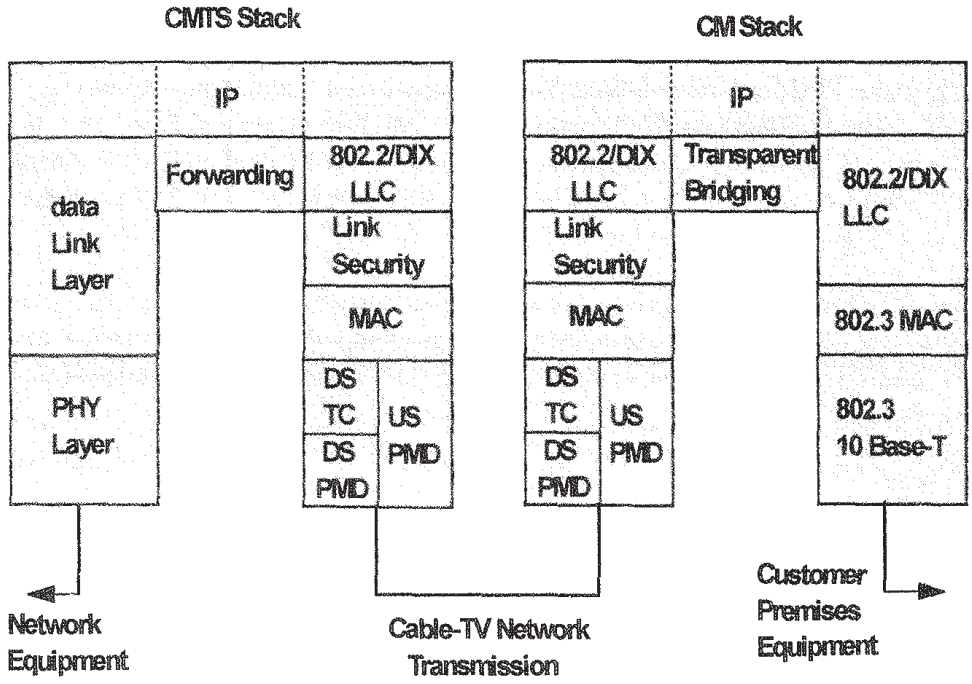


Figure 11.2 Data forwarding through a CM and a CMTS. After Ref. [1].

There are various forwarding rules for the CM and the CMTS, which are similar to the IEEE 802.1D standard, but with some modifications as described in DOCSIS 1.1 protocol standard [1]. The forwarding rules are beyond the discussion here, and further reading is encouraged [9].

11.2 Downstream PHY Layer

The DOCSIS protocol standard defines the procedure and requirements for high-speed data transmission between the subscriber's CM and the cable-modem-termination-system (CMTS) over HFC cable TV network. The PHY layer of DOCSIS protocol stack for down-stream data transmission is divided into two sublayers as follows:

- PMD sublayer (both downstream and upstream)
- Downstream TC sublayer, which is sandwiched between the PMD sublayer the MAC layer, exists only for downstream data transmission

The next two subsections discuss the technical specifications of each of these sublayers.

11.2.1 Downstream PMD Sublayer

The downstream PMD sublayer defines the RF transmission parameters of both the CM and the CMTS. The downstream PMD transmission parameters are specified to conform to ITU-T Recommendation J.83 Annex B for low-delay video applications [10]. These downstream RF parameters for the CMs have been discussed in Chapter 7 on QAM modems, and

Table 11.1 CMTS RF output parameters according to DOCSIS 1.1 standard.

CHARACTERISTICS	SPECIFICATION
Center Frequency Range (f_c)	91 MHz to 857 MHz ± 30 kHz[1]
RF Output Level	50-dBmV to 61 dBmV (adjustable)
Symbol Rate	5.056941 Mbaud for 64-QAM 5.360537 Mbaud for 256-QAM
Spectrum Shaping Filter	SRRC with $\alpha \cong 18\%$ (64-QAM) SRRC with $\alpha \cong 12\%$ (256-QAM)
Phase Noise	1–10 kHz: –33 dBc DS noise power 10–50 kHz: –51 dBc DS noise power 50 kHz to 3 MHz: –51 dBc DS noise power
Output Return Loss	> 14 dB up to 750 MHz > 13 dB above 750 MHz
Total Discrete Spurious In-Band	< –57 dBc for $f_c \pm 3$ MHz
In-Band Spurious and Noise	< –48 dBc
Adjacent Channel Spurious and Noise	< –58 dBc in 750 kHz from $f_c \pm 3$ MHz to $f_c \pm 3.75$ MHz < –62 dBc in 5.25-MHz from $f_c \pm 3.75$ MHz to $f_c \pm 9.0$ MHz[2] < maximum of –65-dBc or –12-dBmV in 6 MHz from $f_c \pm 9.0$ MHz to $f_c \pm 15$ MHz
Spurious and Noise in Other Channel	< –12 dBmV in each 6-MHz channel
Output Impedance	75-ohms
Connector	F connector per IPS-SP-406
CMTS Master Clock Frequency	10.24 MHz ± 5-ppm over 0°C to 40°C temperature range and up to 10 years
CMTS Timestamp Jitter	< 500 ns

[1] ± 30-kHz was specified to allow up to 25-kHz frequency offset due to the QAM RF upconverters at the headend.
[2] Excluding up to 3 spurs, where each spur must be < –60-dBc when measured in 10-kHz band.

thus will not be repeated here. However, let us briefly review the CMTS RF modulated output requirements. The CMTS must transmit to the CM according to the standard, IRC, or HRC frequency plans, but it is not required to transmit 64/256-QAM channels below 91-MHz. The rationale was to set aside a frequency gap (42 to 91-MHz) to minimize potential performance degradation due to nonlinear distortions and spurious noise leaking from upstream to the downstream frequency band.

Table 11.1 summarizes the CMTS RF output parameters according to DOCSIS 1.1 standard. The total in-band spurious and noise specification in Table 11.1 includes all the discrete spurious noise, interference peaks, AWGN, and undesired downstream QAM transmitter products. In order to reduce the effect of adjacent channel interference (ACI) on the transmitted QAM channel, the relative magnitude of the spurious noise outside the desired channel is reduced from less than –58-dBc to less than –65-dBc, depending on the frequency location of the spurious noise. For discussion of the upstream spurious output from a CM, see Section 11.3.4.

11.3 Upstream PHY Layer

The upstream PMD sublayer specifies the use of frequency-division-multiple access (FDMA) and time-division-multiple access (TDMA) methods in a burst mode with two modulation formats, QPSK and 16-QAM, operating at different symbol rate and channel bandwidths. Before discussing the different burst attributes and parameters, let us review the building blocks of the upstream CM transmitter and their requirements.

The various signal-processing building blocks of the upstream QAM burst transmitter are shown in Figure 8.4. The first building block separates the input packets into codewords, where each packet is equal to the number of information bytes in a codeword. This step is called blocking the data. The next building block is the FEC encoder. Note that the upstream PHY layer FEC encoder for a CM is different than the one used in a digital STB (see Section 8.4.1). It consists of R-S coding, bit-to-symbol ordering, and randomizer. The R-S codes over GF(256) can be selected from T = 1 to T = 10 with the following R-S generating polynomial:

$$g(X) = (X + \alpha^0)(X + \alpha^1)\ldots(X + \alpha^{2T-1}) \tag{11.1}$$

where the primitive α is 0x02. The primitive polynomial for the R-S code over GF(256) is given by:

$$p(X) = X^8 + X^4 + X^3 + X^2 + 1 \tag{11.2}$$

The codeword sizes that the upstream CM transmitter can provide range from 18 bytes (16 information bytes plus two parity bytes for T = 1) up to a maximum of 255 bytes. Note that the uncoded word size can be as small as one byte.

The input serial bit stream to the R-S encoder, which was received from the MAC layer in the CM, is mapped into R-S symbols at the encoder. The first bit of the stream is mapped into the MSB of the first R-S symbol. The MSB of the first R-S symbol out of the encoder is mapped into the first bit of the serial stream before it is fed to the randomizer.

After the bit-to-symbol mapping, the symbols are randomized or scrambled to ensure equal probabilities to all the QPSK and 16-QAM constellation points. Figure 11.1 shows the randomizer structure using linear shift registers. The randomizer generating polynomial is given by:

$$g(X) = X^{15} + X^{14} + 1 \tag{11.3}$$

The randomizer works as follows. First, the randomizer's registers are cleared and loaded with the seed value at the beginning of each burst. Then, the first output bit from the randomizer is calculated by XOR, the seed value with the first bit of data of each burst, which is the MSB of the first data symbol. The seed value of the randomizer, which can take an arbitrary value, is calculated in response to the *upstream channel descriptor* (UCD) message from the CMTS, which will be discussed later. The next building block, after the FEC block, prepend a variable-length preamble to the coded data symbols. The preamble length

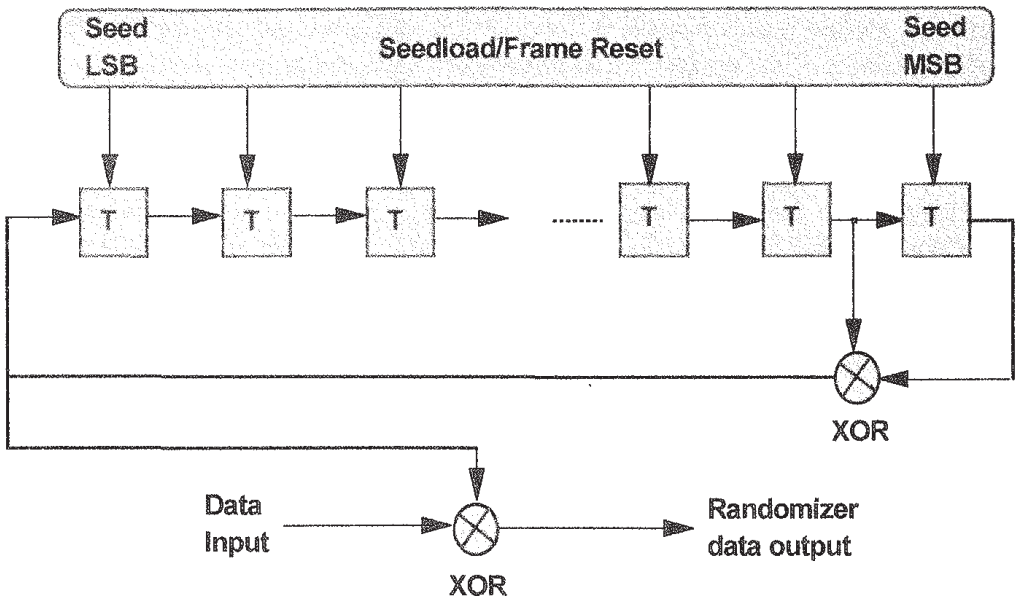


Figure 11.3 Randomizer structure in upstream CM transmitter. After Ref. [1].

is up to 1024 bits for both QPSK and 16-QAM modulation formats, and its value is programmable and must be an integer number of modulation symbols. Thus, the maximum preamble length is 512 QPSK symbols and 256 16-QAM symbols. The first bit of the preamble pattern, which is the also the first bit into the symbol mapper, is designated by the preamble value offset (PVO) to identify the bits to be used for the preamble value. The maximum length of the PVO is 1022 bits. The preamble length and values are calculated based on the transmitted UCD message from the CMTS.

The next building blocks in the upstream CM transmitter, namely, the symbol mapper, SRRC filters, and modulator, are similar to the one already described in Chapter 8 and will not be repeated here. In general, the upstream transmission specifications are divided into three main categories as follows: (A) channel parameters, (B) burst profile attributes, and (C) unique user parameters. Let us review the upstream channel parameters for CM as specified by DOCSIS 1.0 standard [1].

11.3.1 Upstream Channel Parameters and Requirements

The upstream channel parameters include the allowed symbol rates, channel center frequency, and the 1024-bit preamble. The Table 11.2 shows the five different symbol rates with the corresponding upstream channel bandwidths. Notice that the upstream channel bandwidth is the –30-dB bandwidth and not the –3-dB bandwidth as typically used in communication systems. The upstream spectrum is shaped by the SRRC filter with a roll-off factor of 25%. Thus, according to Table 11.2, the maximum transmission rate is 10.24-Mb/s using a 16-QAM modulation format. The required burst profile attributes as well as timing from an upstream CM transmitter are discussed in the next section.

Table 11.2 Upstream symbol rates and channel bandwidths.

Upstream Symbol Rate	Upstream Channel Bandwidth
160 kbaud	200 kHz
320 kbaud	400 kHz
640 kbaud	800 kHz
1.28 Mbaud	1.6 MHz
2.56 Mbaud	3.2 MHz

11.3.2 Burst Profiles

To successfully transmit upstream packets, the CM must generate each burst at the appropriately allocated time. All the burst profile attributes are specified via the burst descriptors in the UCD, and are assigned to the CM for upstream transmission in the upstream *bandwidth allocation map* (MAP) by the CMTS. A burst length of 0 mini-slots in the upstream channel

profile means that the burst length is variable on that channel for the particular burst type. Tables 11.3 and 11.4 summarize the burst profile attributes as well as the unique burst parameters for each subscriber.

Table 11.3 Burst profile attributes according to DOCSIS 1.1 standard.

Burst Profile Attributes	Specification
Upstream Modulation Format	QPSK or 16-QAM
Differential Encoding	On or Off
Preamble Length	Up to 1024 bits
Preamble Offset Value	0 to 1022
FEC	T = 0 to 10 (0 implies no FEC)
FEC Codeword Information Bytes (k)	Fixed or Shortened, 16 to 253 (FEC on)
Randomizer Seed	15 bits
Randomizer Setting	On or Off
Maximum Burst Length	0 to 255 (mini-slots)
Guard Time	5 to 255 symbols
Last Codeword Length	Fixed or Shortened

The CM ranging process provides the correct timing offset such that the transmitted packets are aligned to the proper mini-slot boundary. Since the timing delays between the CM and the CMTS are essentially constant, any additional time delay must be accounted by the CMTS in the guard time of the transmitted packets to synchronize the upstream TDMA transmission. The ranging offset parameter in Table 11.4 is the time-delay correction applied by the CM to the CMTS, and it is essentially equal to the round-trip delay of the CM from the CMTS. In return, the CMTS provides feedback timing offset correction to the CM,

Table 11.4 Upstream unique burst parameters for each user according to DOCSIS 1.1

User Unique Parameters	Specification
Upstream Power Level Range	+8 dBmV to +55 dBmV (16-QAM) +8 dBmV to 58 dBmV (QPSK)
Power Level Increment	1 dB
Channel Frequency Offset	± 32 kHz in 1-Hz increments, but with ± 10-Hz implementation
Ranging Offset	0 to $(2^{16}-1)$ in increments of 6.25-μs/64
Burst Length Variations	1 to 255 mini-slots
Transmit Equalizer Coefficients	Up to 64 coefficients
Equalizer Coefficient Length	4 bytes (2 real and 2 imaginary)

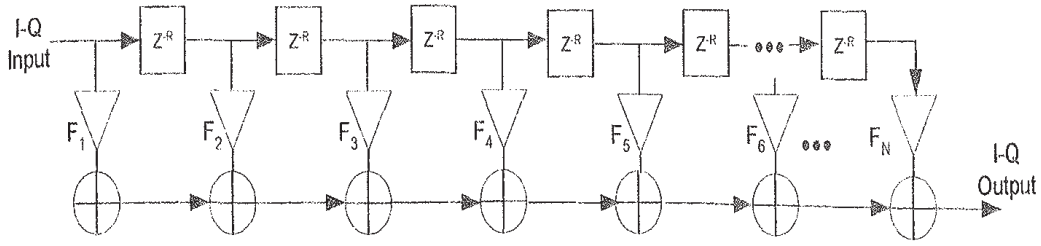


Figure 11.4 Pre-equalizer structure in upstream CM transmitter. After Ref. [1].

based on successful reception of one or more bursts with an accuracy of 1/2 symbol and timing resolution of 1/64 of the frame tick increment (6.25-μs/64 = 97.65625-ns = 1/10.24-MHz). In other words, the timing resolution is equal to the inverse of the CMTS clock frequency. The CM responds to the ranging offset correction with a resolution of 1 burst symbol and with accuracy of ±0.25-μs ± 1/2 symbol, relative to the mini-slot boundaries.

Adaptive pre-equalization, which is also known as precoding, in the upstream CM transmitter is a well-known method to combat the effect of linear distortions in the transmission channel [11, 12]. DOCSIS 1.1 specifies the use of up to 64 fractional-spaced complex taps with 4 bytes for each complex tap coefficient. The total number of taps per symbol varies from 1 to 4. The upstream channel characteristics are learned by the burst receiver in the CMTS, which sends the updated pre-equalizer coefficients for the CM transmitter using the ranging response message. The ranging response message is transmitted by the CMTS in response to the received ranging request (RNG-REQ) from the CM. The CM transmits initially and periodically the RNG-REQ as requested by the CMTS to determine network time-delay to adjust its power level. The ranging and synchronization process will be further discussed in this chapter.

Prior to making an initial ranging request and whenever the upstream channel frequency or symbol rate changes, the CM must initialize the coefficients of the pre-equalizer to a default setting in which all coefficients are zero except the real coefficient of the first tap (i.e., F1). During initial ranging, the CM must compensate for the delay (ranging offset) due to a shift from the first tap to a new main tap location of the equalizer coefficients sent by the CMTS. The pre-equalizer coefficients are then updated though the subsequent ranging process (periodic station maintenance). The main tap location cannot change during periodic station maintenance by the CMTS. Equalizer coefficients may be included in every RNG-RSP message, but typically they occur only when the CMTS determines that the channel response has significantly changed. The frequency of equalizer coefficient updates in the RNG-RSP message is determined by the CMTS. The CM must normalize the pre-equalizer coefficients in order to guarantee proper operation (such as not to overflow or clip). The CM must also compensate for the gain (or loss) due to any coefficient scaling performed locally.

11.3.3 Burst Timing

The DOCSIS standard requires a CM to switch between different burst profiles without a reconfiguration time between consecutive bursts. However, for the following burst profile parameters: (A) output power, (B) modulation format, (C) symbol rate, (D) offset frequency, (E) channel frequency, and (F) ranging offset, the CMTS has to allocate at least 96 symbols reconfiguration time to the CM. Figure 11.5 shows the burst timing convention according to DOCSIS 1.1 protocol standard. The ramp-up and ramp-down times represent the time spreading of the transmitted symbols beyond their nominal symbol duration Ts (= 1/Rs) due to the spectral shaping filter at both the upstream CM transmitter and CMTS receiver. In this figure, ten-symbol ramp-up time with eight-symbol ramp down time are shown with no guard band and assuming no timing errors. Notice that the timing is referenced to the symbol center of the first symbol of each burst. Thus, the 96-symbols reconfiguration time is measured from the last symbol center of one burst to the first symbol center of the following burst. If the output power of the CM is changed by more than 1-dB or less than 1-dB, the reconfiguration time is increased to 96 symbols plus 10-μs and 96 symbols plus 5-μs, respectively. It should be pointed out that the output power of the upstream CM transmitter is

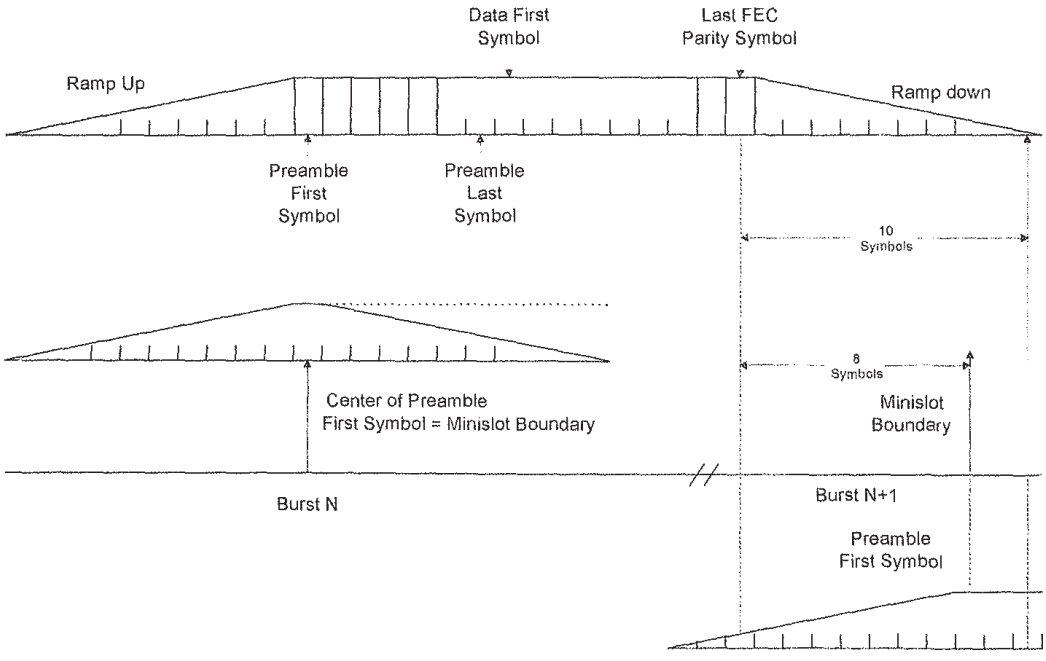


Figure 11.5 Upstream burst timing convention. After Ref. [1].

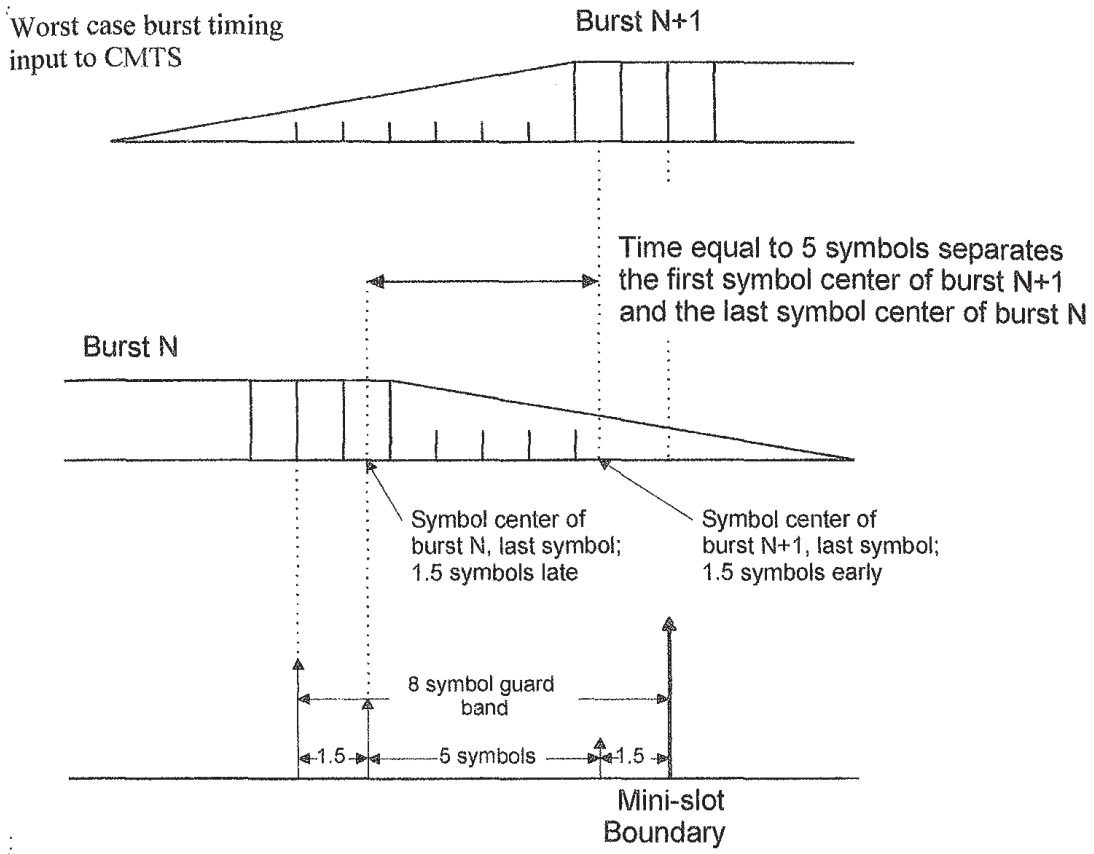


Figure 11.6 Worst case upstream burst timing. After Ref. [1].

required to be essentially constant (less than ± 0.1-dB) within any given TDMA burst. If the channel frequency is changed, the reconfiguration time is increased to 96 symbols plus 100-ms.

Figure 11.6 shows the worst-case burst timing transmission for a CM according to DOCSIS 1.1 standard [1]. Burst N arrives 1.5 symbols late, while the following burst (N+1) arrives 1.5 symbols early, reducing the symbol guard band to 5 symbols, which is the minimum time separation between consecutive bursts required by DOCSIS 1.1 protocol.

11.3.4 Upstream Spurious Power Outputs

Due to the harsh upstream channel characteristics, there is a need to improve the CM trans-

Table 11.5 Upstream spurious emission specifications for a CM.

Parameter	Transmitting Burst	Between Bursts
Inband Spurious Power	–40 dBc	Max {–72 dBc, –59 dBmV}
Adjacent Band Spurious Power	–45 dBc @ 160-kBaud[1] –42 dBc @ 160-kBaud[2] –39 dBc @ 160-kBaud[3] –45 dBc @ other symbol rates[4] –44 dBc @ 1280-kBaud[5] –41 dBc @ 2560-kBaud[6]	Max {–72 dBc, –59 dBmV}
≤ 3 Carrier-Related Frequency Bands	–47 dBc	Max{–72dBc, –59 dBmV}
Spurious Power within 5–42-MHz	–53 dBc @ 160-kBaud –50 dBc @ 320-kBaud –47 dBc @ 640-kBaud –44 dBc @ 1280-kBaud –41 dBc @ 2560-kBaud	Max{–72 dBc, –59 dBmV}
CM Integrated Spurious Power Limits (in 4-MHz)	Max {-40 dBc, -26 dBmV} in 42–54-MHz –35 dBmV in 54–60-MHz –40 dBmV in 60–88-MHz –45 dBmV in 88–880-MHz	 –26 dBmV –40 dBmV –40 dBmV Max {–45 dBmV, –40 dBc}
CM Discrete Spurious Power Limits	Max {–50 dBc, 36 dBmV} in 42–54-MHz –50 dBmV in 54-880-MHz	 –36 dBmV –50 dBmV

[1] Assuming adjacent channel symbol rates of 160-kBaud, 320-kBaud, and 640-kBaud, with measurement intervals from 20-kHz to 180-kHz, 40–360-kHz, and 80–720-kHz relative to channel edge.
[2] Assuming adjacent channel symbol rate of 1280-kBaud, with a measurement interval from 160-kHz to 1440-kHz relative to channel edge.
[3] Assuming adjacent channel symbol rate of 2560-kBaud, with a measurement interval from 320-kHz to 2880-kHz relative to channel edge.
[4] Assuming adjacent channel symbol rates of 160-kBaud, 320-kBaud, and 640-kBaud, with the same measurement intervals as in footnote 1.
[5] Assuming adjacent channel symbol rate of 1280-kBaud, with measurement interval from 160-kHz to 1440-kHz relative to channel edge.
[6] Assuming adjacent channel symbol rate of 2560-kBaud, with a measurement interval from 320-kHz to 2880-kHz relative to channel edge.

mission fidelity. Consequently, this rationale led the DOCSIS 1.1 standard to impose streak limits on the upstream and downstream spurious power levels at different frequency bands relative to the CM transmitted burst power level. The transmission performance of a CM operating at a given symbol rate may be degraded due to adjacent channel spurious emissions from other CMs operating at different symbol rates. Table 11.5 specifies the required in-band, discrete, and integrated spurious power levels from a CM during burst transmission (active state) and between bursts (idle state). The spurious power measurement is done in the adjacent channel interval, which corresponds to the adjacent channel symbol rate. However, the measurement interval does not start at the channel edge, but at a frequency spacing of 12.5% of the adjacent symbol rate relative to the channel band edge. This is because the channel bandwidth is the bandwidth measured at –30-dB, while the symbol rate bandwidth is the bandwidth measured at –3-dB. For example, the 200-kHz channel bandwidth has only a 160-kHz noise bandwidth or 20-kHz excess bandwidth on each side of the channel band. Thus, the spurious measurement interval is specified to start from 20-kHz away from the channel edge up to 180-kHz. The measurement of the upstream spurious emissions in the 5–42-MHz band starts at initial distance of 220-kHz from the channel band edge for a symbol rate of 160-kBaud, and it is repeated until at increasing frequency spacing from the channel until the upstream band edge is reached. For these specifications, the spurious measurement interval starts beyond the adjacent channel. Consequently, 200-kHz (channel bandwidth) is added to 20-kHz, which is initial starting frequency from the channel edge. In addition, the CM must control its spurious output levels immediately before and after the TDMA burst; namely, it's burst on and off transients. This on/off spurious output levels must be less than 100-mV, and occur not faster than 2-μs of constant slewing when the CM is operating at +55-dBmV or more. For each 6-dB drop in output power level from 55-dBmV, the transient voltage must be reduced by a factor of 2, down to 7-mV at +31-dBmV or below.

11.3.5 Burst Frame Structure

The CM can operate in either a fixed-length codeword mode or in a shortened last codeword mode. A codeword consists of FEC parity bytes and payload data bytes, where the minimum codeword length (number of information bytes) is 16 bytes. These two modes are illustrated in Figure 11.7. In the fixed-length codewords, the preamble starts at the mini-slot boundary, and after all the data are encoded, zero-fill occurs in the last codeword to reach the assigned k-bytes per codeword. The zero-fill continues until no additional fixed-length codewords can be inserted before the end of the last allocated mini-slot in the grant. In the shortened last codeword mode, let k' (k' < k) be the number of remaining information bytes in the last codeword. We assumed that the full-length burst was partitioned into k-bytes length codewords. Also, let k" (k' < k") be the number of burst bytes plus zero-fill bytes in the shortened last codeword. In this mode, the CM zero fill (k"–k') bytes until the end of the mini-slot allocation, which in most cases are next to the mini-slot boundary. In example 2 (Figure 11.7), the packet length satisfies the following relation: $k + k' \leq k + k'' \leq 2k$. It

should be pointed out that if after the zero-fill of additional codewords, each with k-bytes, there are less than 16 bytes remaining in the allocated grant of the mini-slot, then the CM must not create a shortened codeword.

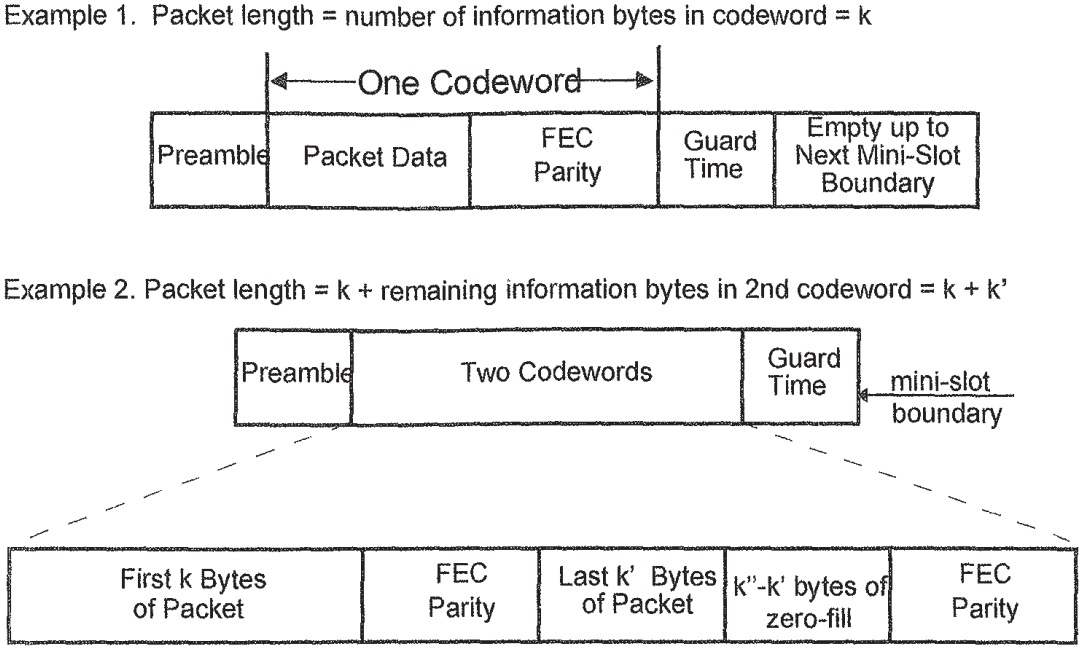


Figure 11.7 Burst frame format examples with fixed and flexible burst length packets. After Ref. [1].

11.4 Downstream Transmission Convergence Sublayer

The purpose of the downstream TC sublayer is to provide a common interface between the PMD sublayer and the MAC layer for future multiplexing/de-multiplexing of MPEG-2 video and data over the PMD sublayer. The downstream bit-stream is defined as continuous stream of 188-byte long MPEG packets [13]. The format of MPEG packet carrying DOCSIS data is shown in Figure 11.8. The 4-byte MPEG header identifies the content of the MPEG payload as either carrying DOCSIS MAC payload or digital video payload. The MPEG header format conforms to the MPEG standard, but its use is restricted to prevent the inclusion of an adaptation_field in the MPEG packets.

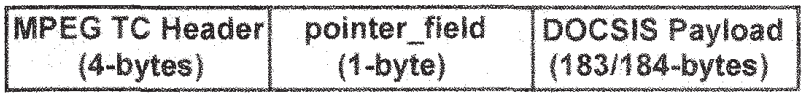


Figure 11.8 Format of MPEG packet according to the DOCSIS protocol.

The MPEG payload portion of the MPEG packet carries the DOCSIS MAC frames. The first byte following the MPEG header, which is called the pointer_field, is present if the payload_unit_start_indicator (PUSI) bit of the MPEG header is set. The pointer_field indicates the number of bytes in the transmitted packet that the CM decoder must skip immediately after the pointer_field for the beginning of a DOCSIS MAC frame. The pointer_field is also present to indicate any stuff_byte(s) following the MAC frame. Stuff_bytes, which have the value of 0xFF, are used within the DOCSIS payload to fill possible gaps between contiguous DOCSIS MAC frames. This value (0xFF) was chosen as an unused value for the first byte of the DOCSIS MAC frame. Note that MAC frame may begin anywhere within the MPEG packet, and several MAC frames may exist within one MPEG packet. The MAC frames may be concatenated one after the other or may be separated by optional stuffing bytes. If a long MAC frame is used such that it spans multiple MPEG packets, the pointer_field of the succeeding frame points to the byte following the last byte of the tail of the first frame.

Another important point is related to the multiplexing of MPEG packets carrying DOCSIS data with digital video data. The CMTS is required not to transmit MPEG packets with the DOCSIS PID consisting of only stuffing bytes. Instead, null MPEG packets should be transmitted. The reason for this requirement is to preserve the timing information that exists in the DOCSIS MAC during the multiplexing operation.

11.5 Media Access Control (MAC) Layer

The MAC layer in the DOCSIS 1.1 protocol standard over HFC networks defines the procedure and parameters in which the CM can interact with the CMTS in order to support various services on both downstream and upstream channels. The primary features of the MAC layer protocol are as follows:

- Upstream bandwidth allocation controlled by the CMTS
- Upstream allocation of mini-slots to the CM by the CMTS
- Dynamic mix of contention and reservation-based upstream transmit opportunities
- Bandwidth efficiency through support of variable length packets
- Support of quality of service (QoS) including:
  1. Support of bandwidth and latency guarantees

2. Packet classification
3. Dynamic service establishment

- Extensions provided for security at the data link layer
- Support of a wide range of data rates

Before we discuss the MAC layer frame formats, let us introduce the concept of service flow, which is an essential part of the DOCSIS MAC protocol. A service flow is a MAC-layer transport service, which provides unidirectional transport of packets between the CM and the CMTS. The service flow also shapes, polices, and prioritizes traffic according to QoS traffic parameters, which are defined for the flow. A service flow ID (SFID) is a 32-bit identifier, which is assigned to a service flow by the CMTS. The CMTS can assign one or more SFIDs to each CM, depending on the requested service flows from the particular CM. This unique mapping can be negotiated between the CMTS and the CM during CM registration or via dynamic service establishment. With an active or admitted upstream service flow, the CMTS assigns the so-called service ID (SID) in addition to the SFID. The SID provides the necessary means for the CMTS to implement the requested upstream QoS. Multiple SIDs allow advance CM to support multiple service classes and to be interoperable with basic CMs, which support only a single SID. The length of the SID parameter is 14 bits.

The second parameter is called mini-slot, which is a unit of granularity for upstream transmission opportunities. A mini-slot is 2^K6.25-μs (K = 1,...,7). Notice that one mini-slot corresponds to the inverse of the smallest symbol rate, namely, 160-kHz. The minimum mini-slot is 12.5-μs, and has two time ticks.

11.5.1 MAC Frame Format

Since upstream request packets and data packets are transmitted in a contention manner, the MAC frame, which is a variable-length packet, is the basic unit of data exchanged at the data link layer (DLL) between the CM and the CMTS over the cable TV network. Figure 11.9 shows a generic MAC frame format. Preceding the MAC frame is either a PMD sublayer overhead (for upstream transmission) or MPEG TC sublayer header (for downstream transmission). The PMD sublayer overhead indicates to the MAC layer the start of a burst at the mini-slot boundary, where the MAC frame is required to start. Thus, the MAC layer can account for the PMD overhead when upstream bandwidth allocation is done (see Section 11.4.2). It should be pointed out that the FEC overhead is spread throughout the MAC frame and is assumed to be transparent to the data stream. The MAC frame consists of a MAC header and an optional variable-length data protocol-data-unit (PDU).[7] The MAC header uniquely identifies the contents of the MAC frame, including the presence of data PDU in the MAC frame. Four different types of data PDUs are supported: (A) variable-

[7] PDU is a unit of data specified in a layer protocol and consisting of protocol control information and layer user data.

length packets (18 to 1518-bytes), (B) ATM packets (n x 53-bytes), (C) MAC specific header (no PDU), and (D) reserved PDU for future use.

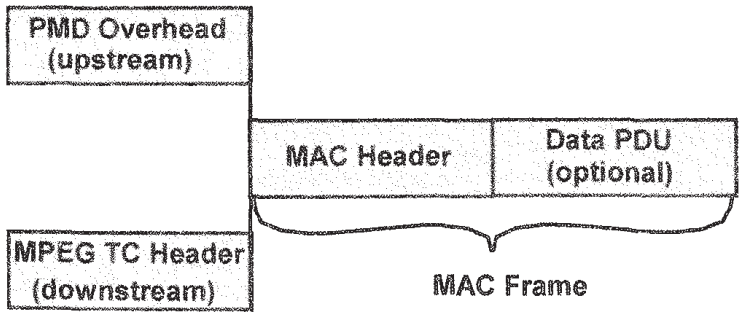


Figure 11.9 Generic MAC frame format according to the DOCSIS protocol.

Many MAC messages incorporate the use of type-length-value (TLV) fields. The TLV represents encoding of three fields, in which the first field indicates the type of element (1-byte), the second field indicates the length of the element (1-byte), and the third field indicates the value. This encoding allows new parameters to be added and correctly interpreted by the CM and CMTS. If the CM or CMTS do not recognize the new parameters, they must skip them and not handle them as errors.

11.5.2 MAC Management Messages

Figure 11.10 shows the MAC header and the MAC management message header formats, which are common across all the MAC management messages. The first byte of the MAC header is the frame control (FC) field, which defines the type and format of data protocol data unit (PDU). Four different types of data PDUs that are supported are (A) variable-length packets (18 to 1518-bytes), (B) ATM packets (n x 53-bytes), (C) MAC specific header (no PDU), and (D) reserved PDU for future use. The MAC specific header can be further divided into five categories as follows: (I) timing header, (II) MAC management header, (III) request frame, (IV) fragmentation header, and (V) concatenation header. The MAC specific headers are used for specific functions including downstream timing and upstream ranging or power adjustments, bandwidth requests, and fragmentation and concatenation of multiple MAC frames.

Timing Header:
This specific MAC header, which is followed by a packet data PDU, is used to transport the *Global Timing Reference* in the downstream channel for synchronization all the CMs. CM MAC synchronization is achieved if the CM has received two SYNC messages within the maximum SYNC interval (= 200-ms). Each SYNC message contains the CMTS timestamp,

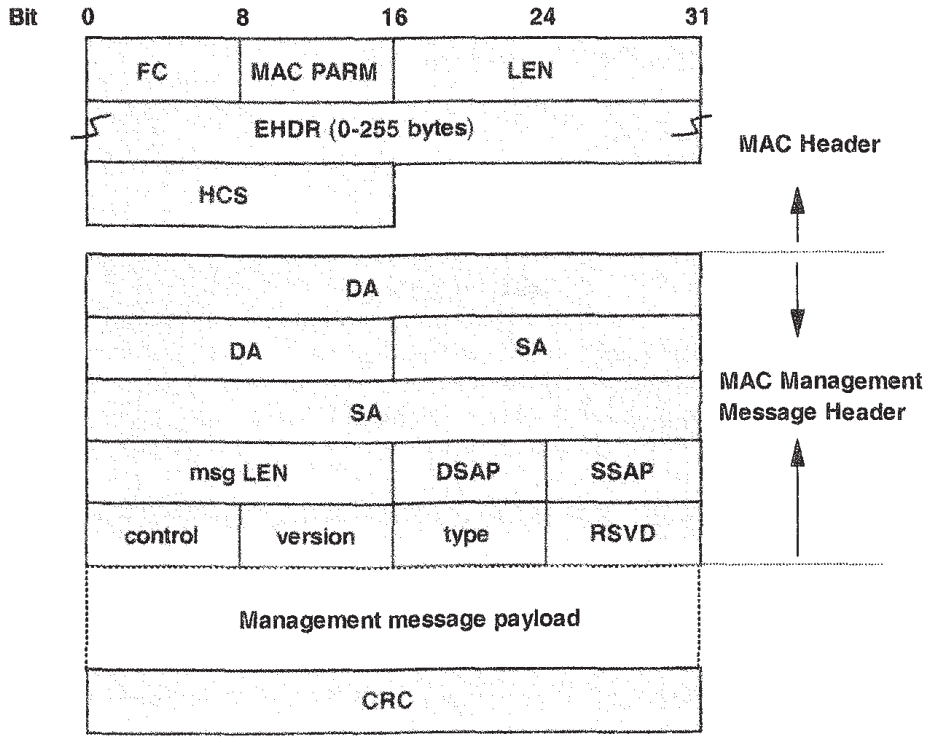


Figure 11.10 MAC header and MAC management header fields.

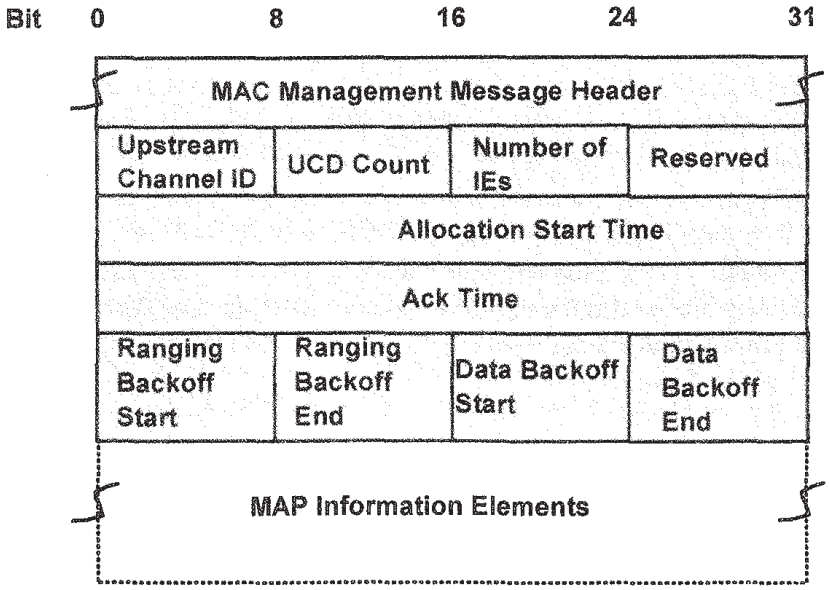


Figure 11.11 Upstream bandwidth allocation MAP format.

which tells the CM when exactly the CMTS has transmitted the message. The CM then compares the actual time the message was received with the CMTS timestamp, and adjusts its local clock accordingly. In this way, the CM can time its transmission to accurately arrive at the CMTS in the cable headend (see Section 11.6). For upstream transmission, the timing header is used as part of the ranging request (RNG-REQ) message, which is needed to adjust the time and power of the CM.

The FC field is followed by 3 bytes of MAC control. The MAC_PARM field of the MAC header is used for different purposes, depending on the FC Field. If the EHDR_ON = 1, then the MAC_PARM field is used as the extended-header-length (ELEN), which can vary up to 240-bytes. For concatenated MAC header, the MAC_PARM field represents the number of concatenated MAC frames. For request MAC header (REQ), the MAC_PARM field represents the amount of requested bandwidth. The 2-bytes LEN field is used in most cases to indicate the length of the MAC frame. However, for the REQ case, this field is used to indicate the CM SID.

The optional extended header (EHDR) field, which provides extension to the MAC frame format, is used to add support for additional functions such as data link security and frame fragmentation. The header check sequence (HCS) field is a 16-bit CRC that is used to detect errors in the entire MAC header, particularly in the presence of collisions. The HCS is calculated using the following CRC-CCITT generating polynomial [14]:

$$g(X) = X^{16} + X^{12} + X^5 + 1 \tag{11.4}$$

MAC Management Header:

This is a specific MAC header that is used to support MAC management messages. The Destination Address (DA) can be a specific CM unicast or multicast address, and the Source Address (SA) is the address of the source CM or CMTS. The "msg LEN" field is the total length of the MAC message from DA to the end of the MAC management message payload. For the other fields in the MAC management header, the reader is encouraged to see the DOCSIS 1.1 protocol specifications.

MAC Management Payload:

There are many different types of MAC management messages with variable lengths, which are briefly outlined as follows:

- CMTS Timestamp: 32-bit counter, which is locked to the CMTS 10.24-MHz master clock.
- Upstream channel descriptor (UCD): The UCD, which is transmitted periodically by the CMTS, defines the upstream channel characteristics. The UCD parameters include the upstream channel ID, the downstream channel ID on which this message was transmitted, the number of mini-slots in the upstream channel, counter for any changes in the CM configuration, and channel type-length-value (TLV) parameters.

- Upstream bandwidth allocation MAP (MAP): The MAP format, which is generated by the CMTS, is shown in Figure 11.11. The upstream bandwidth allocation MAP has a fixed length header and various housekeeping parameters such as the upstream channel ID, the number of information elements (IEs) in the MAP, UCD counter, and a number of important time references. The allocation start time (Alloc Start Time) parameter shows the effective start time from the CMTS initialization (counted in mini-slot) for the first entry in this MAP. The parameter Ack Time in the MAP indicates the latest time from the CMTS initialization (in mini-slots) processed in the upstream that generated a Grant, Grant Pending, or Data Ack messages. Ranging Backoff Start and Ranging Backoff End indicate the initial and final backoff windows for initial ranging contention (see Section 11.5). Data Backoff Start and Data Backoff End parameters indicate the initial and final backoff windows for contention data and requests.

As the name indicates, IEs define individual grants or deferred grants in the transmitted MAP from each CM. Each IE is a 32-bit quantity, where the most significant 14-bits represent the SID (for unicast, multicast, or broadcast services), the middle 4-bits represents interval usage code (IUC), and the last 14-bits represent the mini-slot offset. Since all the CMs must scan all their IEs, it is important that the IEs be short. A null IE is used to terminate the list. The DOCSIS 1.1 protocol standard defines the following IEs:

- Request IE: It provides an upstream interval for all CMs to request upstream bandwidth for data transmission.
- Request/Data IE: It provides upstream interval for either bandwidth or short data packets. For example, under "light" network loading, the allocation algorithms in the CM may use this IE to provide for "quick" data contention.
- Initial Maintenance: It provides an upstream interval for new CMs to join the cable TV network (ranging opportunity). This interval is equal to the round-trip propagation delay between the CM and CMTS plus the transmission time of the ranging request message.
- Station Maintenance IE: It provides an interval in which some stations are expected to perform some aspects of routine network maintenance, such as ranging or power adjustments.
- Short and Long Data Grant IEs: A data grant IE provides an opportunity for a CM to transmit upstream one or more data PDUs.
- Data Acknowledge IE: It provides an acknowledgement that a data PDU was received. The CM has to request this acknowledgement within the data PDU.
- Null IE: It terminates all actual allocations in the IE list. All Data Acknowledge and Data Grant Pending IEs must follow the Null IE.

There are also various request and response messages that are used with the MAC management message payload, which will be briefly introduced as follows:

1. Ranging Request (RNG-REQ):
A CM at initialization must transmit a ranging request and periodically as requested by the CMTS to determine cable TV time delays and requests for output power level adjustments.

2. Ranging Response (RNG-RSP):
A ranging response must be transmitted by the CMTS in response to RNG-REQ. This response message must include TLV encoded parameters such as SID, upstream channel ID, ranging status, timing/power/frequency adjust information. In addition, if the CM transmitter employs a pre-equalizer, then the adjustments of the equalization coefficients are transmitted in the downstream channel.

3. Registration Request (REG-REQ):
A CM at initialization must transmit a registration request after receipt of a CM parameter file. This request includes initialization SID as well as the CM configuration file settings such as downstream frequency, upstream channel ID, network access control object, downstream packet classification, upstream service flow, class of service, baseline privacy configuration, and others.

4. Registration Response (REG-RSP):
A registration response must be transmitted by the CMTS in response to receive REG-REQ. The response includes the SID from the corresponding REG-REQ as well as TLV encoded parameters such as service flow, payload header suppression, classifier and classifier error set, service flow set, payload header suppression error set, service not available, modem capabilities, and vendor-specific data.

5. Registration Acknowledge (REG-ACK):
The CM in response to REG-RSP to the CMTS must transmit a registration acknowledgment. This message confirms the acceptance of the quality-of-service (QoS) parameters of the flow by the CM as reported by the CMTS.

6. Upstream Channel Change Request (UCC-REQ):
An upstream channel change request must be transmitted by the CMTS to cause a CM to change the upstream channel on which it is transmitting.

7. Upstream Channel Change Response (UCC-RSP):
An upstream channel change response must be transmitted by a CM in response to a receive UCC-REQ to indicate to the CMTS that it has received the request and it is complying with the UCC-REQ.

11.6 Random Access and Contention Resolution Methods

Before we can discuss the primary contention resolution methods for upstream transmission by a CM, let us review the conventional random access protocols that were used in early cable TV data networks. Some of these random access methods are still used by many cable TV operators to access their digital STBs.

11.6.1 Random Access Methods

The earliest random access method, which was developed at the University of Hawaii to interconnect several of its computers with a communication satellite, is the Aloha protocol [15]. In the Aloha system, a station can transmit at any time, encoding its transmission with error detection code. Then, the station listens for time duration equal to maximum roundtrip propagation time on the network for an acknowledgment from the receiver. In case of collisions, the station receives a negative acknowledgment, and it re-transmits the message after a random time delay. After repeated negative acknowledgments, the station stops. It can easily be shown that the Aloha protocol is quite inefficient, achieving a maximum traffic throughput of 18% [16]. To improve the maximum throughput of the Aloha system, the slotted Aloha (S-Aloha) protocol was developed. In the S-Aloha system, a central clock is used to synchronize all the stations by broadcasting a sequence of synchronization pulses. The transmission time is divided into uniform slots, and each station can begin to transmit only at the slot boundary. This simple modification reduces the rate of collisions by half, since collisions only occur when two or more stations attempt to transmit within the same time slot. Thus, the maximum traffic throughput for S-Aloha is increased to 1/e or 36.8%. DAVIC 1.2 standard uses the S-Aloha protocol to manage the upstream transmission over HFC networks [17]. The DAVIC upstream 64-byte slot consists of a 4-byte unique word (UW), 53-bytes of data payload, 6-bytes of R-S parity, and 1-byte of guard time. Thus, there are 500 and 3000 slots per second for upstream data rates of 256-kb/s and 1.544-Mb/s, respectively, in the DAVIC 1.2 standard. Appendix A summarizes the upstream and downstream PHY layer parameters between DAVIC 1.2 and DOCSIS 1.1 specifications.

To improve over the Aloha and S-Aloha access schemes, let us review the access methods that were developed in the 1980s to interconnect computers over a local area network [18, 19]. Let us assume that a station began to transmit multiple packets over a local area network. However, it may take some time before other stations know about the first transmitting station. Thus, one or more stations may also try to transmit multiple packets, resulting in a collision with the previously transmitted packet, and neither of the packets is getting through. If the propagation time to the other stations is much smaller than the packet transmission time, and all the stations are listening before talk (LBT) when a given station begins to transmit, then collisions can be avoided since these stations know it almost immediately. Thus, collisions can occur only when a station has begun transmitting within the propagation time delay interval. This approach is sometimes called carrier-sensing multiple access (CSMA) or LBT method. Using the CSMA method raises two important questions. First,

what should a station do when the network is found to be busy? There are two common algorithms to address this problem as follows:

- Non-persistent: If the network is busy, the station has to wait a random amount of time and try to transmit again.
- p-Persistent: If the network is busy, delay by a fixed time slot and try to transmit again with a probability of p ($0 \leq p \leq 1$). A special case of this method is 1-persistent, where a station continues to listen when the network is busy, and transmit as soon as the network becomes available. If collision occurs due to lack of acknowledgment, the station waits a random amount of time and tries to transmit again ($p = 1$).

There are drawbacks to each method. In the non-persistent method, the network capacity is not efficiently utilized since the network remains idle following a station transmission. In the 1-persistent method, a collision is guaranteed when two or more stations are waiting to transmit at the same time. A compromise is achieved in the p-persistent method by setting p low such that $n \cdot p < 1$, where n is the number of stations waiting to transmit, resulting in a collision and unnecessary delays.

The CSMA method can be improved by adding two more transmission rules as follows:

- When a collision is detected, the transmitting station aborts the transmission and sends a short jamming signal to inform all he other stations that a collision has occurred.
- After the jamming signal, the station tries to re-transmit after a random time-delay using CSMA. The time-delay before the nth attempt is a uniformly distributed random number from 0 to 2n -1, where the re-transmission time delay unit is 512 bits.

This is essentially the CSMA with collision-detection (CSMA/CD) algorithm, which is the most commonly used access method in today's Ethernet local-area networks. The maximum Ethernet packet size is 1536 bytes, which consists of 8-byte preamble, 14-byte header, 4-byte parity, and 1500-byte payload. The baseband physical layer of the Ethernet using CSMA/CD was issued as the IEEE802.3 standard [20], while the broadband physical layer for a two-way cable TV system as provided as supplements to IEEE 802.3 standard [21]. In the early 1980s, various two-way cable TV systems were implementing the CSMA/CD method. In the CSMA/CD method, the amount of unused bandwidth is reduced to the time it takes to detect a collision. However, broadband Ethernet has a severe drawback over the HFC network. For example, due to time-delay constraint of 10-Mb/s Ethernet, the maximum distance of a station to the headend is required to be less than 2-km.

To overcome this limitation, two MAC protocols have been proposed and standardized for contention resolution of data over cable. The p-persistent with binary exponential backoff algorithm [22] has been selected for the DOCSIS 1.0/1.1 standard, and the ternary-tree algorithm for IEEE 802.14 [23]. In our discussion here, we are primarily focusing on the p-persistent binary exponential backoff algorithm since the DOCSIS 1.1 is the only widely used standard for CMs in North America.

11.6.2 p-Persistence with Binary Exponential Backoff Algorithm

The contention resolution method for upstream transmission, which is used by DOCSIS 1.1 standard, is based on a truncated binary exponential backoff algorithm, where the initial backoff window (W_i) and the maximum backoff window (W_m) are controlled by the CMTS at the cable headend [22]. In order for a station to enter the contention resolution process, it must set its internal backoff window equal to W_i. Then, the station must select random number X within its backoff window, which is between 0 and R, where R is given by:

$$R = 2^{\max[W_i + K - 1, W_m]} - 1 \tag{11.5}$$

where K is the number of collisions. For example, for $W_i = W_m = 4$, the backoff window is between 0 and 15. If the station selects X = 7, then it has a total of seven contention opportunities.

After the contention transmission, the station must wait for feedback information from the CMTS, which could be a data grant or data acknowledge in the upstream allocation MAP. The contention resolution process is completed once the station receives the feedback information. However, if there is no feedback information or if the station determines that the contention transmission was lost due to collision, the station must increase its backoff window by a factor of 2, as long as it is less than maximum backoff window (W_m). The station must select another random number within its new backoff window and repeat the process as described above. The maximum number of contention resolution re-tries is 16, and it is independent on the initial and maximum backoff windows as defined by the CMTS.

It should be pointed out that the p-persistent contention resolution algorithm is a free-access algorithm, since it allows new stations to content for mini-slots at any time. This type of algorithm is sometimes called a non-blocking algorithm. In contrast, the IEEE802.14 contention resolution protocol based on the ternary tree algorithm is essentially a blocking algorithm. It precludes new stations contending for mini-slots from entering into an ongoing contention resolution process. Each protocol has its own advantages and disadvantages. The p-persistent algorithm cannot guarantee the contention resolution duration, since new stations can always join the ongoing resolution process. In other words, there is no upper bound on the longest resolution time for successful transmission.

The contention resolution in the MAC protocol of the IEEE 802.14 standard uses the ternary-tree algorithm with variable entry persistence. Performance comparison results between the ternary-tree and the p-persistent contention resolution algorithms in terms of the mean access delays and throughput indicate that the ternary-tree-blocking algorithm outperforms both blocking and non-blocking p-persistence algorithms [23].

11.7 MAC Layer Protocol Operation

As we have learned in Section 11.4, a stream of mini-slots defines the upstream channel in the DOCSIS protocol, which is referenced to the CMTS clock. The upstream bandwidth allocation MAP, which is a MAC message transmitted by the CMTS on a downstream channel, specifies the granted mini-slots for particular stations to transmit, the available mini-slots for contention transmission, and other mini-slots as an opportunity for new stations to join in. An upstream transmit opportunity is defined as any mini-slot in which the CM may be allowed to start a transmission. Each mini-slot is number relative to a master reference clock maintained by the CMTS, which distributes the clocking information to the CMs using the synchronization (SYNC) packets. The allocation MAP, which is a variable-length MAC management message, defines the upstream transmit opportunities for a given CM on a given channel. The allocation MAP consists of a fixed-length header and a variable number of information elements (IEs), which defines the allowed usage for the granted mini-slots. Each IE consists of a 14-bit SID, a 4-bit type code, and a 14-bit starting offset parameter. There are four different types of SID as follows: (A) Broadcast SIDs intended for all the CMs, (B) Unicast SID intended for a particular CM or a particular service within that CM, (C) Multicast SID intended for a group of CMs, and (D) Null SID addressed to no CM. The maximum size of an allocation MAP is limited to 240 IEs, and it is bounded to no more than 4096 mini-slots.

Before we explain the MAC message exchange mechanism between the CM and the CMTS for upstream transmission, we will assume that initial CM ranging between the CM and the CMTS has been established. The CM initialization is discussed in the next section. Figure 11.12 illustrates the MAC message exchange example. The CMTS transmits a MAP in a downstream channel at time t_1 with effective starting time of t_3. This time difference (t_3-t_1) is needed to compensate for downstream propagation delay to allow the CM to receive the MAP message, processing time at the CM, and upstream propagation delay. At t_2, the CM receives the transmitted MAP and scans it for request opportunities. The CM has to request bandwidth from the CMTS for upstream data transmission using the Request IE in the MAP message. Thus, the CM sends the Request IE to start at t_5, and calculates a new time t_6 as a random offset based on the Data Backoff Start value (e.g., the initial backoff window starting time) in the most recently transmitted MAP. At t_4, the CM transmits a request to the CMTS for a particular number of mini-slots needed to accommodate the required data packet data units (PDUs). Notice that t_4 is selected such that the transmitted request will arrive at the CMTS at t_6. If, for example, due to collision with requests from other CMs, the CMTS does not receive the transmitted MAP, the CM must perform the binary exponential backoff algorithm and re-try to transmit. At t_6, the CMTS received the transmitted request from the CM and schedules it for upstream data PDU transmission in the next MAP. At this point the scheduling algorithm of the CMTS determines which request to grant, depending on various factors such as class of service requested and any competing

requests from other CMs. It should be pointed out that if the CMTS scheduler cannot grant the CM request in the next MAP message, it must either reply with a zero-length grant in that MAP or discard the request by not giving a grant. In addition, the CMTS must indicate to the CM that the request is still pending by continuing to reply with a zero-length grant in the MAP message until the request can be granted. At t_7, the CMTS transmits an allocation MAP to the CM with an effective starting time t_9, and with a data grant starting time t_{11}. When the CM receives the transmitted MAP at time t_8, it scans the MAP for its data grant and then transmits its data PDU at t_{10} to arrive at the CMTS at t_{11} as shown in Figure 11.12.

Multiple upstream and downstream channels can be transmitted to and from a single CM. If multiple upstream channels are associated with a single downstream channel, then the CMTS must transmit one allocation MAP per upstream channel.

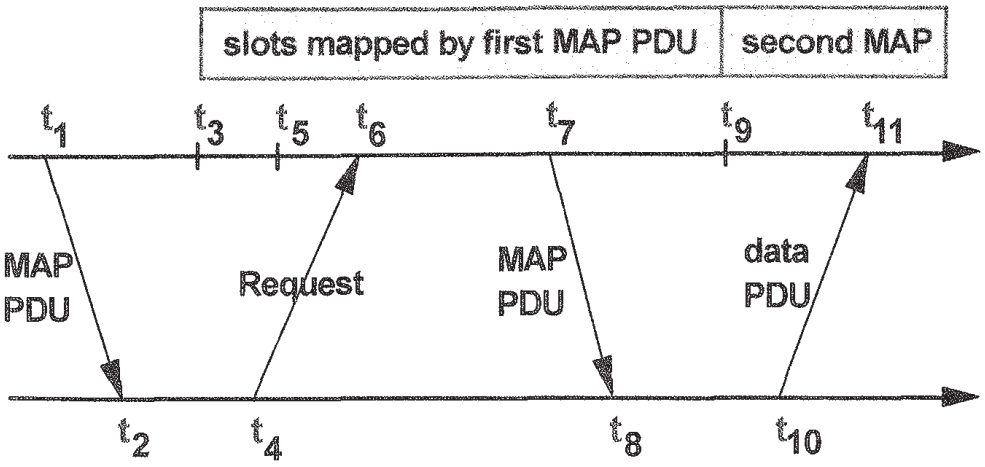


Figure 11.12 Example of MAC protocol between CM and CMTS. After Ref. [1].

11.8 Quality of Service (QoS) and Fragmentation

Several new concepts related to QoS have been introduced in the DOCSIS 1.1 protocol standard as compared with the DOCSIS 1.0 standard [24]. Classifying the transmitted packets over the DOCSIS MAC interface into service flows provides enhanced QoS. As we have learned earlier, a service flow defines a unique unidirectional mapping of packets between the CM and the CMTS to provide a particular QoS. A service flow is characterized by a set of QoS parameters such as latency or end-to-end delay, timing jitter, and throughput assurances. Both the CM and CMTS provide QoS by shaping, policing, and prioritizing the

traffic according to the QoS parameter set defined for the service flow. The SFID exists for all service flows, while SID exists only for admitted or active upstream service flows.

The following subsection discusses several basic concepts related to QoS, including packet classification and types of service flows.

11.8.1 Basic Concepts and Operation

The first important concept is the classification of QoS parameter set or service flows. The QoS parameter set for a given service flow can be divided into three different categories as follows:

Provisioned QoS Parameter Set:
This set of QoS parameters appears in the configuration file of the CM and is present during its registration. The provisioned QoS parameter set is defined when the service flow is created in the CM registration process. Notice that if the service flow is created dynamically, the provisioned QoS parameter set is null.

Admitted QoS Parameter Set:
The CMTS and possibly the CM are reserving resources for this set of QoS parameters. The primary reserved resource is upstream bandwidth, but may also include the required memory or a time-based resource to activate the service flow. The admitted QoS parameter set can be thought as a subset of the provisioned QoS parameter set.

Active QoS Parameter Set:
This QoS parameter set defines the actual service that is being provided to the service flow. Only an active service flow may forward packets. The active QoS parameter set can be thought of as a subset of the admitted QoS parameter set. It should be pointed out that SID exists only for admitted or active upstream service flows.

One can also think in terms of three different types of service flows. The provisioned service flow is provisioned through the configuration file in the CM, while the admitted service flow has reserved resources by the CMTS that are not active. Only for the active service flow, the CMTS has committed resources by its QoS parameter set such as allocation upstream bandwidth.

Another important concept is the concept of Classifiers and packet classification within the MAC layer. A Classifier is a set of matching criteria applied to each transmitted packet over the cable TV network. The packet matching criteria can be, for example, destination IP address, a reference to a service flow, or scheduling priority. If the packet matches the specified packet matching criteria, then it is delivered on the referenced service flow. Downstream Classifiers are applied by the CMTS to the packets it is transmitting, while upstream classifiers are applied at the CM and may be applied by the CMTS in order to police the classification of upstream packets. Packet classification by the CMTS or CM is

done in a table format, and consists of multiple Classifiers. Each Classifier has a priority field, which determines the search order for the Classifier. The highest priority Classifier must be applied first. The Classifier priority is used for ordering the application of Classifiers to packets. Classifiers can be added to the packet classification table using either management operations such as configuration file and registration, or via dynamic operation such as dynamic signaling.

The CMTS approves or denies every change to the QoS parameter set and Classifiers associated with a given service flow using a logical function called *authorization module*. The authorization module defines the range and acceptable values of the admitted and active QoS parameter sets that can be used. Such changes include requesting an admission control decision to set, for example, the admitted QoS parameter set, and requesting activation of a service flow. There are two types of authorization models in which the authorization module functions. In the static authorization model, the authorization module receives all registration messages and stores the provisioned status of all the service flows. Admission and activation requests for these provisioned service flows are permitted, as long as the active QoS parameter set is a subset of the admitted QoS parameter set and the admitted QoS parameter set is a subset of the provisioned QoS parameter set. The static authorization model can be thought of as a nested set of envelopes, with the smallest envelope defining the active QoS parameter set. Thus, in the static model, all the possible services are defined in the initial configuration of the CM. In the dynamic authorization model, the authorization module not only receives all registration messages, but also communicates them through a separate interface to an independent policy server. The policy server provides advance notice of upcoming admission and activation requests, and specifies the correct authorization action to the authorization module. The authorization module checks all the admission and activation requests from the CM. Only those admission and activation requests from the CM that are signaled in advance by the policy server are permitted. All other requests are either refused by the authorization module or sent for real-time query to the policy server. In the dynamic authorization model, it is possible to change the parameters of an existing service flow using the so-called *dynamic service change request* (DSC-REQ).

For any given service flow, its QoS parameter set may be explicitly specified, including all the traffic parameters, or indirectly by specifying a Service Class Name, which is referred to a set of traffic parameters.

11.8.2 Upstream Service Flow Scheduling

In order for the DOCSIS protocol to support constant bit rate (CBR) services such as voice over IP (VoIP) packets, the CMTS needs to schedule a steady stream of grants. These grants are referred to as unsolicited grants because there is no need for the CM to request them. The CMTS may reserve specific upstream opportunities for real-time traffic flows by providing data grants at periodic interval to the service flow. The term *unsolicited grant service* (UGS) is a type of upstream flow scheduling service that is used to map CBR traffic onto a service flow. Upstream flow scheduling services are associated with service flows

through the use of SID. Each service flow may have multiple Classifiers, where each Classifier may be associated with a unique CBR media stream. When a service flow is provisioned for UGS, the Nominal Grant Interval is selected to be equal to the packet interval in the CBR application. In other words, the size of the grant is chosen to satisfy the bandwidth requirements for the CBR application.

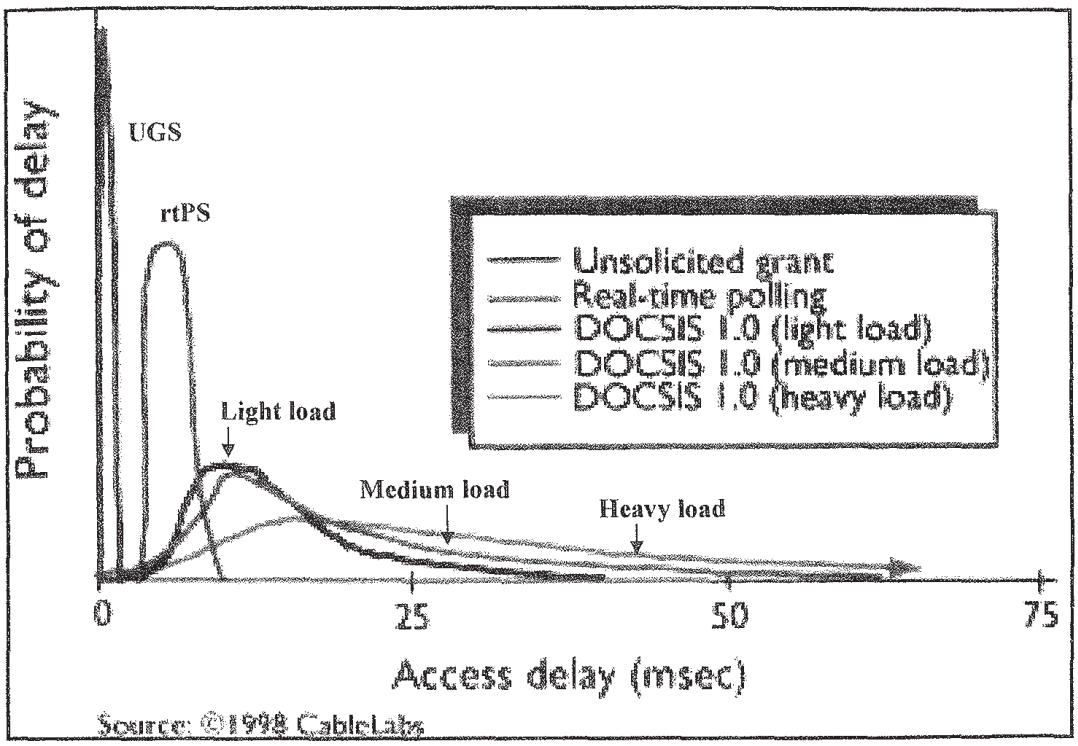


Figure 11.13 Probability of time delay versus the access delay (ms) for (A) unsolicited grant service, (B) real-time polling service, and (C) best effort service capabilities using DOCSIS 1.0 with light, medium, and heavy traffic load. After Ref. [26].

Besides UGS, there are other types of upstream service flow scheduling services, including real time polling service (rtPS), UGS with activity detection (UGS-AD), non-real time polling service (nrtPS), best effort (BE) service, and committed information rate (CIR) service. Let us briefly describe each of these scheduling services. The rtPS flows periodically receive transmission opportunities regardless of network congestion, and they release their transmission reservations to other service flows when inactive [25]. The CMTS polls rtPS SIDs on a periodic basis for upstream transmission traffic usage by using unicast request opportunities. The CM must use both unicast request opportunities as well as unsolicited data grants for upstream transmission.

For active service flows, the CMTS provides periodic unicast grants, but when the service becomes inactive, the CMTS must provide periodic unicast request opportunities. The problem is that the algorithm for detecting when a service flow is changing from an active to inactive state is dependent on the CMTS implementation. In the UGS-AD, one is trying to conserve system resources by taking advantage of the reduced latency of UGS for active service flows, and increase the efficiency of rtPS for inactive service flows. The UGS-AD is particularly tailored for VoIP applications, where meeting packet latency is essential. In this application, the CM must not send packets during the inactive state. This requirement implies that the CMTS has to support silent detection and the CM silent suppression.

The goal of nrtPS was to reserve upstream transmission opportunities for non-real-time traffic flows. The CMTS typically polls nrtPS SIDs on a periodic or random time interval (about one second or less). The CM must use both contention requests and unicast requests opportunities to obtain upstream transmission bandwidth. In the BE service, one is trying to provide efficient service to the upstream traffic on a best-effort basis. In the BE service, the CM must use all contention and unicast request opportunities as well as all unicast data transmission opportunities. Figure 11.13 compares the probability of time delay versus the access delay (in msec) for the following services: (A) UGS, (B) rtPS, and (C) BE service using DOCSIS 1.0 with light, medium, and heavy traffic load [26]. Other services such as a CIR service can be configured in many different ways, including a combination of some of the previously discussed types of scheduling services.

11.8.3 Upstream Fragmentation

The goal of the upstream fragmentation concept, which was introduced to the DOCSIS 1.1 protocol standard by both the Broadcom and Nortel corporations, is to improve the upstream traffic latency, particularly to support CBR services such as VoIP. The CMTS initiates an upstream packet fragmentation when it grants bandwidth to the requesting CM with a grant size smaller than the requested bandwidth. This is known as a Partial Grant. Fragmentation is encapsulation of only a portion of a MAC frame within a fixed-size fragmentation header and a fragment CRC. A single PDU or concatenated PDUs are encapsulated in the same way. At the CMTS, the fragment packets are processed similarly to non-fragmented packets except when baseline privacy is used; it starts just after the fragmentation header. The CMTS supports two different modes for packet fragmentation. In the first mode, which is called *multiple grant* mode, the CMTS allows multiple outstanding partial grants for any given SID. The CMTS can break a request up into two or more grants in a single MAP or over successive MAPs, and calculates the required additional overhead in the remaining partial grants to satisfy the request. If the CMTS cannot grant the remainder in the current MAP, it must send a grant pending (i.e., zero-length grant) in the current MAP and in all subsequent MAPs to the CM until it can grant additional upstream bandwidth. If there is no grant or grant pending in the subsequent MAPs, the CM must re-request for the packet payload remainder. To prevent the CM from being out of synchronization, the CMTS has to make sure that the packet payload remainder is at least greater than a mini-slot.

The second mode of the CMTS to perform fragmentation is called the *piggyback* mode, where it is assumed that the CMTS does not retain any fragmentation state. Thus, there is only one outstanding partial grant, and the CM must insert the payload remainder into the piggyback field of the fragment header. The CM calculates how much of a frame can be transmitted in the granted bandwidth, and forms the packet fragment to send it. Using the piggyback field in the fragment extended header, the CM requests the necessary bandwidth for the payload remainder to be sent. In this mode, the CM must track the physical-layer and fragmentation overhead of the payload remainder to be sent. At the CMTS, once the fragment HCS is correct, the payload fragment is ready for re-assembly with the original MAC frame, and then forward to the appropriate destination. From a practical perspective, the piggyback mode is easier to implement than the multiple-grants mode since the CMTS does not have to keep track of all the outstanding multiple partial grants for any given SID.

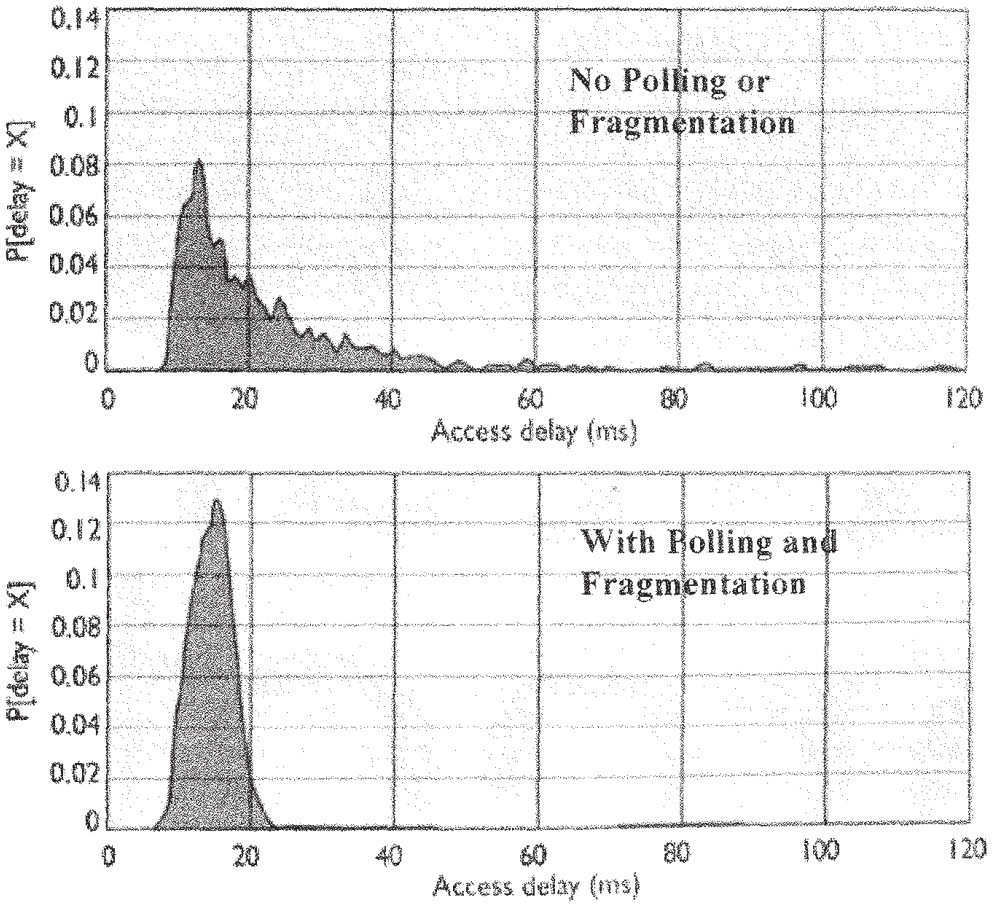


Figure 11.14 Time delay performance of CBR sources with and without polling and packet fragmentation. After Ref. [27].

Each CMTS vendor, based on an implementation specific algorithm, can select one or a combination of these operating modes, depending on the specific services the CMTS is supporting.

The advantage of using both polling and packet fragmentation when CBR and BE traffic are mixed is illustrated in Figure 11.14 [27]. Ten cable modems, each with a 64-Kb/s constant bit rate (CBR) source, modeled low latency voice traffic. Additional 44 CMs with packet sizes distributed over a range from 64 bytes to 1,500 bytes modeled BE traffic. The average bit rate for the best effort sources was 16-Kb/s. Notice that without polling and fragmentation, voice packets can occur time delays in excess of 100-ms. In contrast, the voice packets access time delays are upper bounded around 25-ms. However, there are still some delay variations, resulting from the frame-to-frame shifts in where a packet will lie within a particular frame.

11.9 CM and CMTS Interaction

The interaction between the CM and the CMTS can be divided into five basic categories as follows: (A) initialization, (B) authentication, (C) configuration, (D) authorization, and (E) signaling. The CM initialization procedure can be divided into the following steps:

1. Scan for a downstream channel and establish synchronization with the CMTS.
2. Obtain transmit parameters from the UCD message.
3. Perform ranging.
4. Establish IP connectivity.
5. Establish time of day.
6. Transfer operational parameters.
7. Perform registration.
8. Establish security association if provisioned to run Baseline Privacy.

When a CM is shipped from the manufacturer, the following information is sent:

- A unique IEEE 802 48-bit MAC address that can be used to identify the CM to the CMTS or to other provisioning servers during initialization
- Security information that can be used to authenticate the CM to the security server and authenticate the responses from the security and provisioning servers

Let us explain in more details each of the CM initialization steps.

1. Scanning and Synchronization:

The first step of the CM initialization is to scan and acquire the downstream channel. A downstream signal is considered valid when the CM has achieved the following steps: (A) synchronization of the QAM symbol timing, (B) synchronization of the FEC framing, (C)

synchronization of the MPEG packetization, and (D) recognition of timing synchronization (SYNC) MAC message. As we have noted earlier, the SYNC messages must be periodically transmitted by the CMTS to establish MAC layer timing.

2. Obtain Upstream Parameters:
After synchronization has been established, the CM must wait for the UCD message from the CMTS in order to retrieve the transmission parameters for a possible upstream channel. It should be pointed out that the CMTS periodically broadcasts on the cable TV network all available upstream channels using UCD messages. The CM must determine whether it can use a given upstream channel from the UCD parameters. If yes, the CM extracts the upstream channel parameters, and then it must wait for the next SYNC message and extract the upstream mini-slot timestamp from this message. The CM must also wait for the upstream bandwidth allocation MAP for the selected channel, and then may begin to transmit.

3. Ranging and Automatic Adjustments:
After receiving the upstream bandwidth allocation MAP, the CM transmits a ranging request (RNG-REQ) in a contention mode to the CMTS using a temporary SID = 0. The CMTS receives recognizable ranging packets, allocates temporary SID, sends ranging response, and adds the temporary SID to its poll list. The CM is using a temporary SID before it is registered with the CMTS and is changing the upstream channel. When the CM receives the ranging response, it stores the temporary SID and adjusts its local parameters such as output power level, timing information, and upstream channel ID.

4. Establish IP Connectivity:
After adjusting its local parameters, the CM must transmit *dynamic host configuration protocol* (DHCP) request to the server at the cable TV headend to obtain an IP address and any other parameters, which are needed to establish IP connectivity. The DHCP protocol is typically used to assign network-layer IP addresses. The server DHCP response must contain all the necessary configuration parameters for the CM.

5. Establish Time of Day:
Both the CM and the CMTS need to have the proper time of day and date for time-stamping of various events, which can be retrieved by the management system. The CM creates its current local time by retrieving the time from the server, which is adjusted by the timing offset from the DHCP response.

6. Transfer of Operational Parameters:
After successful DHCP operation, the CM must download its configuration file using trivial file transfer protocol (TFTP). TFTP is an Internet protocol for transferring files without requiring user names or passwords, and it is typically used for automatic downloads of data and software. If the downloaded configuration file has different upstream and/or downstream channels from what the CM is currently using, then the CM must not send a registra-

tion request message to the CMTS but must redo its initial ranging using the configured upstream and/or downstream channels.

7. Registration:

To register with the CMTS, the CM must send a registration request with its assigned SID and all the downloaded configuration file settings as follows:

- Downstream frequency configuration setting
- Upstream channel ID configuration setting
- Network access control object
- Downstream packet classification configuration setting
- Class of service configuration setting
- Upstream service flow configuration setting
- Downstream service flow configuration setting
- Baseline Privacy configuration setting
- Maximum number of Classifiers
- Privacy enable configuration setting
- Payload header suppression
- TFTP server timestamp
- TFTP server provisioned modem address
- Vendor specific information configuration setting
- CM MIC configuration setting
- CMTS MIC configuration setting

In addition, the CM must send the CM ID assigned by the vendor and the CM IP address as well as the encoding capabilities of the CM. The CM must wait for a registration response from the CMTS, authorizing it to transmit data to the network.

8. CM Security Initialization:

After the registration process is completed, the CM can initialize cable TV network security operation if it is provisioned to run Baseline Privacy [3]. The CM is provisioned to run Baseline Privacy if its configuration file includes a Baseline Privacy configuration setting.

References

1. CableLabs, *Data-Over-Cable Service Interface Specifications (DOCSIS): Radio Frequency Interface Specification*, SP-RFIv1.1-I02-990731 (1999).

2. IEEE Standards Department, IEEE Project 802.14/a Draft 3 Revision 3, *Cable TV Access Method and Physical Layer Specification*, October (1998).
3. CableLabs, *Data-Over-Cable Service Interface Specifications, Baseline Privacy Plus Interface Specification*, SP-BPI-W02-981228 (1998).
4. C. Huitema, *Ipv6: The New Internet Protocol*, Prentice Hall PTR (1996).
5. Ethernet Protocol Version 2.0, Digital, Intel, Xerox (1982).
6. D. Plummer, Ethernet Address Resolution Protocol: Or Converting Network Protocol Addresses to 48-bit Ethernet Address for Transmission on Ethernet Hardware, November (1982).
7. K. Sollings, *The Trivial File-Transfer Protocol*, Revision 2, Internet Engineering Task Force RFC-1350, July (1992).
8. R. Droms, *Dynamic Host Configuration Protocol*, Internet Engineering Task Force RFC-2131, March (1997).
9. ISO/IEC 10038, ANSI/IEEE Standard 802.1D: Information technology - Telecommunication and Information Exchange between Systems; Local Area Networks Media Access Control Bridges (1993).
10. ITU-T Recommendation J.83 Annex B, *Digital Multi-program Systems for Television Sound and Data Services for Cable Distribution*, April (1997).
11. H. Harashima and H. Miyakawa, "Matched-Transmission Technique for Channels with Intersymbol Interference," *IEEE Transaction on Communications* **COM-20**, 774–780 (1972).
12. M. Tomlinson, "New Automatic Equalizer Employing Modulo Arithmetic, " *IEE Electronics Letters* **7**, 138–139 (1971).
13. *MPEG Video Compression Standard*, Edited by J. L. Mitchell, W. B. Pennebaker, C. E. Fogg, and D. J. LeGall, Chapman and Hill, New York (1997).
14. ITU-T Recommendation X.25, *Interface between Data Terminal Equipment and Data Circuit-Terminating Equipment for Terminals Operating in the Packet Mode and Connected to Public Data Networks by Dedicated Circuit*, March (1993).
15. N. Abramson, "The ALOHA System, Another Alternative for Computer Communications," Proceedings, Fall Joint Computer Conference AFIPS vol.37, 281–285 (1970).
16. B. Sklar, *Digital Communications Fundamentals and Applications*, PTR Prentice Hall, Englewood Cliffs (1988).
17. Digital Audio-Visual Council (DAVIC), *Lower Layer Protocols and Physical Interfaces*, DAVIC 1.2 Specification Part 8 (1997).
18. W. Bux, "Local-Area Subnetworks: A Performance Comparison," *IEEE Transactions on Communications* **COM-29**, 1465–1473 (1981).
19. W. Stallings, "Local Network Performance," *IEEE Communications Magazine* **22**, 27–36 (1984).
20. IEEE, *Carrier Sense Multiple Access with Collision Detection (CSMA/CD) Access Method and Physical Layer Specifications*, American National Standard ANSI/IEEE Standard 802.3 (1985).

21. IEEE, *Broadband Medium Attachment Unit and Broadband Medium Specifications, Type 10 Broad36 (Section 11)*, Supplements to ANSI/IEEE Standard 802.3 (1988).
22. R. Citta and J. Xia, "Adaptive P-persistive Algorithm with Soft Blocking for Contention Resolution," IEEE 802.14/97-037, March (1997).
23. N. Golmie, D. H. Su, G. Pieris, and S. Masson, "Performance Evaluation of Contention Resolution Algorithms: Ternary Tree versus p-Persistence," IEEE 802.14/96–241, October (1996).
24. CableLabs, *Data-Over-Cable Service Interface Specifications (DOCSIS): Radio Frequency Interface Specification*, SP-RFI-I04-980724 (1998).
25. R. Rabbat and K.-Y. Siu, "QoS Support for Integrated Services over CATV," *IEEE Communications Magazine* **1**, 64–68 (1999).
26. F. Dawson, "Is IP Telephony in Your Future?" *Communications Engineering & Design Magazine* **11** (1998).
27. T. Quigley and D. Hartman, "Future Proofing MCNS Data-Over-Cable Protocol," *Communications Engineering & Design Magazine* **3** (1998).

CHAPTER 12

DIGITAL SET-TOP BOX SOFTWARE ARCHITECTURE AND APPLICATIONS

So far, we have learned about the key system technologies that enable the current and emerging two-way cable TV networks. In the final chapter, we review first the STB software architecture, including the real-time operating systems; the middleware layer; and applications. The different types of STB applications are divided into native applications and TV-based and Internet-based applications and are discussed in more detail. The native applications, which include electronic program guides (EPGs) and parental control, are discussed in Section 12.2. The TV-based applications include pay-per-view (PPV), enhanced broadcast, interactive and targeted advertisements, and video-on-demand (VOD), which are discussed in Section 12.3. The Internet-based applications, which include webcasting, e-mail, e-commerce, home banking, education, gaming, and others, are discussed in Section 12.4. Section 12.5 discusses the ongoing customized integration of TV-based and Internet-based applications. It should be pointed out that since there are many different middleware and applications vendors, which are operating on different platforms, the review here of the software architecture and applications is intended not to be exhaustive but to provide the reader with different examples.

12.1 Digital Set-Top Box Software Architecture

In Chapter 8, our discussion focused primarily on the hardware architecture of the digital STB. The software architecture of the STB is a critical part of the STB operation, enabling cable operators to offer new services to their subscribers. Let us review the basic building blocks of the STB software architecture. A generic block diagram of the software architecture of a digital STB is shown in Figure 12.1 [1,2]. It consists of the following layers: (A) hardware abstraction layer, (B) native middleware layer, (C) real-time operating system (RTOS) layer, (D) standard application program interface (API) layer, and (E) native and high-level application layers.

The hardware abstraction layer consists of software drivers to control the various underlying hardware devices in the STB such as cable modem, cable TV tuner, QAM transceiver, and others. Any design upgrade of an existing hardware device or the addition of new hardware components may require the STB manufacturer to modify the device driver. In the

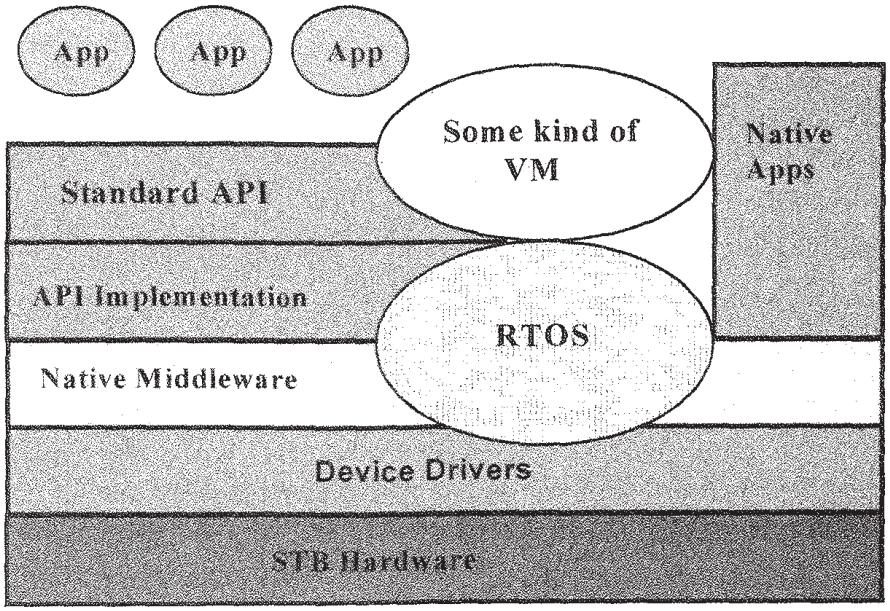


Figure 12.1 Generic software architecture block diagram of digital STB. After Ref. [1].

RTOS layer, the kernel, which is typically stored in flash memory and can be as large as several megabytes, is first loaded when the STB is powered-up. The RTOS kernel is typically responsible for managing the STB memory resources, real-time applications, and high-speed data transmission. Another important feature of the RTOS kernel is its support of multithreading and multitasking, namely, different portions of a program or different programs can be simultaneously executed [2]. In addition, the RTOS performs other important functions such as managing the network communication stacks, graphics, audio and video subsystems, and conditional access system, as well as service acquisition download, system information management, and return-path transmission.

The native middleware layer isolates the native applications and the various APIs from the underlying hardware devices, allowing these applications to operate transparently across the network. In other words, the software vendor may benefit from having the same middleware environment on different STB models, allowing these applications to be easily ported. This can significantly reduce the development complexity of new applications, cutting their development cycle. The standard APIs, such as the ATSC DTV application software environment (DASE), form the necessary interface between a specific RTOS and high-level applications and provide the environment to write applications that are independent of a specific STB hardware or RTOS vendor. The API implementation, on the other hand, is most likely RTOS specific (see Section 12.1.1).

The flexibility of the software architecture enables the cable operators to add new services. The different STB applications can be categorized in terms of orthogonal groups of applica-

tions. Common groups of applications are, for example, native versus non-native or STB-independent applications, broadcast versus resident applications, and passive versus interactive applications [1,3,4]. Resident applications are programs, which typically reside in the STB flash memory, and are downloaded from the headend by the cable operators to the subscriber STB. The RTOS must have a loader to enable the cable operator to upgrade resident applications, download new applications, and/or download patches to the existing RTOS. When multiple applications are running simultaneously, it is essential to prevent possible conflicts as well as to provide a consistent look and feel among these applications. This goal is a function of the middleware implementation and will be discussed in Section 12.1.2. Broadcast applications are typically programs that are synchronous and related to the video content with which they are broadcast. Such broadcast applications, for example, include stock tickers, sports and weather information, and enhanced advertisement. Interactive applications can have local interactivity where the same content is sent to all the STBs and the user makes a choice locally, or transactional applications where the user actually interacts with the headend server (i.e., VOD, web browsing, and e-commerce). These types of applications are discussed in more detail in Section 12.2.

12.1.1 Real-Time Operating System (RTOS)

The operating system (OS) is one of the key components of the digital STB software that enables it to function. Since there are many different types of STB, the OS should be as independent as possible from the hardware devices, shielding the various applications running on top of it. Furthermore, unlike the PC, a digital STB can have multiple operating systems to enable the widest range of applications over the cable TV network. The OS of the STB must be fast, functioning in a real-time environment, and handling sophisticated tasks in a limited memory size and in a smaller hardware system than a desktop PC. The primary RTOS responsibilities include:

- Controlling the use of the CPU and memory management
- Controlling video, graphics, and data outputs to TV, hard drives, and other devices
- Controlling smooth operation of different applications
- Controlling communications to other devices such as cable modems or PCs
- Managing STB hardware functions and data storage, and scheduling real-time tasks

Currently, there is no standard RTOS for digital STB, and some of the most common RTOSs are Microsoft Windows CE [5], PowerTV [6], Java OS [7], VxWorks [8], and Microware David OS-9 [9]. Let us very briefly discuss the features and functionality of two popular OSs, namely, Windows CE and PowerTV.

Microsoft Windows CE is a modular RTOS designed to run on variety of TV-centric devices such as digital STBs and hand-held devices such as a Pocket PC. In order to lure cable operators to use its software, Microsoft has developed the so-called TV platform adaptation kit (TVPAK), which consists of Windows CE and a software headend server called Micro-

soft TV server [2]. The modularity of Windows CE means that software developers can customize the RTOS for a specific hardware platform using Windows CE platform builder of development tools. In order to connect the various Windows CE modules, Microsoft uses dynamic link libraries (DLLs), where a DLL is a library of executable functions or data that can be used by Windows CE applications.

To accelerate their TVPAK strategy, Microsoft has added various drivers to its Windows CE (version 2.12) to support the underlying STB hardware components. The STB hardware components include CMs, smart cards for conditional access and e-commerce, IP telephony module, IEEE 1394 bus, hard disk drives, and cable TV tuner. Another useful feature of Windows CE is its registry, which is a small-footprint database used by the operating system to store the various STB configurations. From a cable operator perspective, the digital STB must be able to communicate securely and efficiently over the cable TV network. Consequently, Microsoft has provided support for a variety of communications and security protocols. Windows CE is one of the possible OSs that can run on Motorola/GI DCT5000+ advanced digital STBs.

The PowerTV OS, which has been developed by PowerTV since 1994, is specifically designed for the digital STB environment [6]. This means that it exists in a low-cost ROM or flash memory that can easily be upgraded and customized by the cable operators through network downloads to deliver integrated and secure enhanced TV services. The PowerTV RTOS consists of the following layers:

- Hardware-independent porting layer, which contains all the necessary device drivers for the STB
- PowerCore layer that provides the base functionality required by the applications, including a multitasking PowerKernel designed to operate in a small memory footprint
- High-level processing functions built on top of the PowerCore are encapsulated as software PowerModules, providing efficient and hardware-independent application services. The set of PowerModules enables cable operators to offer customized network-delivered applications and content.

In addition, the PowerTV platform provides cable operators with the necessary STB middleware to enable Internet-based applications. PowerTV RTOS has been running on Scientific Atlanta Explorer 2000/3000 digital STBs.

12.1.2 Set-Top Box Middleware

As mentioned earlier, the STB middleware is an important link between the native applications and APIs and the underlined hardware devices. Currently deployed digital STBs support a wide range of enhanced interactive applications, including web browsing and video and audio streaming. In order to create applications that are not limited to proprietary hardware, developers have started to write middleware interpreters that are capable of decoding many different types of applications, independently from the hardware. The most popular

web content formats are hypertext markup language (HTML), JavaScript language, and Java bytecodes. The Java language is a general-purpose object-oriented programming language with similar syntax to C/C++, but omits many of the features that make C and C++ complex and confusing. It was designed to support multiple host architectures and to allow secure delivery of software components. The compiled Java code had to survive transport across networks, operate on any client, and assure the client that it was safe to run. The interesting capabilities of Sun's Hot Java browser to embed Java programs, which are known as applets, inside HTML pages were demonstrated before most other web browsers added support for the Java JM and applets. The applets are transparently downloaded into the HotJava browser along with the HTML pages in which they appear. Before being accepted by the browser, applets are carefully checked to make sure they are safe. Like HTML pages, compiled Java programs are network- and platform-independent, and behave the same way regardless of where they come from, or what kind of machine they are being loaded into and run on. Consequently, web browsing was no longer limited to a fixed set of capabilities.

The essential component of the Java technology, which is responsible for Java portability, is called the *Java virtual machine* (JVM) [10]. The Java source code (*.java files) are compiled into bytecodes (*.class files), which are interpreted by the JVM. A java class is a collection of data and related methods that operate on the data. The JVM does not know the Java programming language except for a particular file format called the class file format. It

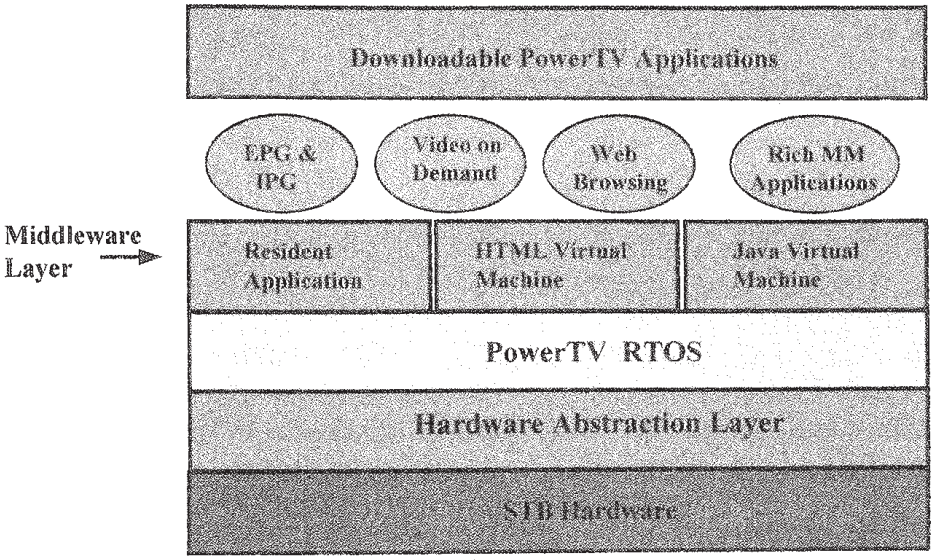


Figure 12.2 Architecture of PowerTV STB software showing the middleware layer with the various applications. After Ref. [2].

contains JVM instructions (or bytecodes) and a symbol table, as well as other ancillary information. For secure delivery, the JVM imposes strong format and structural constraints on the code in the class file. However, any language with functionality that can be expressed in terms of a valid class file can be hosted by the JVM. Personal Java (P-Java), which is a Java API and application development environment, consists of a modified JVM, a set of core libraries, and optional libraries that can be used as needed.

Another related popular virtual machine is called JavaScript virtual machine. JavaScript is a scripting language rather than a programming language, which uses less complex rules, and it is easier to learn and use than Java. Since JavaScript code is typically embedded within an HTML document, it can perform more complex tasks than HTML alone. New extensions to JavaScript are being developed by middleware vendors to provide an enhanced TV viewing experience. It should be pointed out that JavaScript is the only interpreted language in which the source code files are executed directly in the virtual machine and stored in the STB.

The emerging API standardization efforts want to eliminate porting of applications to all the different RTOSs in a given STB. The middleware platform must have a common set of APIs to make downloadable content and applications interoperable among different STBs. In other words, the ultimate goal of the software vendor is to develop applications once using standard APIs, which are STB hardware and RTOS independent. The STB is only required to support a chosen VM such as JVM and a set of APIs such as Java APIs. This increases the STB deployment cost because the JVM and the API implementation layer must be included on top of the native middleware in the STB software architecture as shown in Figure 12.1.

Currently, various companies are offering middleware platforms that are mostly proprietary solutions. However, these solutions are evolving towards the emerging open standard middleware, which is split between two main efforts. One effort, which is led by the DVB organization in Europe [11], is called the DVB Multimedia Home Platform (DVB-MHP) standard. The DVB-MHP standard, which intends to enable a wide variety of home terminals such as a PC, an integrated TV, and a digital STB, is responsible to define user requirements for enhanced cable TV services (i.e., dual broadcast audio/video and Internet), and provide a solution for interactive television. The DVB-MHP 1.0 specification, which has been recently released, consists of the JVM, Java APIs, and other APIs such as Java TV APIs. MediaHighway middleware, which has been developed by Canal+ Technologies and internationally indorsed by many countries, provides a powerful and flexible solution in this category [12]. The latest version of this software is called MediaHighway+, which is integrating the open technical specifications of DVB-MHP middleware standard.

A second alternative effort led by a subgroup of advanced television systems committee (ATSC) in the US, which is known as T3/S17, is defining the software architecture standard for digital STB called DTV DASE [13]. DASE has two environments as follows: (1) a procedural environment (called Application Execution Engine), which is generally written in Java, and (2) a declarative environment (called Presentation Engine), which is for declarative application content (HTML) [14]. The T3/S17 group has selected Sun's Java TV APIs

[15], P-Java APIs [16], Java Media Framework APIs [17], and Home Audio/Video Interoperability (HAVi) User Interface APIs [18] as the standard development environment for digital interactive services. The Java TV APIs, which have also been adopted by other standards organizations such as DVB, provide a high-level, protocol-independent, common set of APIs for applications to be used on different hardware platforms. The complete set of DASE APIs is expected to be implemented on top of P-Java platform, and it is also expected that TV applications written in a Java programming language will be able to run on digital STBs that comply with the DASE effort.

In addition to the standard efforts, there is also a consortium effort, consisting of US-based companies, including Microsoft, Intel, Disney, DirecTV, and others, and it is called advanced television enhancement forum (ATVEF) [19]. The ATVEF group is proposing to use HTML virtual machine and JavaScript virtual machine for the middleware standard. ATVEF version 1.1 specification, which has been released last year, defines the fundamentals for creating HTML-enhanced TV content for reliable delivery to many different access terminals such as digital STBs across a wide variety of networks, including terrestrial (i.e., over the air), cable, satellite, and the Internet.

To illustrate the middleware platform concepts that have been discussed so far, let us look at the following example. Figure 12.2 shows a block diagram of the PowerTV software architecture, which has been implemented on Explorer 2000/3000 digital STB by Scientific Atlanta [6]. Notice that the middleware layer contains both JVM and HTML virtual machine APIs. The use of HTML virtual machine allows the PowerTV enabled STB to process web content which has been broadcasted over the cable TV network. The downloadable PowerTV applications are applications that can be used, for example, to control other devices on the home network. It is expected that both Scientific Atlanta and Motorola will support ATVEF content delivery on their digital STBs.

Finally, let us mention the proprietary middleware efforts such as OpenTV and Liberate TV Navigator for DTV by Liberate Technologies [20]. OpenTV software environment for digital STBs consists of a middleware platform, a set of authoring tools, a library of APIs, and utilities, which can fit into a small-footprint configuration (350–560 kB flash memory), for cost-effective integration into interactive TV applications. The addition of O-code VM, which translates the OpenTV scripting language into native instructions, shields the OpenTV applications from the hardware layer. Recently, OpenTV has begun to implement jointly with Panasonic a fully compliant DVB-MHP extension to their STB software.

Liberate Technologies, which was originally founded by Oracle and Netscape and was known as Network Computers, Inc., has developed a platform solution, which integrates Internet-based applications with TV-based content to digital STB subscribers. Liberate TV Navigator platform integrates HTML extensions for TV with JavaScript 1.2 content. The Liberate middleware platform, which is competing with Microsoft's WebTV solution, has been installed on various STBs, including Motorola's DVi5000+ to allow European subscribers access to a wide variety of applications.

As mentioned earlier, the middleware implementation determines the feel and look of the content display for a specific digital STB. This can be achieved by using (1) native master

application to manage all the concurrent applications when they are launched, and assign priority for sharing hardware resources, (2) a set of implementation APIs for all the downloadable and broadcast applications, and (3) non-native resident application to control the TV display.

There are many different ways to classify the various STB applications. For reasons that will become clearer later on, let us classify the various STB applications into three main groups as follows:

(A) Native applications, which are specific to a given STB, such as Electronic Program Guides (EPGs)
(B) TV-based interactive applications, which include local and server interactivity, such as pay-per-view (PPV) and video-on-demand (VOD)
(C) Internet-based applications, which include a wide range of applications from web surfing to e-commerce

From here to the end of this chapter, these applications are reviewed.

12.2 Native Applications

Native applications, which typically reside above the STB native middleware layer as shown in Figure 12.1, are STB specific applications that do not require the use of the RTOS or APIs. EPGs and parental control are examples of native applications, and are discussed in the next subsections.

12.2.1 Electronic Program Guides (EPGs)

As the possibility of 500 or more TV channels with potentially hundreds or even thousands of additional web sites becomes closer to a reality, the necessity of software tools to help navigate through large number of options becomes clear. EPGs became available in the ear ly 1970s and provided consumers with onscreen guides of the channel line-ups. The EPG development in the 1980s and early 1990s had a limited functionality with mostly text-based onscreen display due to hardware limitations of the analog STBs. With the development of interactive digital STBs, a new type of advanced multimedia EPGs, which are sometimes called interactive program guide (IPG), were developed that changed the consumer TV experience. Some of the most popular EPGs are TV Guide [21] and StarSight [22], running on the most widely deployed digital STBs such as Motorola's DCT2000/5000+ and Scientific Atlanta's Explorer 2000/3000. The basic EPG provides onscreen display of program lineup and episode information for every channel for the next seven days. The viewer typically navigates around the program grid menu using the arrow keys on his remote control, and can

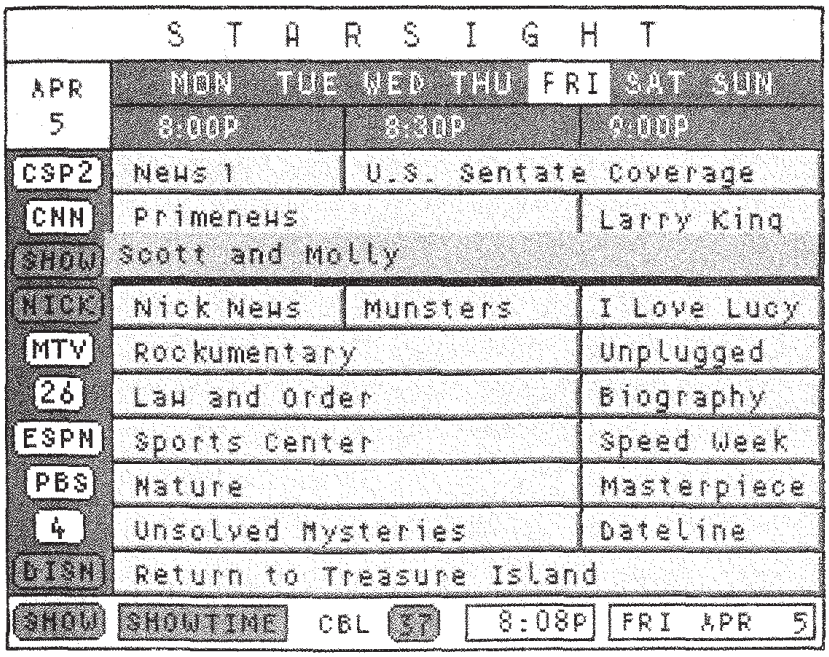


Figure 12.3 StarSight electronic program guide features where the selected program is highlighted in the program menu. Courtesy of Gemstar TV Guide International.

receive immediate information for any available program, including show description, main actors, and rating. Figure 12.3 illustrates, for example, StarSight EPG with the available program menu within the selected time slot, and with the desired program highlighted [22].

Advanced EPGs offer new features in addition to the basic EPG features, and can be configured for personalized TV viewing as well as provide detailed program information in multiple languages. For example, StarSight EPG let the viewer arrange the TV channels in the program grid menu (available channels versus time) such that the favorite channels are placed first, and delete those channels that the viewer never wants to watch. Furthermore, StarSight lets the viewer turn on his or her VCR, record the selected programs, and turn it off. Advanced EPGs may also include additional features such as alerting the viewer before his selected program is shown, control of the disk storage device within the digital STB, and searching capabilities for a particular episode on a specific time and date.

The EPG information has exploited the digital characteristics of MPEG-2 video streams. Special control data structures, which help to identify the transmitted programs within a multiplexed stream or among different multiplexed streams, have been defined by ITU/ISO MPEG-2 system specifications (ISO-13818 section 1) [23]. A packet identifier (PID) field in the header identifies each video or audio stream. The PID streams, which form virtual channels, are multiplexed and transmitted, for example, within a 64-QAM channel. A special reserved PID of 0 is used only for the periodic transmissions of the so-called program

assignment table (PAT). The PAT contains a list of the available program numbers for the transmitted multiplex as well as the list of the associated PID numbers. The program map table (PMT), which is transmitted on an assigned PID in the PAT, lists descriptors about the program, stream type, and PIDs for each stream that is associated with that program as well as descriptors for each stream. Since some of the transmitted programs may be encrypted, PID 1 is reserved for the conditional access table (CAT). The CAT lists the associated entitlement management messages (EMMs) or the decryption keys for the addressable digital STBs that are allowed to receive the specific programs that were paid for by the subscriber.

It should be pointed out that there are two EPG extensions to this MPEG-2 system specification, which have been specified by the European Telecommunications Standardization Institute (ETSI)/DVB [24] and by ATSC [25]. Unfortunately, these extensions are not compatible with each other and will not be discussed here [26].

The ongoing development of advanced EPGs is still in its early stages. The integration of web-based applications with enhanced TV services will require the next-generation EPGs to become more personalized, intelligent, and highly interactive to reduce the increasing complexity and offer more TV friendly viewing. For example, the EPG can group TV channels based on a common content such as sporting events or children programs. Other features may include a personalized agent who is familiar with your viewing habits and interests can scan the available TV and web programs when asked. By interacting with the intelligent agent, the viewer can reduce the list of choices according to his preferences. The personalized agent can also alert you to future programs based on your viewing schedule and your interaction with him. Such advanced interactive EPGs will surely transform the TV viewing experience from a passive one to an interactive and exciting one.

The discussion on EPGs is not complete without mentioning intellectual property rights. Gemstar TV Guide International, in the US, holds various key patents for the functionality, look, and feel of the basic and advanced EPGs. For example, Gemstar has the patent rights for the typical TV program grid design (see Figure 12.3). Since this grid look is familiar with many consumers, various software vendors and STB manufacturers have licensed the patent rights rather than engage in an expensive legal battle with Gemstar International.

12.2.2 Parental Control

Another application related to the EPG application is called parental control. The parental control service allows viewers to control access to certain programs or channels that are viewed at the subscriber's location. The parental control service, which can be launched on the TV screen using a lock or a secret PIN number, allows the subscribers to specify the category of programs to be restricted, such as adult movies, as well as how much Can be spent when ordering a non-restricted PPV event. The parental control of certain TV programs is typically accomplished by highlighting the selected program rating from the on-screen menu and pressing the lock button. Figure 12.4 shows, for example, a parental control screen with no lock on the selected channel. To keep the lock secret, which is only

known to several family members, the cable operators typically advise the subscriber to change the lock periodically, say every three months.

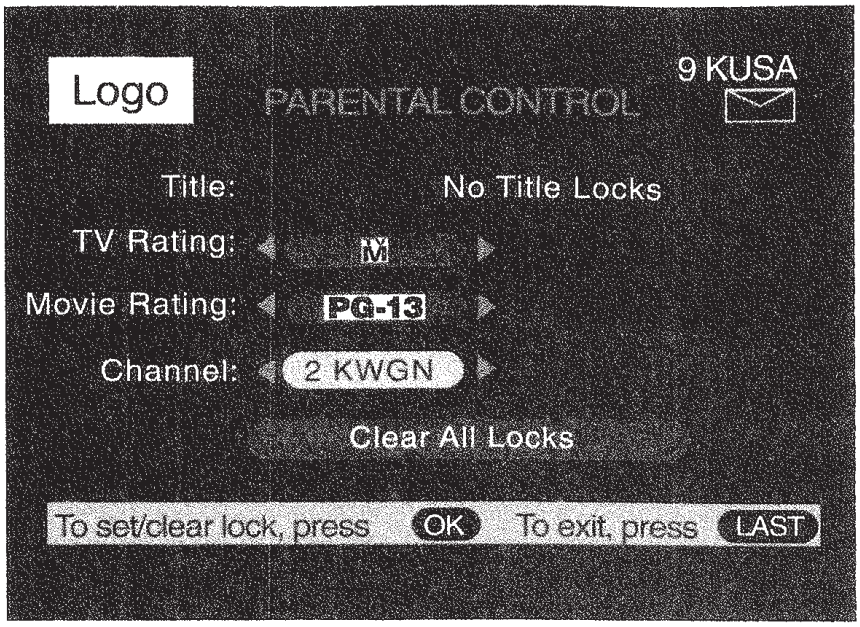


Figure 12.4 A parental control screen showing the selected title and the lock status.

12.3 TV-Based Interactive Applications

The TV-based applications can be divided into two main groups. The first group of TV-based interactive applications, which enables the user's local interactivity, includes applications such as PPV, impulse PPV (IPPV), and parental control, which are discussed in Section 12.3.1. In addition, there are non-native applications such as enhanced broadcast and interactive and targeted advertisements, which may require an increasing level of local user interactivity and are discussed in Section 12.3.2. The second group of TV-based applications, which require server interactivity, includes applications such as VOD and are discussed in Section 12.3.3. Although Near VOD (NVOD) application requires only weak server interactivity, it is also discussed here due to its close relationship with VOD.

12.3.1 Pay-Per-View (PPV) and Impulse PPV (IPPV)

PPV and IPPV enable consumers to watch a broadcast program such as a movie or a sporting event by purchasing it within a designated time window. The cable operators typically allow the viewer to purchase the desired event from several weeks before the starting time of the event up to 15 minutes after the event starts. Different PPV menus have a different look and feel in terms of the screen layout and appearance. The PPV menu may be organized, for example, according to movie titles, titles by time, or according to the type of programs such as children, adult, and sport. Each cable operator can insert his logo on the PPV screen and further customize the PPV menu. The concept of PPV application was implemented as call-ahead PPV (CAPPV) service, where the subscriber had to call ahead using a toll-free number before receiving authorization for the requested event. The IPPV application allowed the subscriber to watch the requested programs and then pay for them up to a maximum predetermined credit. The calling was done automatically using a low-speed (9600-kb/s) telephone modem built into the STB. Figure 12.5 shows an example of an IPPV menu selected according to the desired time slot, where the viewer is reviewing his order for the movie "Batman Forever" rated PG-13. After the viewer has purchased the desired movie, the billing information such as the time, date, title, and charge for the movie is transmitted (not real-time and low-speed) to the billing system server located at the cable headend through the return OOB channel. The subscriber billing information is typically stored in a

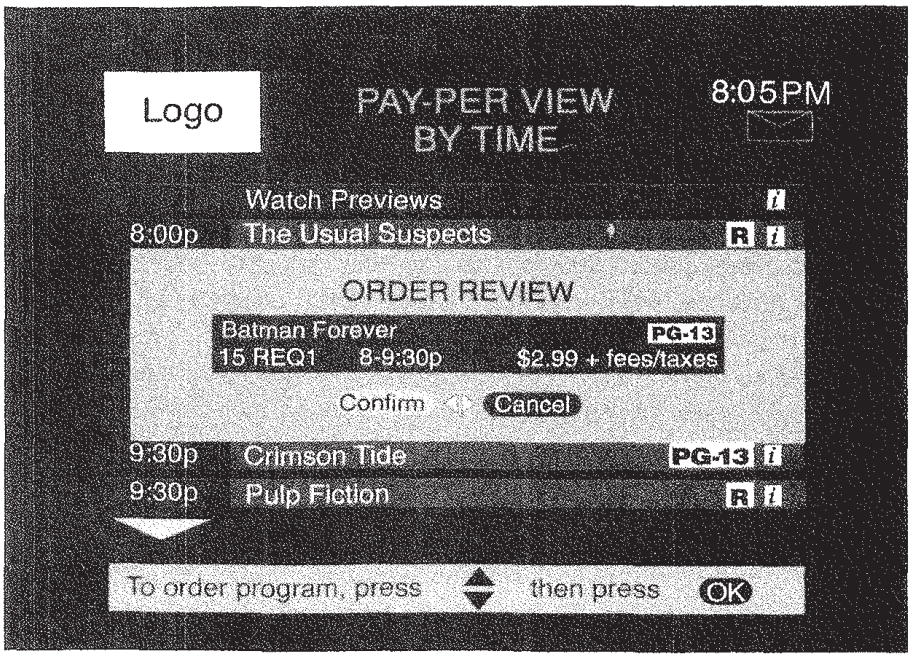


Figure 12.5 Pay-per-view menu selected according to desired time slot.

non-volatile memory such as flash memory in the STB. Some international cable operators allow subscribers to use the so-called prepaid smart cards to purchase the requested PPV events. It should be pointed out that some cable operators might have cumbersome and/or noisy return-path network architecture, which require an expensive upgrade. Consequently, IPPV applications cannot be implemented, and the cable operators have to resort to using low-speed telephone modems or call-ahead options.

12.3.2 Enhanced Broadcast, Interactive, and Targeted Advertisements

Enhanced broadcast (EB) and interactive and targeted advertisements are non-native STB applications that are associated with the audio/video stream and are enabled via the subscriber's local interactivity. EB, which is targeted by DVB-MHP and ATSC-DASE, is represented by additional information (i.e., text, graphics, and some level of interactivity) sent to the subscriber along the audio/video stream to enhance the broadcast video program. For example, such information may be sports scores of an ice hockey team playing, which can be displayed on the screen when the subscriber pushes a specific button on his remote control. Other examples may include a customized stock ticker during a CNN business news program or an additional text/press release during an evening news program. Some of these features are also being targeted by ATVEF [19].

Interactive and targeted advertisement applications, which offer potentially lucrative opportunities to many businesses, require higher user's interactivity than EB, depending on the particular implementation of these applications. For example, during a commercial break, the user may click on a specific button on his remote control and either request further information on the displayed product or service, or even purchase it. The application may allow the subscriber to print a coupon of the advertised product or service in the convenience of his home, or connect him to the web for e-commerce transactions (see Section 12.4.3). In addition, different subscribers may see different commercials during the same program break, depending on their location and/or personal preferences. For example, some people who live in Miami may prefer to see commercials in Spanish rather than English, and some people who live in Phoenix may not want to see winter tire ads during the winter months.

12.3.3 Video-on-Demand (VOD) and Near VOD (NVOD)

One of the primary applications of digital TV is VOD and Near VOD (NVOD) [2]. In the VOD system, the consumer can purchase a program on demand using the STB remote control and view it when he wants to. In other words, VOD system offers the viewer the convenience of renting a movie from the cable operators without having to leave his home. Figure 12.6 shows, for example, the interactive VOD grid menu by Diva, where the viewer can search, purchase, and view the desired movie from the available movie menu [27]. VOD



Figure 12.6 Interactive video-on-demand grid menu, showing the available movie categories to be selected. Courtesy of DIVA.

is sometimes called "pull" technology because the media server "pulls-in" the subscriber's requests over the cable TV network. In the NVOD system, a limited number of programs start on different digital channels with a fixed time interval (i.e., every 30 minutes) such that the consumer can easily choose the desired time and date to view his selected program. Currently, there are various vendors who offer commercially scalable VOD system solution, including Diva [27], SeaChange International [28], and Vivid Technologies. Generally speaking, the VOD system architecture consists of high-performance video servers, which have a large library of movies, connected to a network management system and a billing system at the cable TV headend. For example, the DIVA DVS5000 video server consists of multiple processor modules that stream movies from disk drive arrays over VOD networks. Each processor module uses a twelve-disk redundant array of independent (or inexpensive) disks (RAID) storage. The DVS 5000 includes a 34-Gb/s non-blocking MPEG switch that can be configured up to 16 ports, and can interconnect server modules to form video server clusters. A DVS 5000 cluster can deliver anywhere from 500 to over 20,000 3.4-Mb/s streams. The different MPEG-2 video streams are then encrypted, multiplexed, and coded for 64-QAM or 256-QAM transmission over the cable TV network to the subscriber's digital STB. In practice, it is cheaper and simpler for the cable operators to offer NVOD service rather than VOD service, since the NVOD system can be implemented using low-cost PC-

based digital media servers and there is no need for high-throughput real-time MPEG-2 switching and decoding. Furthermore, some NVOD vendors offer a scalable NVOD solution to VOD, depending on the cable operator penetration rates and number of subscribers.

12.4 Internet-Based Applications

Internet-based applications are perhaps the most important emerging application class for the digital STB. In fact, web-based applications are converging with broadcast and interactive TV-based applications [29]. Before discussing the different web-based applications, let us discuss how web-based content is implemented to enhance broadcast TV content. For the broadcast analog channel, the web content is carried in the VBI according to North American basic Teletext specification (NABTS) [30] and Internet standard IP over VBI [31]. For the broadcast digital channel, there are several options. An extension to the ATSC *program and system information protocol* (PSIP) supports data broadcast as defined by ATSC T3/S13, specifying how IP data is carried in the MPEG-2 TS [32].

In the next section, we provide a brief overview, which is not intended to be exhaustive, of the various web-based applications for a digital STB, including webcasting, e-mail, e-commerce, home banking, education, and gaming.

12.4.1 Set-Top Box Web Browsers

Internet-based applications are the most important emerging application class for a digital STB. Similar to PC-based web browsers, STB-based browsers allow subscribers to receive multimedia web content displayed on their TV. However, the web browsers in the STB environment are operating with some constraints such as limited memory size and CPU processing power. As a result, it may not be possible to support all the different forms of web content such as 3D graphics or a virtual reality content. The Internet access of the STB is accomplished by connecting to a file server at the headend through the cable TV network. The file server listens and responds to requests from the subscriber STB browser using *hypertext transfer protocol* (HTTP). In addition, the web server is responsible for other important tasks such as protecting the web content from unauthorized users, and sending requests to other web servers on the Internet. To help browse the web, the digital STB often incorporates Proxy server software. The Proxy server acts as a gateway with firewall-class security between the cable TV network and the public Internet, while providing easy-to-use management features. The Proxy server offers distributed (hierarchical and array-based) web caching, scalability, fault tolerance, resulting in improved network response time and efficiency by as much as 50%. Some Proxy servers provide network filtering, allowing cable operators and subscribers to restrict access to certain web site containing inflammatory or inappropriate content.

The security between the digital STB and the Proxy server is typically established using *secure sockets layer* (SSL) protocol, which is supported by most web browsers using 40-bit

or 128-bit keys for data encryption [34]. The SSL protocol runs above the TCP/IP layer and below the high-level application protocols such as HTTP and IMAP. The transmitted data is encrypted using a public key, but can only be decrypted using a private key. The SSL server authentication allows a user to confirm the identity of a server. This feature may be critical when the STB subscriber, for example, is sending his credit card information over the cable TV network and wants to check the receiving server identity. Furthermore, the SSL authentication running on the user's STB allows a server to confirm the users' identity. This confirmation may be important, for example, to a bank sending financial information to its client. The SSL protocol uses both public-key and symmetric-key encryption. First, the server authenticates itself to the STB, or the STB can authenticate itself to the server using public-key encryption. Then, symmetric keys are created for rapid encryption, decryption, and tamper detection during the session between the server and the STB.



Figure 12.7 Web browsing through a standard TV using a digital set-top box. Courtesy of Interactive Channel.

An interesting and important feature of the web browser, in contrast to the VOD application discussed in Section 12.2.3, is called *webcasting* ("push" technology). Set-top webcasting is the process of distributing multimedia content by the web server to the STB subscriber over the cable TV network. The reason it is called push technology is because the server "pushes" the multimedia content to the user rather than waiting for his request. In practice,

the push of the multimedia content is triggered by either the user or the cable operator, and arrives only as a result of the user request.

In webcasting, the STB user subscribes to his favorite "channels" that are frequently accessed. A channel consists of the main web page and any related web pages. The set-top browser periodically monitors the selected channels and notifies the user when a new content is available. As the updates arrive, they are either stored for you to view the first time you click on a "channel" or, if a channel is already active, the information is presented to you immediately. Microsoft has developed a channel specification called *channel definition format* (CDF) that permits the subscribed STB user to automatically receive new multimedia content posted on the selected channel. The CDF file, which is typically written in extensible markup language (XML), contains a list of all the necessary uniform resource locators (URLs) to point to the selected multimedia content on the Internet [35]. Using some type of a scheduling tool, the cable operators can decide how often the multimedia content needs to be updated on the Internet [2].

12.4.2 E-mail

The use of electronic mail or e-mail has become very popular with the recent explosive use of the Internet. E-mail is a non-real-time electronic communication between computers that are connected, for example, via a LAN or WAN. It is a fast and economical way for anyone with a PC and a modem to exchange information with friends and colleagues around the globe. Thus, the e-mail information, which may include multimedia-rich content, promotes the virtual office concept, where people can communicate with each other wherever they are and whenever they want. Since e-mail is cheaper and faster than making phone calls or sending faxes, the use of e-mail is expected to grow dramatically to more than a billion global users within three years.

E-mail application can be viewed as part of the STB client/server family of applications. In the client/server computing model, the client STB interacts with the cable operator e-mail servers equipped with a firewall at the cable headend. Every subscriber receives a unique e-mail address and mailbox, which is stored and managed for billing purposes at the e-mail server. The e-mail server acts as a gateway to the Internet using common protocol standards such as *simple message transfer protocol* (SMTP) and *secure multipurpose Internet mail extensions* (S/MIME). As part of the TCP/IP protocol stack, the SMTP is a reliable and efficient mail transfer protocol, which specifies how the messages should be transmitted from the sender to the recipient 's mailbox, for only plaintext files. Then, the STB user can retrieve the messages using either a *post-office protocol* (POP) or an *Internet message access protocol* (IMAP). The newest version of POP is POP3, which is used by most e-mail applications and can be used with or without SMTP [36]. The latest version of IMAP is IMAP4, which is similar to POP3, but supports additional features such as selecting which messages on the e-mail server to download to your STB [37].

The S/MIME protocol, which is a new version of the MIME protocol for secure transmission, allows subscribers to send non-ASCII messages such as graphics, audio, and video

files over the public Internet network [38]. The S/MIME supports RSA public-key encryption (see Section 8.6.1). The advantage of the S/MIME protocol is that it will allow people to send secure e-mail messages to one another using different STB e-mail clients. A STB e-mail client is an application that runs on STB that enables one to send, receive, and organize his e-mail messages.

12.4.3 E-Commerce

Electronic commerce or e-commerce is one of the most significant emerging Internet applications. E-commerce is typically defined as buying and selling goods on the Internet. According to Forrester Research, the on-line Business-to-Consumer (B2C) e-commerce is predicted to reach $200 billion in consumer purchases by 2004. This kind of explosive growth is not only fueled by ease of use and broad range of available products, but also because it drives prices down, and there are no taxes for goods and services purchased on-line. Consequently, cable operators are faced with a compelling e-business opportunity to deploy new e-commerce applications. In this e-business model, cable operators are forming profit-sharing partnerships with various existing on-line merchants. Examples of popular e-commerce services over cable TV networks are [39]:

- Home catalog shopping
- Travel services (airline tickets, hotels, car rental)
- E-auction (i.e., art, antiques, jewelry)
- E-gambling
- On-line ticket sales (i.e., concerts, shows, and sports)
- Local fulfillment (flowers, stamps, food)

The key component of this e-business model is payment for the purchased on-line goods and services. The consumer can pay for his on-line transactions in two ways, namely, electronic cash (e-cash) or credit cards. E-cash is a new form of payment that allows subscribers to make electronic transactions over the cable TV networks. Currently, there are three main categories for e-cash as follows: anonymous cash, micro-payments, and smart cards. The anonymous cash method is just like real cash where the subscriber can spend cash anywhere in the world while being anonymous. An example in this category is eCash, which uses digital signatures based on public-key cryptography, provides authentication, non-repudiation, data integrity, and confidentiality [40]. In the eCash system, only the bank signs the payment data, and the same bank verifies its signature and the integrity of the payment data when a payment recipient submits an eCash payment for validation. The eCash software eliminates the complex key management issues associated with issuing or verifying digital signatures from millions of consumers or merchants.

The micro-payments method allows subscribers to make small payments just as one would use coins in the real world. Since the micro-payments method handles transaction typically up to $10, it is generally not economical for the merchant to use a credit card. For example,

the Pay2See system uses a browser-like payment system, which handles specially encrypted web pages and lets the subscriber see them only if he pays.

Smart cards are electronic cards that can store a limited amount of cash in them. Since most digital STB have a built-in smart card reader, cable operators can download a fixed cash amount to the smart card for e-commerce transactions. Examples of such e-cash systems include BarclayCoin, NetFare, Mondex, and Smartcard Axis.

The use of credit cards for electronic transactions over the cable TV network is similar to in-person transactions. There are two main categories for credit card payments. The first category simply requires the subscriber to enter his credit card at the STB e-commerce application when he decides to make a purchase. The credit card information can be sent encrypted or unencrypted (not recommended) across the cable TV network to the merchant's web server. The second category of credit card payment involves the use of the so-called electronic or digital wallets. Electronic wallet, which is securely stored in the STB, is a software program that has the subscriber's credit card and billing information. This information is sent encrypted to the desired merchant once a secure connection has been established between the merchant and the subscriber. The advantage of electronic wallet is that the subscriber does not have to enter his credit card information every time he wants to purchase.

12.4.4 Home Banking, Education, and Gaming

Home banking, education, and gaming can also be viewed as part of the client/server family of applications. These applications, like e-commerce application, require the establishment of a secure means to transmit the sensitive subscriber information over the cable TV network. Home banking service is an important emerging new application typically via the cable TV network. This service offers both convenience and time saving opportunity to the STB subscribers. For example, it enables subscribers to obtain up-to-date information on their checking and saving accounts, and allows them to transfer funds between accounts and pay bills 24 hours a day, 7 days a week. The home banking service is also advantageous to the financial institution as well as the cable operator. From the financial institution's point of view, it lowers its operating costs, and allows it to offer new financial services to its customers. From the cable TV operator's point of view, it increases subscriber satisfaction and could generate additional revenues through adding additional subscribers and through targeted advertisement campaigns.

STB education is also a promising new application that is expected to have an explosive growth. Generally speaking, STB education is the delivery of STB educational materials to subscribers in the convenience of their homes. This application essentially creates a virtual classroom, where students at different locations receive specially broadcast audio and video content from a central location and can interact with each other and the teacher as if they were all in same physical classroom. The educational material may include, for example, university curriculums, training courses, or even lectures and speeches given by subject matter experts. To enable the STB education service, the cable operator has to provide the sub-

scriber with a downloadable resident application to the STB, and must have some kind of database server that stores and manages the educational material. To reach the STB user, the educational content can be multiplexed with other MPEG-2 video stream to form a 64/256-QAM channel that is transmitted over the cable TV network.

The popularity of interactive video games has been increasing in recent years. However, most of these games are limited to a single user. With the evolution of cable TV networks toward DWDM high-capacity digital networks, multi-user interactive video games are expected to become very hot applications for many people. From the cable TV operator's perspective, it may be easier to implement than home banking or e-commerce applications. The operator can simply download one or more resident applications for specific games to the STB user over a dedicated gaming channel when the subscriber tunes in. The gaming application can be stored in the STB if it has enough flash or RAM memory. Then, the list of authorized games will be displayed on the subscriber's TV monitor, and he can select the desired games using his remote control. The selected game request is then forwarded to the game application server at the cable headend, which authorizes the request, and starts the game session. The game server also manages the game interaction among multiple users.

12.5 Integrated Set-Top Box Applications

In the previous sections so far, we have reviewed separately the different TV-based and Internet-based applications. These applications are sometimes called third-party applications since software vendors independently from the RTOS or STB vendors have developed them. In order to deliver enhanced TV and web content, several software vendors such as Microsoft, Liberate Technologies, and WorldGate Communications are developing a customized interactive menu that integrates the various STB applications. This important point is best illustrated by the following example. Figure 12.8 the shows the WorldGate home page menu, showing the available services, including web browsing, e-mail, and TV programming using a digital STB [41]. Using a wireless keyboard or a remote control, the subscriber logs in to the WorldGate home page menu that can be customized to his city or community. In addition to web surfing, the WorldGate menu supports the so-called Channel HyperLinking, which enables the viewer to go directly to the corresponding web site related to the viewed TV channel or advertisement by pressing a special key on the keyboard. This feature offers a smooth transition between TV and web-watched programming. Using the WorldGate menu, the viewer can activate parental control filters such as Surf Watch to assist parents who wish to block certain types of web sites such as those dedicated to gambling or guns. The WorldGate menu also offers a home banking capability, which allows subscribers up-to-date account information as well as safe direct bill payment. New emerging applications such as VOD and distance learning can also be integrated into the current interactive menu. Liberate TV Navigator is also offering similar features by integrating web browsing, e-mail, and an interactive program guide for TV programming for enhanced TV viewing.



Figure 12.8 WorldGate home page menu with accesses to standard TV programs, e-mail, as well as customized web browsing features. Courtesy of WorldGate Communications, Inc.

Emerging applications for digital STB should be able to support these technologies:

- Animated and virtual reality graphics
- High-definition TV (HDTV) display
- Video and audio streaming
- 3-D video display

As subscribers become more comfortable with the enhanced TV viewing, they will demand more advanced interactivity to TV programs using, for example, Channel HyperLinking. Advanced TV interactive applications (not limited to specific web content) will open the door to a whole new TV experience where many people will be able to interact with each other based on the viewed TV or webcasting programs.

References

1. P. Peterka, "Interactive TV Applications: Standard APIs for Digital TV Receivers," *NCTA Technical Papers*, 134–143 (1999).
2. G. OÆdriscoll, *The Essential Guide to Digital Set-Top Boxes and Interactive TV*, Prentice Hall PTR (2000).
3. R. F. Annibaldi, J. Buehl, and S. Johnson, "System Implementation of a Resident Application and User Interface for Digital Set-Tops," *NCTA Technical Papers* (1998).
4. R. W. Brown, "Pegagus Set-Top Terminal," *NCTA Technical Papers*, 24–31 (1997).
5. Product information on Windows CE can be found at http://www.microsoft.com/tv/
6. Product information on PowerTV RTOS can be found, for example, at http://www.powertv.com/product/product.html
7. Product information on Java OS and APIs can be found at http://www.sun.com/javaos.
8. Product information on VxWorks OS can be found at http://www.vxworks.com/
9. Product information on Microware DAVID OS-9 can be found at http://www.microware.com/ProductsServices/Technologies/david.html.
10. Java Virtual machine (JVM): http://java.sun.com/docs/books/vmspec/index.html.
11. See for example http://www.dvb.org/.
12. For more information on MediaHighway middleware platform see for example http://www.canalplus-technologies.com/media/mediahighway.htm.
13. ATSC T3/S17 DTV Application Software Environment (DASE): http://toocan.philabs.research.philips.com/misc/atsc/dase/.
14. For example, look at www.w3c.org.
15. Suns' Java TV: http://java.sun/com/products/javatv.
16. Personal Java: http://java.sun.com/products/personaljava/spec-1-1/pJavaSpec.html.
17. Java Media Framework (JMF): http://java.sun.com/products/javamedia/jmf/forDevelopers/playerguide/index.html.
18. Home Audio/Video Interoperability (HAVi): http://www.havi.org.
19. For information on ATVEF specifications, see for example http://www.atvef.com/index.html.
20. Liberate product information can be found at http://www.liberate.com.
21. See, for example http://www.tvguide.com/.
22. See, for example http://www.starsight.com/.
23. International Telecommunication Union (ITU) H.222/ISO 13818 Section 1, Generic Coding of Moving Pictures and Associated Audio Information: Systems (1997).
24. European Telecommunications Standardization Institute (ETSI) ETS 300468, Digital Broadcasting Systems for Television Sound and Data Services; Specification for Service Information (SI) in Digital Video Broadcast (DVB) Systems (1996).

25. A/65 Program and System Information Protocol (PSIP) for Terrestrial Broadcast and Cable, Advanced Television Standardization Committee, *Digital Television Standard* (1997).
26. D. Ruiu, "Electronic Program Guide Standards", in *Testing Digital Video*, Hewlett Packard (1997).
27. For information on Diva VOD system, see http://www.divatv.com/diva_home.html.
28. For SeaChange International VOD product, see http://www.schange.com/products/resvod.html.
29. R. W. Brown, "Where Web and TV Collide," *NCTA Technical Papers*, 95–102 (1998).
30. Joint EIA/CVCC Recommended Practice for Teletext: North American Basic Teletext Specification, ANSI/EIA-516-88 (1988).
31. The Transmission of IP Over The Vertical Blanking Interval Of A Television Signal, Internet draft of IPVBI working group (1998). http://www.ietf.org/internet-drafts/draft-ietf-ipvbi-tv-signal-00.txt.
32. A/90 Data Broadcast Standard, Advanced Television Standardization Committee (August, 2000).
33. Information Technology – Generic Coding of Moving Pictures and Associated Audio: Digital Storage Media and Control – ISO/IEC 13818-6 International Standard, ISO/IEC JTC1/SC29/WG11 MPEG96/N1300p1 (1996).
34. More information on the SSL protocol can be found at http://home.netscape.com/eng/ssl3/draft302.txt.
35. Tutorial on Microsoft's CDF standard can be found at http://msdn.microsoft.com/workshop/delivery/channel/cdf1/cdf1.asp?RLD=363.
36. For more information on POP version3 protocol standard, see for example http://www.cis.ohio-state.edu/htbin/rfc/rfc1939.html.
37. For more information on IMAP version4 protocol standard, see for example http://www.cis.ohio-state.edu/htbin/rfc/rfc2060.html.
38. For more information on S/MIME protocol standard, see for example, http://www.ietf.org/ids.by.wg/smime.html.
39. T. Wasilewski, "E-Commerce over Cable: Providing Security for Interactive Applications," *NCTA Technical Papers*, 122–133 (1999).
40. For more information on eCash, see for example http://www.ecash.net/.
41. WorldGate user guide, WorldGate communications, Inc. (1999).

APPENDIX A

COMPARISON OF DAVIC AND DOCSIS SPECIFICATIONS

In Chapter 11, we reviewed CableLabs DOCSIS protocol, which is the primary standard in the United States for high-speed data transmission. The Digital Audio Video Council (DAVIC) protocol standard is a competing standard, which is used mainly in Europe. In an attempt to bridge this gap, CableLabs has added Appendix N (EuroDOCSIS) to the DOCSIS 1.1 standard, which provides PHY layer specifications for CMs operating in European cable plants. The intent of this appendix is simply to highlight the primary PHY layer differences between the DAVIC and DOCSIS protocol specifications; accordingly, what is presented should not be viewed as a complete comparison. Table A.1 summarizes the primary PHY layer differences between DAVIC 1.2 and DOCSIS 1.1 specifications.

Table A.1 Comparison of DAVIC 1.2 and DOCSIS 1.1 Specifications.

Parameter	DAVIC 1.2	DOCSIS 1.1
OOB Modulation Format	Differentially encoded QPSK	N/A
OOB Transmission Rate	1.544 Mb/s	N/A
OOB Error Correction	R-S T = 3 (59,53)	N/A
OOB Link Layer(s)	ATM-like/ extended superframe	N/A
Inband Modulation Format	64/256-QAM	64/256-QAM
Transmitted Spectrum 64-QAM 256-QAM	Square-root raised cosine shaping $\alpha = 0.13$ (6-MHz) $\alpha = 0.15$ (8-MHz)	Square-root raised cosine shaping $\alpha = 0.18$ (6-MHz) for 64-QAM $\alpha = 0.12$ (6-MHz) for 256-QAM
Inband Information Rate	29.172/38.896 Mb/s (6-MHz) 38.236/50.981 Mb/s (8-MHz)	26.97035 / 38.8107 Mb/s (6-MHz)
Inband Error Correction 64-QAM 256-QAM	 R-S (204,188) T = 8 R-S (204,188) T = 8	R-S T= 3 (128,122) +14/15 rate TCM R-S T = 3 (128,122) +19/20 rate TCM

Parameter	DAVIC 1.2	DOCSIS 1.1
Convolutional Interleaver	I = 12, J = 17 for 64-QAM I = 204, J = 1 for 256-QAM	Variable I = 8, 16, 32, 64, 128 J = 16, 8, 4, 2, 1 for both 64/256-QAM
CNR @ Receiver Input (only AWGN)	≥30 dB @ BER = $1 \cdot 10^{-12}$ (64-QAM)[1] ≥36 dB @ BER = $1 \cdot 10^{-12}$ (256-QAM)[2]	≥23.5 dB @ BER ≤$1 \cdot 10^{-8}$ (64-QAM) ≥ 30 dB @ BER≤$1 \cdot 10^{-8}$ (256-QAM) at RF input −6 to +15 dBmV ≥ 33 dB @ BER≤$1 \cdot 10^{-8}$ (256-QAM) @ RF input −15 to < −6 dBmV
Adjacent QAM Channel Level	≤ 3 dB (same QAM channels) ≤ 6 dB (diff. QAM channels)	0 dB for both 64/256QAM
Adjacent Analog Channel Level	0 to 10 dBc for 64-QAM 0 to 6 dBc for 256-QAM	10 dBc for both 64/256-QAM
RF Input Level Range (Downstream)	−8 to 20 dBmV (64-QAM) +2 to 20 dBmV (256-QAM)	−15 to +15 dBmV (64/256-QAM)
Inband Link Layers	ATM	DIX or 802.3 over DOCSIS MAC
Assumed Set-top Addressing Architecture	48 bits	48 bits
Upstream Modulation Format	Differentially encoded QPSK	QPSK and 16-QAM
Upstream Frequency Band	8–26.5 MHz	5–42 MHz
Upstream Transmitted Spectrum	$\alpha = 0.30$ for QPSK Square-root raised cosine shape	$\alpha = 0.25$ for QPSK or 16-QAM Square-root raised cosine shape
Upstream Transmission Rate(s)	256 kb/s for Grade A 1.544 Mb/s for Grade B 3.088 Mb/s for Grade C	160, 320, 640, 1280, and 2560 kSym/s
Upstream Channel Spacing	200 kHz for Grade A 1 MHz for Grade B 2 MHz for Grade C	200, 400, 800, 1600, and 3200 kHz

[1] EuroDOCSIS specifies CNR of 25.5 dB or greater (post FEC) at BER=10^{-8} for 64-QAM.

[2] EuroDOCSIS specifies CNR of 31.5 dB (post FEC) at BER=10^{-8} at RF input from −15 dBmV to > −6 dBmV, and 34.5 dB or greater (post FEC) at BER=10^{-8} at RF input level from −6 dBmV to +15 dBmV for 256-QAM.

Parameter	DAVIC 1.2	DOCSIS 1.1
Upstream Transmitter Output Power	+25 to +53 dBmV (RMS) QPSK	+8 to 58 dBmV (QPSK) +8 to 55 dBmV (16-QAM)
Upstream Demodulator Input Power (in each carrier)	N/A	−16 to +14dBmV @ 160 kSym/s −13 to +17 dBmV @ 320 kSym/s −10 to +20 dBmV @ 640 kSym/s −7 to +23 dBmV @ 1280 kSym/s −4 to +26 dBmV @ 2560 kSym/s
Upstream CNR (Only AWGN)	≥ 20 dB @ BER = $1 \cdot 10^{-6}$ (post FEC packet loss)	@ SER=$1 \cdot 10^{-6}$ (uncoded) ≤14.29 dB for QPSK ≤21.42 dB for 16-QAM
Upstream Error Correction	R-S T = 3 (59,53)	RS over GF(256) with T = 1–10
Upstream Data Link Packet Structure	UW = 4 bytes, Pay Load = 53 bytes, RS parity = 6 bytes, Guard band = 1 byte	FC = 1-byte, MAC_PARM = 1 byte, LEN=2 bytes,HCS = 2 bytes, Packet PDU = 18–1518 bytes
Upstream Link Layer(s)	ATM cell	Variable-length Ethernet/802.3
TDMA Synchronization Approach	OOB Extended Superframe synchronization bits	Time synchronization MAC management messages

N/A	Not Applicable
R-S	Reed-Solomon Code
FC	Frame Control: Identifies type of MAC header
MAC_PARM	Parameter field whose use is dependent on FC
LEN	The length of the MAC frame
HCS	MAC header check sequence
PDU	Protocol Data Unit
SER	Symbol Error Rate

APPENDIX B

INTERNATIONAL CABLE TV FREQUENCY PLANS

B.1 CCIR System B/G Frequency Plan

The North America cable TV frequency plans, namely, the standard, HRC, and IRC, were discussed in Chapter 2. In this appendix, we provide selected cable TV frequency plans commonly used in various parts of the globe. In particular, the CCIR system B/G cable TV plan, which is used in Western Europe, the CCIR system I, which is used in Great Britain, and the CCIR system D, which is used in China, are listed in the tables that follow. Notice that E-2 to E-12 channels (Table B.1) are 7-MHz wide, while all the channels from E-21 and above are 8-MHz wide. However, the sound carrier is fixed at 5.5-MHz above the picture carrier frequency for either the 7-MHz or 8-MHz wide channels.

Table B.1 CCIR System B/G Cable TV Frequency Plan Used in Western Europe.

Channel	Picture Carrier Frequency (MHz)	Sound Carrier Frequency (MHz)
E-2	48.25	53.75
E-3	55.25	60.75
E-4	62.25	67.75
E-5	175.25	180.75
E-6	182.25	187.75
E-7	189.25	194.75
E-8	196.25	201.75
E-9	203.25	208.75
E-10	210.25	215.75
E-11	217.25	222.75
E-12	224.25	229.75
E-21	471.25	476.75
E-22	479.25	484.75
E-23	487.25	492.75

Channel	Picture Carrier	Sound Carrier
E-24	495.25	500.75
E-25	503.25	508.75
E-26	511.25	516.75
E-27	519.25	524.75
E-28	527.25	532.75
E-29	535.25	540.75
E-30	543.25	548.75
E-31	551.25	556.75
E-32	559.25	564.75
E-33	567.25	572.75
E-34	575.25	580.75
E-35	583.25	588.75
E-36	591.25	596.75
E-37	599.25	604.75
E-38	607.25	612.75
E-39	615.25	620.75
E-40	623.25	628.75
E-41	631.25	636.75
E-42	639.25	644.75
E-43	647.25	652.75
E-44	655.25	660.75
E-45	663.25	668.75
E-46	671.25	676.75
E-47	679.25	684.75
E-48	687.25	692.75
E-49	695.25	700.75
E-50	703.25	708.75
E-51	711.25	716.75
E-52	719.25	724.75
E-53	727.25	732.75
E-54	735.25	740.75
E-55	743.25	748.75
E-56	751.25	756.75
E-57	759.25	764.75
E-58	767.25	772.75
E-59	775.25	780.75
E-60	783.25	788.75
E-61	791.25	796.75
E-62	799.25	804.75

Channel	Picture Carrier	Sound Carrier
E-63	807.25	812.75
E-64	815.25	820.75
E-65	823.25	828.75
E-66	831.25	836.75
E-67	839.25	844.75
E-68	847.25	852.75
E-69	855.25	860.75

B.2 CCIR system I Frequency Plan

The CCIR system I frequency plan, which is used in Great Britain, is similar to the CCIR system B/G used in Western Europe. In fact, the picture carrier frequencies from Channel 21 to channel 69 in Table B.2 are the same as E-21 to E-69 in Table B.1. However, the sound carrier frequency is 6-MHz above the picture carrier frequency, instead of 5.5-MHz as in Table B.1. See Section 2.1.3.

Table B.2 CCIR System I Cable TV Frequency Plan used in Great Britain.

Channel	Picture Carrier Frequency (MHz)	Sound Carrier Frequency (MHz)
21	471.25	477.25
22	479.25	485.25
23	487.25	493.25
24	495.25	501.25
25	503.25	509.25
26	511.25	517.25
27	519.25	525.25
28	527.25	533.25
29	535.25	541.25
30	543.25	549.25
31	551.25	557.25
32	559.25	565.25
33	567.25	573.25
34	575.25	581.25
35	583.25	589.25

Channel	Picture Carrier Frequency (MHz)	Sound Carrier Frequency (MHz)
36	591.25	597.25
37	599.25	605.25
38	607.25	613.25
39	615.25	621.25
40	623.25	629.25
41	631.25	637.25
42	639.25	645.25
43	647.25	653.25
44	655.25	661.25
45	663.25	669.25
46	671.25	677.25
47	679.25	685.25
48	687.25	693.25
49	695.25	701.25
50	703.25	709.25
51	711.25	717.25
52	719.25	725.25
53	727.25	733.25
54	735.25	741.25
55	743.25	749.25
56	751.25	757.25
57	759.25	765.25
58	767.25	773.25
59	775.25	781.25
60	783.25	789.25
61	791.25	797.25
62	799.25	805.25
63	807.25	813.25
64	815.25	821.25
65	823.25	829.25
66	831.25	837.25
67	839.25	845.25
68	847.25	853.25
69	855.25	861.25

B.3 CCIR System D Frequency Plan

The CCIR system D consists of 8-MHz wide channels. However, unlike its location in systems B/G and system I, the sound carrier frequency in system D is located 6.5-MHz above the picture carrier frequency.

Table B.3 CCIR System D Cable TV Frequency Plan used in China.

Channel	Picture Carrier Frequency (MHz)	Sound Carrier Frequency (MHz)
DS-1	49.75	56.25
DS-2	57.75	64.25
DS-3	65.75	72.25
DS-4	77.25	83.75
DS-5	85.25	91.75
DS-6	168.25	174.75
DS-7	176.25	182.75
DS-8	184.25	190.75
DS-9	192.25	198.75
DS-10	200.25	206.75
DS-11	208.25	214.75
DS-12	216.25	222.75
DS-13	471.25	477.75
DS-14	479.25	485.75
DS-15	487.25	493.75
DS-16	495.25	501.75
DS-17	503.25	509.75
DS-18	511.25	517.75
DS-19	519.25	525.75
DS-20	527.25	533.75
DS-21	535.25	541.75
DS-22	543.25	549.75
DS-23	551.25	557.75
DS-24	559.25	565.75
DS-25	607.25	613.75
DS-26	615.25	621.75
DS-27	623.25	629.75
DS-28	631.25	637.75
DS-29	639.25	645.75
DS-30	647.25	653.75

Channel	Picture Carrier Frequency (MHz)	Sound Carrier Frequency (MHz)
DS-31	655.25	661.75
DS-32	663.25	669.75
DS-33	671.25	677.75
DS-34	679.25	685.75
DS-35	687.25	693.75
DS-36	695.25	701.75
DS-37	703.25	709.75
DS-38	711.25	717.75
DS-39	719.25	725.75
DS-40	727.25	733.75
DS-41	735.25	741.75
DS-42	743.25	749.75
DS-43	751.25	757.75
DS-44	759.25	765.75
DS-45	767.25	773.75
DS-46	775.25	781.75
DS-47	783.25	789.75
DS-48	791.25	797.75
DS-49	799.25	805.75
DS-50	807.25	813.75
DS-51	815.25	821.75
DS-52	823.25	829.75
DS-53	831.25	837.75
DS-54	839.25	845.75
DS-55	847.25	853.75
DS-56	855.25	861.75

APPENDIX C

SATELLITE TRANSPONDER PARAMETERS FOR CABLE TV NETWORKS

The downstream information rate for a 6 MHz cable TV channel operating at a 64-QAM modulation is 26.97035-Mb/s according to the DOCSIS specifications. As pointed out previously in Chapter 7, many cable TV headends receive their downlink digital video feed from various satellite transponders operating at a QPSK modulation format with a matching information rate. The downlink C-Band satellite transponders are operating on vertically and horizontally polarized 36 MHz channels having center frequencies ranging from 3.72/3.74-GHz to 4.16/4.18-GHz with 40-MHz spacing between adjacent channels. The downlink K-Band satellite transponders are operating on right-hand and left-hand circularly polarized 24-MHz channels. Since these are bandwidth-limited systems, robust transmission is achieved using FEC code consisting of a R-S block code, which is interleaved and concatenated with convolutional code. Table C.1 summarizes the 36-MHz (wide) and 24-MHz (narrow) satellite transponder characteristics.

Table C.1 Common Satellite Transponder Parameters That Are Used by Cable TV Operators.

Parameter	Wide QPSK	Narrow QPSK
Transponder Bandwidth	36 MHz	24 MHz
Information Bit Rate	26.97035 Mb/s	26.97035 Mb/s
Total Channel Bit Rate	58.53140 Mb/s	39.02093 Mb/s
Symbol Rate	29.2657 MBaud	19.51047 MBaud
R-S Code	RS (204,188) T = 8	RS (204,188) T = 8
Trellis Code	R = 1/2	R = 3/4
Interleaver	I = 12, J = 19	I = 12, J = 19
Standard IF	70 MHz	70-MHz

According to Table C.1, the channel information rate of 26.97035 Mb/s is identical for both the wide and narrow QPSK channels. From a historical perspective, scientists at General Instrument have successfully selected the proper channel coding (R-S and Trellis codes) such that the 26.97035 Mb/s information rate would match that of ITU-T J.83 Annex B 64-QAM channel transmitted over the cable TV networks. Therefore, the information payload of the received satellite QPSK channel at the cable-TV headend can be used directly for a 64-QAM transmission with no need for bit stuffing. The corresponding symbol rate for a wide bandwidth QPSK channel is calculated as follows:

26.97-Mb/s x 204/188 x 2/1 = 58.53-Mb/s / 2bits/symbol = 29.266-MBaud

and for a narrow bandwidth QPSK channel

26.97-Mb/s x 204/188 x 4/3 = 39.02-Mb/s / 2bits/symbol = 19.51-MBaud

Unfortunately, there is no QPSK channel convolutional coding that can match the required information rate of 38.8107-Mb/s for an ITU-T J.83 Annex B 256-QAM channel.

ACRONYMS

ADC	Analog to Digital Converter
ADSL	Asymmetric Digital Subscriber Line
AGC	Automatic Gain Control
AM	Amplitude Modulation
AOTF	Acousto-Optic Tunable Filter
APC	Automatic Power Control
APE	Annealed Proton Exchange
API	Application Programming Interface
ARP	Address Resolution Protocol
ASE	Amplified Spontaneous Emission
ATC	Automatic Temperature Control
ATM	Asynchronous Transfer Mode
ATSC	Advanced Television System Committee
ATVEF	Advanced Television Enhancement Forum
AWG	Array Waveguide Grating
AWGN	Additive White Gaussian Noise
BBI	Balanced Bridge Interferometer
BCC	Binary Convolutional Code
BER	Bit Error Rate
BNU	Broadband Network Unit
BPF	Band Pass Filter
CCIR	Commite' Consulatif International Radiocommunications
CDF	Channel Definition Format
CDLI	Chroma Luma Delay Inequality
CIF	Common Intermediate Format
CM	Cable Modem
CMA	Constant Modulus Algorithm
CMTS	Cable Modem Termination System
CNR	Carrier to Noise Ratio
CPB	Constrained Parameters Bit stream
CSMA	Carrier Sensing Multiple-Access
CSMA/CD	Carrier Sensing Multiple-Access with Collision-Detection
CSO	Composite Second Order
CTB	Composite Triple Beat

DAC	Digital to Analog Converter
DASE	Digital television Application Software Environment
DAVIC	Digital Audio Visual Council
DBR	Double Rayleigh Backscattering
DBS	Direct Broadcast Satellite
DCT	Discrete Cosine Transform
DDFS	Direct Digital Frequency Synthesizer
DES	Data Encryption Standard
DFE	Decision Feedback Equalizer
DH	Double Heterostructure
DHCP	Dynamic Host Configuration Protocol
DLL	Data Link Layer
DOCSIS	Data-Over-Cable Service Interface Specifications
DSF	Dispersion Shifted Fiber
DVB	Digital Video Broadcast
DVS	Digital Video Subcommittee
DWDM	Dense Wavelength Division Multiplexing
ECM	Entitlement Control Message
EDF	Erbium-Doped Fiber
EDFA	Erbium-Doped Fiber Amplifier
EIA	Electronics Industry Association
EMM	Entitlement Management Message
EPG	Electronic Program Guide
EPM	External Phase Modulation
ESA	Excited state Absorption
ETSI	European Telecommunications Standardization Institute
EVM	Error Vector Magnitude
FBG	Fiber Bragg Grating
FCC	Federal Communications Commission
FDM	Frequency Division Multiplexing
FDMA	Frequency Division Multiple Access
FEC	Forward Error Correction
FFE	Feed-Forward Equalizer
FIR	Finite Impulse Response (filter)
FITL	Fiber In The Loop
FM	Frequency Modulation
FP	Fabry Perot
FPR	Free Propagation Range
FSR	Free Spectral Range
FTTC	Fiber To The Curb
FTTH	Fiber To The Home
FTTN	Fiber To The Node

FSS	Frequency Stacking Scheme
GDV	Group Delay Variation
GF	Galois Field
GOP	Group Of Pictures
GSA	Ground State Absorption
HCS	MAC Header Check Sequence
HDT	Host Digital Terminal
HDTV	High Definition Television
HFC	Hybrid Fiber Coax
HRC	Harmonically Related Carrier
HTML	Hyper Text Markup Language
HTTP	Hyper Text Transfer Protocol
IIN	Interference Intensity Noise
IIR	Infinite Impulse Response (filter)
IMAP	Internet Message Access Protocol
IPG	Interactive Program Guide
IPPV	Impulse Pay Per View
IRC	Incrementally Related Carrier
ISI	Inter-Symbol Interference
ITU	International Telecommunication Union
JBIG	Joint Bilevel Image experts Group
JPEG	Joint Photographic Experts Group
JVM	Java Virtual Machine
LLC	Logical Link Control
LMS	Least Mean Square
LOD	Level Of Detail
LPF	Low Pass Filter
LSB	Least Significant Bit
LTE	Linear Transversal Equalizer
MAC	Media Access Control
MER	Modulation Error Ratio
MGCP	Media Gateway Control Protocol
MHN	Mode Hopping Noise
MIPS	Million Instructions Per Second
MPEG	Moving Picture Expert Group
MPN	Mode Partition Noise
MQW	Multiple Quantum Well
MSB	Most Significant Bit
MSE	Mean Square Error
MZI	Mach-Zehnder Interferometer
NA	Numerical Aperture
NABTS	North American Basic Teletext Specification

NCO	Numerically Controlled Oscillator
NCTA	National Cable Television Association
NEP	Noise-Equivalent Photocurrent
NF	Noise Figure
NPR	Noise Power Ratio
NRZ	Non-Return to Zero
NTSC	National Television System Committee
NVOD	Near Video-On-Demand
OI	Optical Isolator
OOB	Out-Of-Band
OTN	Optical Transition Node
PAL	Phase Alteration Line
PBS	Polarization Beam Splitter
PCM	Pulse Code Modulation
PCR	Program Clock Reference
PDL	Polarization Dependent Loss
PDU	Packet Data Unit
PES	Packetized Elementary Stream
PGA	Programmable Gain Amplifier
PHB	Polarization Hole Burning
PID	Program (or packet) Identification
PLL	Phase Locked Loop
PMD	Physical Media Dependent
PMT	Program Management Table
POD	Point of Deployment
POP	Post-Office Protocol
PPV	Pay Per View
PSIP	Program and System Information Protocol
PSTN	Public Switched Telephone Network
PTS	Presentation Time Stamp
QAM	Quadrature Amplitude Modulation
QoS	Quality of Service
QPSK	Quadrature Phase Shift Keying
RAID	Redundant Array of Independent (or inexpensive) Disks
RAM	Random Access Memory
RGB	Red Green Blue
RGW	Residential Gateway
RIN	Relative Intensity Noise
RLS	Recursive Least Squares
ROM	Read Only Memory
RTOS	Real Time Operating System
SAW	Surface Acoustic Wave

SBS	Stimulated Brillouin Scattering
SCM	Sub-Carrier Multiplexing
SCTE	Society of Cable Television Engineers
SDRAM	Synchronous Dynamic Random Access Memory
SER	Symbol Error Rate
SFID	Service Flow ID
SHB	Spectral Hole Burning
SID	Service ID
SL	Strained Layer
SMF	Single Mode Fiber
S/MIME	Secure Multipurpose Internet Mail Extensions
SMTP	Simple Message Transfer Protocol
SNMP	Simple Network Management Protocol
SNR	Signal to Noise Ratio
SONET	Synchronous Optical Networks
SPM	Self Phase Modulation
SRRC	Square Root Raised Cosine
SRS	Stimulated Raman Scattering
SS7	Signaling System number 7
SSL	Secure Sockets Layer
STB	Set-Top Box
TCM	Trellis Coded Modulation
TDM	Time Division Multiplexing
TDMA	Time Division Multiple Access
TEC	Thermo Electric Cooler
TFTP	Trivial File Transfer Protocol
TGW	Trunking Gateway
TLV	Type Length Value
TVPAK	Television Platform Adaptation Kit
UCD	Upstream Channel Descriptor
UGS	Unsolicited Grant Service
UMA	Unified Memory Architecture
USB	Universal Serial Bus
URL	Uniform Resource Locator
UW	Unique Word
VBI	Vertical Blanking Interval
VBR	Variable Back Reflector
VCO	Voltage Controlled Oscillator
VITS	Vertical Interval Test Signals
VOD	Video-On-Demand
VoIP	Voice Over IP
VSB	Vestigal Side Band

WDM	Wavelength Division Multiplexing
XML	Extensible Markup Language
XMOD	Cross Modulation
XPM	Cross Phase Modulation
YAG	Yttrium Aluminum Garnet
YIG	Yttrium Iron Garnet

INDEX

A

AC-3, audio coding, 35
Absorption cross sections, 157–161
Acousto-optic tunable filters, *see* Filters
Adaptive equalizers, 208–214, *see also* Equalizers,
Address resolution protocol (ARP), 359
Advanced set-top box, 260–261
Advanced TV enhancement forum (ATVEF), 401, 407
Advanced Television System Committee (ATSC), 35, 382, 386, 389, 392
Aloha protocol, 380–381
Alpha blending, 254
AM hum modulation, 55, 273, 276
Amplified spontaneous emission (ASE), 157–161, 165–174, *see also* Noise
Amplifiers, optical, *see* Erbium-doped fiber amplifiers
Amplifiers, RF, 43–45, 90, 133–139, 142–144, 207–208, 232, 234
Amplitude ripple, QAM channel, 270–271
Analog to digital converter (ADC), 29 206–207, 354–356
Application program interface (API), 395–39, 400–401
Architecture:
 downstream HFC access, 4–6, 348–349
 downstream DWDM access, 349–351
 fiber-in-the-loop (FITL), 14–16
 digital set-top box software, 395–402
 upstream DWDM access, 352–354
Array waveguide grating (AWG), 150–152
Asymmetric digital subscriber line (ADSL), 12–14
Aural carrier, 22, 24
Authorization module, 386
Automatic gain control (AGC), 46, 85–86, 119, 296
Automatic power control (APC), 85–86
Automatic slope control (ASC), 46
Automatic temperature control (ATC), 85–86

B

Backoff window, 382
Balanced-bridge interferometer (BBI) modulator, *see* Modulators
Bandwidth allocation, *see* Upstream,
Bipolar-junction transistors (BJT), 139, 143
Bit error rate (BER), of M-ary QAM signals, 223–226
Blind equalization, 212–213, *see also* Equalizers
Bragg grating, 152–153
Bragg wavelength, 153
Broadband network unit (BNU), 14–16
Burst frame structure, 371–372

Burst noise, 56, 271–273
Burst profiles, 365–367
Burst timing, 368–369
Bursty nonlinear distortions, 294–299

C

Call agent, 10–11
Cable modem (CM):
 downstream physical layer, 361–363
 downstream transmission convergence sublayer, 372–373
 interaction, with CMTS, 390–392
 media access control (MAC), see MAC layer
 random access methods, 380–382
 synchronization, 375–377
 upstream burst timing, 368–369
 upstream fragmentation, 388–390
 upstream physical layer, 351–352
 upstream quality of service, 384–388
 upstream spurious power outputs, 357–358
 upstream transmitter, *see* Upstream
Cable modem termination system (CMTS), 360–362, 366–367, 374–379, 390–392
Cable TV frequency plans, 38–42, 423–428
Carrier-to-noise-ratio (CNR), of single and cascaded amplifiers, 47–48
Coaxial cable, 42–44
 return-path characteristics,
 RF tuner, *see* Tuner,
 RF amplifiers, 44–47, 90, 133–139
 taps, 47
Carrier sensing multiple access (CSMA) method, 380–381
Carrier recovery methods, in QAM receivers, 214–217
Cascode preamplifier configuration, 143–144
Channel definition format (CDF), 411
Channel model, of HFC networks, 53–55, 268–269
Characteristic temperature, of lasers, 71
Chroma-luma delay inequality (CLDI), 25–27
Ciphertext, 247
Circuit model, large signal response, 79–82
Clipping noise:
 BER of QAM channels due to, 283–287
 dynamic, 290–292
 double-level, 289–290
 reduction methods, 292–294
 statistical properties of, 281–282
Coding gain, of TCM, 196–197
Constant-modulus algorithm (CMA), 213
Constellation diagrams, 64/245-QAM, 221–222, 265–266
Contention resolution protocols, 380–382
Composite second order (CSO), 49–50, 265, 275, 294–299, *see also* Distortions
Composite triple beat (CTB), 49–50, 265, 275, 294–299, *see also* Distortions
Constraint length, 193–196
Costas loop, 215–216
Cross phase modulation (XPM), 322–323,
Coupled mode equations, 148, 150

D

Damping coefficient, 78
Data encryption standard (DES), 247
Data link layer (DLL), 359–361

Dense-wavelength-division multiplexing (DWDM), *see* Architecture
Decision-directed loops, 216–217
Decision-feedback equalizer (DFE), *see* Equalizers
Depletion region, p-i-n photodiode, 126–127
Differential detection scheme, 340–342
Differential gain (DG), NTSC signal, 25–27
Differential quantum efficiency, 72
Differential phase (DP), NTSC signal, 25, 27
Differential precoder, 200–201
Diffusion process,124–126
Digital encryption and decryption, 246–248
Digital Audio and Video Council (DAVIC), 183, 227, 380, 419–421
Digital to Analog converter (DAC), 206, 355
Digital video broadcast (DVB), 400–401, 404, 407
Digital video signals, *see* Video signals
Digitized return-path transport, 354–356
Direct broadcast satellite (DBS), 16–17
Discrete cosine transform (DCT), 30–31, 35
Dispersion shifted fiber (DSF), 311, 314, 318
Dissymmetrization scheme, 294
Distortions:
  chroma differential gain, 25–27
  chroma differential phase, 25–27
  composite second-order (CSO), 49–50, 265, 275, 294–299
  composite triple beat (CTB), 49–50, 265, 275, 294–299
  dispersion-induced, 309–311
  gain tilt, in EDFA, 346–348
  intermodulation, 49–50, 136–137
  polarization-induced, 344–346
Double-heterostructure (DH), semiconductor lasers, 69–70
Double Rayleigh backscattering (DRB), 300–301
Downstream transmission parameters: ITU-T J.83 Annex A and B, 226–227
Dynamic service change request, 386
Dynamic host configuration protocol (DHCP), 360, 391
DTV application software environment (DASE), 400–401

E

Early-late timing recovery, 218–219
Einstein relation, 124
Electron mobility, 124–126
Electronic:
  commerce (E-commerce), 412–413
  home banking, 413–414
  mail (E-mail), 411–412
  predistortion techniques, *see* Linearization methods
  program guides (EPGs), 402–405
  wallets, 413
Emission cross sections, 157–161
Enhanced broadcast, 407
Entitlement control message (ECM), 239–240
Entitlement management message (EMM), 248–249, 404
Entropy coding, 31
Equalizers:
  adaptive, 208–214
  blind, 212–213
  decision feedback (DFE), 53, 212–214, 268–270
  feedforward, 53, 212–214, 268–270

fractionally spaced, 209
linear transversal (LTE), 209
zero-forcing, 210
Erbium doped fiber amplifier (EDFA):
basic configurations, 163–165
carrier-to-noise ratio (CNR), calculation,167–169
dual-stage configurations, 164–165
energy-level diagrams, 154–156
gain-flattened, 176–178
gain spectra, 159–161, 171–172
noise figure (NF), measurement, 169–170
pump lasers, *see* Lasers
requirements for cable TV networks, 170–176
three-level model, 156–160
Error vector modulation (EVM), 219–223
Excited State Absorption, 154–156
External phase modulation (EPM), 319, 342–344

F

Faraday effect, 87–88
Fiber:
Bragg grating, 152–153
Erbium doped, *see* Erbium doped fiber amplifiers (EDFA)
In-the-loop (FITL), 15–17
Filters:
acousto-optic tunable, 153–154, 177–178
bandpass, 214, 233–234, 283
diplex, 46, 231–232, 261
interpolation, 198
Kalman, 212
Nyquist, 202–203
raised cosine, 203, 222–223
SAW, 206–207
square-root raised cosine (SRRC), 203–205, 208, 222–223
Flash memory, *see* Memory
Fractionally spaced equalizers, 202, *see also* Equalizer,
Free propagation region (FPR), 152
Free spectral range (FSR), 152
Frequency chirp, of semiconductor lasers, 81–82, 311, 309, 318, 346
Frequency Division Multiplexing (FDM), 14
Frequency division multiple access (FDMA), 363
Frequency stacking scheme, 352–354

G

Gain:
coefficient, optical, 64,
compression coefficient, in lasers, 75–79
flattened EDFAs, 176–178
optical coefficient, 66
spectra, *see* Erbium doped fiber amplifier (EDFA)
tilt, in EDFA, 346–348
Galois field (GF), 188–190, 238, 242, 363
Generating polynomial, 188–190, 238, 242, 363
Ground state absorption, 154
Group delay variations (GDV), 54–55, 270–271

H

HBT, 139–140
Harmonically related carriers (HRC), 37–38, 49, 423
Headends, master, primary and secondary, 4–6, 332, 348–349, 353
Hole mobility, 119–122
Hybrid fiber/coax (HFC) networks,
architecture, 4–6, 348–349
channel models, 55, 268–269
two-way, overview, 6–9
Hypertext transfer protocol (HTTP), 395 409–410, *see also* Protocol
Hypertext markup language (HTML), 399–401

I

IEEE 802.14, model, 53–55, 268–269
Impulse pay per view (IPPV), 6–7, 406–407
Incrementally related carriers (IRC), 37–38, 423
Index-guided lasers, *see* Lasers
Interferometric noise, *see* Noise
Interference intensity noise, *see* Noise
Interleaving, downstream QAM channel, 191–193
Intermodulation distortions, *see* Distortions
Internet-based applications, set-top box, 409–414
Intersymbol interference (ISI), 51, 202, 205, 209, 211, 213–214
IP telephony, 9–11
Isolators, optical, 87–88, 323–326, 344
ITU-T J.83 Annex A, downstream parameters, 226–227
ITU-T J.83 Annex B, downstream parameters, 226–227

J

Java, language, 399–401
Java virtual machine (JVM), 399–401

L

Large-signal circuit model, 79–81
Lasers:
buried heterostructure (BH), 69–70
directly modulated, transmitter, 287–289, 303–304, 308–309, 311, 316, 318
see Laser Transmitter Design
distributed-feedback (DFB), 72–73, 85–87, 90–92
dynamic characteristics, 74–82
externally modulated, transmitter, 116–120
Fabry Perot (FP), 67–68, 92, 94
frequency response, small-signal, 75–79
gain-guided, 68–69
index-guided, 69–70
linewidth, 84–85
multimode, 68
multiple-quantum well (MQW), 70–71
Nd-YAG, 116–118
package and parasitics, 79–81
pump, 161–162
return-path, transmitters, 92–96, 342–343

structures, 68–70
Laser transmitter design:
directly modulated DFB, 85–90
externally modulated DFB, 119–120
externally modulated YAG, 116–118
Least mean square (LMS) algorithm, 211–212
Lightwave multichannel trunking systems, 333–334
Linearization:
circuits, 110–112
feedforward, 107–110
methods, overview, 106–115
optical dual parallel, 112–114
optical dual cascade predistortion, 114–115
predistortion, 108–110
Lithium Niobate modulator, basic operation, 100–104
Lumped circuit-element modulator, 101

M

Media access control (MAC) layer, DOCSIS protocol:
frame format, 374–375
format and messages, 373–379
management messages, 375–379
operation, 383–384
quality of service (QoS), 384–388
ranging, 379, 391
registration, 379, 391
synchronization, 375–377
upstream fragmentation, 388–390
Mean square error (MSE), 210–211
Memory, see also Set-top box:
flash, 232, 258–260
random access (RAM), 258–260
read only (ROM), 258
synchronous dynamic random access (SDRAM), 232, 258-260
Middleware layer, 398–402
Mini-slot, 365–369, 371–374, 378
Modulation:
AM hum, 55, 273, 276
cross-phase (XPM), 322–323
error vector (MER), 219–223
external-phase (XPM), 319, 342–344
index, optical, 87, 90, 227–280
quadrature amplitude (QAM), modem, building blocks, 183–185
self-phase (SPM), 316–319, 342–344
trellis coded (TCM), 193–200
Modulators:
balanced-bridge interferometer (BBI), 102–105, 118
Lithium Niobate modulator, basic operation, 100–104
lumped circuit-element, 97–98
Mach-Zehnder interferometer (MZI), 102–105, 108, 112–114
M-ary QAM modulator, upstream, 239–243, 363–365, *see also* Upstream Burst Transmitter
traveling-wave, 101–102
Multichannel multipoint distribution services (MMDS), 18–19
Multipath reflections, 50–55, 267–270, 276
Multiple reflections, optical, 299–309
Multiplexing:
frequency-division (FDM), 354
time-division (TDM), 352
wavelength-division (WDM),
Multiple grant mode, 388
Multiple quantum well (MQW) lasers, 73–74, 85, 92

N

Narrowcasting, 350
National Television Standard Committee (NTSC) video format, 21–27, 244–245
Native middleware, 396, 398–402
Native applications, 402–405
Near video on demand (NVOD), 8 407–409
Noise:
 additive white Gaussian (AWGN), 223, 227, 262–267, 273
 amplified spontaneous emission (ASE), 157–161, 165–175, 336
 burst, 57, 271–273
 clipping, 281–283, *see also* Clipping Noise
 equivalent photocurrent (NEP), 132
 funneling effect, 58–59
 impulse, 56, 271–273
 ingress, 56–60
 interference intensity (IIN), 300, 305
 interferometric, due to DBR, 300–301
 Langevin, 82–83
 mode-partition (MPN), 92–94
 mode-hopping (MHN), 92, 94
 phase, 254–256
 power ratio (NPR), 355–356
 relative-intensity (RIN), 82–84, 91–92, 132, 289, 306–307
 shot, 129–130, 133–134
 signal-spontaneous beat, 162–164
 spontaneous-spontaneous beat, 162–164
 spurious, upstream, 370–371
 thermal, 130–134
Noise figure:
 optical amplifiers, 167–175
 RF amplifiers, 47–48
 saturated, 174–175
Non-blocking algorithm, 382
Nonlinear distortions, *see* Distortions
Nyquist bandwidth, 202

O

OpenCable, set-top box, 249–250, 273, 275–276
Optical isolator, 87–88, 323–326, 344
Optical reflections, 299–309
Out-of-band (OOB):
 interleaver, 238–239
 mapping, 239
 R-S coding, 238
 parameters, receiver, 236
 randomizer, 237–238
 receiver, 232, 235–239, 261

P

p-persistent binary exponential backoff, 382
Packet data unit (PDU), 240, 374–375, 379, 383–384
Pay per view (PPV), 402, 406–407
Parental control, 404–405
Parity bytes, 188–190, 238, 363
Parity check matrix, 186–187
Peak optical gain, 66
Piggyback mode, cable modems, 389
p-i-n photodiode, 123–129
Physical media dependent (PMD) sublayer, downstream, 361–363
Pockels effect, 100
Point of deployment (POD) module, 249–250
Polarization-dependent distortions,

323–326, *see also* Distortions,
Polarization coupling, 300–301
Polarization hole burning (PHB), 170
Polygon mesh, 252
Power TV software, 398–399
Preamble, 240, 364–366
Preclipping methods, 292–294
Pre-equalization, adaptive, 367
Program identification (PID), 243, 245
Protocol:
address resolution (ARP), 359
data-over-cable interface specifications (DOCSIS), stack, 359–361
dynamic host configuration (DHCP), 360, 391
hypertext transfer (HTTP), 395, 409–410
Internet message access (IMAP), 411
network-based call signaling (NCS), 11–12
post-office (POP), 411
program and system information (PSIP), 409
simple network management (SNMP), 411
simple message transfer (SMTP), 411
trivial file transfer (TFTP), 360, 391–392
Public key encryption, 247–248
Public switched telephone network (PSTN), 2, 10–11
Punctured convolutional coding, 193–195, 198
Pump lasers, 161–162, *see also* Lasers
Push pull amplifiers, 90, 139–140

Q

Quadrature amplitude modulation (QAM), *see* Modulation
QPSK, *see* Upstream Burst Transmitter
Quality of service (QoS), 384–388

R

RSA, cryptosystem, 247–248
Randering, 255–257
Random access methods, 366–369
Random access memory (RAM), 249–250, *see also* Memory
Randomizer, 201–202, 242–243, 364
Ranging request, 379, 391, *see also* Cable Modem
Ranging response, 379, 391, *see also* Cable Modem
Rate equations, 75–76, 156–157
Rayleigh distribution, 282, 291
Rayleigh scattering, 299–300
Read-only-memory (ROM), *see* Memory
Registration:
request, 379, 392
response, 379
acknowledge, 379
Receiver:
basic configurations, 138–144
front-end design, optical, 140–142
M-ary QAM, operation, 206–208
nonlinear behavior, p-i-n photodetectors, 135–138
optical, configurations, 133–139
out-of-band (OOB),8, 232, 235–239, 248–250, 260–261, 419
quantum efficiency, 128–129
responsivity, 127–128
transimpedance front-end design, 141–143
Recursive least square (RLS) algorithm, 212

Real time operating system (RTOS), 395–398
Reed Solomon (R-S) code, 183–185, 188–193, 227, 236, 238, 241–242, 267, 363–364, 419, 421
Resonance frequency, laser, 77–78
RMS modulation index, 91, 291–292

S

SECAM, signal format, 27–29
S-Aloha, 380
Saturated noise figure, 174–175
Secure sockets layer (SSL) protocol, 409–410
Semiconductor structures, *see* Lasers,
Semiconductor lasers, *see* Lasers
Self-phase modulation (SPM), 316–319, 342–344, *see also* Modulation
Service ID (SID), 374, 385, 387–389, 391
Service flow ID (SFID), 374
Set-top box:
 architecture, hardware, 231–233, 249–250, 260–261
 conditional access, 246–250
 CPU, 257–258
 graphics processor, 250–257
 memory, 249–250
 MPEG demultiplexer and decoder, 235–237
 on-screen video, 255–257
 renewable security, 249–251
 RF tuner, 231–235, 250, 260–261, 263–265
 system budget link, 273–274
 upstream transmitter, 239–243
Skin effect, 43
Simple message transfer protocol (SMTP), 411
Signaling system number 7 (SS7), 11
Spectral-hole burning (SHB), 75–76
Spontaneous emission, 76, 154, 156–157
Square-root raised cosine (SRRC) filter, *see* Filters
Stimulated Brillouin scattering (SBS), 119, 312–316, 326
Stimulated emission, 75–76, 154, 156, 161
Stimulated Raman scattering (SRS), 319–323
Subcarrier multiplexed (SCM) lightwave systems, 91, 94, 149, 292, 294, 303–306 319–320
Stark levels, 155–156
Synchronization, upstream packets, *see* Cable Modem
Synchronization trellis group, for QAM, 199–200

T

Thermoelectric cooler (TEC), 86, 88–89
Time-Division Multiplexing (TDM), 6, 352, 363
Timing, burst, 355–357
Timing recovery methods, 217–219
 early-late, 218–219
 forward-acting, 217–218
Transimpedance receivers, 141–143, see *also* Receivers
Transmission convergence (TC) sublayer, DOCSIS protocol, 372–373
Traveling-wave modulator, 101–102
Trellis-coded modulation (TCM), 193–200
Trellis groups, for 64/256-QAM, 191–194

Trivial file transfer protocol (TFTP), *see* Protocol
Tuner, RF double-conversion, 231–235, 250, 260–261, 263–265
Turn-on delay, 290–291
TV platform adaptation kit (TVPAK), 397–398

U

Unsolicited grant service (UGS), 386–388
Unified memory architecture (UMA), 259
Unique word (UW), 240, 421
Uniform resource locator (URL), 411
Universal serial bus (USB), 232, 261
Upstream:
  channel descriptor (UCD), 364, 377–378, 391
  bandwidth allocation map, 365, 378, 383–384, 388
  channel change request, 379
  channel change response, 379
  fragmentation, 388–390
  channel parameters, 365–366
  service flow scheduling, 386–388
Upstream burst transmitter:
  block diagram, 239–242, 367
  forward-error-correction coding, 242–243, 363–365
  packet format, 240
  parameters, RF, 241, 419–421
  PHY layer, cable modem, 363–365
Upstream spurious output, cable modem, 370–371

V

Video on demand (VOD), 8, 402, 405 407–409
Video signals:
  DigiCipher I and II, 35–36
  NTSC system, 21–27
  MPEG-1 standard, 29–33, 37
  MPEG-2 standard, 33–34
  MPEG-4 standard, 35–36
  PAL system, 27–28
  SECAM system, 28–29
Visual carrier, 22, 24–25
Vertical blanking interval (VBI), 24, 245–246
Viterbi decoding, 195–197

W

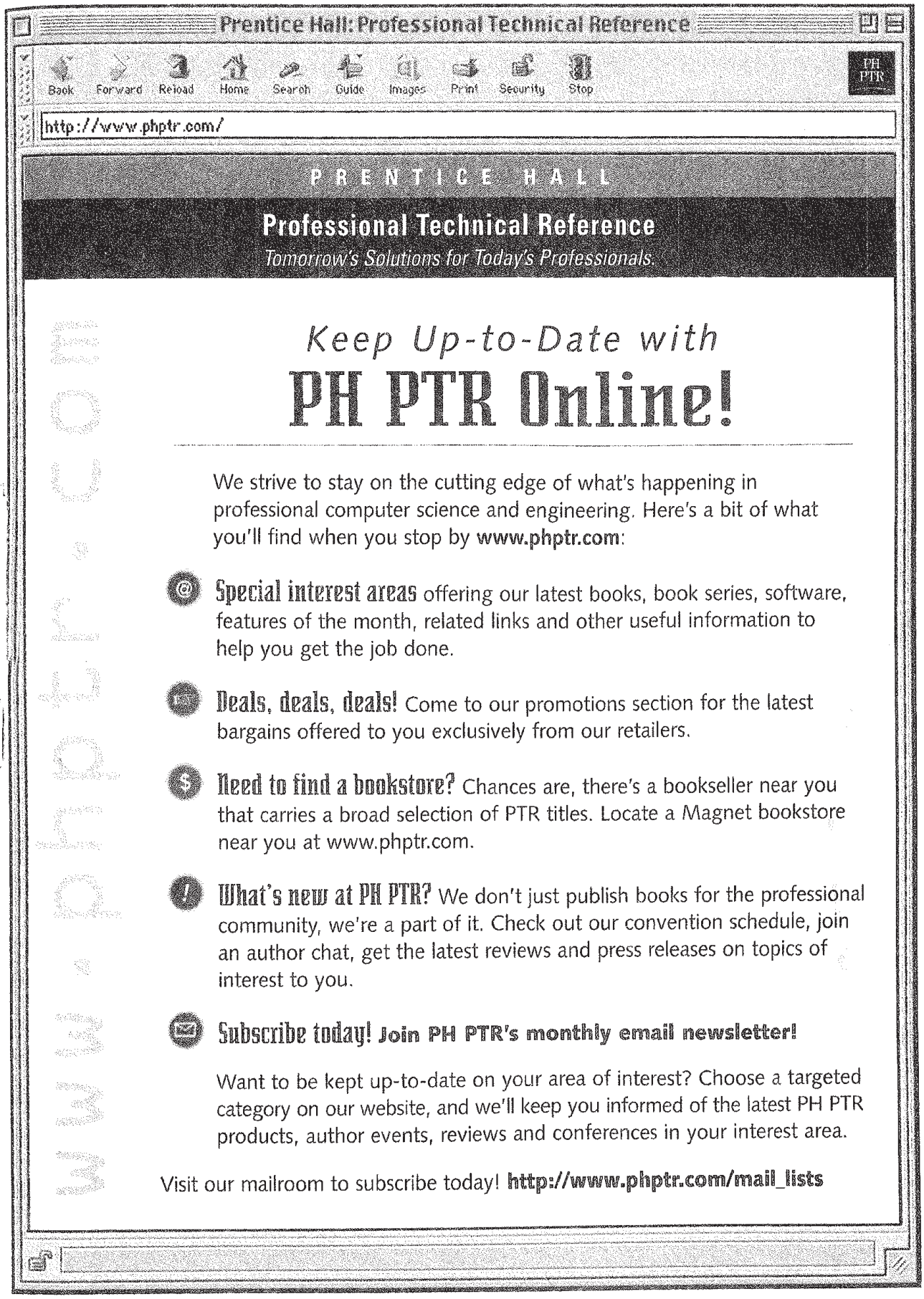
Web browsers, set-top box, 409–411
Webcasting, 410–411
Window CE operating system, 397–398

Y

YAG laser transmitter, 116–118
Yttrium iron Garnet (YIG), 88
Y junction coupler, 102–103

Z

Z buffering technique, 253–254


Prentice Hall: Professional Technical Reference
Back
Forward
Reload
Home
Search
Guide
Images
Print
Security
Stop
PH PTR
http://www.phptr.com/
PRENTICE HALL
Professional Technical Reference
Tomorrow's Solutions for Today's Professionals.
www.phptr.com
Keep Up-to-Date with
PH PTR Online!
We strive to stay on the cutting edge of what's happening in professional computer science and engineering. Here's a bit of what you'll find when you stop by www.phptr.com:
Special interest areas offering our latest books, book series, software, features of the month, related links and other useful information to help you get the job done.
Deals, deals, deals! Come to our promotions section for the latest bargains offered to you exclusively from our retailers.
Need to find a bookstore? Chances are, there's a bookseller near you that carries a broad selection of PTR titles. Locate a Magnet bookstore near you at www.phptr.com.
What's new at PH PTR? We don't just publish books for the professional community, we're a part of it. Check out our convention schedule, join an author chat, get the latest reviews and press releases on topics of interest to you.
Subscribe today! Join PH PTR's monthly email newsletter!
Want to be kept up-to-date on your area of interest? Choose a targeted category on our website, and we'll keep you informed of the latest PH PTR products, author events, reviews and conferences in your interest area.
Visit our mailroom to subscribe today! http://www.phptr.com/mail_lists

InformIT

Solutions from experts you know and trust.

Articles | Free Library | eBooks | Expert Q & A | Training | Career Center | Downloads | MyInformIT

Login | Register | About InformIT

Topics

Operating Systems

Web Development

Programming

Networking

Certification

and more...

Expert Access

Free Content

www.informit.com

- Free, in-depth articles and supplements
- Master the skills you need, when you need them
- Choose from industry leading books, ebooks, and training products
- Get answers when you need them - from live experts or InformIT's comprehensive library
- Achieve industry certification and advance your career

Visit InformIT today and get great content from PH PTR

Prentice Hall and InformIT are trademarks of Pearson plc / Copyright © 2000 Pearson

Made in the USA
Las Vegas, NV
07 February 2022



43175538R00256

Communications

BROADBAND CABLE TV ACCESS NETWORKS

From Technologies to Applications

SHLOMO OVADIA

Next-generation CATV systems: architecture, protocols, technologies, and applications

Broadband cable TV networks are undergoing a massive transformation, from simply broadcasting analog TV channels to providing sophisticated, two-way interactive services such as high-speed Internet access and video-on-demand. Now, one of the field's leading experts reviews the technologies, protocols, and applications associated with the CATV revolution, and previews the migration path from today's two-way hybrid fiber/coax networks to the awesome capacities of tomorrow's DWDM fiber networks. Coverage includes:

- **HFC cable networks vs. the competition: DSL, FTTL, DBS, and MMDS**
- **Key fiber-optics transmission technologies: directly and externally modulated laser transmitters, optical receivers, and Erbium-doped optical fiber amplifiers (EDFAs)**
- **Architecture of DWDM access networks**
- **Hardware architecture and operation of digital set-top boxes and cable modems**
- **Software architecture and applications for digital set-top boxes**

Ovadia offers in-depth analyses of single-and multiple-wavelength fiber-optics transmission impairments over HFC and DWDM networks, and presents the emerging two-way DWDM network architecture. Finally, he discusses the DOCSIS cable modem protocol, as well as key set-top box applications such as electronic program guides (EPGs), video-on-demand (VOD), Internet-based applications such as e-mail, and e-commerce.

Whether you're an engineer, scientist, cable professional, manager, or investor, if you want to understand where cable is headed, you need *Broadband Cable TV Access Networks: From Technologies to Applications*.

About the Author

SHLOMO OVADIA is a Principal System Architect in the Cable Network Operation business unit at Intel. Prior to joining Intel, he was involved in the development of digital set-top boxes and cable modems as a Principal Scientist at Digital Network Systems, General Instrument/Motorola. He is a Senior Member of IEEE, and has written more than 60 technical publications and conference presentations. He currently has eight patents pending, and his personal biography is included in the millennium edition of *Who's Who in America: Science and Engineering*.

PRENTICE HALL
Upper Saddle River, NJ 07458
www.phptr.com

ISBN 0 13 086421 8
90000
9 780130 864215